Infrastructure Technology Institute
McCormick School of Engineering and Applied Science
Northwestern University

Design and Verification of Blast Densification for Highway Embankments of Liquefiable Sands

Final Report

by

Richard Finno

October 26, 2012

Measuring the effect of occluded gas bubbles on stress-strain response of a loose to medium sand

Hilde B. Knai

Abstract

As part of a larger effort to investigate the effects of blast densification on the properties and behavior of compacted sand deposits, this study presents a procedure for replicating in the laboratory the occluded gas bubbles believed to exist in the ground after blasting, and a preliminary evaluation of the effect of these bubbles on the stress-strain response of loose to medium samples of a fine sand. The procedure for creating gassy soil specimens relied on the exsolution of CO_2 gas from carbonated water when the applied pressure was reduced. A system was developed for replacing the pore water in a sand sample with water saturated with CO_2. After replacing the pore water, a given amount of bubbles could be produced in the sample by lowering the backpressure by a controlled increment. Using this setup, a series of drained and undrained triaxial compression tests were performed on sand samples with void ratios ranging from 0.62 to 0.82 and containing varying amounts of gas. It was concluded that the presence of free gas lowered the effective friction angle of the sand by 1.0 to 1.5 degrees compared to fully saturated samples at the same void ratio. This effect may explain the reduction in cone penetration resistance after blasting which is often observed in the field.

Contents

List of tables

List of figures

Chapter 1 – Introduction

This study is part of a larger effort to investigate the effect of blast densification on soil properties and develop a quantifiable design methodology and verification system for improving liquefiable sands through blast densification. The liquefaction of loose, saturated sands due to seismically induced ground motions has been recognized as one of the most damaging effects of earthquakes since the 1960s (Kramer, 1996). Various methods of soil improvement have been used to reduce liquefaction susceptibility through densifying the soil, one of the most common being blast densification. Although it is widely used, blasting procedures are typically based on individual contractors' experience rather than established theory. To develop a design methodology based on soil mechanics theory, the soil conditions during and after blast densification must be understood in more detail. One aspect of these conditions is the behavior of gases produced during blasting and their interaction with the sand grains and water in the soil. It is believed that the influence of occluded gas bubbles dispersed throughout the sand may explain some surprising trends in soil behavior after blasting, particularly the decrease in cone penetration resistance which is often observed in the field. The goal of this particular study is to develop an experimental procedure to replicate these bubbles in the laboratory, and to perform some preliminary triaxial tests on sand containing bubbles.

A review of the available literature on triaxial testing of gassy sand, and some previous results of tests on sands containing gas bubbles is presented in Chapter 2. Chapter 3 describes the experimental setup developed for introducing gas bubbles into the soil, the methods used for specimen preparation, the testing program and the methods of analysis used. Chapter 4 presents the results of triaxial tests on saturated and gassy samples in drained and undrained shear, and describes the effect of gas on the effective friction angle of the sand samples. The conclusions of this study are summarized in Chapter 5.

Chapter 2 – Literature review

The goal of this study is to develop an experimental procedure to produce well-dispersed gas bubbles in sand samples for triaxial testing, and to perform some preliminary tests on these gassy samples to study how their stress-strain behavior compares to fully saturated samples at the same density. To do so, it is necessary to understand how blasting introduces gases into the soil, the effects gas bubbles are believed to have on the soil response, and what laboratory procedures have been established for triaxial testing of gassy soils.

2.1 Blast densification

2.1.1 Procedure and practice

Blast densification has been used to densify loose, saturated sands since the 1930s. The technique relies on the shockwave created underground by the detonation of an explosive, most often ammonium nitrate/fuel oil (ANFO). The pressure wave breaks any interparticle bonds due to cementation, and the sudden increase in pore water pressure enables soil grains to "move around" and rearrange themselves as the effective confining pressure is reduced. As these excess pore water pressures dissipate and the effective stresses return to normal, the sand reconsolidates into a denser configuration than before. Depending on the grain size distribution, the initial density of the sand, and the design of the blasting process, settlements up to 10% of the initial thickness of the soil layer can be achieved in a single pass. Several passes can be used to achieve further compaction. (Narin van Court and Mitchell, 1994)

2.1.2 Use in liquefaction mitigation

Blast densification is a useful method for reducing the risk of liquefaction of sands following an earthquake, because the type of sand deposits that are susceptible to liquefaction are exactly the type most suited for blast densification. Liquefaction can occur in a saturated sand layer if cyclic loads (such as those imposed by seismic shear waves) lead to a buildup of pore water pressure

sufficiently high to balance the confining stresses on the sand, so the effective confining stress approaches zero. As the name of the phenomenon implies, the sand behaves as a viscous liquid and can no longer support significant shear loads, which can lead to catastrophic failures such as lateral spreading and flow of massive soil sections or complete bearing failure under large buildings, levees or dams. Liquefaction and flow can only occur if the sand has a contractive response to shear, which occurs when the sand is loose of critical state. If the sand is compacted sufficiently, for example through blasting, its response will change to dilative type behavior, meaning that positive pore pressures will not build up significantly during undrained cyclic shear. Therefore, a sand that is sufficiently dense (for a given confining pressure) will not be at risk of liquefying. Blast densification has been used to densify sand to reduce the risk of earthquake-induced liquefaction for a range of applications, as described by Narsilio et al. (2009).

2.1.3   Effect on Cone Penetration Test (CPT) results

The effectiveness of blasts densification has traditionally been judged based on surface settlements and cone penetration tests (Dowding and Hryciw, 1986). Surface settlements can usually be observed within hours, and are reasonably simple to interpret, although some loosening of the upper soil layers can occur due to the upward movement of gases and excess pore water, obscuring the densification of the lower layers. For a given soil, CPT results are usually directly proportional to the relative density (Kulhawy and Mayne, 1990). However, even in cases where significant settlement is observed, CPT results have been shown to decrease after blasting (Mitchell and Solymar, 1984; Narin van Court and Mitchell, 1994, Narsilio et al. 2009.).

2.1.4   Gases produced during blasting

Hryciw (1986) described the amount of gas produced during blasting and the behavior of the gases in the soil. Although many different types of explosives can be used for blast densification, they all produce the same types of byproducts in the form of gas. The main products from a well-designed explosive (i.e. enough oxygen is provided so that complete combustion takes place) are nitrogen gas, carbon dioxide gas, and water vapor. These gases are produced in the approximate

ratio of $CO_2 : N_2 : H_2O$ of $1 : 2 : 5$. ANFO explosives, which are the type most commonly used for blast densification, typically produce about 43 moles of gas per kg of explosive used. The water vapor condenses quickly, while the remaining 3/8 of the explosion products will remain in gas form at the temperatures and pressures considered here. Depending on temperature and pressure, a small amount of this gas will dissolve in the pore water, while the rest remains in free form.

2.2   Behavior of gassy soil

Although most soil mechanics research has been focused on saturated soils, it has long been known that the presence of gases in soil can influence the soil behavior. Terzaghi (1943) noted that suspended pockets of gas could exist in soil, and distinguished between the effects of small and large bubbles. As summarized by Wheeler (1986), most research on soils containing gas bubbles has focused on marine deposits under high pressures. Most of the free gas in these deposits is found in the form of large bubbles (larger than the soil grains and the normal void spaces), as opposed to small occluded bubbles which exist within a continuous pore fluid (Wheeler, 1988). The gases encountered in these deposits are most often methane or biogenic gases produced by bacteria, which include carbon dioxide, hydrogen sulfide, and ethane, in addition to methane. Although the bubbles created in shallower, on-shore deposits by blast densification or other soil improvement methods may not be directly analogous to the conditions in these marine soils, some findings from previous research are applicable to the in-situ conditions and stress ranges evaluated herein.

2.2.1   Loose sands

Grozic et al. (1999) performed a series of laboratory tests on reconstituted samples of Ottawa sands. The samples were all loose to very loose, with void ratios ranging from 0.77 to 1.02, and were tested at a relatively high mean normal effective stress of 300 kPa. At this stress, the fully saturated samples all developed positive excess pore water pressures during undrained shear. As shown in Figure 2.1, the shear response of the gassy samples varied with the gas content, with

11

samples with an initial degree of saturation over 90% exhibiting strain-softening behavior, and those with an initial degree of saturation below 90% exhibiting strain-hardening responses. This would suggest that the presence of gas decreases the risk of liquefaction and flow at these stress conditions, as the undrained shear strength of the soil increases in the presence of a sufficient amount of gas.
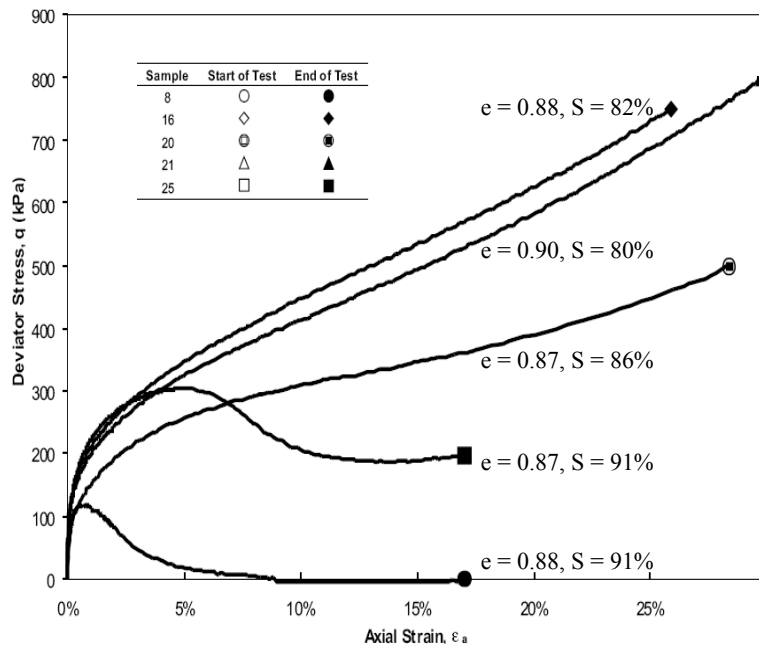
Figure 2.1 – Stress-strain response of specimens with similar void ratios and varying gas content (Grozic et al., 1999)

2.2.2 Dense sands

Rad et al. (1994) performed a series of static and cyclic triaxial tests on a fine river sand reconstituted to void ratios ranging from approximately 0.65 to 0.80. Relatively low confining pressures were used, and the fully saturated reference samples all exhibited dilative-type behavior when tested in drained shear. Because the specimens tested in undrained shear developed negative excess pore pressures, they had higher shear strengths than the drained samples at the same void ratio. Figure 2.2 shows the results of two fully saturated samples, one tested in drained shear (no. 13) and one in undrained shear (no. 6), as well as two gassy samples in "undrained" shear.

12
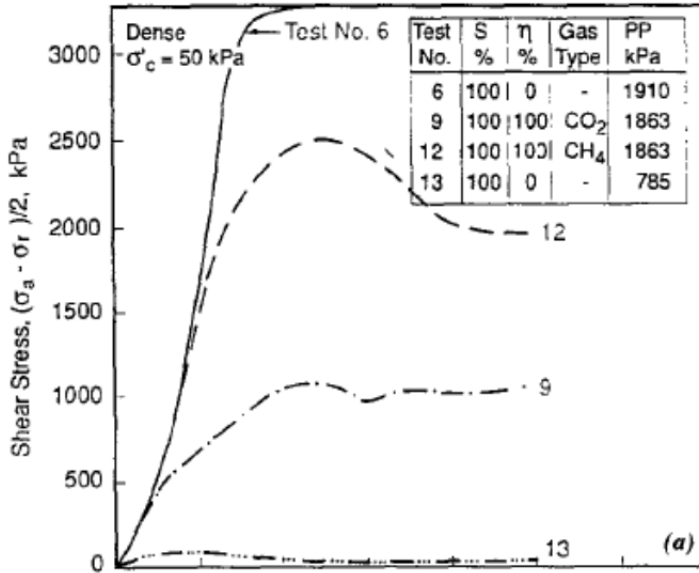
Figure 2.2 – Effect of gas on undrained shear strength of dense sand samples: Test no. 6 is a fully saturated sample in undrained shear, 9 and 12 are gassy samples in "undrained" shear, and 13 is a fully saturated sample in drained shear. (Rad et al., 1994)

In the samples where the pore water had been saturated with CO_2 or methane gas prior to shearing, gas bubbles formed when the pore pressure started to decrease. With gas bubbles present, the pore fluid could expand, allowing the soil to dilate without developing large negative pore pressures. Because of this effect, the measured "undrained" shear strength of gassy specimens was lower than that of fully saturated samples, as shown in Figure 2.2. However, it should be noted that as the volume of these gassy samples could change during shear, the shear stage was not undrained in the usual sense of the word.

2.2.3   Longevity of gas bubbles

Gas bubbles have been found to remain in otherwise saturated soil deposits for several decades. Okamura et al. (2006) obtained high-quality frozen samples of sands that had been improved using sand compaction piles, a technique which introduces large amounts of air when installing sand piles in previously saturated sand layers. The samples were obtained from sites that had been improved 4, 8, and 26 years previously. The degree of saturation was well below 100% for

all the samples, with the samples containing 26-year-old bubbles having a degree of saturation of 92%. Although these bubbles had been introduced by sand compaction piles rather than blasting, they confirm that gas bubbles can remain in the soil for considerable amounts of time and should be considered in any investigation of previously improved soils where the presence of gas is expected.

2.3   Laboratory testing procedures developed for gassy soils

Wheeler (1986) described a procedure for triaxial tests on remolded samples of Combwich Mud, a clayey silt into which methane bubbles were introduced by means of a chemical reaction using a method developed by Nageswaran (1983). These specimens were consolidated and sheared in a modified triaxial setup which included an inner "jacket" filled with mercury used to monitor the volumetric strain of the sample.

Rad et al. (1994) performed a series of static and cyclic triaxial tests on dense reconstituted samples of Baskarp sand in which the pore water in a saturated specimen was replaced with water that had been saturated with carbon dioxide or methane gas. Most of the samples were fully saturated at the beginning of shear, with gas bubbles appearing only if the pore pressures decreased as a consequence of dilative type behavior of the soil. A similar procedure was used by Grozic et al. (1999) on very loose specimens of Ottawa sand. These samples were isotropically consolidated by maintaining a constant cell pressure while the backpressure was lowered, so gas exsolution occurred during consolidation. This method of replacing the pore water with carbonated water was found to work very well, and was used in this study.

2.4   Summary

Blast densification is a reliable method for compacting loose, saturated sand deposits, but CPT test results often show little improvement even though significant settlements have taken place and the sand must have been compacted. This indicates that some aspect of the soil conditions besides the void ratio must influence the CPT resistance after blasting. Blasting introduces large amounts of gas into the soil, and it seems likely that some of the gas will remain in the soil,

whether dissolved in the pore water or in the form of free gas bubbles. The chemical composition of the explosion products is relatively similar to that of air, consisting of mostly nitrogen. Air bubbles introduced into a soil deposit during installation of sand compaction piles, another ground improvement technique, have been found to remain in the soil for decades, so it can be assumed that bubbles created during blasting may endure for considerable periods as well.

In the laboratory, gas in the pore space has been found to have a noticeable effect on sands both loose and dense of critical. Although triaxial tests have been performed on reconstituted samples, most researchers have focused on marine deposits with higher fines content, tested at higher pressures than the stresses used in this study. The laboratory methods developed for sands by Rad et al. (1994), however, were found to be applicable to the stress conditions used in this study, and were modified for use here.

Chapter 3 – Experimental Program and Procedures

3.1 Material tested

The sand used for testing was obtained from a blast densification test site in South Carolina described by Narsilio et al. (2009). It is a light brown, clean, fine sand with subrounded to subangular grains. A photograph of a sample from the same source is shown in Figure 3.1, below. The grain size distribution is shown in Figure 3.2. As the figure shows, 100% of the material passed a #4 sieve, 95% passed a #40 sieve, and less than 1% was finer than a #200 sieve, so the bulk of the material is fine sand. The coefficients of uniformity and curvature are 1.98 and 0.95, respectively, so the sand is poorly graded and is categorized as a poorly graded clean sand (SP) according to USCS.
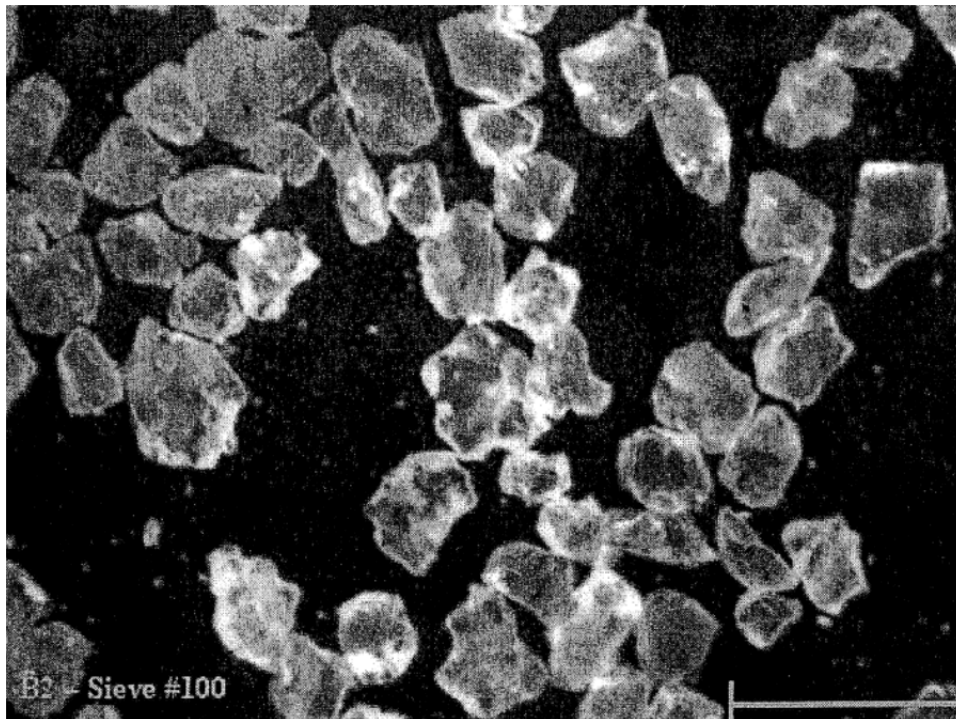
Figure 3.1 – Grains retained on a #100 sieve photographed at 60X magnification, from Narsilio et al. (2009)
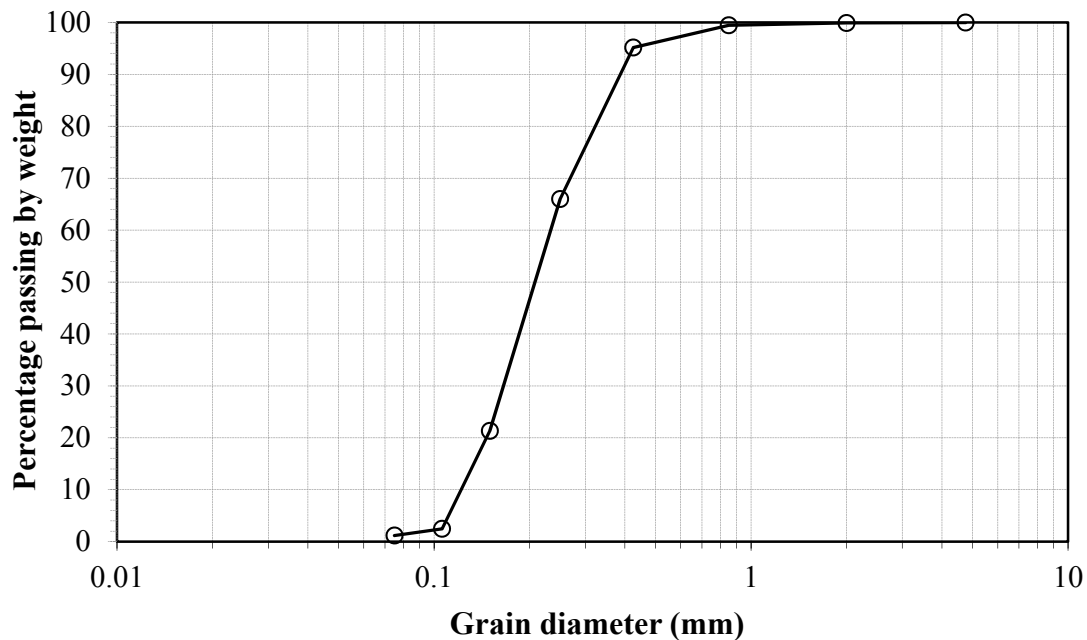
Figure 3.2 – Grain size distribution of the sand used for triaxial testing

A limited amount of sand had been extracted for testing. Since the testing program consisted of triaxial tests at relatively low pressures, it was assumed that no grain crushing would occur during testing, so the sand could be dried and reused for several rounds of triaxial testing without affecting the soil response. To check this hypothesis, a second grain size analysis was performed on a sand sample that had been reused several times. The resulting grain size distribution was virtually identical to the initial one, which confirmed that no grain crushing had taken place. A visual inspection (with a microscope) also indicated that the grains in the sample remained the same shape as before and had not been noticeably rounded off by the testing process.

3.2   Triaxial device and additional instrumentation

The triaxial tests were performed with two CKC e/p Cyclic Loader devices described in detail by Gassman (1994). In addition to the sensors built into this apparatus, an internal load cell and three linear variable differential transformers (LVDTs) were used to measure the axial force applied to the sample and its deformation. Two LVDTs were installed in the axial direction and

one was mounted on a circumferential frame to measure the radial expansion of the sample, as shown in Figure 3.3. The LVDTs were installed on the central third of the specimen to minimize the effects of barreling on the measurements. The components and specifications of these sensors were described in detail by Holman (2005).
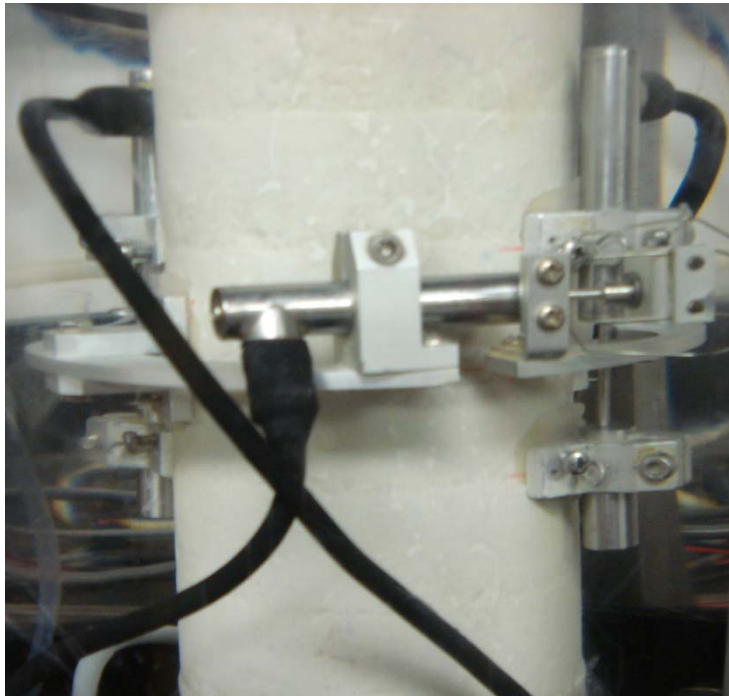
Figure 3.3 – Axial and radial LVDTs mounted on triaxial sample

The velocity of flexural waves traveling through the sample was measured using bender elements. The bender elements consisted of a transmitter embedded in the top cap and a receiver embedded in the pedestal. When excited by an applied voltage, the transmitter deflects horizontally, creating a flexural wave which travels through the sample and is detected by the receiver at the base of the specimen. Although the wave mechanics are not identical to that of a shear wave in an infinite medium, it has been shown that at the frequencies used here, the velocity at which the flexural wave travels through samples of this size and stiffness is the same as the in-situ shear wave velocity in the soil (Holman and Finno, 2005). The construction, installation, and calibration of the bender elements used were described by Holman (2005).

3.3   Dissolution of CO_2 gas in water

To create evenly distributed occluded gas bubbles of the type believed to exist in sand after blast densification, the pore water in the sample was replaced with carbonated water, after which the applied pressure was lowered to bring the CO_2 out of solution in the form of gas bubbles. This process is the same as what happens when the cap is taken off a bottle of soda water, and should produce small, evenly dispersed bubbles throughout the body of the soil sample.

To produce the carbonated water, a container was filled with deaired water and CO_2 gas under pressure. The solubility of gas in water at standard temperature (T = 298 K) is governed by Henry's law, which relates the applied pressure to the concentration at which water is completely saturated with the given solute:

$$c = \frac{p}{k_H} \tag{3.1}$$

where c is the concentration of the solute (CO_2) in the water, p the partial pressure of the gas above the water, and k_H the solubility or Henry's law coefficient, which depends on the chemical properties of the solute. Carbon dioxide gas was chosen because of its relatively low solubility coefficient of 2979 L·kPa/mol, which meant that significant amounts of gas could be dissolved in water at manageable pressures. Because pure CO_2 was used, the partial pressure of the gas was equal to the total pressure in the container. (Stumm and Morgan, 1996)

When a gage pressure of 200 kPa (i.e. 300 kPa absolute pressure) is applied to a system consisting only of deaired water and CO_2 gas, the amount of gas that can be dissolved in the water is

$$c = \frac{300 \text{ kPa}}{2979 \frac{\text{L} \cdot \text{kPa}}{\text{mol}}} = 0.101 \frac{\text{mol}}{\text{L}} \tag{3.2}$$

If the applied pressure were lowered to 200 kPa absolute pressure, the amount of CO_2 that could remain in solution would be c = 0.067 mol/L, and the remaining 0.033 mol/L would precipitate out of solution in the form of gas bubbles.

Stumm and Morgan describe how the rate of dissolution of CO_2 gas in water changes with the concentration of CO_2 in the water. The rate of molecular transfer is

$$F = \frac{D_{CO_2}}{z_w}([CO_2]_i - [CO_2]_w) \tag{3.3}$$

where F is the rate of transfer in mol/m^2·s, D_{CO_2} the molecular diffusion coefficient, z_w the thickness of the saturated film that forms the gas/water interface, and $[CO_2]_i$ and $[CO_2]_w$ the instantaneous concentrations of CO_2 in this interface and in the water, respectively. D_{CO_2} and z_w are constant during the saturation process: $D_{CO_2} = 2 \times 10^9$ m^2/s, $z_w = 40$ μm (Stumm and Morgan, 1996). As the container is continuously replenished with CO_2 gas, the gas/water interface is fully saturated throughout and $[CO_2]_i = 0.101$ mol/L as calculated previously. The rate of transfer, therefore, is simply a function of the concentration of dissolved CO_2 in the water, $[CO_2]_w$, which will increase with time from an initial value of zero as dictated by the flux of gas molecules across the gas/water boundary. This flux is found by multiplying the rate of transfer F by the area of the interface. The rate of transfer and $[CO_2]_w$ can then be calculated by iteration and are shown in Figure 3.4.
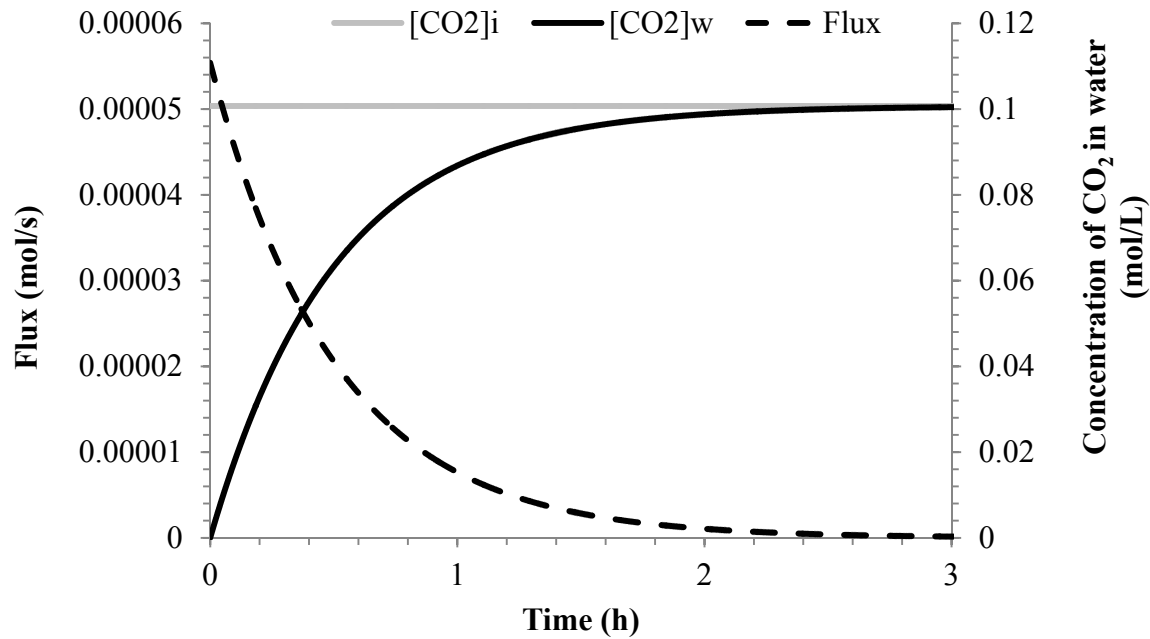
Figure 3.4 – Variation in flux of CO_2 molecules across gas/water interface and concentration of CO_2 in water with time

3.4   CO₂ system design and use
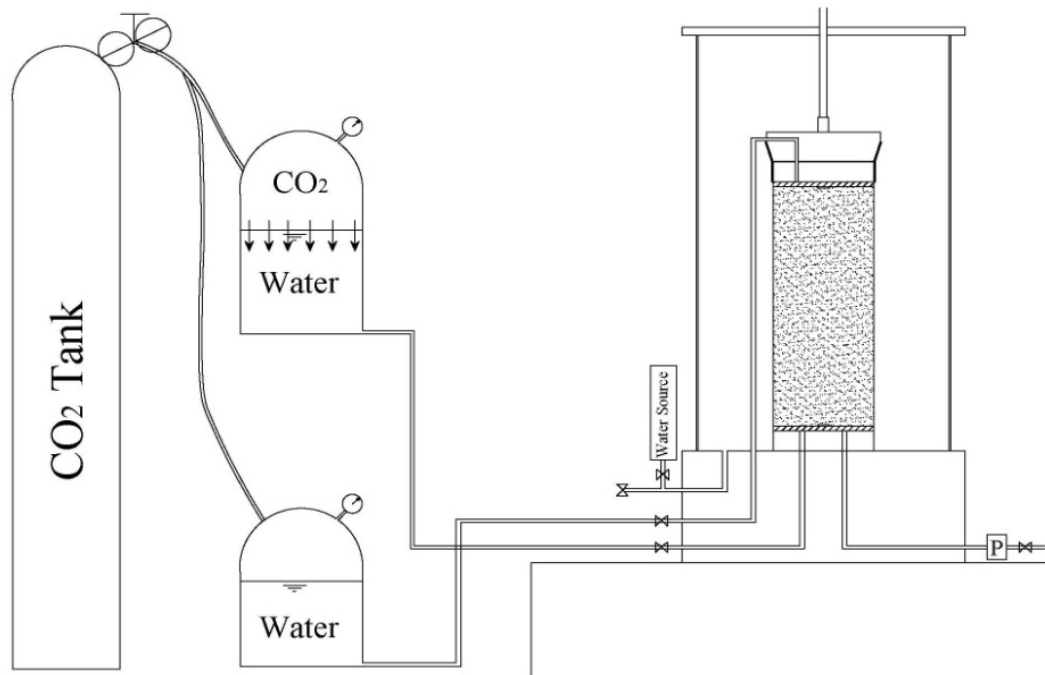
Figure 3.5 – CO₂ saturation system: After the water in the top container had been fully saturated with CO₂, it was fed through the sand specimen (going in at the base and out at the top), replacing the pore water.

As shown in Figure 3.5, the system developed for replacing the sample pore water with carbonated water consisted of two containers of deaired water, a pressurized CO_2 canister and two additional valves attached to the base plate of the triaxial cell that were used to circumvent the backpressure system on the CKC device. One container was elevated while the other was kept at floor level, so the head difference was about two meters. The CO_2 canister was used to apply an absolute pressure of 300 kPa to both tanks. To produce the carbonated water, the top container was filled with deaired water and CO_2 gas from the canister was percolated through the water for about an hour, after which the system was left under pressure overnight to ensure that all the water in the system would be completely saturated with CO_2. As Figure 3.4 shows, the water in the container would be almost completely saturated with CO_2 in about three hours. It is important to note that the initial step of percolating the CO_2 gas through the water was not considered in this calculation, as this model for molecular transfer only considers static interfaces. The rate of dissolution increases when gas is bubbled through the water (Shindo et al.,

1995), so it can be safely assumed that the water was completely saturated with CO_2 at a concentration of 0.101 mol/L at the end of the 12-hour saturation process.

3.5 Experimental procedures

3.5.1 Preparation of sample

Sand samples were prepared by moist tamping using a procedure similar to that described by Ladd (1978). The soil was moistened with 5% water by weight and placed in six layers of approximately 24 mm using a tamping rod. Undercompaction of the lower layers was attempted, but as the samples were all relatively loose, the target values for the initial thicknesses of the layers varied by less than 1 mm, which could not be reliably measured using the gradation on the tamping rod. A split mold was used to hold the sample membrane in place during preparation, before a vacuum of about 20 kPa was applied to the sample after the top cap was installed. The frames for the LVDTs were mounted using pins and silicone sealant. The vacuum was held for an hour to check that the membrane was intact and sealed sufficiently at both ends of the sample and around the pins supporting the LVDTs. The exact dimensions of each sample were measured and used to calculate the initial (unconsolidated) void ratio. The samples all measured about 72 mm in diameter and 143 to 145 mm in height.

3.5.2 Saturation

Once the triaxial cell was assembled, a cell pressure of 30 kPa was applied to hold the sample in place as the vacuum was released. To drive out air and achieve saturation at lower backpressures than would otherwise have been necessary, CO_2 gas was percolated through the sample for 20 minutes before it was saturated with deaired water. A volume of water corresponding to about three times the pore volume of the loosest samples was flushed through the sample, after which the water lines to the CKC apparatus were connected and a backpressure of 200 kPa was applied. The sample was then left overnight to saturate completely. After backpressure saturation, the B-value was measured and testing proceeded if the value was over 0.96. An isotropic effective stress of 30 kPa was maintained throughout this process.

3.5.3 Consolidation and creep

The tested sand was obtained from a depth of about nine meters. The water table at this site was located at a depth of about one meter, so the in-situ effective vertical pressure was estimated to be 100 kPa. The samples were anisotropically consolidated with a K_c value of 0.6. This value was found to be close to the K_0 value since minimal radial expansion or contraction occurred during consolidation (the largest radial strain measured for any of the samples was 0.03%). The target stress state at the end of consolidation, therefore, was $\sigma'_1 = 100$ kPa, $\sigma'_3 = 60$ kPa, which gives a mean normal effective stress of 73 kPa and a deviatoric stress of 40 kPa. Because of some initial problems with instability at low effective stresses when following a direct constant stress ratio path, samples were consolidated from the initial isotropic effective stress of 30 kPa using a bilinear stress path in which the effective confining pressure was first increased to 60 kPa, and deviatoric stress was then increased to 40 kPa, as shown in Figure 3.6. Both steps were done at a rate of 1 kPa per minute. The average strain rate calculated from the total axial strain and the duration of the test stage ranged from 0.07%/hr to 0.30%/hr, varying with the initial density of the samples. The backpressure was maintained at 200 kPa throughout the consolidation and creep stages.
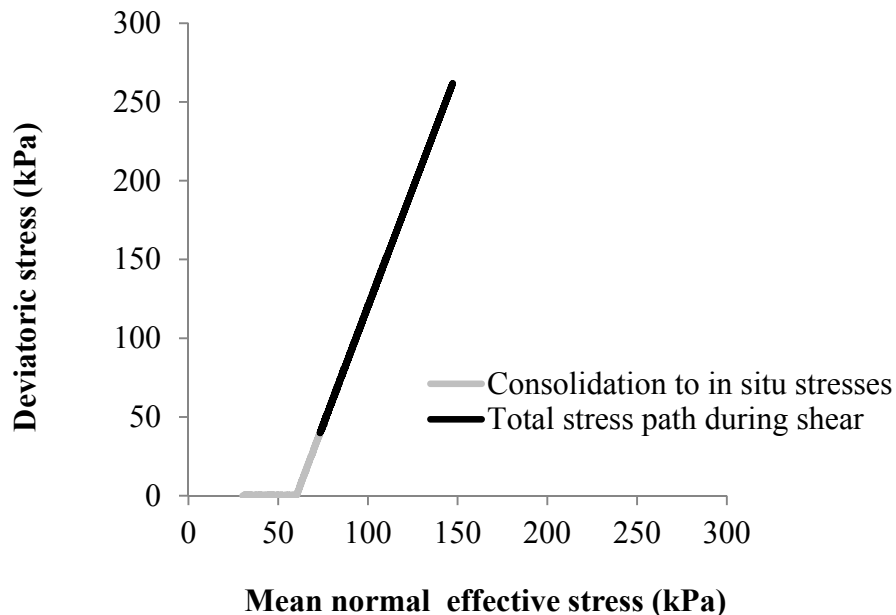
Figure 3.6 – Total stress path applied to all samples: Bilinear K_0 consolidation to p' = 73 kPa, q = 40 kPa, shear by direct triaxial compression to q = 240 kPa.

Samples were allowed to creep for one hour, at which point the axial strain rate was well below 0.01% per hour for all the specimens. The consolidated void ratio was calculated from the initial void ratio and the total axial strain measured during consolidation and creep.

3.5.4   Introducing CO_2 bubbles

To produce the gassy samples, gas bubbles were introduced after the consolidation and creep stages. The first step of this process was to replace the sample pore water with CO_2-saturated water. The valves illustrated in Figure 3.5 were opened to allow the carbonated water to flow from the top container into the sample and from the sample into the bottom container. Since the pressure in both tanks and the backpressure in the sample were all the same, the only driving force was the head difference between the top and bottom containers. A volume of carbonated water corresponding to about three times the total pore volume of the loosest samples was flushed through the sample to ensure that the pore water was completely replaced with carbonated water. This step took 30 to 45 minutes depending on the density of the sample.

After the pore water had been replaced, bubbles were created by lowering the backpressure by the increment necessary to induce exsolution of the desired amount of CO_2 gas. As described in section 3.3, the water in the CO_2 system was completely saturated with the gas at 300 kPa absolute pressure. The concentration of CO_2 in water at this point was 0.101 mol/L. The amount of CO_2 that could remain in solution was proportionate to the applied pressure after it had been adjusted, so the amount of gas could be controlled by adjusting the increment by which the backpressure was reduced. For example, reducing the applied backpressure to 260 kPa would lower the saturation concentration to

$$c = \frac{260 \text{ kPa}}{2979 \frac{\text{L} \cdot \text{kPa}}{\text{mol}}} = 0.087 \frac{\text{mol}}{\text{L}} \tag{3.4}$$

and the remaining 0.014 mol/L of CO_2 which had been dissolved in the water would come out of solution.

The theoretical degree of saturation of the different samples was calculated from the sample volume, the void ratio, and the amount of gas that should come out of solution after a given reduction in backpressure, and are listed in Table 3.1 – Gassy samples tested, backpressure after reduction and degree of saturation calculated from gas solubility. The degree of saturation as a function of final backpressure is shown in Figure 3.7.

Table 3.1 – Gassy samples tested, backpressure after reduction and degree of saturation calculated from gas solubility

Sample no.	Final backpressure	Degree of saturation
C0816	200 kPa	100 %
C0908	160 kPa	87 %
C0831	140 kPa	79 %
C0920	100 kPa	59 %
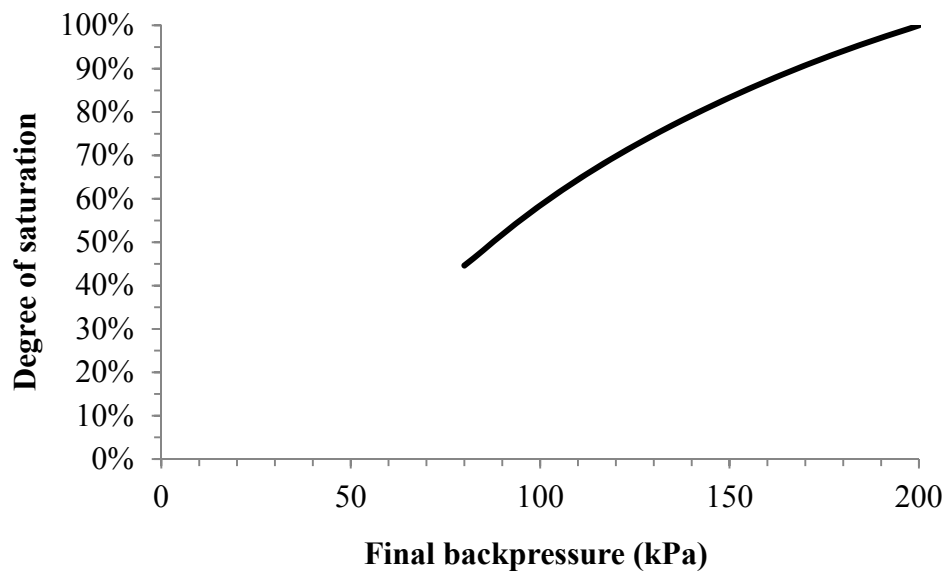
Figure 3.7 – Theoretical degree of saturation after lowering the applied pressure from an initial value of 200 kPa

After the backpressure had been reduced, the sample was allowed to rest for 30 minutes at constant effective stress with the drainage lines open for the gas/water ratio to stabilize. Gas was

observed coming out of solution in the tubes and volume control cylinders almost instantly when the pressure was lowered, and water was observed flowing out of the sample as the gas came out of solution. The water level in the volume control tubes increased rapidly at first but stabilized after about 10 minutes for all samples, indicating that near-complete exsolution occurred relatively quickly.

These additional steps of substituting carbonated water for the pore water, lowering the backpressure, and waiting for the gas to come out of solution added 60 to 90 minutes to the age of the gassy specimens compared with the fully saturated specimens which were sheared immediately after the creep stage. As the sand specimens were all about 18 hours old at the beginning of the shear stage, this additional time should not influence the soil behaviour in any way. The effective vertical and horizontal stresses were kept constant throughout this procedure, and axial and radial strains were monitored using the internal LVDTs to ensure that no excessive deformation of the sample occurred. The total axial strain measured during these stages was in the range of 0.004-0.010% for all the samples.

3.5.5   Undrained triaxial compression tests

For the undrained tests on gassy specimens, the valves were closed after this stabilization period, and the sample was sheared by increasing the deviatoric stress at a rate of 1 kPa/min until failure or 20% axial deformation took place. The average axial strain rate during the shear stage ranged from 5.2 %/hr to 10.8 %/hr. It should be noted that one "gassy" specimen (C0816) had undergone the same process of pore water replacement as the other gassy samples, but the backpressure had not been reduced, so no bubbles were present at the beginning of shear. It was sheared in undrained triaxial compression like the samples containing gas bubbles. The tests are listed in Table 3.2.

Table 3.2 – Summary of triaxial tests performed

Specimen no.	Procedure	Consolidated void	CO_2 introduced	Saturation
1007	CK_0D TXC	0.82	No	100 %
0930	CK_0D TXC	0.80	No	100 %
0328	CK_0D TXC	0.76	No	100 %
0331	CK_0D TXC	0.71	No	100 %
0405	CK_0D TXC	0.68	No	100 %
0412	CK_0D TXC	0.62	No	100 %
C0816	CK_0U TXC	0.76	Yes	100 %
C0908	CK_0U TXC	0.75	Yes	87 %
C0831	CK_0U TXC	0.76	Yes	79 %
C0920	CK_0U TXC	0.75	Yes	59 %

3.5.6   Drained triaxial compression tests

For the drained tests on fully saturated specimens, the valves remained open and the samples were sheared by increasing the deviatoric stress at a rate of 0.5 kPa/min to minimize the buildup of excess pore water pressures in the specimen. The average axial strain rate during the shearing stage ranged from 0.6 %/hr for the densest sample to 5.4%/hr for the loosest.

3.6   Data analysis

Three different sets of data were recorded in parallel for each test: The CKC system logged the basic triaxial test parameters, the GDSLAB system recorded the internal instrumentation measurements, and the GDS BES program recorded the readings from the bender elements.

The computer connected to the CKC device was used to record the cell pressure, deviatoric stress, backpressure, axial strain (measured with an external LVDT mounted on the piston), and volumetric strain based on water flow in and out of the sample at 10 second intervals throughout all test stages. These data were used to calculate the principal effective stresses and produce stress-strain plots.

The measurements from the internal load cell and LVDTs were recorded with the GDSLAB software. As described in section 3.2, these sensors measured the axial and radial deformations at the center of the specimen. These data were used to calculate more precisely the volumetric

strain of the sample, as the resolution of the LVDTs was much higher than that of the volumetric strain sensors in the CKC device. Because the specimens usually take on a barrel shape at late stages of testing, a calculation based on a radial measurement at the center of the sample would tend to overestimate the volumetric strain at these stages. However, the limited range of the LVDTs prevented this from becoming a problem, as they only recorded deformations during the initial part of the shear stage, before the barrel shape becomes prominent. Measurements from the radially mounted LVDT were also used to verify that the assumed K_0 value resulted in minimal radial strain during consolidation.

The GDS BES software was used to record the waveforms transmitted and received by the bender elements at different stages of the test. For each recorded waveform, ten to twenty individual shots were taken at 1-2 second intervals and "stacked" by the software to produce an averaged output waveform. The current (deformed) length of the specimen was calculated from the measured axial strain at the time of each test. The length of the embedded section of the bender elements was subtracted to obtain the tip to tip distance, which was recorded for use in calculating the velocity of the flexural waves. Bender element tests were performed every three to ten minutes depending on the test stage and duration.

The shear wave velocity was calculated from each averaged waveform using a procedure developed by Kim (2011) which uses a window function to eliminate noise, and compares basic peak-to-peak measurements, cross-correlation of the input and output signals, and a frequency domain analysis of the trigger and response. Whereas the peak-to-peak and cross-correlation measurements calculate the velocity directly from the time-domain waveforms, the frequency domain method evaluates the phase difference between the input and output signal in the frequency domain. This means that the resolution of the signal can be enhanced by zero-padding of the waveforms before a Fourier transform is applied to convert the signal to the frequency domain. Because of this improved resolution, the frequency domain method is more accurate than the other analysis methods. The shear wave velocities reported here were all calculated using this procedure, while the results of the peak-to-peak and cross-correlation methods were used as a check on the shear wave velocities calculated using the frequency domain method.

3.7 Summary

Triaxial tests were performed on a clean, fine, poorly graded sand. A series of fully saturated triaxial specimens of varying void ratios were consolidated to $\sigma'_1 = 100$ kPa, $\sigma'_3 = 60$ kPa, allowed to creep at a constant stress with the drainage lines open, and sheared in drained triaxial compression to establish the variation in effective friction angles with density. Another series of samples were consolidated to the same stress conditions, after which the water in the pore space was replaced with carbonated water and the backpressure was lowered to bring CO_2 gas out of solution and produce occluded bubbles throughout the specimens. These samples, all at the same void ratio but containing varying amounts of gas, were sheared in undrained triaxial compression. Shear wave velocity measurements were taken throughout all test stages for all the samples.

Chapter 4 – Experimental results

4.1 Stress-strain responses and mobilized friction angles

4.1.1 Drained triaxial compression tests on saturated specimens

A series of specimens with consolidated void ratios ranging from 0.68 to 0.83 were tested in drained triaxial compression, and are listed in Table 4.1. As described in Chapter 3, the major principal stress was increased at a rate of 0.5 kPa/min to minimize differences in pore pressure across the specimen during shearing, which gave average strain rates of 0.6%/hr to 5.4%/hr, varying with the density of the specimens. The stress-strain responses for these tests are presented in Figure 4.1. The individual test results are also shown in Appendix A.

Table 4.1 – Drained triaxial compression tests performed

Specimen no.	Consolidated void ratio	Saturation
1007	0.82	100 %
0930	0.80	100 %
0328	0.76	100 %
0331	0.71	100 %
0405	0.68	100 %
0412	0.62	100 %

The volumetric strain in each specimen was measured directly by the CKC device and calculated from the internal LVDTs. For clarity, the CKC measurements alone are plotted in Figure 4.1, and the LVDT results can be seen in the figures in the appendix. There was generally good agreement between the two measurements, except for test 1007 where the internal LVDTs indicated much larger volumetric strains than the CKC device measurements, probably due to barreling of the sample. For test 0405, because of an error in installation of the radial LVDT, radial deformation could not be measured and only the volume change measured by the CKC device is presented.
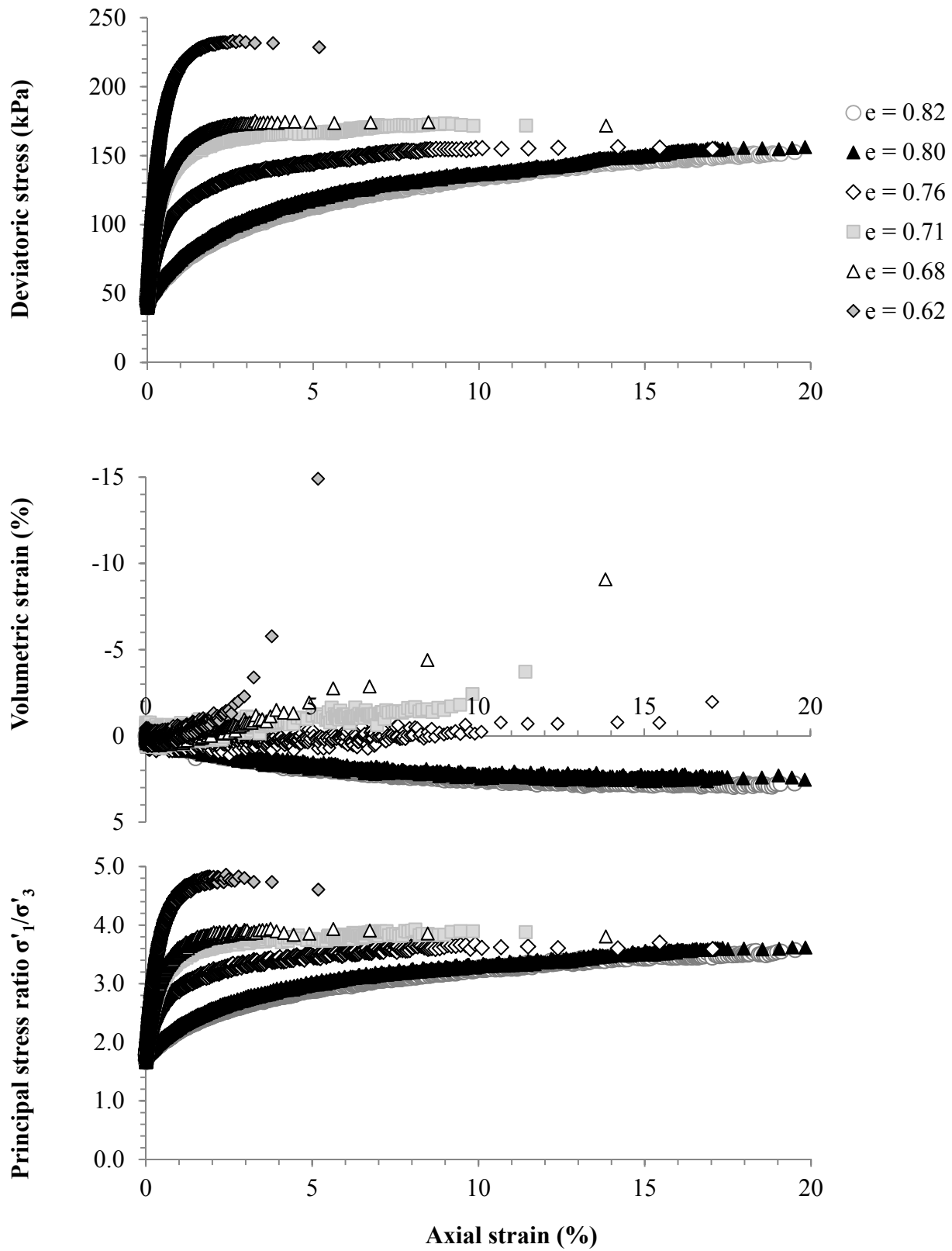
Figure 4.1 – Stress-strain results of CK$_0$D TXC tests on fully saturated specimens with varying void ratios

Figure 4.1 shows quite clearly how the soil response changed with density: At the higher initial void ratios (0.82 and 0.80) the stress-strain response was entirely contractive, with a final volumetric strain of about 3% for both samples. At consolidated void ratios of 0.76 and 0.71, the samples initially contracted but changed to dilation at about 6% and 2% axial strain, respectively. At the lowest initial void ratios (0.68 and 0.62) the response was entirely dilative and quite large volumetric strains (9% and 15%) were reached before failure. The critical void ratio, at which minimal volumetric strain would occur during shearing, seems to be about 0.75 for the effective confining stress of 60 kPa used here.

Since the sand is cohesionless, the effective friction angle is calculated directly from the peak principal stress ratio

$$\varphi' = \sin^{-1} \frac{1 - \frac{\sigma'_1}{\sigma'_3}}{1 + \frac{\sigma'_1}{\sigma'_3}} \qquad (4.1)$$

The results are summarized in Table 4.2 and plotted in Figure 4.2. The observed friction angles ranged from 34.3 degrees for the loosest sample (e = 0.82 at the beginning of shear) to 40.8 degrees for the densest (e = 0.62). As expected, the apparent effective friction angle increased with increasing density, i.e. with decreasing void ratio. The friction angle at the assumed critical void ratio of 0.75 would be about 35 degrees.

Table 4.2 – Peak friction angles from drained tests, varying void ratios

Test no.	Consolidated void ratio	Peak σ'_1/σ'_3	φ' (degrees)
1007	0.82	3.58	34.3
0930	0.80	3.61	34.5
0328	0.76	3.70	35.1
0331	0.71	3.92	36.4
0405	0.68	3.94	36.5
0412	0.62	4.76	40.8
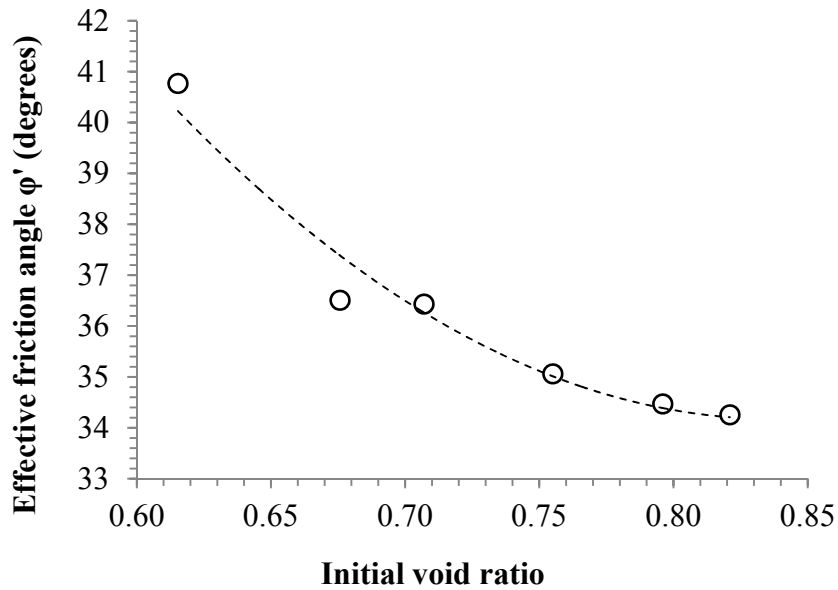
Figure 4.2 – Friction angles from drained tests

4.1.2   Gassy samples

The samples containing CO_2 gas bubbles are listed in Table 4.3. To evaluate the effect of gas on soil response, these samples were all compacted to the same density, while the level of saturation was varied from test to test. As described in Chapter 3, the gassy samples were prepared and consolidated in the same manner as the fully saturated samples, but the creep stage was prolonged to include the replacement of the pore water with CO_2-saturated water, reduction of the backpressure to bring CO_2 gas out of solution, and an additional 30-minute waiting period to ensure that pore water and pore gas pressures in the sample had time to stabilize before shearing. These samples were sheared in triaxial compression like the fully saturated samples, but with the drainage lines closed. The theoretical degrees of saturation of the samples listed in Table 4.3 were calculated based on the amount of CO_2 that could be dissolved in water at the initial and final backpressure, as described in Chapter 3.

Table 4.3 – Gassy samples tested

Test no.	Consolidated void ratio	Saturation	Procedure
C0816	0.76	100 %	CK_0U TXC
C0908	0.75	87 %	CK_0U TXC
C0831	0.76	79 %	CK_0U TXC
C0920	0.75	59 %	CK_0U TXC

The stress-strain responses of these samples during shear are shown in Figure 4.3, and individual test results are shown in Appendix B. As can be seen from the plot of pore water pressure versus axial strain, the fully saturated sample (C0816) initially developed positive excess pore water pressures of about 40 kPa which gradually dissipated during shearing. This response was consistent with the contractive-dilative behavior of the drained sample with the same void ratio (see Figure 4.1). For the other specimens, as the backpressure was reduced and more gas came out of solution, the soil response gradually changed from contractive-dilative to purely dilative, as illustrated by the pore water pressures measured during shear for C0908, C0831, and C0920. The samples with estimated degrees of saturation of 79% and 87% developed quite low positive excess pore pressures, peaking at 10 kPa and 7 kPa, respectively, while the sample with the most gas (S = 59%) developed a negative excess pore pressure of 45 kPa. The deviatoric stress plot confirms that the overall stiffness of the samples increased noticeably with the amount of gas, as the amount of stress needed to reach a given amount of axial strain increased with decreasing degree of saturation.
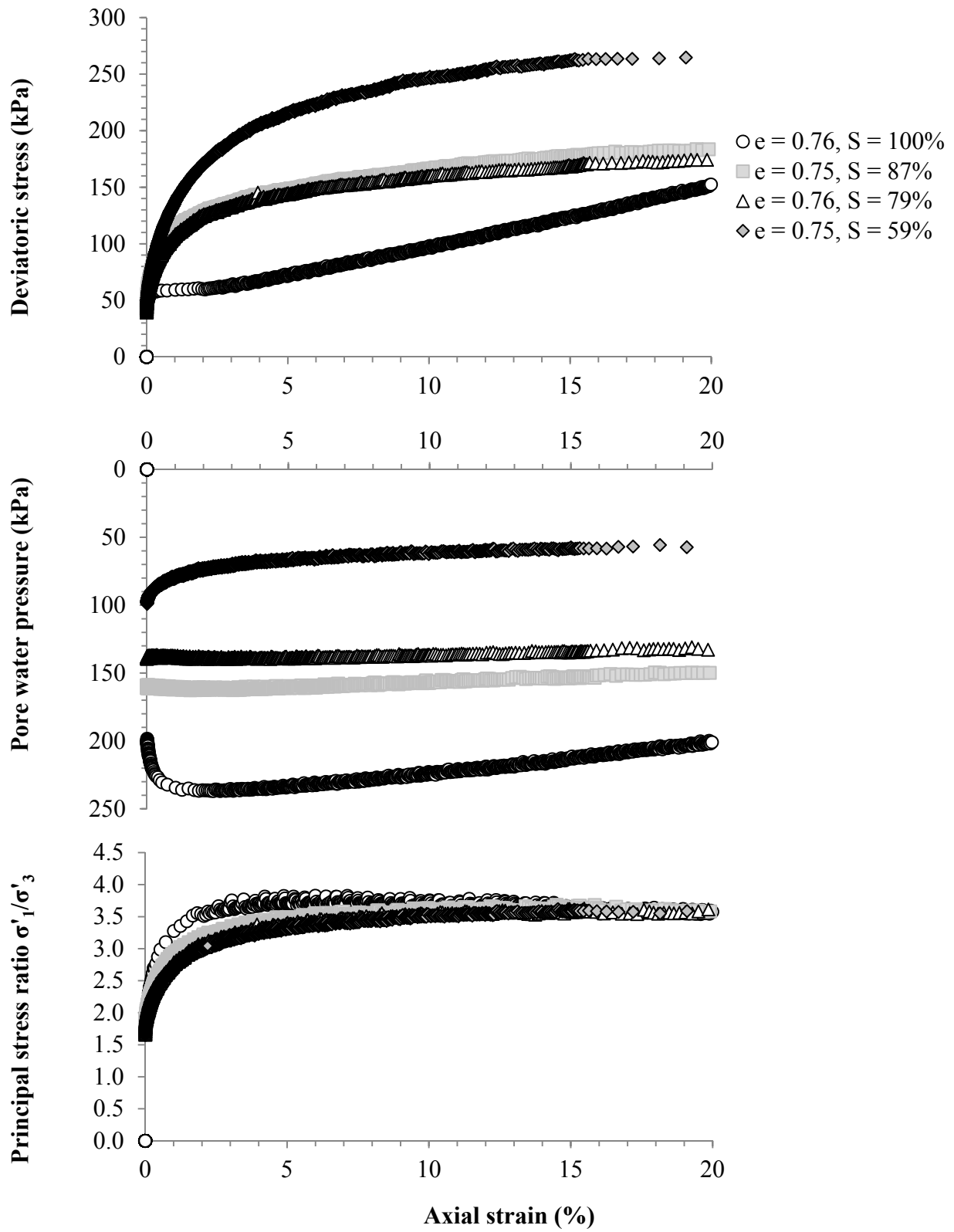
Figure 4.3 – Stress-strain results of CK$_0$U TXC tests on samples containing varying amounts of CO$_2$ gas

The effective friction angles can again be calculated directly from the peak of the principal effective stress ratios in Figure 4.3, and are shown in Table 4.4 and Figure 4.4.

The friction angle for C0816 is very close to that obtained from the CK_0D TXC test on sample 0328, which had the same initial void ratio. Sample 0328 had a friction angle of 35.1°, while C0816 had a friction angle of 35.3°. The three samples where the backpressure was reduced and gas was allowed to come out of solution had friction angles of 34.0°, 34.2°, and 34.4°. The difference in average effective friction angles of the saturated and gassy samples is shown by the two dashed lines in Figure 4.4.

Table 4.4 – Friction angles from undrained tests, varying saturation level

Test no.	Consolidated void ratio	Saturation	Peak σ'_1/σ'_3	φ' (degrees)
C0816	0.76	100 %	3.74	35.3
C0908	0.75	87 %	3.57	34.2
C0831	0.76	79 %	3.53	34.0
C0920	0.75	59 %	3.59	34.4
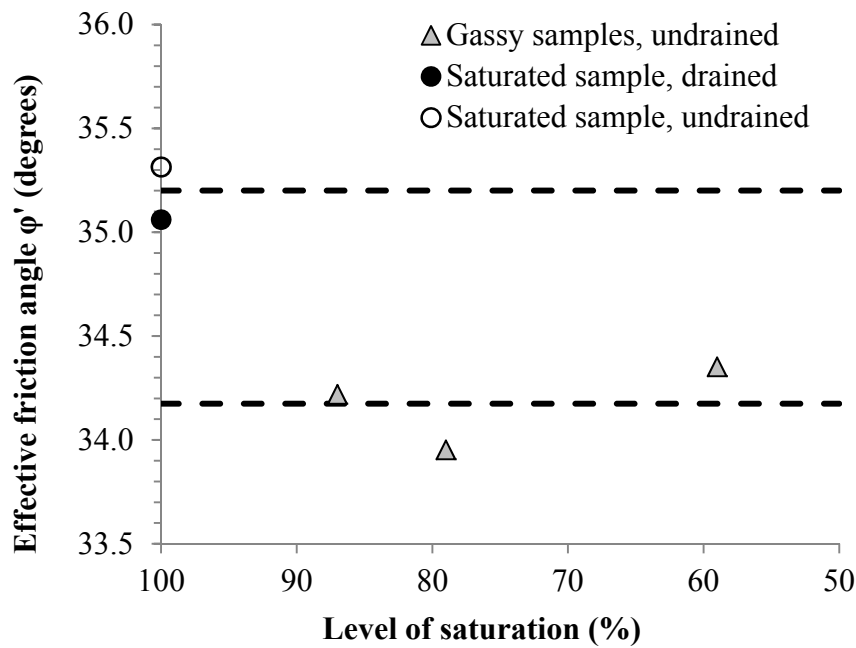
Figure 4.4 – Friction angles from undrained tests, with friction angle from drained test at same void ratio (0.75-0.76)
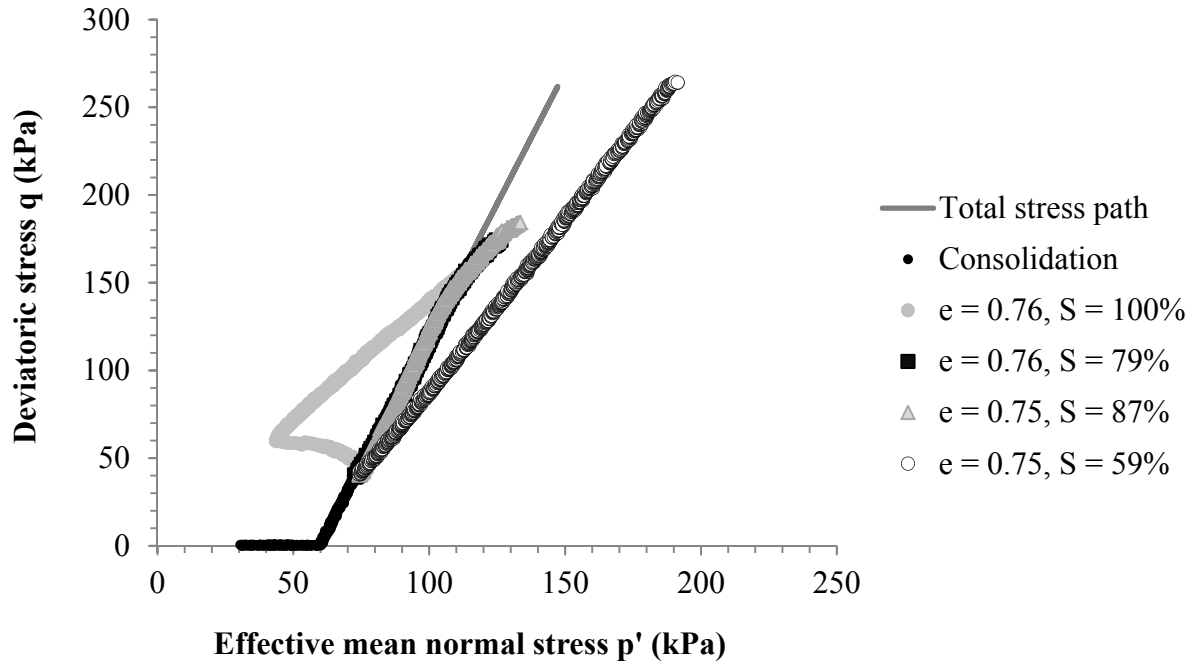
Figure 4.5 – Effective stress paths for undrained tests, and total stress path for direct triaxial compression

The effective stress paths for these four tests are shown in Figure 4.5. The differences in pore pressure development during the shear stage can be seen in the deviation of these paths from the total stress path: the sample with 100% saturation initially develops positive excess pore pressures which then dissipate; the effective stress paths for the samples at 79% and 87% saturation are almost identical to the total stress path, indicating that only very small excess pore pressures develop; and the sample with the most gas (S = 59%) develops negative excess pore pressures throughout the shear stage.

4.2　Shear wave velocity measurements

As described in Chapter 3, the velocity of vertically propagating flexural waves was measured using bender elements embedded in the pedestal and top cap attached to the soil specimens. It has been shown that the velocity of this type of flexural wave is very close to that of an in-situ shear wave at the same soil density and stress conditions (Holman and Finno, 2005). The

velocity of wave transmission was calculated from a compound image of the waveforms of the trigger signal and the received wave front using three different computational methods.

4.2.1 Effects of different methods of analysis

The three methods used to calculate the shear wave velocity were applied to all results from all samples. An example of the generated results is shown in Figure 4.6. As this figure shows, the three methods give very similar values for the shear wave velocity, with the maximum difference between any two values calculated from the same waveform less than 3 m/s for all the tests. As described in section 3.6, the frequency domain method has been found to give more precise results and less scatter than the peak-to-peak and cross-correlation measurements (Kim, 2011). Therefore, the values of shear wave velocity reported here are all calculated using the frequency domain approach.
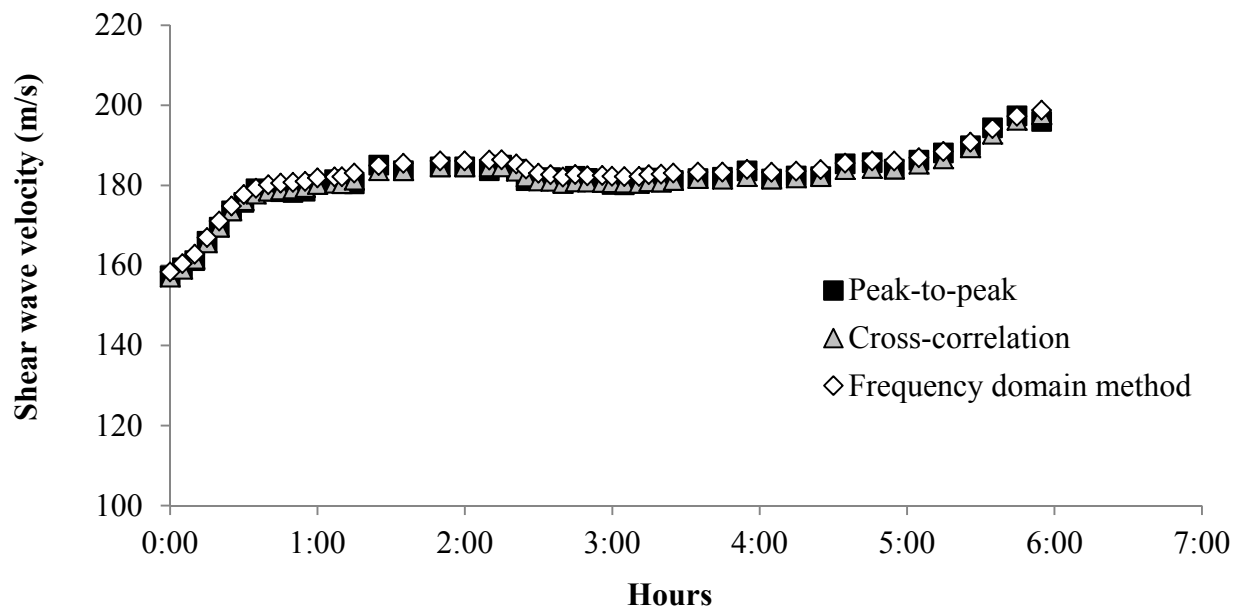
Figure 4.6 – Comparison of three analysis methods for shear wave velocity. Sample C0908, e = 0.75, S = 87%

4.2.2   Shear wave velocity in different stages of testing for fully saturated samples

Shear wave velocity measurements were taken throughout all stages of testing for all the samples. For the fully saturated samples, the different stages of testing were consolidation along a bilinear path, creep, and drained shear until failure or 20% axial strain. The changes in shear wave velocity during different stages of testing for a fully saturated sample are shown in Figure 4.7.
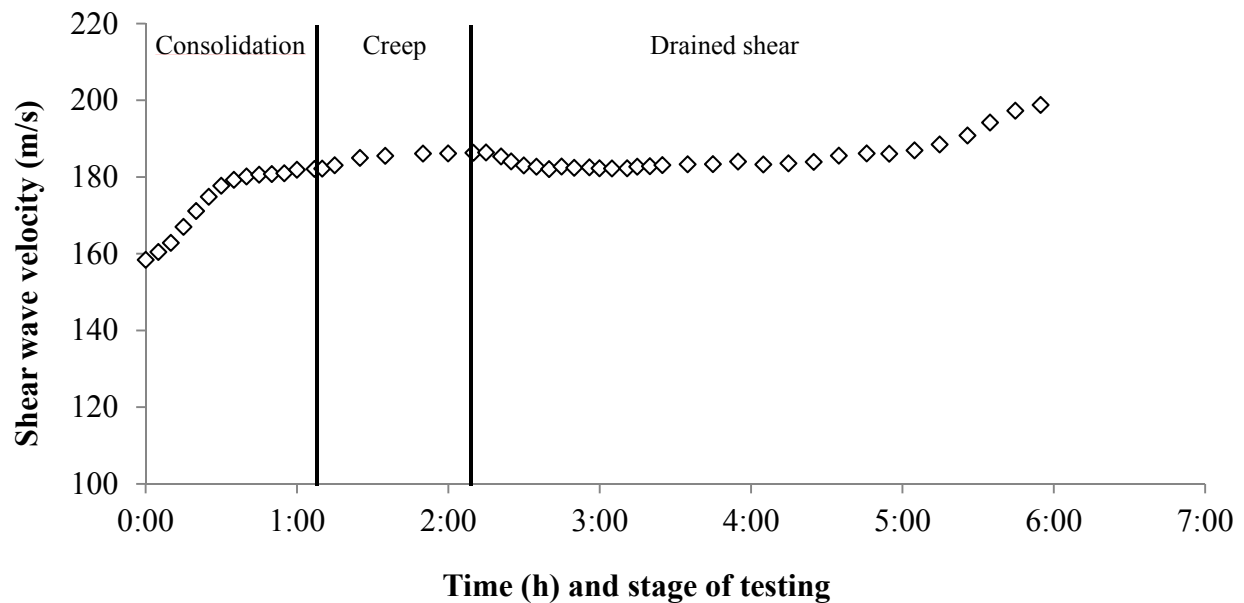
Figure 4.7 – Variation in shear wave velocity with stage of testing for sample 0930 (e = 0.80)

Shear wave velocities generally increase with increasing mean normal effective stress and increasing density (i.e. decreasing void ratio), but generally decrease with increasing shear strains (Jung et al., 2007). During drained shear, all these components change. The main trend in Figure 4.7 is the increase in shear wave velocity during stages of increasing mean normal stress and decreasing void ratio. For example, the measured shear wave velocity increases very rapidly during the first 30 minutes of the consolidation stage, when the cell pressure was increased at a rate of 1 kPa/min. During the remaining 40 minutes of consolidation, the cell pressure was held constant and only the axial load was increased, which leads to a lower rate of increase of the

mean normal stress and also a slower increase in the shear wave velocity. For this specimen, the shear wave velocity decreased somewhat during the first part of the shearing stage but then increased significantly, which is consistent with the conclusions drawn from the stress-strain response of the sample (see Figure 4.1): this specimen was relatively loose, with a void ratio at the end of consolidation of 0.80, and contracted during shearing. The increase in shear wave velocity during the shear stage is consistent with increasing density as the specimen contracts.

Figure 4.8 shows the shear wave velocity results for all the fully saturated samples. Since the shear wave velocity mostly varies with the density of the sample and the mean normal effective stress, plotting shear wave velocity versus mean normal stress rather than time makes it easier to evaluate the differences between the different samples. These specimens were all subjected to the same stress path, so the data points from p' = 30 to p' = 73 kPa were recorded during the consolidation stage, those at p' = 73 kPa during creep, and those over 73 kPa during the shear stage of the test.
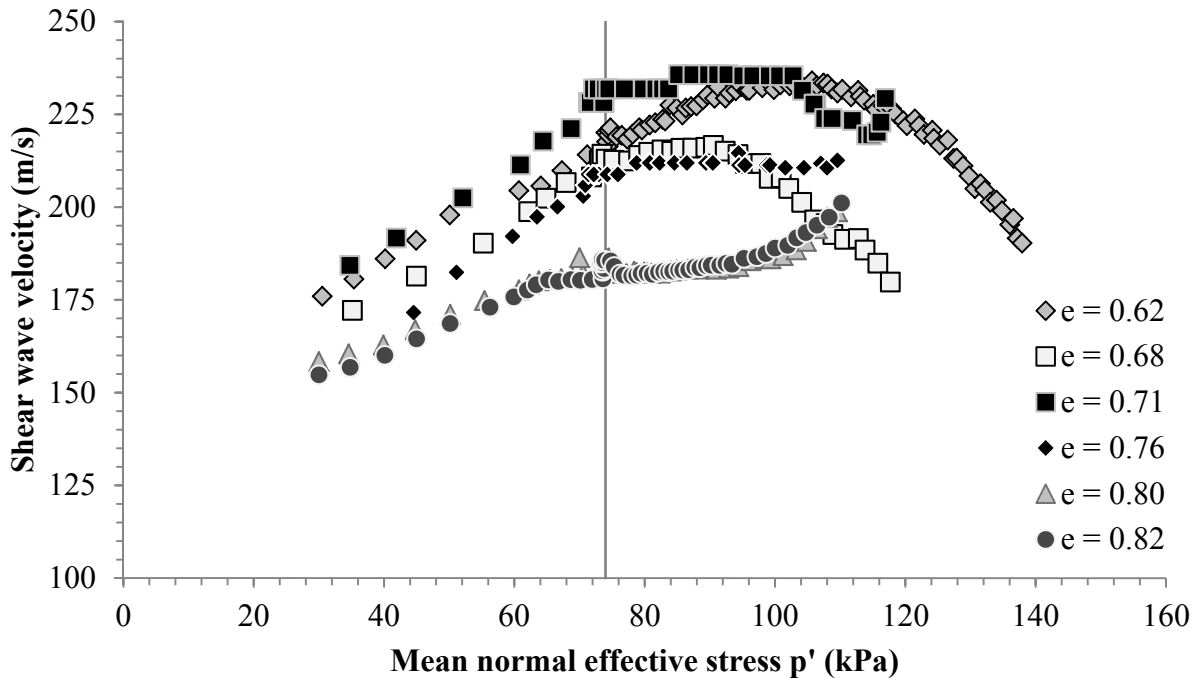
Figure 4.8 – Variation in shear wave velocity with mean normal effective stress during consolidation (p' < 73 kPa), creep (p' = 73 kPa), and drained shear (p' > 73 kPa) for fully saturated samples at varying void ratios

During the consolidation stage, the shear wave velocities measured at a given mean normal effective stress generally increase with increasing sample density (i.e. decreasing void ratio). In the looser samples, the shear wave velocity also increases throughout the shear stage as the specimens contract. The shear wave velocities measured in the denser samples during the shear stage increase at first but then decrease significantly as the samples dilate. This trend is more pronounced for the densest samples (e = 0.62 and e = 0.68) than those of medium density (e = 0.71 and e = 0.76), which is consistent with the volumetric strain results reported in section 4.1. These trends confirm that the samples loose of critical (i.e. a void ratio of about 0.75 for the confining stress used here) contract during shear, while the samples dense of critical dilate.

The trends are generally consistent except for sample 0331, which produced higher shear wave velocities during the consolidation stage than expected for its void ratio of 0.71. This might have been due to an error in the calculation of the void ratio for this sample, but its stress-strain response and friction angle are consistent with a void ratio of 0.71. The shear wave velocities measured in this sample during the shearing stage were also similar to those of the other specimens.

4.2.3 Shear wave velocity in different stages of testing for gassy samples

The shear wave velocity results recorded for a gassy sample during the different stages of testing are shown in Figure 4.9. The shear wave velocity increased during consolidation and stabilized during the creep stage, as for the fully saturated sample shown in Figure 4.7. During the period when the pore water was replaced with CO_2-saturated water, the shear wave velocity initially decreased but then increased back to the same level as at the end of the creep stage. This was probably due to an error in the adjustment of the pressure on the CO_2 system, which led to a small drop in the effective stress applied to the sample. Because the pressure in the CO_2 system was regulated based on a pressure gauge on the CO_2 canister which was not very precise, a small drop in pressure was sometimes observed when the valves were switched to override the backpressure system on the CKC device. The one shown here for specimen C0831 was the largest one observed during testing. It was assumed that the overall effect on the specimens was minimal, as the pressures were given ample time to equilibrate after the valves had been opened

and the shear wave velocity increased to the expected values when the sample was left to creep for the duration of the CO_2 water saturation stage, as indicated by the dashed line in Figure 4.9.
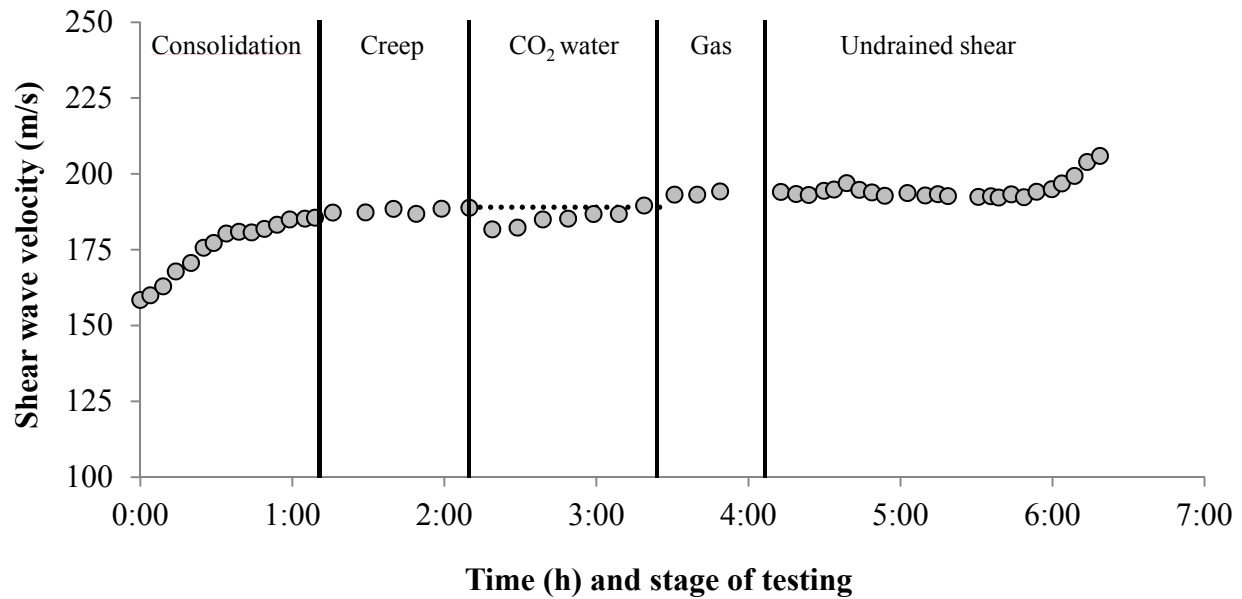

Figure 4.9 – Variation in shear wave velocity with stage of testing for sample C0831 (e = 0.76, S = 79%)

The shear wave velocity results for all four gassy samples are shown in Figure 4.10. The total stress path was the same as for the fully saturated samples, but as the gassy samples were sheared in undrained triaxial compression, the mean normal effective stress during shear was influenced by the excess pore water pressure. Figure 4.10a shows that for the consolidation and creep stages, the overall trend is the same as for the fully saturated specimens, with the shear wave velocity increasing steadily with the mean normal effective stress. As these four samples had virtually identical void ratios and the gas bubbles were not introduced until after the creep stage, the measured shear wave velocities during consolidation and creep were expected to be the same for all the samples. However, there were some differences between the samples, with a variation of 10 m/s in shear wave velocities measured at a given mean normal effective stress during the consolidation stage.
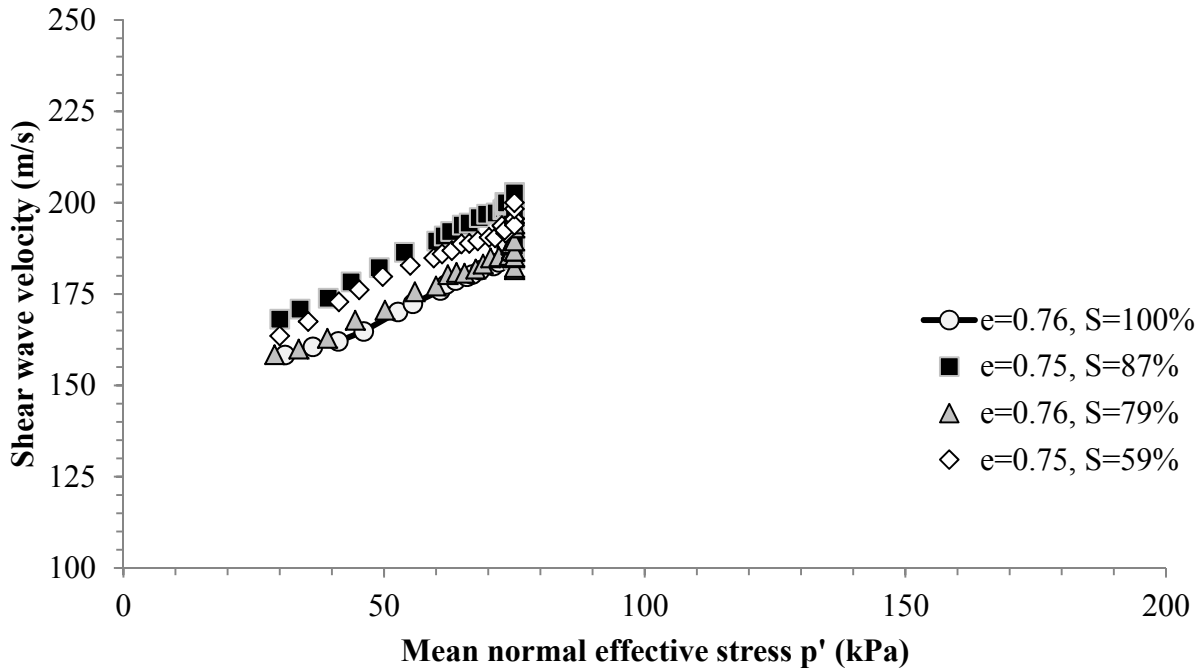
Figure 4.10a – Variation in shear wave velocity with mean normal effective stress during consolidation (p'<73 kPa), creep, pore water replacement, and gas exsolution (p'=73 kPa) for gassy saturated samples with varying degree of saturation.
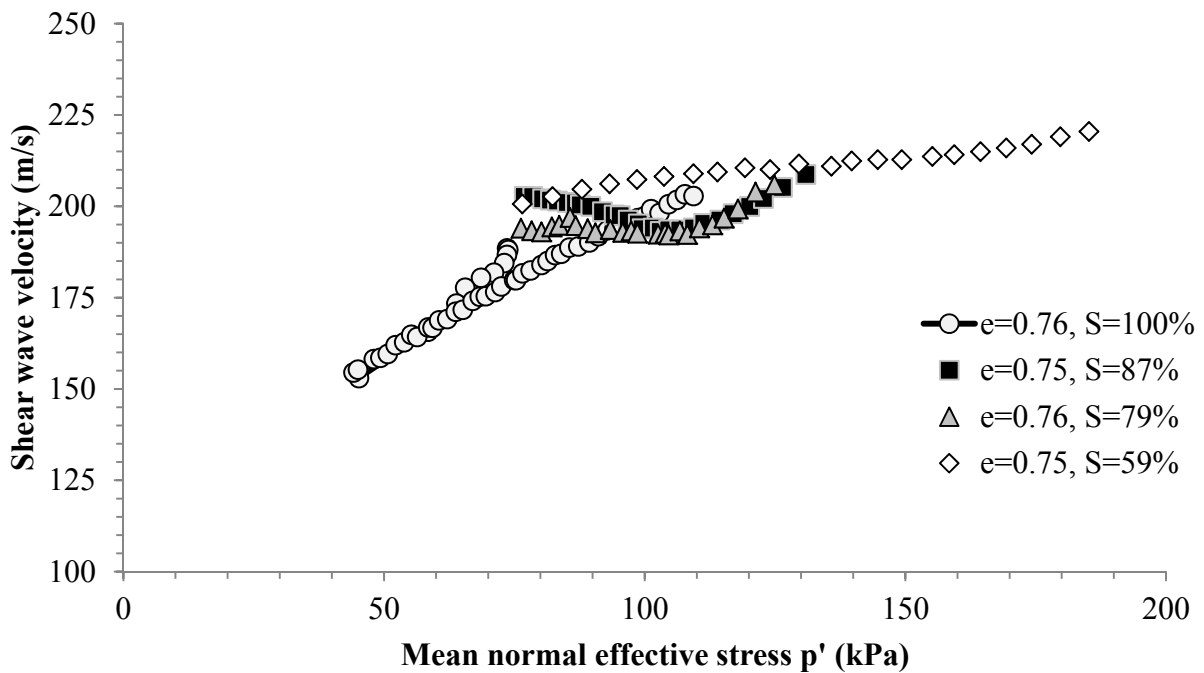
Figure 4.11b – Variation in shear wave velocity with mean normal effective stress during undrained shear for gassy saturated samples with varying degree of saturation.

As described in Section 4.2, the fully saturated sample (in which the pore water had been replaced with carbonated water, but the backpressure had not been lowered, so no CO_2 bubbles were formed before the shear stage) developed a maximum positive excess pore water pressure of about 40 kPa, which reduced the mean normal effective stress. As Figure 4.10a shows, the mean normal effective stress for this sample (e = 0.76, S = 100%) goes from 30 kPa to 73 kPa during the consolidation stage, with steadily increasing shear wave velocities. During shear, plotted in Figure 4.10b, the mean normal effective stress drops back to about 43 kPa at the beginning of the stage as positive excess pore pressures build up in the sample. As the shear stage progresses further, however, the mean normal effective stress increases again, and so does the shear wave velocity. The two specimens with theoretical saturation levels of 79% and 87% developed small positive excess pore water pressures of 10 and 7 kPa, respectively, as reported in section 4.1. The shear wave velocity in these specimens decreased during the first part of the shearing process but then increased as the mean normal effective stress passed 100 kPa. In the sample containing the most gas bubbles (S = 59%), the shear wave velocity increased steadily with the mean normal effective stress. In general, however, the shear wave velocities varied less during the shear stage than for the samples sheared under drained conditions.

4.2.4 Effect of gas exsolution on shear wave velocity

As Figure 4.12 shows, the shear wave velocity in the "gassy" samples did not change much during gas exsolution. As the two main factors that have been found to influence shear wave velocity are void ratio and mean normal effective stress, and as neither of these factors varied much during the gas exsolution stage, this result is consistent with expectations. The figure shows that there was a general trend of increasing shear wave velocity with decreasing void ratio, even though a fair amount of scatter was observed. The shear wave velocities measured for the gassy samples were all somewhat lower than that of the fully saturated sample at the same void ratio, but the variation was not much larger than the observed scatter in shear wave velocities for the fully saturated specimens.
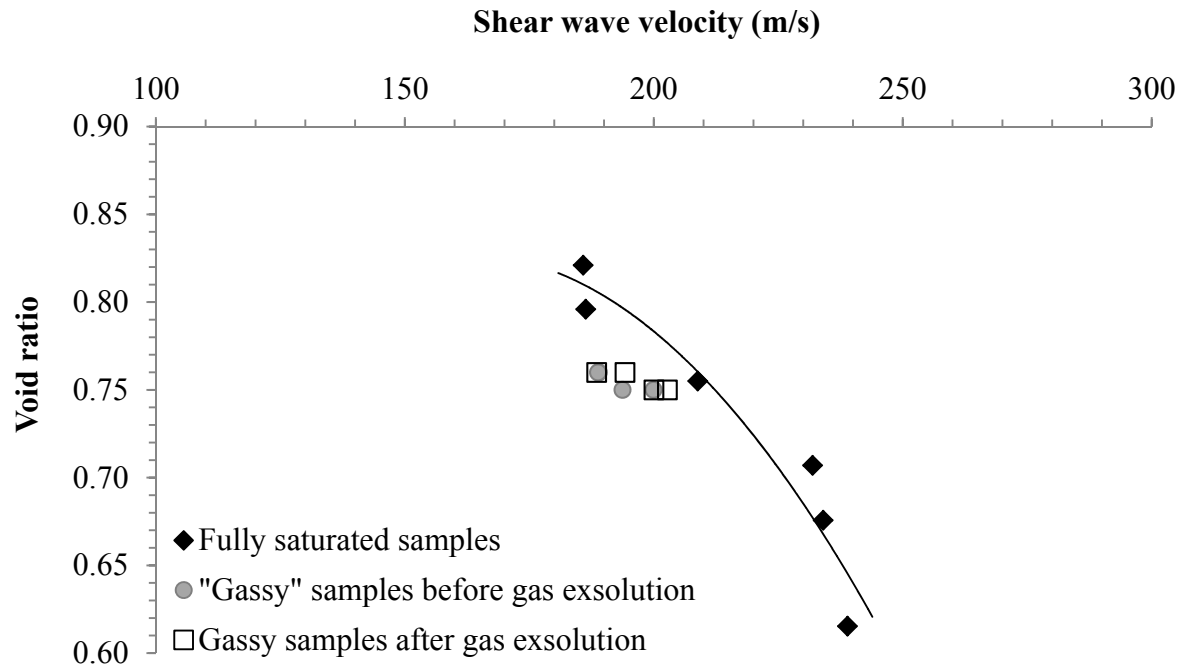
Figure 4.12 – Shear wave velocities measured in fully saturated samples at the end of the creep stage, and in "gassy" samples at the end of the creep stage (before gas exsolution) and after gas exsolution

4.3   Discussion of results

4.3.1   Evaluation of procedures and methods of analysis used

There was some concern about the validity of results obtained from specimens made of sand that had been reused for several tests. As described in Section 3.1, a grain size analysis and microscopic inspection of the sand grains was performed on a sample of sand before testing and then repeated after the sand had been used in triaxial tests several times. As no difference was found in either grain size distribution or grain shape, it was concluded that at the stress levels used here, sand samples can be reused for triaxial testing several times with no adverse effects.

The design and operation of the carbonated water system was generally successful. Circumventing the CKC device backpressure system to replace the pore water with CO_2-saturated water worked well, and the head differential between the two containers was sufficient

to drive the carbonated water through even the densest samples tested here. It did not become necessary to apply an additional pressure to the CO_2-saturated water system, so the effective stress on the sample could be held constant throughout the process of replacing the pore water, and minimal sample disturbance occurred during this step.

More detailed investigation is needed to establish the exact degree of saturation reached in the gassy samples. The actual amount of CO_2 gas that developed in the pore space after the backpressure was reduced could not be established with the equipment used here, and the degree of saturation could only be estimated using a theoretical model of the response of the gas/water mixture to changes in the applied pressure. This model for the kinetics of gas dissolution is well established, but an approach where the levels of saturation could be confirmed experimentally would be very valuable in confirming the model predictions used here. It also seems reasonable to assume that gas dissolution and/or exsolution takes place during shear, in response to changing pore water pressures. For example, in sample C0920, where the pore water pressures decreased by 45 kPa during shear, more most likely came out of solution during the shearing process. Therefore, repeating these tests with more advanced equipment would also be useful to track the amount of gas present in the sample at any given time.

Although the exact amounts of gas produced in each sample could not be confirmed experimentally, observation of the samples confirmed the general trend in decreasing degree of saturation with increasing drop in backpressure. For the fully saturated sample (C0816) no gas bubbles were observed. For samples C0908 and C0831 (with theoretical degrees of saturation of 87% and 79%) a small amount of bubbles could be seen in the drainage lines as the backpressure was lowered. For the sample with the largest drop in backpressure (C0930, S = 59%) a large amount of gas was observed coming out of solution very rapidly, and when disassembled after failure the sand in this specimen was noticeably drier than in the others. These observations, when combined with the noticeable difference in the measured stress-strain responses of the gassy samples, clearly prove that even though the exact degree of saturation could not be confirmed experimentally, enough gas was present in the samples to make a significant difference in the soil behavior.

4.3.2 Triaxial test results and the effect of gas on soil response

The fully saturated samples tested here, which ranged in void ratio from 0.62 to 0.82, exhibited responses in drained shear ranging from complete contraction to pure dilation. The change was gradual with changes in void ratio, and the behavior closest to constant volume in shear was observed for the sample at void ratio 0.76. The effective friction angles increased proportionally with increasing density.

The presence of gas in the soil lowered the effective friction angle for samples with void ratios of 0.75 to 0.76 by 1.0 to 1.5 degrees compared to other specimens at the same void ratio. These friction angle values were approximately equal to those found in drained tests on samples with a consolidated void ratio of 0.80 or 0.82. This decrease in effective friction angle may explain why CPT measurements in sands that have been densified using blast densification are often lower than initial measurements even though observations of surface settlement confirm that the soil has indeed been densified. As a CPT cone is advanced, the soil below it essentially undergoes a bearing capacity failure, and the bearing capacity is a direct function of the effective friction angle. Therefore, if a sand stratum containing gas bubbles has a lower effective friction angle than before the gasses were introduced, its bearing capacity decreases and the CPT reading will be lower than what would be expected based solely on density considerations.

The presence of gas in specimens with void ratio of 0.75 also changed the soil response from contractive to dilative. While fully saturated samples at this void ratio contracted in drained shear and developed positive excess pore pressures of 40 kPa in undrained shear, the samples containing CO_2 bubbles developed very low or negative excess pore pressures in undrained shear. Note that the presence of a very compressible gas in the void space allows volume change to occur in a globally undrained test. The sample containing the most gas had a pronounced dilative response, indicating that the amount of dilative behavior may be proportional amounts of gas in the sample. The introduction of gas bubbles in the soil, therefore, may be a beneficial if unintended consequence of blast densification. One of the common goals of densifying saturated sand strata is to reduce their susceptibility to earthquake-induced liquefaction. If the presence of gas bubbles makes the sand more dilative in shear, it will be less likely to liquefy in the event of an earthquake. The magnitude of this effect may not be significant compared to the established

effect of lowering the void ratio, however. More detailed testing is needed to evaluate the effects of gas on the cyclic resistance of blast-densified sand.

4.3.3   Shear wave velocity results

The shear wave velocities recorded for samples at the same void ratio and same applied stresses varied more than is usually found, so no detailed conclusions can be drawn from these data. However, some observations can still be made. For a given sample, the shear wave velocities clearly increased with increasing mean normal effective stress and increasing density, which is consistent with theory and previous research.

Analyzing shear wave velocities in this manner confirmed that the gassy soil samples had a more dilative response than fully saturated samples at the same void ratio. The gradual change from a contractive response (S = 100%) via a contractive-dilative response (S = 87% and S = 79%) to a purely dilative response (S = 59%) was also confirmed by the trends in shear wave velocity measurements. Based on Figure 4.11, the presence of gas bubbles seems to lower the shear wave velocity somewhat compared to fully saturated samples at the same void ratio and mean normal effective stress. Further research is needed on this topic.

4.4   Summary

The saturated samples tested in drained triaxial compression spanned the range of responses from wholly contractive at void ratios of 0.82 and 0.80, via a contractive-dilative response at intermediate void ratios (0.71 and 0.76) to dilative for the densest samples (0.62 and 0.68). The observations made based on stress-strain responses were corroborated by the shear wave velocity measurements during the shear stage, which increased for the looser samples but decreased for the denser ones, indicating contraction and dilation, respectively. Based on these trends, the critical void ratio for this sand at an effective confining pressure of 60 kPa seems to be about 0.75. For saturated samples, the friction angles increased steadily with decreasing void ratios, varying from 34.3 to 40.8 degrees. The critical state friction angle would be about 35 degrees.

The shear wave velocities also generally increased with increasing density. The presence of CO_2 bubbles changed the response of specimens of medium density from contractive-dilative to dilative, with specimens containing more gas exhibiting a more fully dilative response. The friction angle decreased from 35.3 and 35.1 degrees for saturated samples at void ratios of 0.75 and 0.76 to 34.0 to 34.4 degrees for specimens at the same void ratio with gas bubbles present. The presence of gas did not have a noticeable effect on the measured shear wave velocities.

Chapter 5 – Conclusions

The objective of this study was to develop an experimental procedure for preparing and testing sand samples containing occluded bubbles of CO_2 gas, and to perform some preliminary triaxial tests on these samples. These objectives were achieved and several key differences between fully saturated samples and samples containing CO_2 gas bubbles were observed. Although further research is clearly needed to examine the soil response in more detail, a number of conclusions can be drawn about the procedures developed here and the trends observed in the experimental results:

1. At the stress levels used here, this type of sand can be dried and reused for triaxial tests several times without affecting the results.

2. The CO_2 saturation system and procedures were generally successful. A two-meter head differential was sufficient to replace the sample pore water with carbonated water.

3. The effective friction angles of gassy samples were lower than those of saturated specimens at the same void ratio.

4. When tested in drained shear at a mean normal effective stress of 70-200 kPa, the response of this sand changed from contractive to dilative at a void ratio of about 0.75.The introduction of gas bubbles changed the soil response at this void ratio from contractive to contractive-dilative or purely dilative, varying with the amount of gas present in the specimen.

5. Globally undrained tests on gassy soils are not really undrained, as the compressibility of the gas bubbles allows the sample volume to change even though the drainage lines are closed. Future studies should include equipment to measure the sample volume during "undrained" shear of gassy samples.

Further research is needed to confirm experimentally the results of the analytical method used here to estimate the amount of gas produced in the specimens when the backpressure was reduced. However, even though the exact degree of saturation could not be established

experimentally, significant amounts of gas were observed, confirming the theoretical model of gas exsolution.

Because the degree of saturation is likely to change as gas dissolves into or precipitates out of the saturated pore water in response to changes in pore pressure, future studies should track the volume of gas present in the sample at different points during shear. The pressures in the pore water and in the pore gas should also be measured separately, as they are not necessarily the same if gas exsolution is taking place during shear. Measuring these pressures separately would also give a better estimate of the mean normal effective stress in gassy samples.

References

Cho, W. J., "Recent Stress History Effects on Compressible Chicago Glacial Clay" Dissertation, Northwestern University, June 2007.

Dowding, C. H. and Hryciw, R. D. "A Laboratory Study of Blast Densification of Saturated Sand" *J. Geotech. Eng.* 112, 187, 1986.

Gassman, S., "Undrained Steady State Shear Strength and Instabilities of Fine Sands," MS thesis, Northwestern University, June 1994.

Grozic, J.L., Robertson, P.K., Morgenstern, N.R.. "The behavior of loose gassy sand". *Can. Geotech. J.* 36: 482-492. 1999.

Hardin, B. O., and Richart, F. E.. "Elastic wave velocities in granular soils". *Journal of the Soil Mechanics and Foundations Division, Proceedings of the ASCE*, Vol. 89, No. SM1, February, 1963.

Holman, T., "Small strain behavior of compressible Chicago glacial clay," Dissertation, Northwestern University, June 2005.

Holman, T., and Finno, R.J., "Maximum shear modulus and incrementally nonlinear soils," Proceedings, 16th International Conference on Soil Mechanics and Geotechnical Engineering," Osaka, Japan. Vol. 2, 383-387, 2005.

Hryciw, R. D. "A study of the physical and chemical aspects of blast densification of sand". Dissertation, Northwestern University, 1986.

Jung, Y.-H., Cho, W. and Finno, R.J., "Defining Yielding from Bender Element Measurements in Triaxial Stress Probe Experiments." *J. Geotech. Geoenv. Eng.*, ASCE, Vol. 133, No. 7, 841-849, July 2007.

Kim, T., "Incrementally Nonlinear Responses of Soft Chicago Glacial Clays." Dissertation, Northwestern University, 2011

Kramer, S. L., *Geotechnical Earthquake Engineering*. Prentice Hall, New Jersey, 1996.

Kulhawy, F. H., and Mayne, P. W., *Manual on estimating soil properties for foundation design.* Cornell Univ., Ithaca, NY, 1990.

Mitchell, J. K., and Solymar, Z. V., "Time-Dependent Strength Gain in Freshly Deposited or Densified Sand," *Journal of Geotechnical Engineering,* ASCE, Vol.110, No. 11, pp. 1559-1576, November 1984.

Narin van Court, W. A., and Mitchell, J.K., "Soil improvement by blasting". *Journal of explosives engineering,* vol. 12, issue 3, 34-41, 1994.

Narsilio, G. A., Santamarina, J. C., Hebeler, T., and Bachus, R. , "Blast densification: multi-instrumented case history." *J. Geotech. Geoenviron. Eng.*, 135(6), 723-734, 2009.

Okamura, M., Ishihara, M., and Tamura, K., "Degree of saturation and liquefaction resistances of sand improved with sand compaction pile." *J. Geotech. Geoenviron. Eng.*, 132(2), 258-264, 2006.

Schaefer, V. R. (editor), *Ground Improvement/Ground Reinforcement/Ground Treatment Developments 1987-1997. Proceedings of sessions sponsored by the Committee on Soil Improvement and Geosynthetics of the Geo-Institute of the ASCE in conjunction with Geo-Logan '97. Logan, Utah, July 17-19, 1997*. Geotechnical Special Publication No. 69. Published by the ASCE, NY, 1997.

Shindo, Y., Fujioka, Y., Takeuchi, K., Komiyama, H., "Kinetics on the Dissolution of CO_2 into Water from the Surface of CO_2 Hydrate at High Pressure." *International Journal of Chemical Kinetics* Vol 27, Number 6, 1995.

Stumm, W, and Morgan, J. J., *Aquatic Chemistry – Chemical Equilibria and Rates in Natural Waters.* John Wiley and Sons, New York, New York. Third edition, 1996.

Terzaghi, K., *Theoretical soil mechanics*. John Wiley, 1943.

Wheeler, S. J., "The stress-strain behaviour of soils containing gas bubbles". Dissertation, University of Oxford, 1986.

Wheeler, S. J., "The undrained shear strength of soils containing large gas bubbles" *Géotechnique* 38, No. 3, 399-413, 1988

Appendix A - Stress-strain results from drained triaxial compression tests on saturated specimens
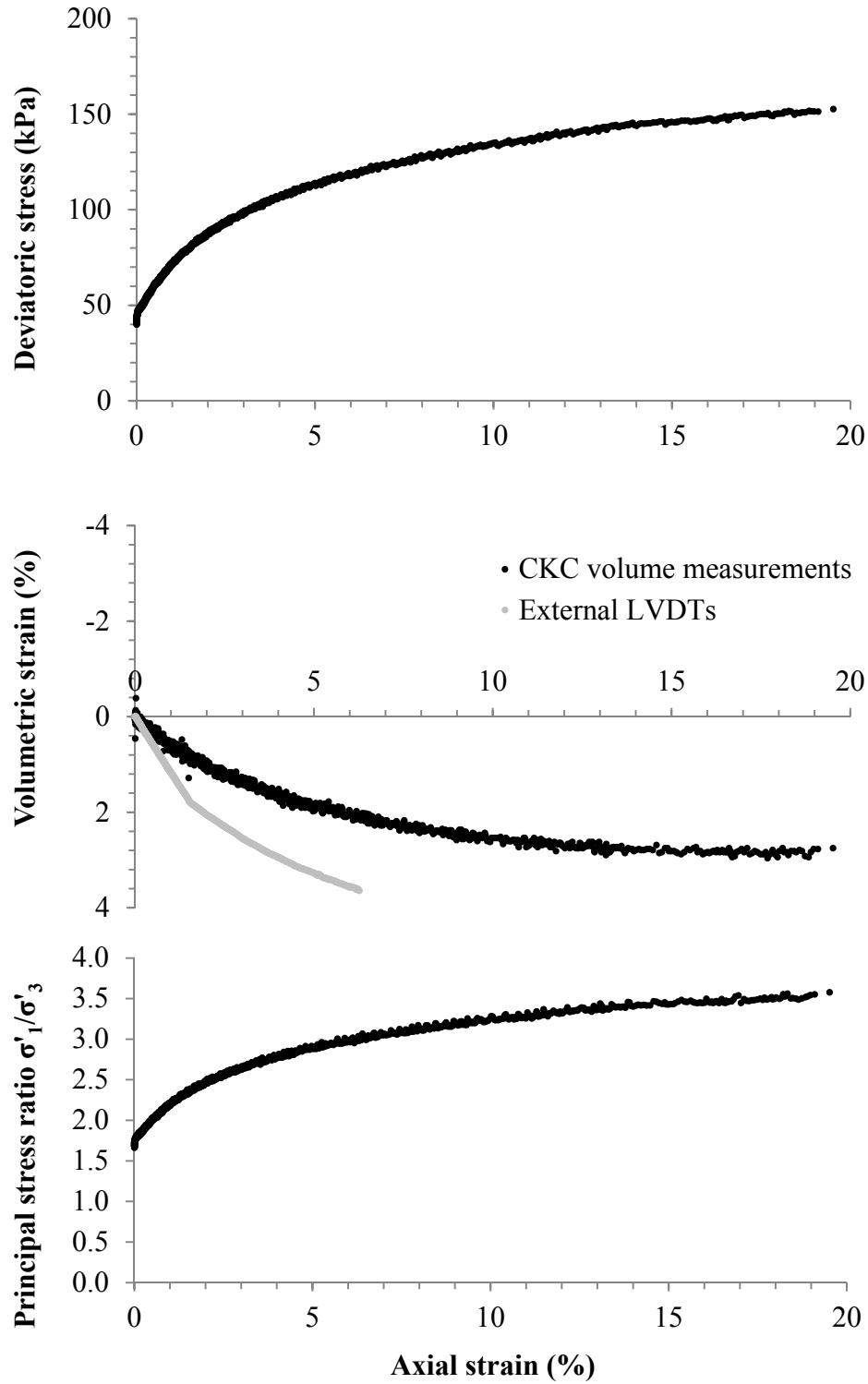
Figure A.1 – CK$_0$D TXC test no. 1007: e = 0.82, S = 100%
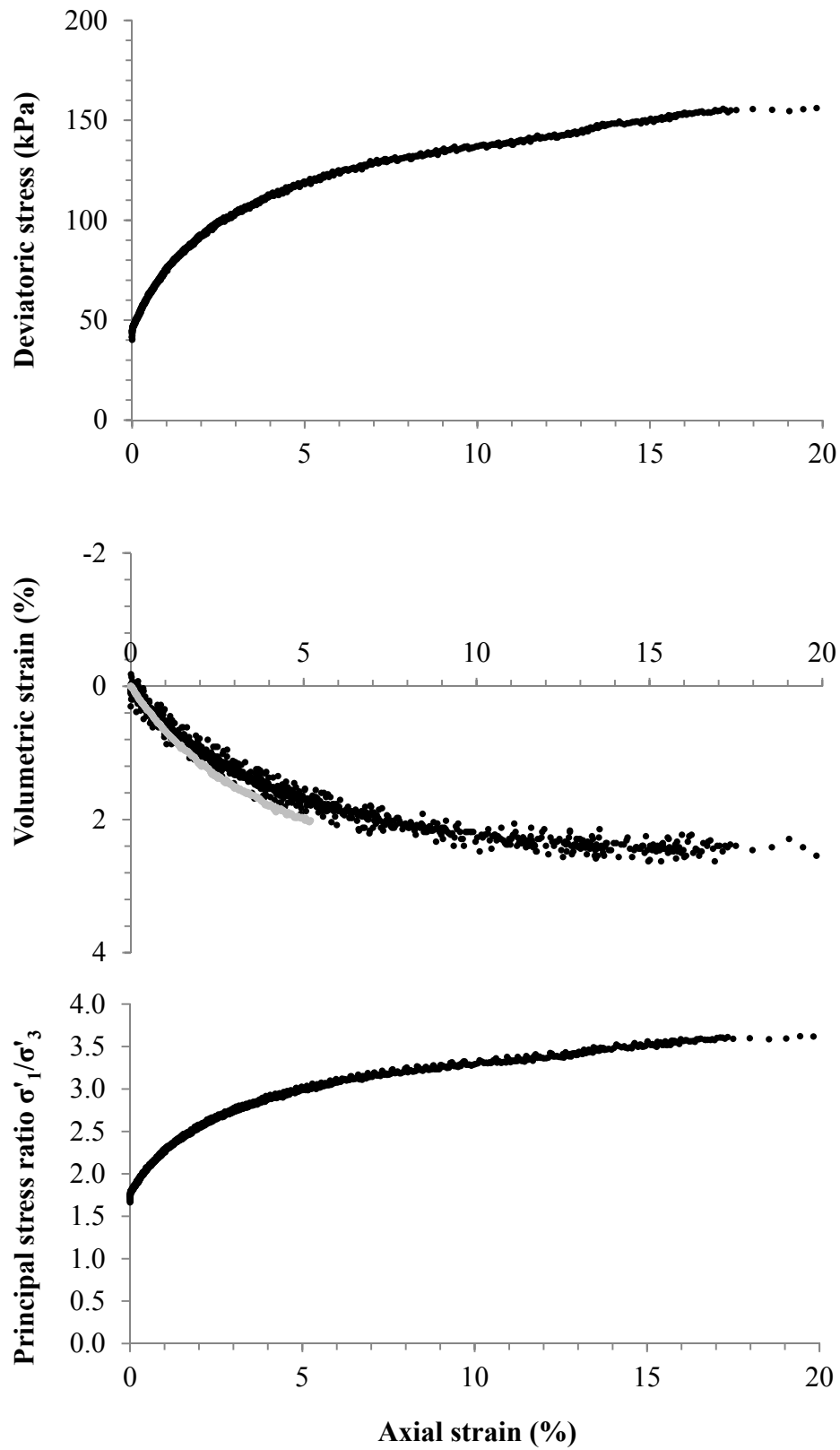
Figure A.2 – CK$_0$D TXC test no. 0930: e = 0.79, S = 100%
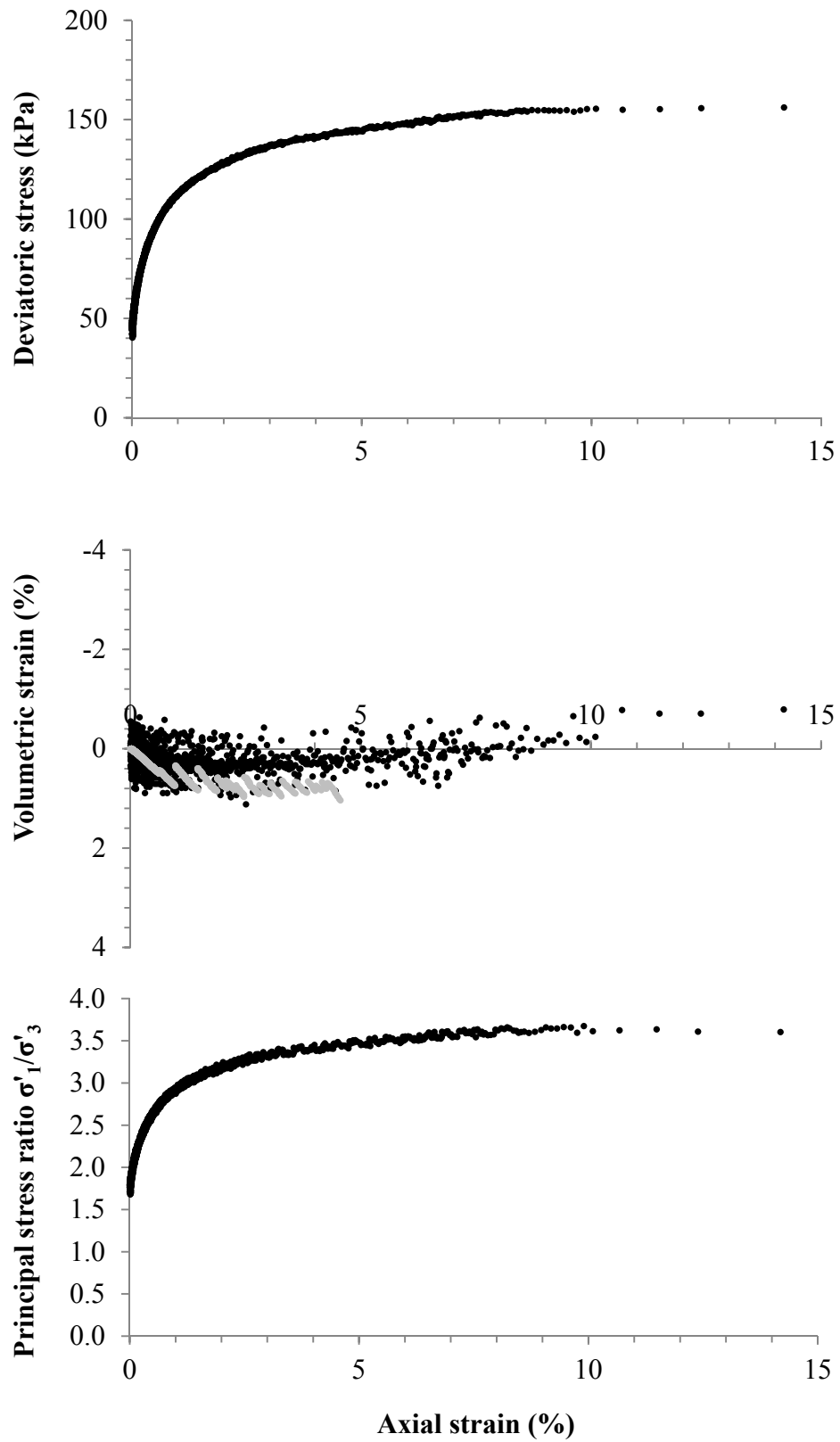
Figure A.3 – CK$_0$D TXC test no. 0328: e = 0.76, S = 100%
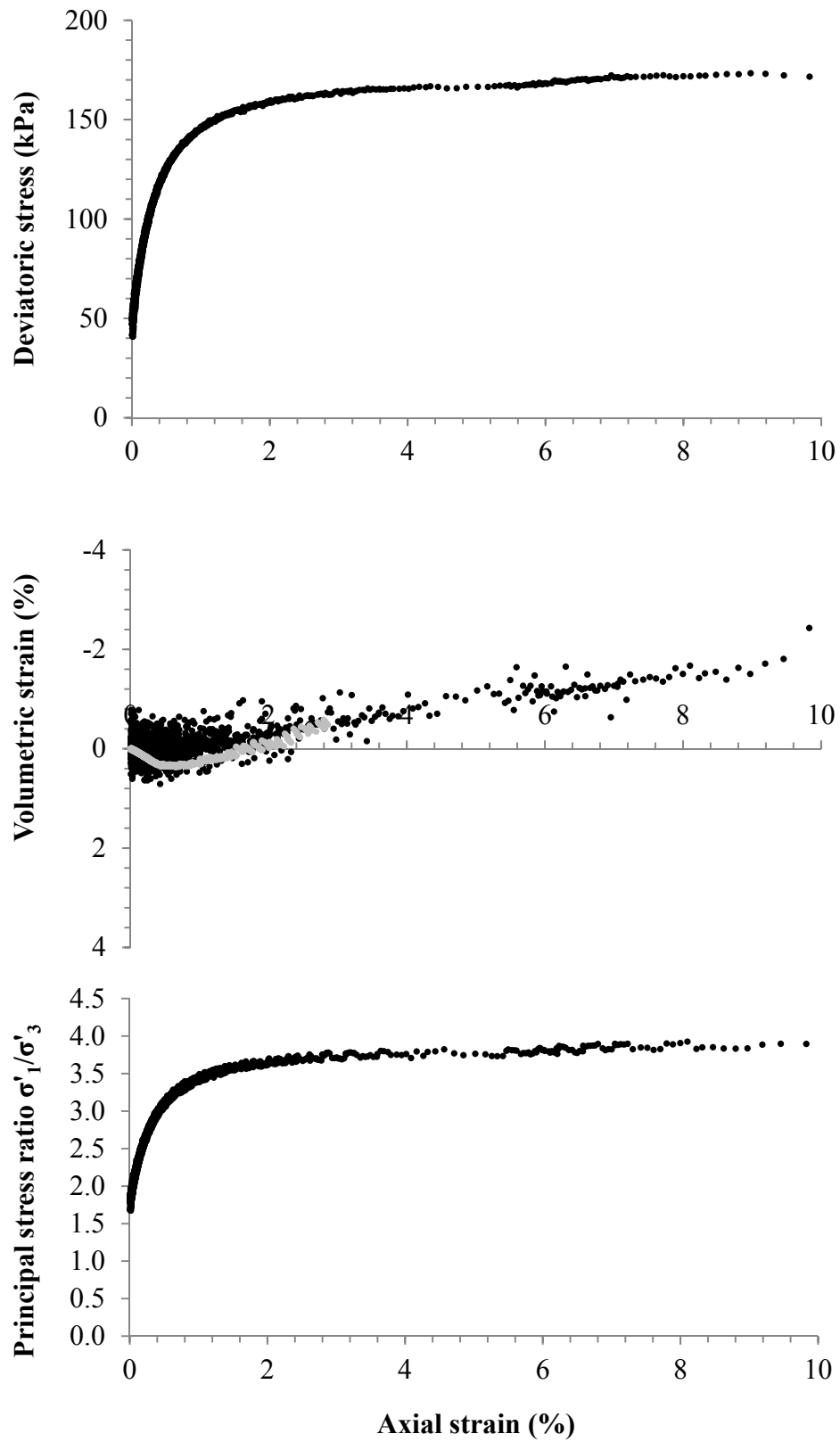
Figure A.4 − CK$_0$D TXC test no. 0331, e = 0.71, S = 100%
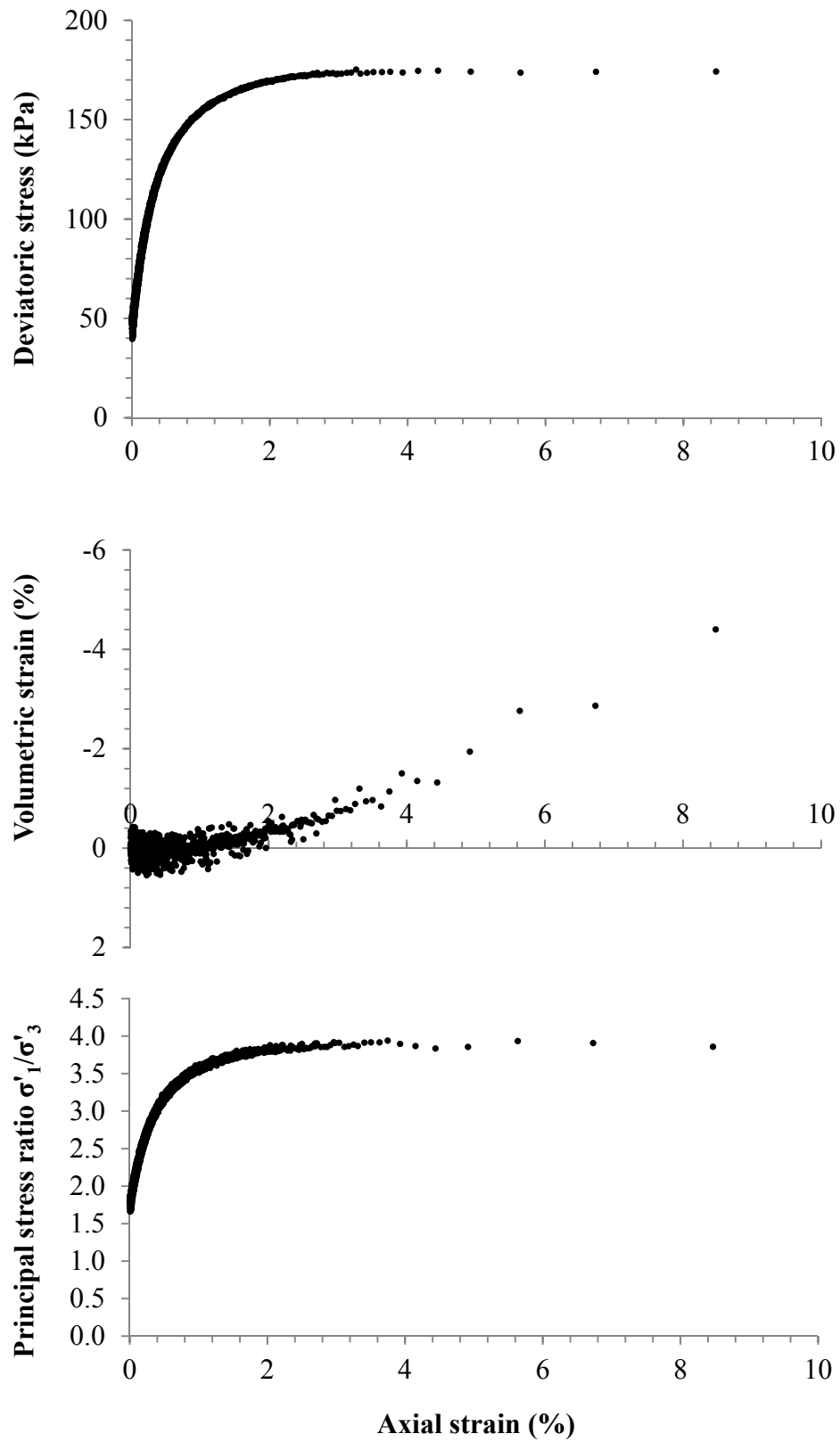
Figure A.5 – CK$_0$D TXC test no. 0405: e = 0.68, S = 100%
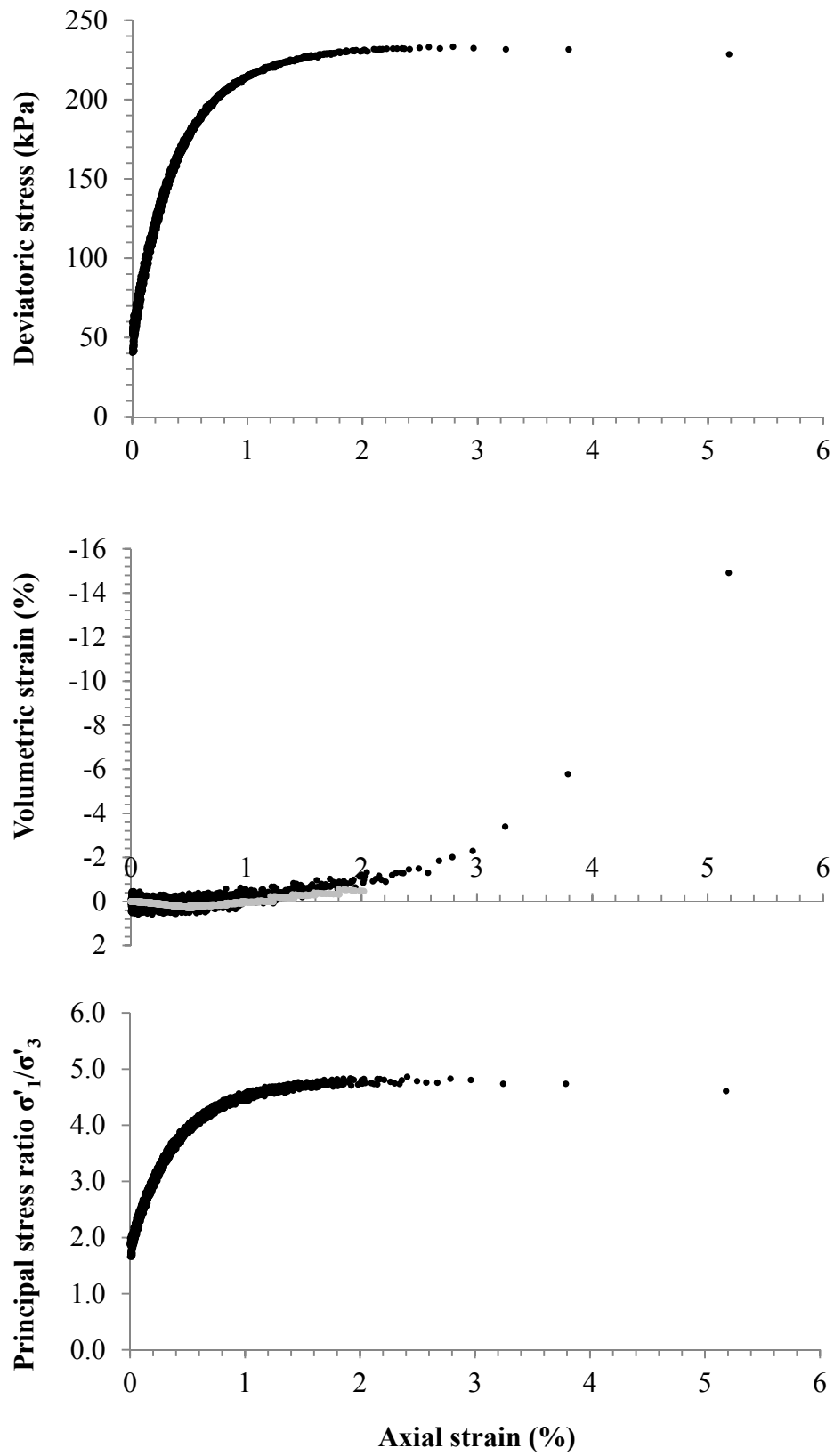
Figure A.6 – CK₀D TXC test no. 0412: e = 0.62, S = 100%

Appendix B - Stress-strain results from undrained triaxial compression tests on gassy specimens
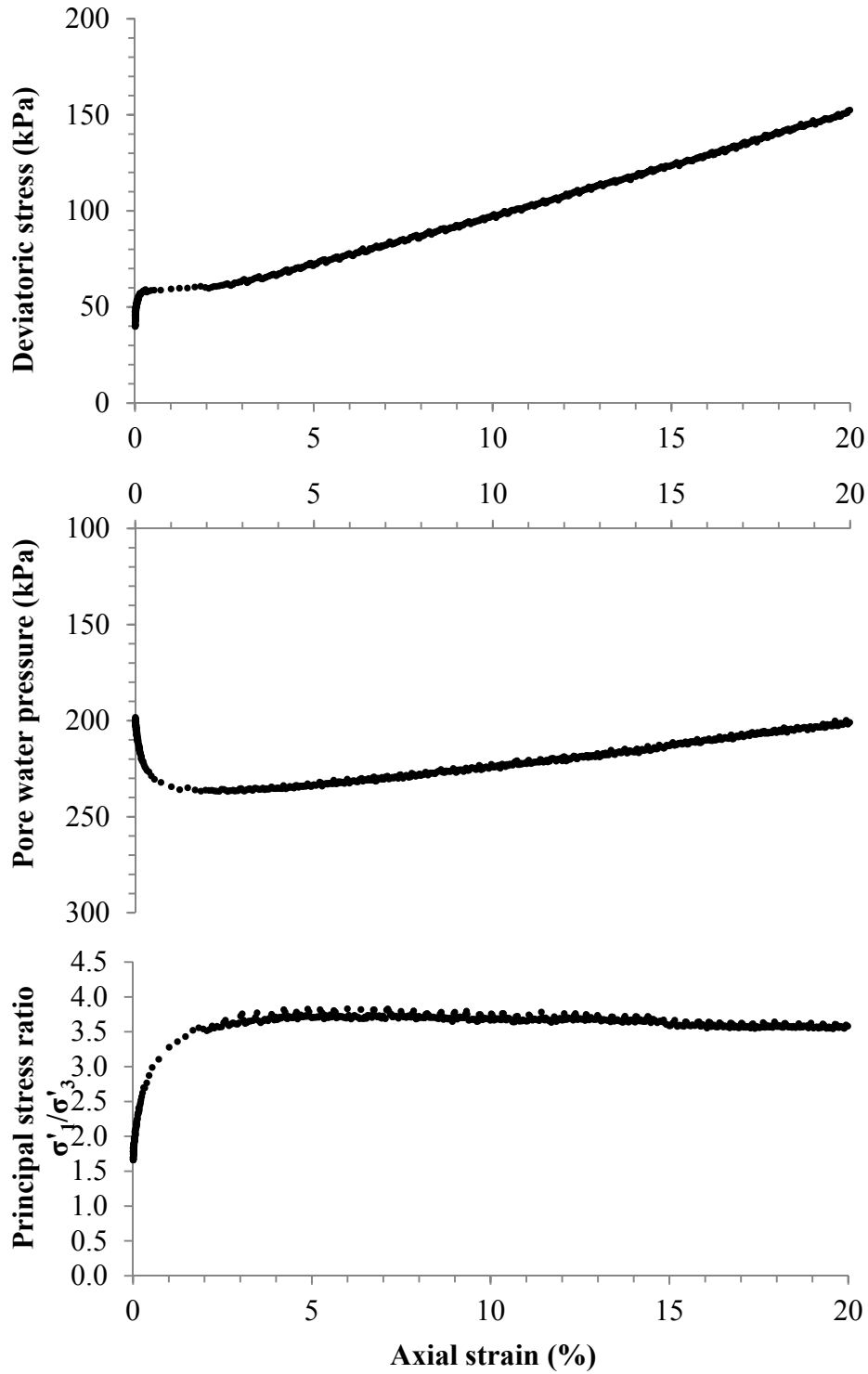
Figure B.1 – CK$_0$U TXC test no. C0816: e = 0.76, S = 100%
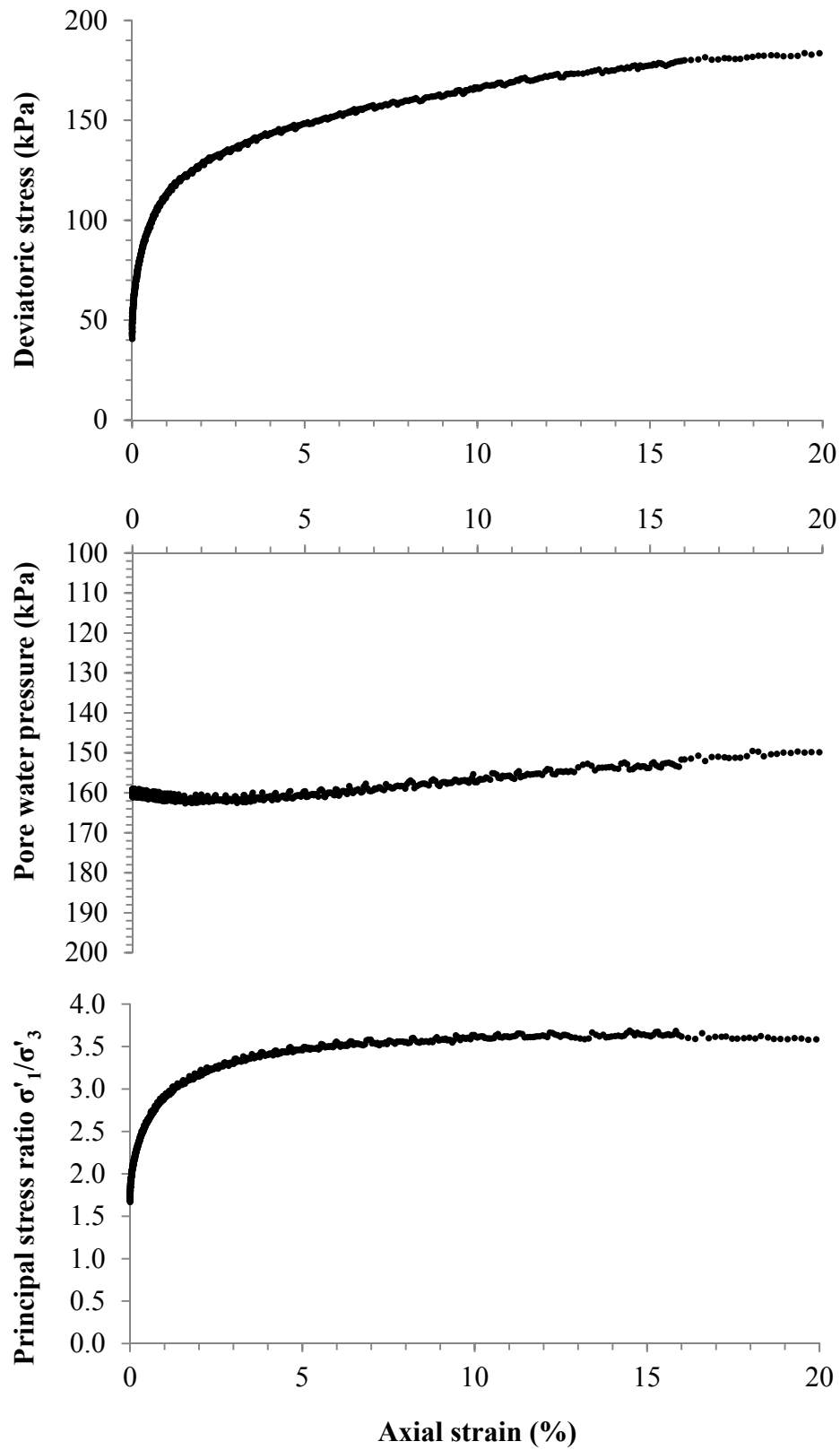
Figure B.2 – CK$_0$U TXC test no. C0908: e = 0.75, S = 87%
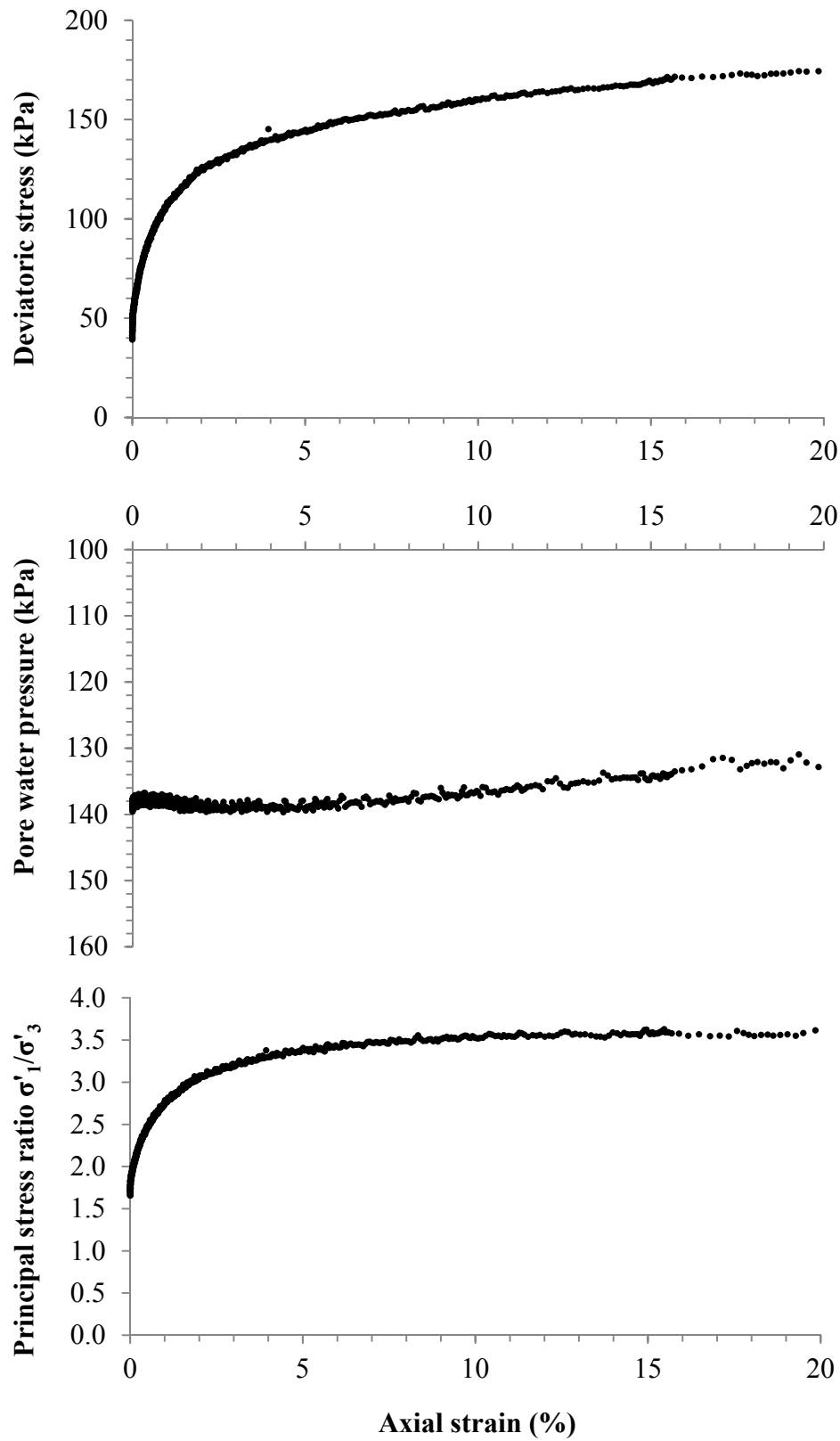
Figure B.3 – CK$_0$U TXC test no. C0831: e = 0.76, S = 79%
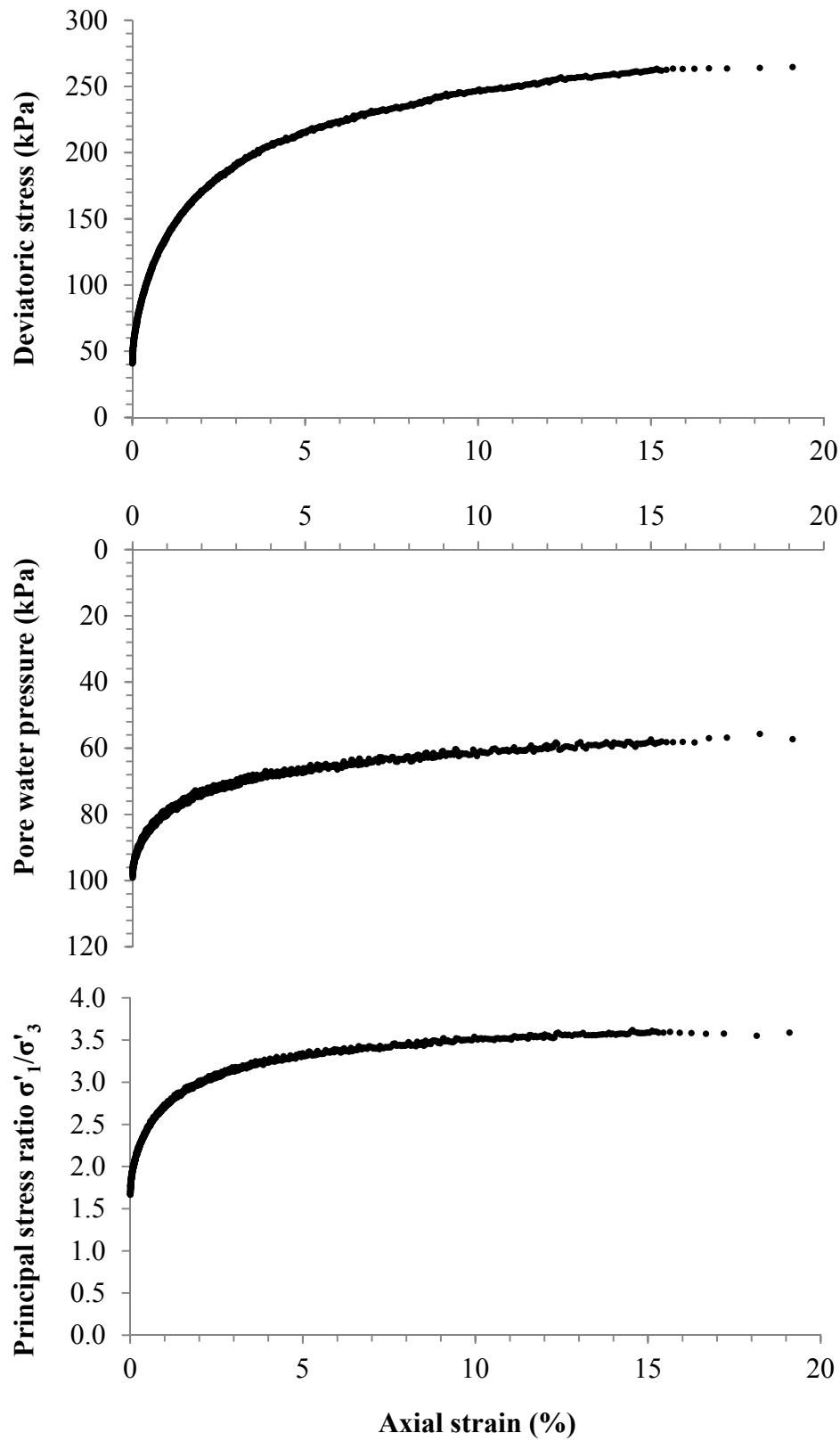
Figure B.4 – CK$_0$U TXC test no. C0920: e = 0.75, S = 59%

NORTHWESTERN UNIVERSITY

Evaluation of Liquefaction Susceptibility of Clean Sands after Blast Densification

A DISSERTATION

SUBMITTED TO THE GRADUATE SCHOOL

IN PARTIAL FULFILLMENT OF THE REQUIREMENTS

for the degree

DOCTOR OF PHILOSOPHY

Field of Civil and Environmental Engineering

By

Carlos Alberto Vega Posada

EVANSTON, ILLINOIS

August 2012

ABSTRACT

Evaluation of Liquefaction Susceptibility of Clean Sands after Blast Densification

Carlos Alberto Vega Posada

The effect of earthquakes on infrastructure facilities is an important topic of interest in geotechnical research. A key design issue for such facilities is whether or not liquefaction will occur during an earthquake. The consequences of this type of ground failure are usually severe, resulting in severe damage to a facility and in some cases the loss of human life. One approach to minimize the effect of liquefaction is to improve the ground condition by controlled blasting.

The main limitations of the blast densification technique are that the design is mostly empirical and verification studies of densification have resulted in contradictory results in some case studies. In such cases, even though the ground surface settles almost immediately after blasting, common verification tests such as the cone penetration test (CPT), standard penetration test (SPT), and shear wave velocity test (V_s) suggest that the soil mass has not been improved at all. This raises concerns regarding the future performance of the soil and casts doubts on whether or not the improved deposit is still susceptible to liquefaction.

In this work, a blast densification program was implemented at the Oakridge Landfill located in Dorchester County, SC, to gain information regarding the condition of a loose sand deposit during and after each blast event. In addition, an extensive laboratory testing program was conducted on reconstituted sand specimens to evaluate the mechanical behavior of saturated and gassy, medium dense sands during monotonic and cyclic loading.

The results from the field and laboratory program indicate that gas released during blasting can remain trapped in the soil mass for several years, and this gas greatly affects the mechanical

behavior of the sand. Gas greatly increases the liquefaction resistance of the soil. If the gas remains in the sand over the life of a project, then it will maintain this increased resistance to liquefaction, whether or not the penetration resistance increases with time. As part of this work, a methodology based on the critical state concepts was described to quantify the amount of densification needed at a certain project to make the soil more resistant to liquefaction and flow.

ACKNOWLEDGEMENT

To my wife and daughter, Maria E. Gallego and Karen Vega,

for their patience, support and love during all this years

To my brother and sister, Cesar A. Vega and Sandra H. Vega,

for their support and encouragement

To my beloved and deceased parents, Gloria E. Posada and Jesus A. Vega,

who raised me to be the man I am today

TABLE OF CONTENTS

LIST OF FIGURES

LIST OF TABLES

1 INTRODUCTION

1.1 Background

Soil liquefaction has long been an important topic of interest in geotechnical research. One method to mitigate the effects of liquefaction is to densify the potentially liquefiable stratum. Thus it is important to understand in detail the response of improved soil to dynamic loads.

For liquefiable soils, the designer must assess the consequences of liquefaction. The consequences of this type of ground failure are usually severe, resulting in significant damage to the facility and in some cases the loss of human life. Some options to minimize the effect of liquefaction are to (i) relocate the facility to a site with more competent soil strata; (ii) design the facility to withstand the effects of liquefaction; or (iii) improve the site to minimize the potential for liquefaction under the expected earthquake. For most practical cases where liquefaction is a concern, the costs of alternatives (i) or (ii) are large and almost prohibitive. Therefore, the most common and economical approach is to improve the engineering characteristics of the ground to withstand the expected earthquake.

To improve the ground over large areas, densification of loose sands by controlled blasting is a relatively economical approach. The main limitations of this densification approach are that the design is mostly empirical because there is not a well-established theoretical procedure available, and verification studies of densification have resulted in some contradictory results in some case studies. In such cases, even though the target soil layer was densified and the ground surface settles almost immediately after blasting, common verification tests such as the cone penetration test (CPT), standard penetration test (SPT), and shear wave velocity test (V_s) suggest that the soil mass has not been improved at all. This raises concerns regarding the future performance of the

soil and casts doubts on whether or not the loose sands have really been improved to the point where liquefaction is not possible.

The counterintuitive observation of increased density with an accompanying apparent absence of increased penetration resistance is central to this research. Because there is much evidence to show the relationship between soil density, penetration resistance, and liquefaction susceptibility, it is not clear why the penetration resistance measured in the field does not increase after a blasting event that is known to have resulted in an increase in an overall density of the loose soil deposit. Since the current design methods for blast densification are largely empirical, a rational procedure is needed to define and confirm how much improvement is required to meet the design objective of a particular project.

1.2 Objectives

The two main objectives of this dissertation are to develop a methodology based on the critical state concepts to quantify the amount of densification required to make the soil resistant to liquefaction and flow in the presence of shear stresses, and to develop a means of reliable in-situ verification of the ground improvement. To achieve the first objective, a laboratory testing program was conducted to define the critical state line and the constitutive response of reconstituted saturated and gassy sand specimens. To achieve the second objective, a field verification program was conducted to monitor the soil response during and after blasts at a test section near Charleston, SC. This program consisted of ground surface settlement measurements, pore pressure measurements, cone penetration soundings, and pore fluid sampling to determine in-situ gas compositions and concentrations.

1.3   Summary

This dissertation consists of eight chapters. Following this introduction, Chapter 2 presents a review of previous studies where explosives were used to densify the soil mass. A summary of case studies is presented and the time-dependent behavior of soils improved with explosives is discussed. The effects of blasting on sands, type of gases produced by explosives, longevity of gas trapped in the soil, influence of gas on soil response, and groundwater and gas sampling techniques are discussed in detail.

Chapter 3 presents a detailed description of previous blast densification programs performed at the Oakridge landfill site. The results from ground surface settlements, subsurface settlements, porewater pressure measurements, and cone penetration and shear velocity tests are presented and discussed in detail.

Chapter 4 describes the field blast densification program conducted at the Oakridge landfill site in 2011 at which Northwestern University measured gases and porewater pressures after blasting. The results from the ground surface settlements, cone penetration tests, porewater pressure measurements, and groundwater/gas samples are presented and discussed in detail. In this field program, emphasis is given to the identification of the type of gases trapped in the soil after blasting and the quantification of their in-situ concentrations. The final degree of saturation of the targeted layer after ground improvement is presented and the short and long term fate of these gases are discussed.

Chapter 5 presents the soil parameters and index properties of the sand used for testing. Summaries are provided to the laboratory testing program implemented to determine the shear resistance and cyclic resistance to liquefaction of saturated and gassy sands.

Chapter 6 presents the analysis and results from the laboratory experimentation program. The testing procedure used to create the saturated and gassy samples is explained. The monotonic and cyclic loading responses of medium to dense saturated and gassy sand samples are presented. The mechanical behavior of the soil is shown to be a function of void ratio and degree of saturation. The shear wave velocities obtained from the bender elements during all the stages of the testing program are presented. In addition, the use of one-dimensional constrained compression test to estimate the volume changes that will occur after blasting is proposed.

Chapter 7 presents the comparison between the void ratios and axial strains measured in the field during the blast densification programs conducted in 2003-2004, 2005, 2007 and 2011 with those estimated from one-dimensional constrained tests. Possible discrepancies between the results are also discussed.

Finally, Chapter 8 presents a summary and the conclusions of this work and provides recommendations for future research.

2 TECHNICAL BACKGROUND

2.1 Ground improvement by blast densification

Blast densification has been used for more than 70 years to densify loose, saturated sand deposits. Although it is considered to be an economical approach when compared with other alternatives, it has not been widely accepted because the design is primarily based on experience rather than on theory (Gohl et al., 2000b). Blast densification consists of placing charges within the loose layer requiring treatment. The charges are detonated with multiple delays to generate a cyclic load. Delays are used to minimize the peak ground acceleration while efficiently inducing cyclic stresses. This cyclic load and the gas produced during blasting increase the pore fluid pressure, and as a consequence, the effective stresses are reduced until a zero vertical effective stress state is reached in the soil. As the blast-induced pore pressure dissipates, the effective stress increases to values near the pre-blast levels and the soil deposit reconsolidates to a denser configuration. As a result, it is believed that the soil's strength and stiffness increase.

Considerable work has been conducted to correlate field tests such as the CPT, SPT, and Vs with the soil strength and liquefaction potential (Youd et al., 2001). These studies show that, in saturated soils, the shear resistance increases and liquefaction potential decreases with increases in density. A few case studies have shown that the ground surface settles almost immediately after blast densification, but when standard field tests such as the CPT, SPT, and Vs are conducted, the results provide rather counterintuitive results. Some of these test results indicate an initial, and in some cases a more lasting, decrease in strength and stiffness of the densified soil mass.

This time-dependent strength behavior has been extensively discussed in the literature since the 1980s, but so far no general agreement has been reached in this respect. The initial lack of increase in the soil strength immediately after densification has been attributed to different factors such as destruction of cementation at the interparticle contacts (Mitchell and Solymar, 1984; Schmertmann, 1991); decrease in the horizontal stresses (Schmertmann, 1987); particle rearrangement and structuration (Mesri et al., 1990; Bowman and Soga, 2003); initial loss of stiffness (Thomann, 1990; Thomann and Hryciw, 1992); static fatigue at the grain contacts (Michalowski and Nadukuru, 2012) and free gas trapped in the soil mass (Dowding and Hryciw, 1986; Hryciw, 1986). Although a great effort has been made to explain this initial decrease in soil resistance, no attempts have been made to study the long term strength behavior of soils densified with explosives.

Numerous case studies of blast-induced liquefaction have focused on the pore pressure responses and peak particle velocities generated by the passage of the blast-induced cyclic stresses (Charlie et al., 1981; Charlie et al., 1992a; Narin Van Court and Mitchell, 1994; Gohl et al., 2000a; Charlie et al., 2001; Ashford et al., 2002; Al-Qasimi et al., 2005; Rollins et al., 2005; Charlie and Doehring, 2007; Saftner et al., 2008). These studies correlate the induced pore water pressure, energy released and peak particle velocity with the cube root-scaled distance ($R/W^{1/3}$). The cube root-scale distance is defined as the distance from the explosive to the seismograph (R), divided by the cube root of the explosive's mass ($W^{1/3}$). These correlations are useful to design the blast densification program (charge weight, charge spacing, charge depth, etc.) and to predict the extent of liquefaction during blast densification.

Table 2-1 presents a summary of case studies where blast densification was used to improve the strength of the soil mass. The soil profile, thickness of the target layer, blast densification program, and ground surface settlements measured after blast densification are presented. When applicable, the results from the cone penetration tests (CPT), standard penetration tests (SPT), and shear wave velocity tests (V_s) are also presented. Table 2-1 is organized in the following fashion. The first category consists of case studies where no increase in soil resistance occurred even several years after ground improvement; the second category consists of case studies where an initial decrease but then an increase in resistance over time to values above initial values was measured; and the third category consists of case studies where an immediate increase in soil resistance was measured.

A detailed look at the summary of the case studies provides some indications of why in some cases the soil resistance does not increase to levels above the pre-blast values even several years after ground improvement. In some cases, the densified layer contains a certain percentage of fines that prevent the gas trapped after blast densification from escaping to the surface. This gas will remain trapped between the grains for several years and it will influence the soil response during the verification field tests. In other cases, there is an impermeable layer overlying the blasted layer that prevents gas from escaping to the surface and promotes the accumulation of gas below it. This may explain why in some cases there is little to no improvement only at the upper half part of the densified layer.

Table 2-1. Summary of case histories

Category 1: No increase in soil resistance after blasting					
Reference	**Soil profile/ thick. layer**	**Generalized blasting program and configuration**	**Ground surface settlement**	**CPT/SPT and Vs results**	**Comments**
(Thomann and Hryciw, 1992)	The soil consists of 9.1m of medium to fine, subangular, light brown sand.	Single charge of 1.1kg placed at a depth of 6.4m.	Ground surface settlements were not reported	CPT tests conducted 217 days after blasting showed no soil improvement. Vs results were inconclusive	Short term data only
(Charlie et al., 1992b)	Starting at the surface: i) 1.5m of poorly graded medium-fine sand; ii) 3.6m of poorly graded gravelly sand; and iii) 2.5m of inorganic silt (ML). – Target layer: layer (ii)	Single blast hole. Charge of 5kg.	Max. settl. = 0.20m	Initial reduction in penetration resistance CPT tests showed little to no improvement after 3 weeks	Short term data only
(GeoSyntec Consultants, 1998)	Starting at the surface: i) 1.5m of fine-medium silty sand; ii) 1.2 - 3m of silty clay and clayey sand; iii) 3 – 4.6m of dense fine to medium sand; iv) 0.3 – 1.5m of very loose fine sand; v)1.5 – 4.6m of loose fine sand; vi) Below 30m - fine sand and silty clay. - Loose layer, t ≈ 5.5m	Charges of 16–25kg/hole detonated at a depth of 10m, with an 18ms delay. Zone A: two square grid coverages. 9 detonation points. Zone B: one square grid coverage. 9 detonation points.	Zone A: on the order of 0.25-0.46 m after both coverages. Average: 0.36m Zone B: on the order of 0.17 – 0.23m. Average: 0.21m	CPTu tests conducted 6 weeks, 17 weeks, and 3 years after blasting showed little to no improvement. Vs showed little to no improvement.	Impermeable layer overlying target loose layer

Reference	Soil profile/ thick. layer	Generalized blasting program and configuration	Ground surface settlement	CPT/SPT and Vs results	Comments
(Liao and Mayne, 2005)	Soil deposit was composed of two layers i) top layer: 5 to 6m of clayey silt; and ii) bottom layer: 25m of clean quartz sands. – Depth of target layer from 7 to 13m	Test Area 1: one single blast point. Single charge of 1180kg. Test Area 2: two single blast points. Charge of 1180kg/hole.	Ground settlements were not reported	CPT tests conducted 8 months after blasting showed no increase in penetration resistance	Impermeable layer overlying target layer
(Camp et al., 2008)	Starting at the surface: i) 1.5m of loose, fine clayey sand; ii) 1.5m of very soft sandy clay; iii) 3.3m of loose fine sand; iv) 3.5m of loose to medium dense sand; v) Cooper Marl	Circular layout. Three coverages. Charges of 2.72 kg distributed along the depth. 20 piezometers at various depths were installed to monitor porewater pressures	Maximum settl. $\approx$ 0.28m, corresponding to an ε_a =9.3%	CPT resistance and Vs tests conducted 7 yrs after blasting showed minimum to no improvement	Impermeable layer overlying target layer
(Narsilio et al., 2009)	Similar to the soil profile reported by GeoSyntec Consultants (1998). - Loose layer, t $\approx$ 5.5m	Charges of 11–34 kg/hole, detonated at a depth of 10m. Four square grid coverages.	Total settl. $\approx$ 0.5m, corresponding to approx. ε_v = 12%	Initial reduction in penetration resistance. CPTu tests conducted 1.3 and 2.8 yrs showed little to no improvement at the upper half part of the layer.	Impermeable layer overlying target loose layer

		Category 2: Initial decrease but then an increase in resistance over time to values above initial values and case studies where no long-term performance data is presented			
Reference	Soil profile/ thick. layer	Generalized blasting program and configuration	Ground surface settlement	CPT/SPT and Vs results	Comments
(Solymar, 1984; Solymar et al., 1984; Solymar and Reed, 1986)	Loose alluvial sand deposit up to 70m in depth. Soil density varies appreciably in both vertical and horizontal directions. Loose to medium dense portions of the deposit were densified. thick.= 15m	Charges of: 20–35kg/hole. Spacing charges = 10m Zones 1, 2, 3 and 4: three square grid coverages. Zones 5: four square grid coverages	Average settlements Zone 1: 0.53 – 0.98m Zone 2: 0.55 – 0.75m Zone 3: 0.50 – 0.85m Zone 4: 0.75 – 0.95m Zone 5: 0.50 – 0.85m	Initial reduction in penetration resistance CPT resistance increased several months after blasting	In some cases, q_c decreased above blasted zones
(La Fosse and Rosenvinge IV, 1992)	Starting at the surface: i) 3m of loose to medium dense sand; ii) 3m of medium dense to dense sand; iii) 9.1m of very loose to loose sand; and iv) 12.1m of medium dense to dense sand. v) 15.2m of silty and clay. Target layer between depths of 6.1 and 15.2m	Two coverages Zone A: charges of 5.1kg/hole Zone B: charges of 6.8kg/hole Zone C: charges of 8.5kg/hole	Max. settl. = 0.35m Aver. settl. = 0.13m	- In general, N values and q_c increased. - A few tests showed a reduction in N values and q_c decreased in the upper 3m.	CPTs were conducted 5 months after blasting
(Kimmerling, 1994)	Starting at the surface: i) 40 m of loose avalanche debris (mixture of sands and gravels containing silt, cobbles and boulders. ii) Dense to very dense silty sands and gravels	Pilot: charges of 47.2 kg/hole for 1st coverage (PF≈15g/m^3) and 81.9 kg/hole for 2nd coverage. Blasting: charges of 81.9 kg/hole (PF≈25g/m^3). Three coverages.	Pilot: total settl. ≈ 0.5m, corresponding to approx. ε_a = 1.2% Blasting: total settl. ≈ 1.5m, corresponding to approx. ε_a = 3.8%	In general, N values increased. Vs did not increase from 0–6 m, increased from 6-24m, and did not increase below a depth of 24m.	Significant data scatter in N-values due to the presence of gravels. Inconclusive results

Reference	Soil profile/ thick. layer	Generalized blasting program and configuration	Ground surface settlement	CPT/SPT and Vs results	Comments
(Gohl et al., 1998)	Starting at the surface: i) 5.8m of loose, sandy silt fill; ii) 0.7m of sandy silt; iii) 2.5m of loose, fine silty sand containing ≈30% fines; iv) Below 9m: loose sandy silt and silt. – Depth of target layer from 6.5 to11.5m	Charges distributed along the depth. i) single blast holes: total charges of 1 - 5kg. ii) multiple blast holes: total charges of 5 kg/hole. - Vs (SASW) were conducted	Max. settl. = 0.37m (1 week after) and 0.42m (5.5 months after blasting) Settlements extended radially up to 20-25m	N-values and Vs slightly increased four weeks after blasting. Post-blast SASW results showed a significant reduction in Vs above the 6.5m depth	Semi-impermeable layer overlying target layer Vs decreased above target layer
(Gandhi et al., 1999)	12m of fly ash from thermal power plants	i) 15 single blast points, total charges of 5.5–28 kg. distributed along the depth. One coverage ii) 3 groups of 25 blasts each. Powder factors 1.9-4.0g/m^3. Two coverages	i) Single blast points: Settl.= 0.25-0.55m, ε_a (%) = 2 – 4.6 ii) 3 groups: 0.21-0.30 m, ε_a= 1.7–2.5%	SPT N-values and static CPT tests after blasting showed minimum to no improvement, especially near the surface.	q_c was inconsistent over the blasted layer
(Ashford et al., 2004)	Starting at the surface: i) 2.5m of clean fine sand with shell fragments; ii) 0.4m of silty sand; iii) 2m of clean fine sand with shell fragments; and iv) 3.1m of interbedded silty sand and silty clay layers	Single charge of 0.5 kg. Two blast coverages. 32 single blast points placed around the periphery of two circles. Transducers were installed to measure pore pressures	Average settl. ranged from 0.025–0.10m. Maximum settl. ≈ 0.10m, corresponding to an ε_a =2.5%	Initial reduction in penetration resistance After 42 days, CPT resistance increased 2.5 times above pre-blasting values	Impermeable layer overlying target layer

Reference	Soil profile/ thick. layer	Generalized blasting program and configuration	Ground surface settlement	CPT/SPT and Vs results	Comments
(Rollins and Anderson, 2008)	Starting at the surface: i) 1m of sand fill (SP); ii) 1.7m of silty sand (SM); 1.8m of silt and sandy silt (ML); and iv) 10m of clean fine sand. – Depth of target layer from 5 to 13m	Two sites: Each site with 4 single blast points, 4 pore press. transducers, and 35 drains. Charges of 1.8–3kg/hole placed along the depth.	Max. settl. = 0.35m (finned-mandrel used to install drains) Max. settl. = 0.10m (smooth pipe mandrel used to install drains)	Initial reduction in penetration resistance CPT resistance increased 2 weeks after blasting	Impermeable layer overlying target layer.
Category 3: Immediate increase in soil resistance					
(Handford, 1988)	Hydraulic fill tailing dam i) top layer: 11 to 16m of medium dense sand ii) lower layer: 5 to 18m of loose sand. – Thick. of target layer ≈ 13m	Pilot program: charge of 9kg/hole. Four coverages, spacing charges =10m Blasting program: charges of 12-16kg. spacing charges =14m	Ground settlements were not reported	N values increased from 43 to 147% with respect to the pre-blasting values	
(Hachey et al., 1994)	40 meters of debris flow composed of very loose silty sand and gravel with boulders and cobbles	Total charges of 47–82 kg distributed along the depth. Pilot: two coverages Blasting: three coverages	Pilot program: max. settl.= 0.46m Blasting program: max. settl.= 1.5m (vertical strains= 4%)	Becker penetration tests - N values increased from 7 to 20 blows/ft	
(Raju and Gudehus, 1994)	Three fill layers having a total depth of 45m. i) top two layers: very loose fine-medium sands; and ii) fine sand + cohesive material	Charge of 15 kg, located at a depth of 11.5 m. 13 pore press. gages at various radial distances. 8 shock gages at 1m horizontal interval.	Max. settlement = 1.3m. Settlements extended radially up to 25m	At a distance of 6m from the blast point, the CPT increased up to a factor of 3	100% liquefaction was achieved

Reference	Soil profile/ thick. layer	Generalized blasting program and configuration	Ground surface settlement	CPT/SPT and Vs results	Comments
(Elliott et al., 2009)	The upper 20m to 40m is composed of loose granular material with the upper 18m section containing boulders, cobbles, sand, and gravel. The material becomes progressively finer with depth	Equilateral triangle layouts. Three coverages. Charges distributed along the depth. Close of existing dam: Charges of 37kg/hole. Further from dam: Charges of up to 120kg/hole	Aver. Settl. ranging from 0.3 to 1.5m. ε_a= 3–15%, assuming a thick. of liquefied layer $\approx$ 10-16m	In general, N values increased	Significant data scatter in N values due to the coarse particles

2.2   Mechanism of densification after blasting

The mechanism that densifies soil as a result of blasting can be explained as follows. Upon detonation, the energy released by the explosives creates a high pressure shock wave that initially increases normal stresses in the soil mass as the shock wave approaches and then decreases it as the shock wave passes (Narin Van Court and Mitchell, 1994). The rapid repetition of compression and extension cycles, coupled with the development of shear stress and the increase in water pressure caused by the expansion of released gas, destroy the existing soil structure and allow the soil grains to rearrange themselves in a denser configuration as the excess pore water pressure dissipates. The amount of blast densification is believed to be greatly influenced by the charge weight, horizontal charge spacing, vertical separation between charges, charge depth, number of coverages, and firing sequence and timing (Narin Van Court and Mitchell, 1994).

One of the most accepted methods for defining whether or not a saturated granular soil will liquefy and flow is embodied in the concepts of the critical state soil mechanics. The critical state line (CSL) represents the relationship between the critical void ratio and effective stresses when a soil has failed (Schofield and Wroth, 1968). The soil response to monotonic or dynamic loads depend strongly on the state variables mean normal effective stress, p', and void ratio, e. This is illustrated on the state diagram shown in Figure 2-1a. For example, a sample in an initial state above the CSL will tend to contract and develop positive excess pore water pressure when subjected to undrained loading until no further changes in effective stress will occur. On the other hand, a sample in an initial state below the CSL will tend to dilate and develop negative pore water pressure, increasing the effective stresses until the critical state line is reached.

After each blast event, the excess pore water pressure rapidly builds up, decreasing the confining effective stresses to zero and triggering a condition of initial liquefaction. As the blast-induced pore pressure dissipates, the effective stresses will increase and a reduction in the soil void ratio (Δe in Figure 2-1b), will occur. Conceptually, no more blast densification is needed once the soil void ratio is below the critical state line (point A' – Figure 2-1b) because at this state a dilative behavior is expected. However, further densification may be needed to account for extra stresses induced by the facility or embankment to be constructed, as noted by point B (Figure 2-1b). If the embankment stresses are large enough to change the soil state to above the critical state line, and hence be loose of critical, it again will be susceptible to liquefaction and flow.
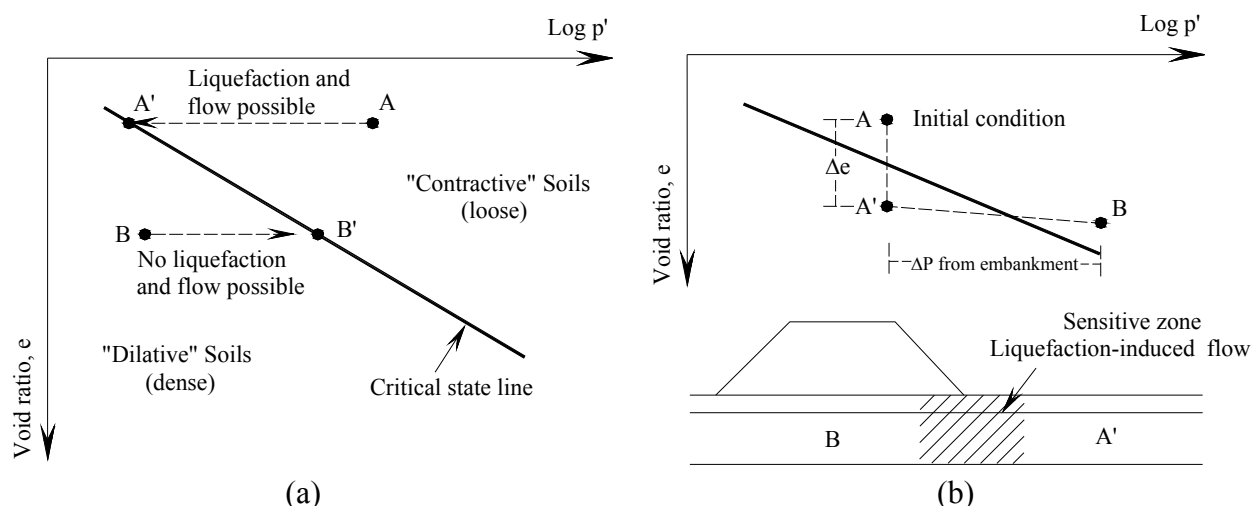
Figure 2-1. a) State diagram indicating liquefaction potential based on undrained test of saturated sands, and b) stresses induced by the facility or embankment.

2.3 Gases produced by explosives and their significance

During blast densification, large amounts of gas are produced and released in the ground. Since some of this gas does not immediately escape to the surface and may remain trapped for months or even years, it is important to determine the type of gases produced by typical

explosives and quantify their in-situ concentrations. It is also necessary to consider the longevity of these trapped gases and their effect on the mechanical response of soils during monotonic or cyclic loading.

2.3.1   Types and amount of gas produced

The principal gases produced by typical explosives are water vapor (H_2O), carbon dioxide (CO_2) and nitrogen (N_2) in a mole ratio of 1:2:5 (U.S. Army Corps of Engineers, 1972). Hryciw (1986) calculated that 1 kg (2.2 lb) of Ammonium Nitrate Fuel Oil (ANFO) will produce approximately 43 moles of these gases, which corresponds to about 1.0 m^3 (35 ft^3) of gas at standard temperature and pressure. However, after blasting some gas will escape to the surface, some will rapidly condense in the presence of cooling groundwater, and some will migrate and diffuse with time, making it difficult to predict a priori the exact amount of gas trapped in the soil.

2.3.2   Longevity of gas trapped in the soil

Figure 2-2 shows the fate of gases following detonation of ANFO. Of these gases, water vapor will condense almost immediately when the groundwater temperature drops to the pre-blasting value and carbon dioxide will gradually dissolve in the pore fluid over time, leaving nitrogen as the main gas present in the ground. In most practical applications where blast densification is used, the absolute pressure acting on the gas is relatively low ($P_{abs} \approx 200$ kPa at a depth of 10 m). This observation, combined with the fact that nitrogen does not dissolve easily in the pore fluid under these pressures (solubility coefficient, β= 0.015 mL of N_2/ mL of water), leaves open the possibility that the amount of nitrogen initially trapped in the soil mass after

blasting will remain in the ground for a long period of time, assuming low hydraulic gradients at the site.
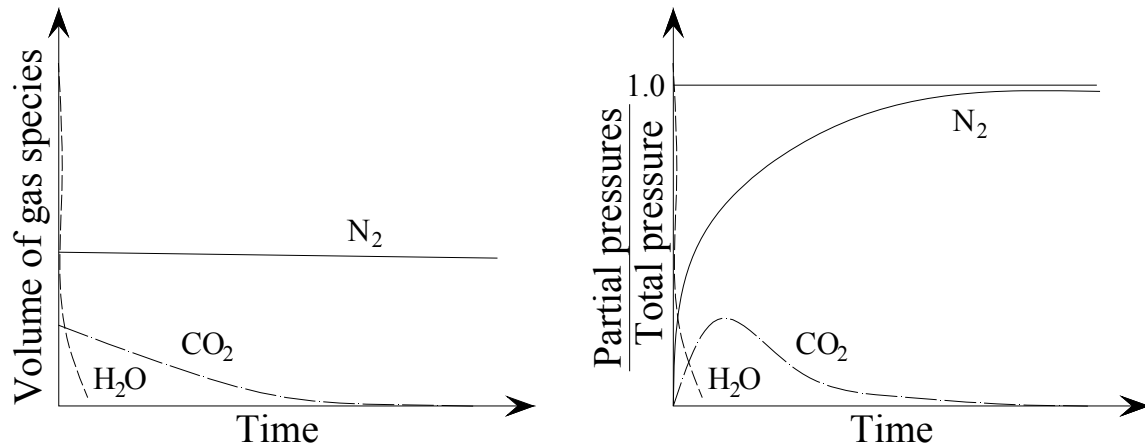
Figure 2-2. Fate of gases following detonation.
After Hryciw (1986)

Recently, several studies have evaluated the persistence of air below the groundwater table by measuring the degree of saturation in the ground at sites that have been improved by using the sand compaction pile technique. This technique consists of installing sand piles into a loose layer to increase both the soil density and the lateral effective stresses. Large amounts of air are introduced in the soil during the installation process (Okamura et al., 2003; Okamura and Teraoka, 2004; Okamura et al., 2006; Okamura and Yasuhara, 2009; Okamura et al., 2011). Okamura et al. (2006) measured the degree of saturation of high-quality undisturbed samples obtained by in-situ freezing at six sites in Japan where this technique was used. Figure 2-3 shows the degree of saturation based on the frozen samples at the sites. They found that air was present at all sites, and even at one site 26 years after the sand compaction piles were installed.
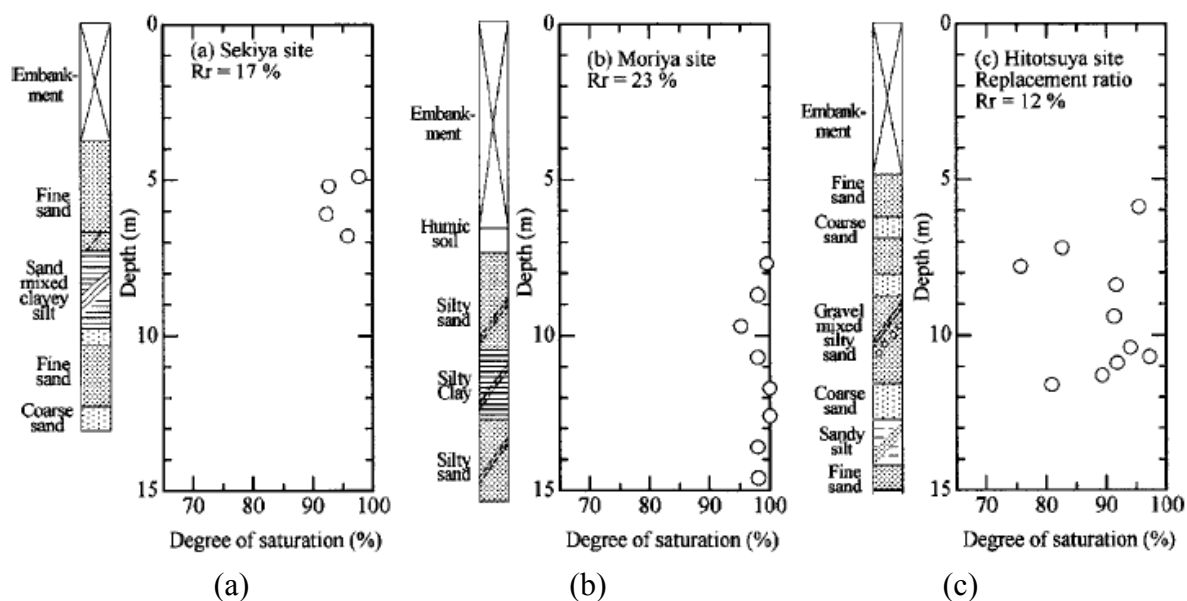
Figure 2-3. Degree of saturation of soils at different improved sites (a) 26 years ago, (b) 8 years ago, and (c) 4 years ago.
Okamura et al. (2006)

As part of an experimental investigation program for liquefaction mitigation, Yegian et al. (2007) prepared a 151 cm column of partially saturated loose Ottawa sand to evaluate the long term tendency of air to diffuse when trapped in a thick soil layer. Partial saturation was achieved in the specimen by using the drainage-recharge method. This method consists on draining the specimen porewater from the bottom and then reintroducing it from the top at a slow rate. The degree of saturation of the sample is computed using the accumulated free water at the top of the sample. The volume of free water is equivalent to the volume of air trapped in the sand column. As shown in Figure 2-4b, the degree of saturation of the sand sample slightly increased from 82.1% to 83.9% during 442 days, indicating little tendency of diffusion of the entrapped air. This increase in the degree of saturation was observed within few days after sample desaturation; after that period the degree of saturation remained mostly constant.
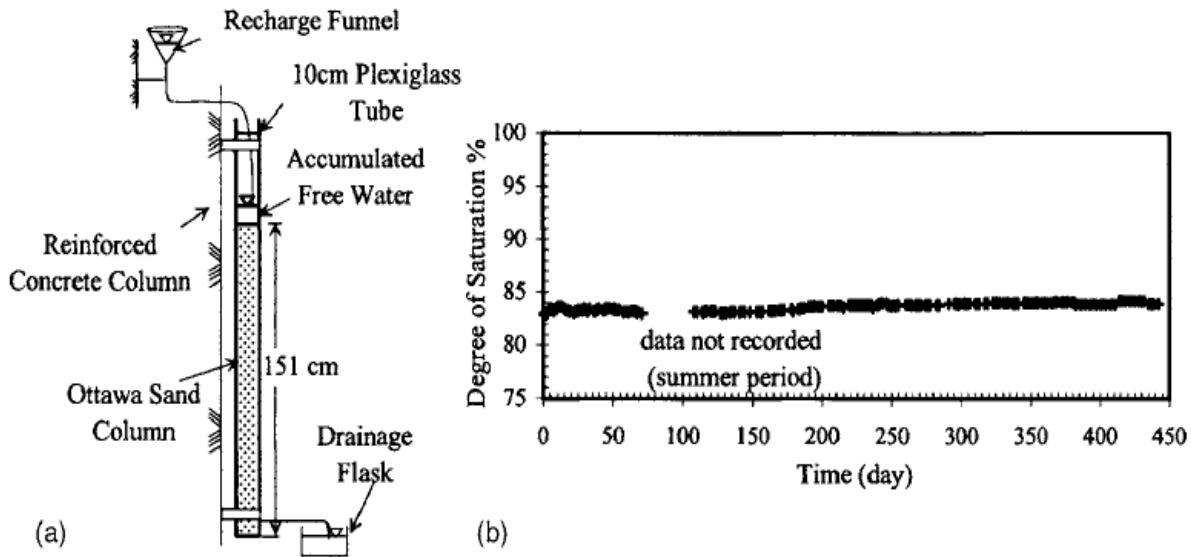
Figure 2-4. (a) Test setup used to investigate the long-term sustainability of air bubbles in a partially saturated sand column and (b) long-term monitoring of the degree of saturation. Yegian et al. (2007)

Because nitrogen is a significant component of both air and explosion product, the long term behavior of the gas bubbles from blasting is expected to be similar to that of air bubbles studied by Okamura et al. (2006). Based on the results obtained from Okamura et al. (2006) and Yegian et al. (2007), the influence of gas on the soil behavior must be taken into account when evaluating the behavior of blast-densified sand at a particular ground improvement project.

2.4 Field tests used to quantify soil improvement

The most common field tests used to quantify the soil improvement after blast densification are the cone penetration test (CPT), the standard penetration test (SPT), and to a lesser extent the shear wave velocity test (Vs). It is well known that the CPT, Vs, and N-values increase as the density of the soil deposit increases. However, several case studies have shown that the values obtained from these tests right after blasting often decrease (Solymar et al., 1984; Ashford et al., 2004; Rollins and Anderson, 2008) and in some cases do not return to levels above to the pre-blasting level (Thomann and Hryciw, 1992; Camp et al., 2008; Narsilio et al., 2009).

Although a loose sand deposit compresses almost immediately after blast densification, there is not yet a clear explanation for the lack of increase in penetration resistance and shear wave velocity which suggest that the strength and stiffness of the soil has not been improved. Figure 2-5 shows the CPT tip resistance and shear wave velocity measurements before and 7 years after blasting at a site located in Charleston, South Carolina, United States (Camp et al., 2008). The results showed that the tip resistance and shear wave velocity were lower than the pre-blasting levels at the "improved" layer, from 3.0 m to 5.5 m.
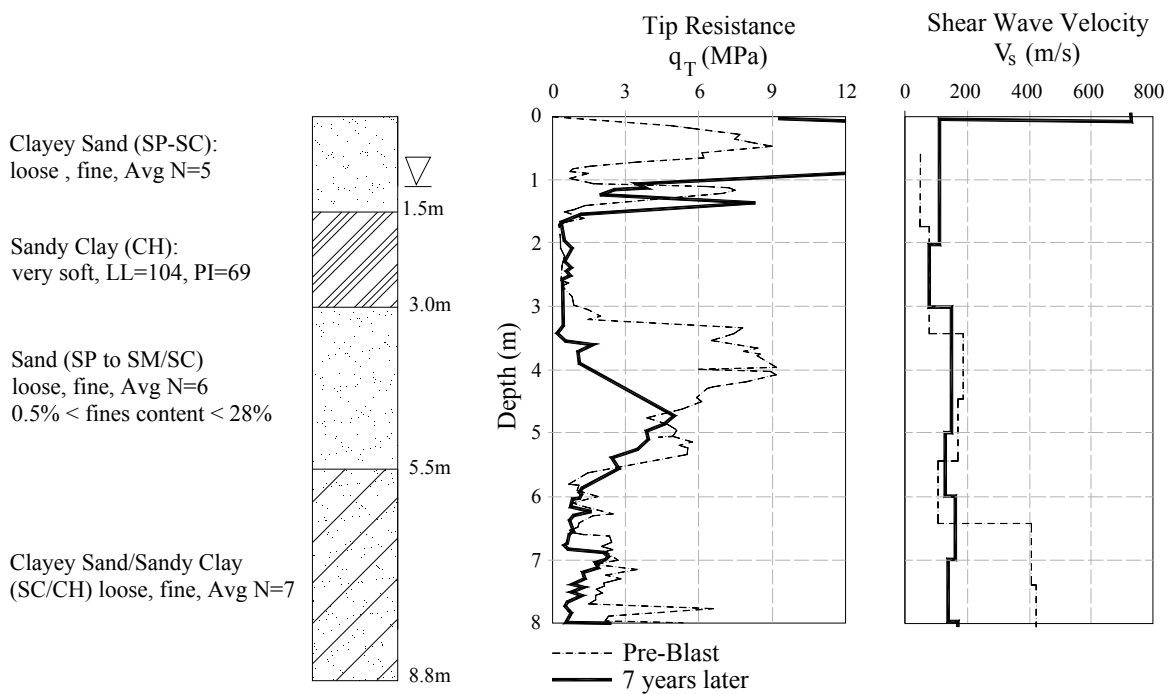
Figure 2-5. CPT tip resistance and shear wave velocity measurements before and 7 years after blasting.
After Camp et al. (2008)

2.5 Influence of gas on soil response

Previous studies (Dusseault, 1979; Thomas, 1987; Rad and Lunne, 1994; Rad et al., 1994; Christian and Cranston, 1997; Christian et al., 1997; Grozic et al., 1999; Grozic et al., 2000;

Fourie et al., 2001; Amaratunga and Grozic, 2009) have shown that the mechanical behavior of soil is significantly affected by the presence of gas in either dissolved or free form. Sobkowicz and Morgenstern (1984) showed that when unloading under undrained conditions, gassy soils behave different from "unsaturated" soils containing degassed pore fluid and from fully saturated soils.

Throughout the remainder of this thesis, gassy soil is assumed to be "a partially saturated soil with sufficiently high degrees of saturation for the gas to exist in discrete bubble form" (Nageswaran, 1983). Gassy soils are a special type of unsaturated soils where the pore gas phase is not connected to the atmosphere. The only effect of the presence of gas in the soil mass is thought to be the increase of the pore fluid compressibility (Sparks, 1963).

Grozic et al. (1999) conducted a series of monotonic triaxial compression tests on loose specimens of gassy sand. They found that the stress-strain soil response is considerably affected by the degree of saturation of the soil. Figure 2-6 shows that the higher the initial degree of saturation, the lower the shear strength under monotonic undrained loading. For reconstituted loose sand specimens consolidated to the same void ratio, the soil stress-strain response changes from strain softening to strain hardening at an approximate degree of saturation of 90%. This is an indication that gas in free form has the effect of increasing the globally undrained shearing resistance of loose sands.
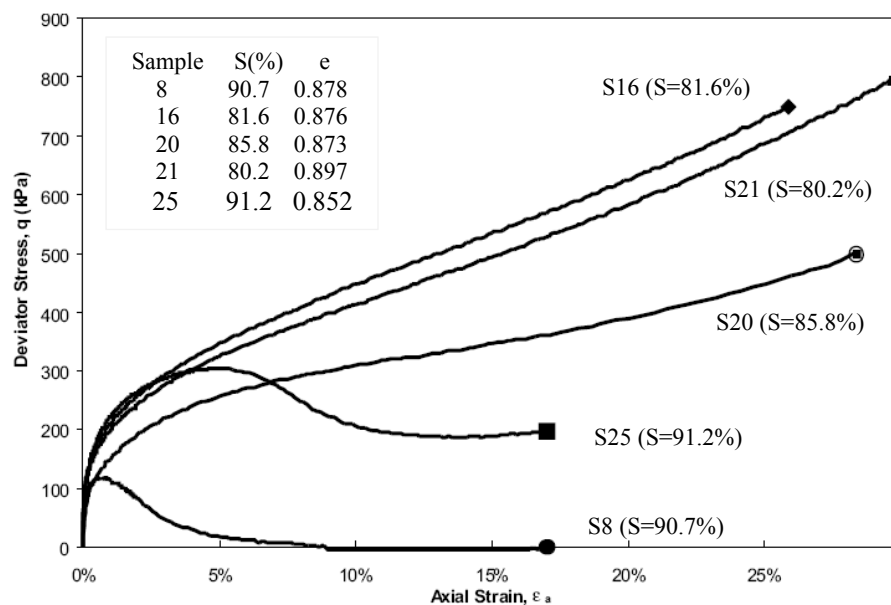
**Figure 2-6. Stress-strain curves for five representative loose gassy specimens.
After Grozic et al. (1999)**

Rad et al. (1994) showed that the shear strength of dense specimens of gassy sand is affected by the gas type, gas amount, and the pore pressure level. In contrast to the case of loose gassy sands, the presence of gas in free form has the effect of reducing the globally undrained shearing resistance of dense sands, because the increase in shear strength will be affected by the reduction in negative pore water pressure development. Fourie et al. (2001) conducted a series of undrained triaxial compression tests on undisturbed and reconstituted medium-dense samples of Syncrude tailing sands. Figure 2-7a shows the change in pore pressure with axial strain during monotonic loading of an undisturbed gassy sample, undisturbed saturated sample, and a reconstituted saturated sample with approximately the same void ratio. A careful examination of the undisturbed gassy samples revealed that the specimens were not fully saturated (Figure 2-7b). The experimental results showed that even a very small amount of air in the pore fluid had a significant effect on the pore water pressure response during loading. At an axial strain of 12%,

the negative pore water pressure developed by the undisturbed gassy sample was 2.5 times less than that developed by the undisturbed saturated sample.
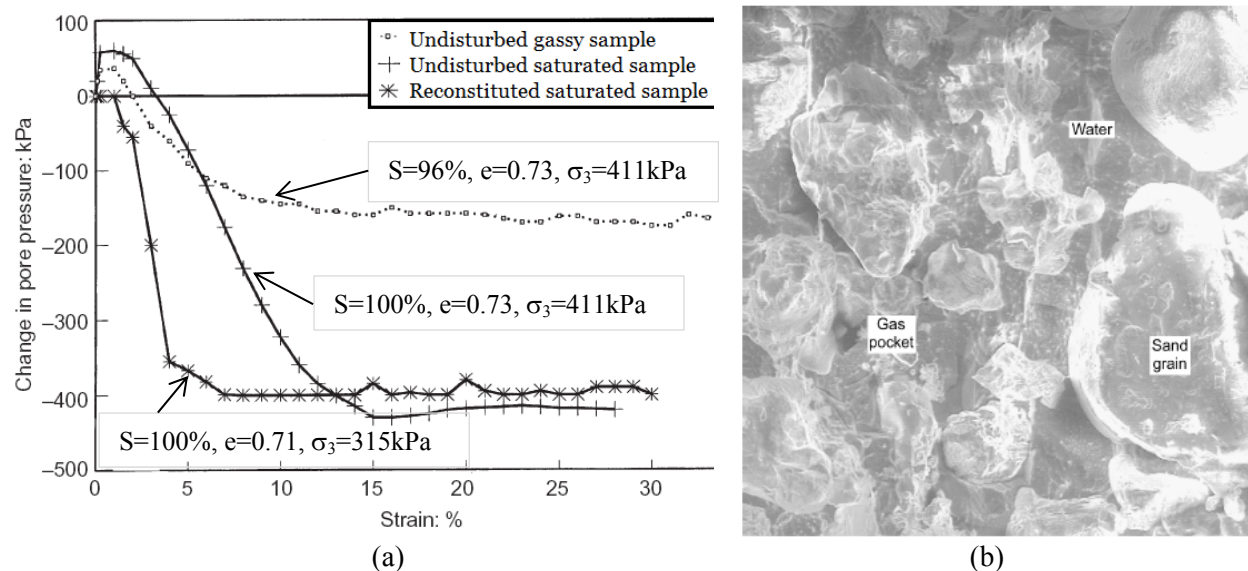
Figure 2-7. (a) Change in pore pressure during undrained triaxial compression of medium-dense specimens of Syncrude tailing sand and (b) microscopic examination (120 μ).
After Fourie et al. (2001)

Previous studies (Xia and Hu, 1991; Rad et al., 1994; Grozic et al., 2000; Tsukamoto et al., 2002; Okamura and Soga, 2006; Yegian et al., 2007; Okamura et al., 2011) have shown that the presence of gas in the soil in either dissolved or free form affects the mechanical response of the soil during cyclic loading. Although limited information is available, the presence of gas has the effect of increasing the cyclic resistance in loose sands and to delay the negative pore water pressure builds up in dense sands.

Xia and Hu (1991) conducted a series of cyclic triaxial tests on four sets of reconstituted loose sand samples with initial degrees of saturation ranging from 97.8% to 100%. It was concluded from this study that a slight decrease in the degree of saturation (say from 100% to 99.5%) increased the cyclic resistance ratio significantly. Grozic et al. (2000) conducted a series

of triaxial tests on loose gassy specimens to determine the influence of gas on soil behavior. The reconstituted sand samples were prepared with a range of gas contents and densities. The results showed that the presence of gas in free form increased the cyclic liquefaction resistance of the soil by 200 to 300%. Okamura et al. (2011) conducted a series of undrained cyclic triaxial tests on undisturbed and reconstituted loose specimens to determine the effect of the sample degree of saturation on the liquefaction resistance. The cyclic stress ratio ($\sigma_d/2\sigma_c'$) needed to cause a double amplitude axial strain of 5% (DA=5%) after 20 cycles was referred as the liquefaction resistance in their study. As shown in Figure 2-8, the authors showed that the liquefaction resistance of gassy loose sand increased as the degree of saturation decreased. The liquefaction resistance of gassy sand was found to be approximately twice the liquefaction resistance of saturated sand.
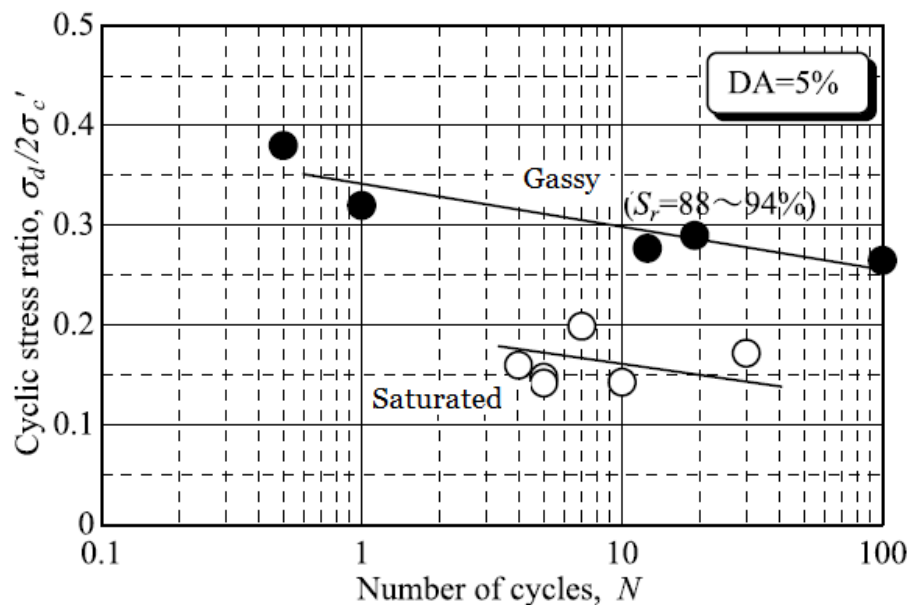
Figure 2-8. Liquefaction resistance curves obtained for saturated and gassy loose specimens. After Okamura et al. (2011)

Rad et al. (1994) performed a series of cyclic triaxial tests on dense sand specimens containing methane dissolved in the pore fluid and in free form. The initial degrees of saturation

varied from 66 to 100% and the average relative density of the samples was 87%. The results of this study showed that gas affects the dilative response of dense sands. The soil specimens containing gas had a tendency to develop large axial strains during extension. These large axial strains were attributed to the fact that the specimens containing gas had less negative pore water pressure build up than the fully saturated samples.

2.6   Identifying gases and their concentrations in-situ

As discussed in previous sections, gas produced and released during blast densification can endure in the ground for years after ground improvement. Therefore, it is important to clearly identify the type and concentration of gases trapped in the ground after blasting. This information is critical to determine in what form gases are present in the ground.

In the field instrumentation program introduced in chapter 4, a BAT probe device was used for pore fluid/gas sampling and in-situ pore pressure and temperature monitoring. The BAT probe system has been successfully used for more than 25 years in groundwater and offshore investigations. This probe was originally designed for sampling in-situ pore fluid, but it was later modified to recover fluid/gas samples in offshore sediments (Rad and Lunne, 1994; Christian and Cranston, 1997). The collected samples are analyzed with a gas chromatograph device to identify the type of gas present in the soil, quantify their concentrations, and identify if the gas is dissolved or present in free form. Rad and Lunne (1994) tested this system in the laboratory to verify its applicability for determining the in-situ fluid/gas condition and concluded that the BAT probe can provide a realistic assessment of in-situ conditions.

2.6.1   BAT probe system description

The BAT system can be used for pore pressure and temperature measurements using the BAT pore pressure configuration or for sampling of groundwater using the BAT permeability

configuration. Figure 2-9 shows the BAT probe system. This system is manufactured and sold by BAT Geosystems AB, Sweden. The main components of the BAT probe are the BAT filter tip, the BAT/IS sensor, the battery unit, and the BAT/IS field unit.

The filter tip is sealed at the top with a flexible septum that will automatically reseal after sampling. The septum can be penetrated with a needle several times without losing its self-sealing functions. The sensor is used for measuring/logging the pore pressure and temperature inside the filter tip. A hypodermic needle attached at the tip of the sensor is used to penetrate the filter tip. The battery unit is used to store the readings. This unit can store up to 3500 measurements (any combination of pressure and temperature readings). If a D-size lithium battery is used, the data can be logged for at least 8 months. The field unit is used to take real-time pressure and temperature readings and is also equipped with an internal atmospheric pressure sensor. Using the field unit, the sensor can be programmed to take readings at pre-established intervals.

2.6.1.1 Pore pressure and temperature measurements

Figure 2-9 shows the BAT probe configuration when used for measuring pore pressure and temperature. The BAT probe in this configuration consists of a filter tip, a guide sleeve, a hypodermic needle, a transfer nipple, a sensor unit, a battery unit, and a field unit. To measure the pore pressure, the BAT probe is assembled and carefully lowered down the extension pipe. The needle mounted in the IS sensor punctures the septum in the top of the filter tip by gravity. In cohesionless soils, readings can begin to be taken approximately one minute after the sensor is coupled to the filter tip. In clays, it could take up to 15 minutes for the pressures to stabilize.
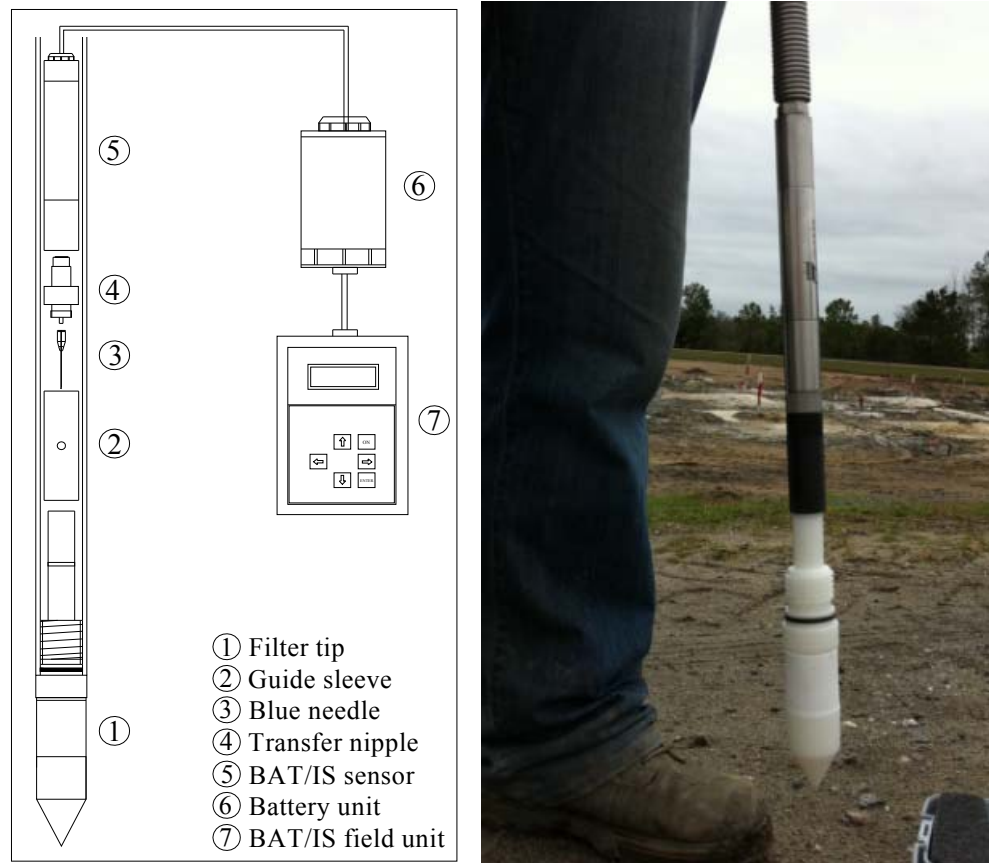
Figure 2-9. Pore pressure and temperature measurement configuration.

① Filter tip
② Guide sleeve
③ Blue needle
④ Transfer nipple
⑤ BAT/IS sensor
⑥ Battery unit
⑦ BAT/IS field unit

2.6.1.2 Groundwater/gas sampling

Figure 2-10 shows the BAT probe configuration when used for groundwater/gas sampling, the BAT probe in this configuration consists of a filter tip, a quick coupling, a double ended needle, a test container housing, a 35 mL test container, an extension adapter, a hypodermic needle, a transfer nipple, a BAT/IS sensor unit, a battery unit, and a BAT/IS field unit.
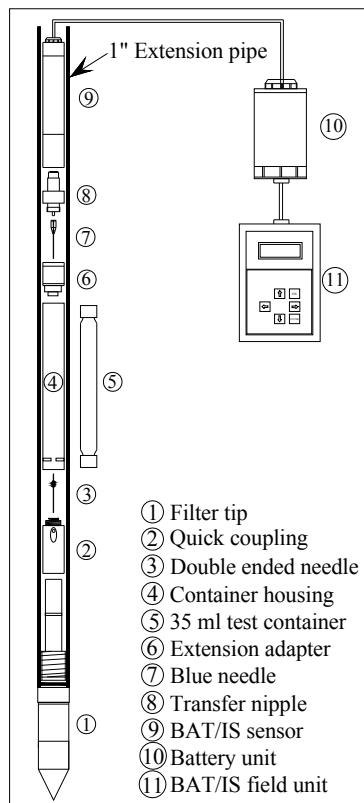
Figure 2-10. Groundwater/gas sampling configuration

A procedure similar to that used for pore pressure measurements is used for groundwater/gas sampling. The only difference is that a double ended needle mounted in a quick coupling simultaneously penetrates the septum in the filter tip and the septum in the bottom of the container, allowing the in-situ liquid/gas to enter the container. Because the sensor is connected to the top of the container with a needle, it is also possible to measure and monitor the pressure changes inside the container at any time during sampling, using the field unit. No change in pressure indicates that coupling was not achieved and sampling has not begun. Another advantage of this testing configuration is that pressurized samples can be also collected, if needed.

2.6.2 Sampling techniques

To collect in-situ groundwater/gas samples, the BAT probe system must be assembled as shown in Figure 2-10. Before placing the test container in the container housing, the air inside the container is removed by either applying vacuum to the container or by flushing and pre-charging the container with an inert gas that is not found in the ground. The time needed to collect a sample may vary from a couple of minutes to up to 24 hours or more. It depends on the soil type, sample collection technique and the difference in pressure between the inside of the container and the in-situ pore pressure. Experience gain during the course of this research indicates that collecting a sample in cohesionless soils can take from 30 to 90 seconds when vacuum is applied to the container and from 3 to 5 minutes when the container is precharged with a gaseous compound.

After sampling, the BAT probe is retrieved and the container is removed and sent to a laboratory for a gas chromatography (GC) test to analyze the free gas in the headspace of the container. The results from the GC test are used to determine the type of gases present in the ground and their concentrations. These results combined with data regarding the total volume of the container, the amount of pore water sampled, the pressure and temperature in-situ, and the solubility of each gas in pore water are used to compute the degree of saturation of the soil at the time of sampling. An example of the calculation of the degree of saturation is shown in Appendix B. If a small groundwater/gas sample is collected, the container can be placed back in the protective housing and the testing procedure can be repeated until a more representative sample is obtained.

2.6.2.1   Vacuum applied to the containers

The main advantage of this approach is that a higher pressure difference between the BAT container and the in-situ pressure is created, forcing the groundwater/gas to enter the container. This approach is ideal for collecting samples at shallow depths, where the in-situ pore pressure acting on the filter tip is relatively low and sampling may otherwise not be possible. To apply the vacuum, a hand vacuum pump is used. The maximum vacuum that can be achieved using the hand pump is in the order of 85-90% of vacuum. The main concern while using this approach is that after vacuum is applied, a small volume of air (10-15% of the volume of container) is left inside the container, introducing a certain degree of uncertainty in the results obtained from the gas chromatography test. The level of uncertainty is higher when the gases to be sampled are those already found in the atmosphere. This is particularly true in the case of blast densification, where the principal gas released during the explosion, nitrogen, is also the main gas present in air.

2.6.2.2   Container flushed and precharged with Helium

A sampling technique used to minimize the uncertainties in the calculations introduced by gases left inside the container consists of flushing and pre-charging the test container with an inert gas that is not found in the ground and, for this application, a gas that is not produced during blasting by typical explosives. For blast densification applications, Helium (He), Nitrous oxide (N_2O), and Argon (Ar) are inert gases that can be used for this purpose. None of these gases are present in the atmosphere at high concentrations, and therefore the gases sampled in the BAT container are a more realistic representation of the in-situ conditions. The gas selected for pre-charging the container must be detectable during a gas chromatography test. Therefore, it

must be a different gas than that used as the carrier gas in the GC test. By doing this, a more accurate and reliable measurement of the gas concentrations can be achieved.

Christian and Cranston (1997) recommended charging the container with a known gas under a pressure of 1 atm and at a temperature of 25 ^{o}C, to allow a simpler sample evaluation and computation of the degree of saturation. However, from the experience gained during this work, a more appropriate approach would be to pre-charge the container under a pressure slightly higher (i.e., 10 kPa) than the atmospheric pressure to ensure that no contamination enters into the container during assembly of the BAT probe or at any other time during sampling.

2.7 Summary

Blast densification is a relatively economical approach to densify loose, saturated sand deposits. Although the ground surface settles significantly after blasting, results from some field verification tests, including the CPT, SPT, and Vs, suggest that the soil mass experienced little to no improvement. Large amounts of gas are released into the soil during blast densification and some of this gas may remain trapped, in the form of free gas bubbles, for months or even years. Several studies conducted on high quality undisturbed samples collected at sites where the soil has been improved by using the sand compaction pile (SCP) technique have shown that air can remain in the soil for decades. Since nitrogen is a significant component of both air and explosion product, the long term behavior performance of the gas bubbles from blasting is expected to be similar to that of air bubbles from the SCP technique.

In the laboratory, several studies have shown that the presence of gas in the pore fluid affects the mechanical response of soil during monotonic and cyclic loading. In loose of critical sands, gas has the effect of increasing the shear resistance and cyclic liquefaction resistance during undrained loading. In dense of critical sands, gas has the effect of delaying the negative

pore water pressure development. The magnitude of the increase in resistance or delay in negative porewater pressure depends on the degree of saturation, initial confining pressure, and initial pore pressure.

The majority of the research conducted on gassy soils has been focused on samples collected from marine deposits with higher fines content and tested at greater stresses than those stresses used in this study. Static and cyclic triaxial compression tests conducted on medium to dense gassy sands are limited. Even more limited for specimens tested at pressures similar to those pressures where blast densification is applicable.

3   BLAST DENSIFICATION AT THE OAKRIDGE SANITARY LANDFILL SITE - PREVIOUS WORK

Blast densification is being used at the Oakridge Sanitary Landfill located in Dorchester county, approximately 55 kilometers from Charleston, SC. This is an ongoing effort that has been conducted by GeoSyntec Consultants and started in 1998. This work involved blasting to densifiy a potentially liquefiable loose sand layer at a depth of 7.5 m -13 m. Figure 3-1 shows an air photo of the site and Figure 3-2 shows a plan view of the site and timeframe for the blast densification program.

Figure 3-1.Tested site location, Dorchester (SC).
Google Earth (05/05/2011)
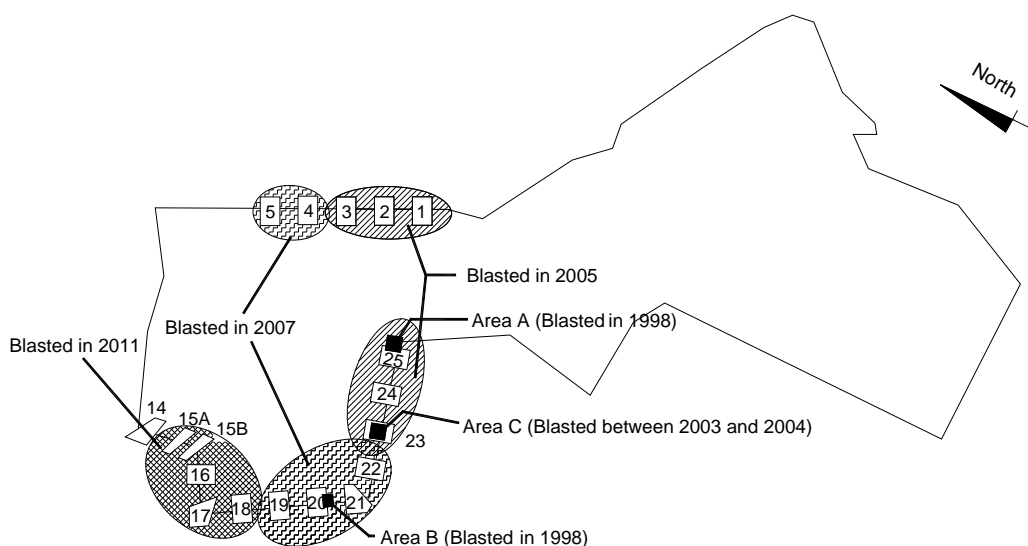
Figure 3-2. Plan view of the site showing blasted zones and timeframe for the blast densification program.

The first field testing program was conducted by GeoSyntec in 1998. The main objective of this pilot program was to evaluate the effect of blasting on a loose sand deposit at a test section. One of the outcomes of this pilot program was the development of significant surface settlements (i.e., 0.15 m to 0.46 m) within the tested area. However, CPT results indicated that little or no soil improvement was achieved after blasting. Based on these conflicting results, GeoSyntec recommended performing a major blast densification and instrumentation program to gain extensive information of the soil response during and after blast densification, and to optimize the blast densification design for the subsequent areas. This major blasting and instrumentation program was conducted between November of 2003 and August of 2004. Since then, blast densification of areas at the site has been conducted in 2005, 2007 and 2011.

3.1   Geology and site description

The geologic origin of a soil deposit is commonly used to assess the soil potential to liquefaction during an earthquake. For instance, soils deposited recently (i.e., within the past few thousand years) are more susceptible to liquefaction than soils deposited millions of years ago. Figure 3-3 and Figure 3-4 show a generalized geologic map of South Carolina and a geologic time scale for South Carolina, respectively. The surface soils in South Carolina were formed during the Quaternary period. The Quaternary period can be subdivided into the Holocene and the Pleistocene epochs. Holocene sediments are sediments that were deposited less than 10,000 years ago and Pleistocene sediments are sediments that were deposited more than 10,000 years ago and less than 1,600,000 years ago. Figure 3-3 shows that approximately 90% of the soils in Dorchester County, including the site location, were formed during the Pleistocene epoch. The age of the soil deposits and the lack of evidence of historic liquefaction in areas near the site (Weems, 1997) suggest that the local soils are not highly susceptible to liquefaction. This

empirical observation is not consistent with the results obtained from the field tests performed at

the site (CPT tip resistance tests, SPT tests, and Vs tests), which suggest that these soils are

susceptible to liquefaction and flow.
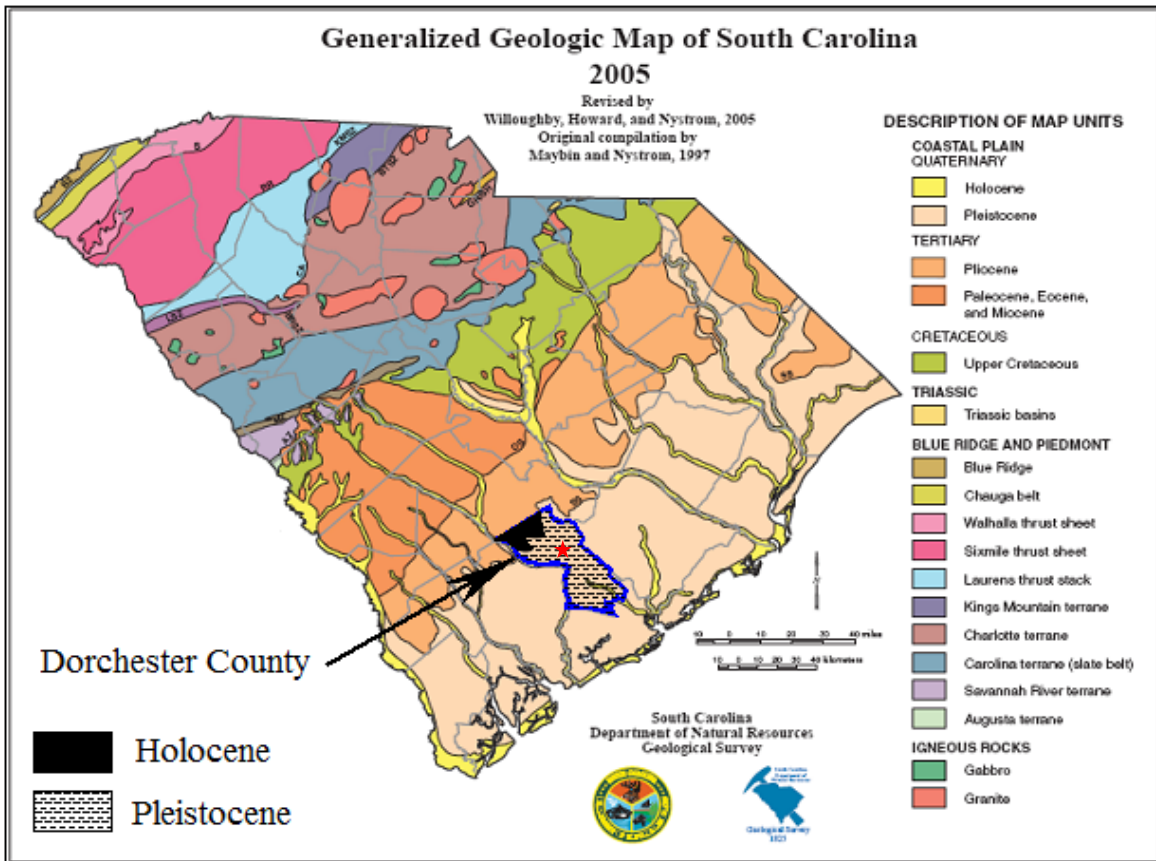
Figure 3-3. Generalized geologic map of South Carolina.
★ **Approximate location of the tested site.**

ERA	PERIOD		EPOCH	Geologic Events in South Carolina	MYA*
CENOZOIC	QUATERNARY		HOLOCENE	Barrier Islands formed; flood plains of major rivers established.	0.01
			PLEISTOCENE	Surficial deposits cover the underlying Coastal Plain formations. Carolina Bays develop; scarps form due to sea level rise and fall	1.6
	TERTIARY	NEOGENE	PLIOCENE	Coastal Plain sediments reflect large-scale regressive cycles. Off-lap of the ocean and scouring responsible for the Orangeburg scarp.	5.3
			MIOCENE	Uplift and erosion of Piedmont and mountains. Fluvial sediments spread over the Coastal Plain. Sandhill dunes deposited.	23
		PALEOGENE	OLIGOCENE	Deposition of carbonates predominates. Arches and embayments continue to influence deposition of Coastal Plain formations.	36.6
			EOCENE	Sand deposited in upper Coastal Plains; limestone deposited in middle and lower Coastal Plain. Fault activity.	53
			PALEOCENE	Fluvial, marginal marine and marine Coastal Plain sediments deposited.	65

Figure 3-4. Geology time scale for South Carolina, (*) million years ago.
(After SCDNR)

South Carolina has a high seismic hazard risk. Figure 3-5 shows that there is 20% probability of an earthquake of magnitude greater than 5.0 to be exceeded within the next 50 years (USGS). According to the 2009 earthquake probability mapping shown in Figure 3-6, the expected peak ground acceleration at the site with a 2 percent probability of exceedance within a 50-year period is between 0.7g and 1.0g
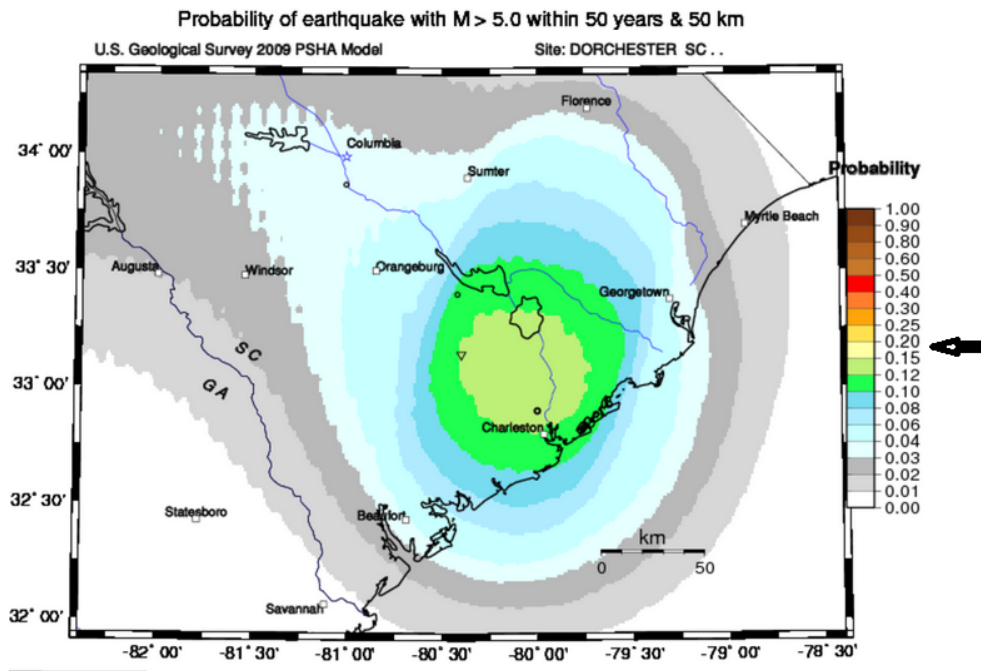
Figure 3-5. Probability of an earthquake with M>5.0 within 50 years.
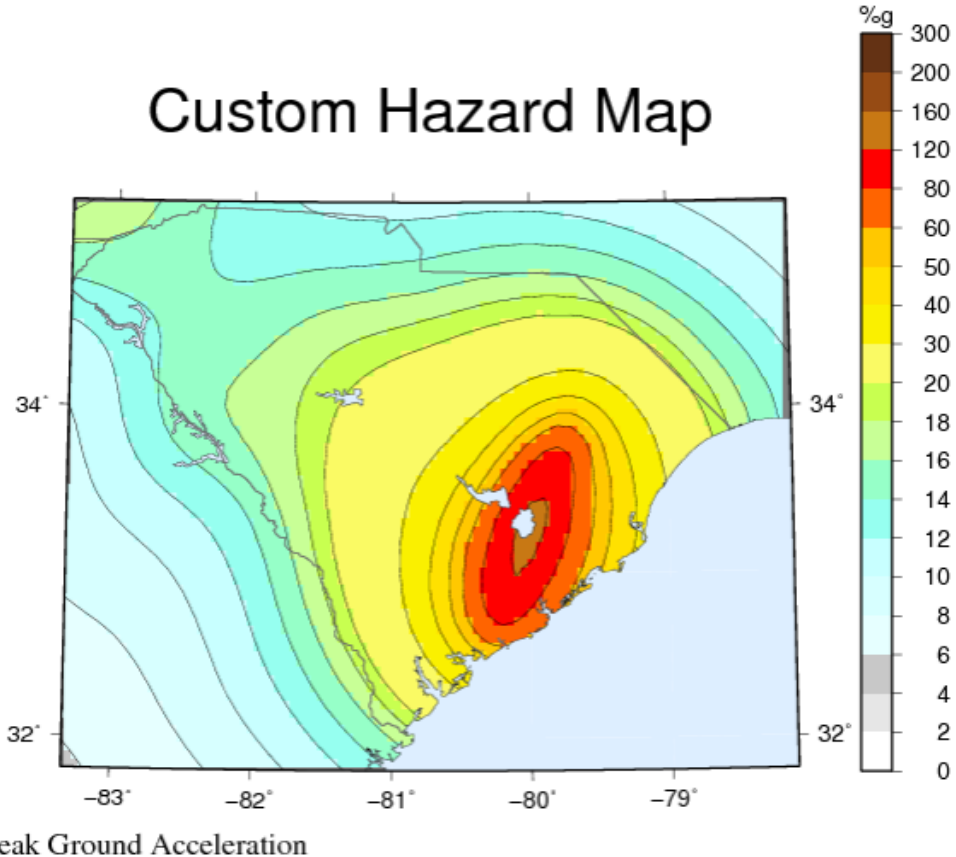
Figure 3-6. Expected PGA (%g) with 2% of probability of exceedance within a 50-year period.

The soil profile at the site is generally composed of six distinctive layers, as shown in Figure 3-7. Starting at the ground surface, the soil profile consists of (i) 1.0 m to 1.5 m fine-medium silty sand; (ii) 1.2 m to 3.0 m of silty clay and clayey sand; (iii) 3.0 m to 4.5 m of dense fine to medium sand; (iv) 0.3 m to 1.5 m of very loose fine sand; (v) 1.5 m to 4.5 m of loose fine sand; and (vi) more than 30 m of a fine sand and silty clay fossiliferous layer regionally known as Cooper Marl (GeoSyntec Consultants, 2005). The water table is located between 0.8-1.5 m below the ground surface.

The relative density inferred from the corrected tip cone penetration resistance at depths between 7.5 m and 12 m was $D_R \cong 12\%$ and the initial in-situ void ratio of this layer was estimated as $e_o \cong 0.97$ (Narsilio et al., 2009).
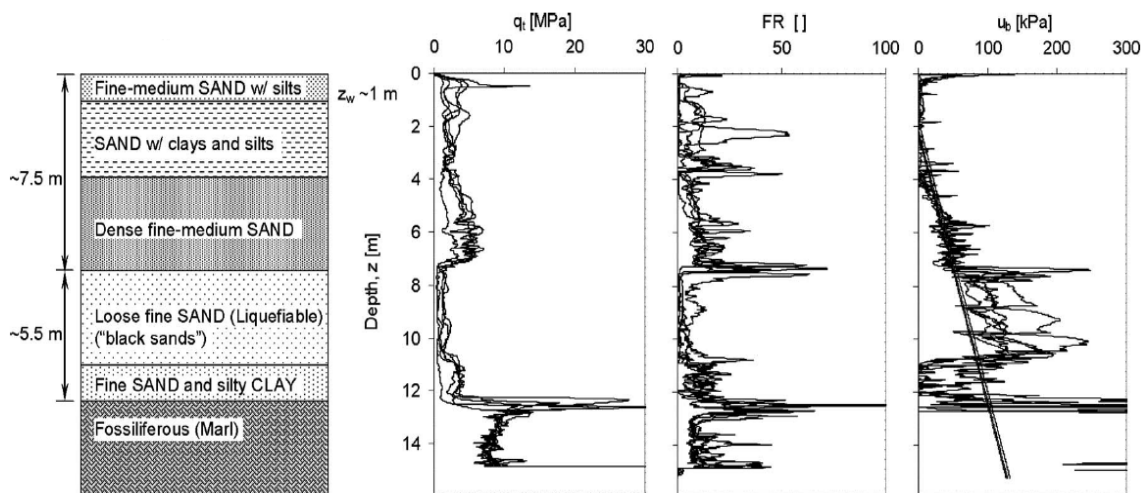
Figure 3-7. Typical soil profile; before-blasting CPT profiles at different locations within the site. Narsilio et al. (2009)

3.2 Soil parameters and index properties

GeoSyntec Consultants conducted a laboratory characterization program to evaluate the index and mechanical properties of the loose sand layer found at depths between 7.5m and 12m. The soil is clean, fine grained sand, SP, white, very angular in shapes; with little or no fines, as

indicated in Figure 3-8. The average uniformity coefficient (C_u) and curvature coefficient (C_c) were 1.47 and 0.87, respectively and the minimum and maximum void ratios were e_{min} = 0.52 and e_{max} = 1.096, respectively. The compression (C_c) and recompression (C_r) indices were C_c = 0.053 and C_r = 0.0036, respectively based on constrained compression test results. The percentage of fines passing sieve #200 was 0.73% by weight when the standard (dry) sieve analysis was conducted. When the washed sieve analysis was conducted, the C_u and C_c coefficients were 1.75 and 1.15, respectively and the percentage of fines passing sieve #200 was 3.8% by weight.
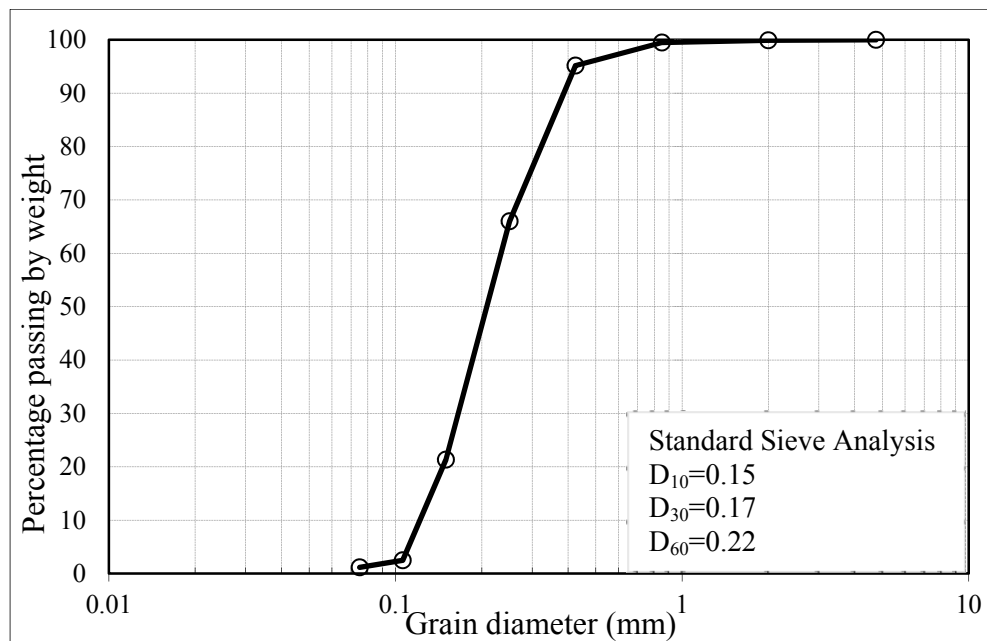
Figure 3-8. Typical grain size distribution.

3.3   Previous blast densification programs at the test site

Since 1998, GeoSyntec Consultants has been in charge of designing and evaluating the ground improvement of the loose sand layer at the site to prevent liquefaction and flow during an earthquake. The loose sand is generally located between 7.5 m and 13 m below the ground

surface. As shown in Figure 3-9, the ground improvement is to be conducted around the 1500 m

perimeter berm in the Phase II area before construction of the Phase II cells begins. The target

perimeter was divided into approximately 25 ground improvement zones (only 18 of these zones

are shown in Figure 3-9), with most of the zones measuring 30.5 m x 45.7 m and separated by a

distance of 30.5 m along the perimeter alignment.
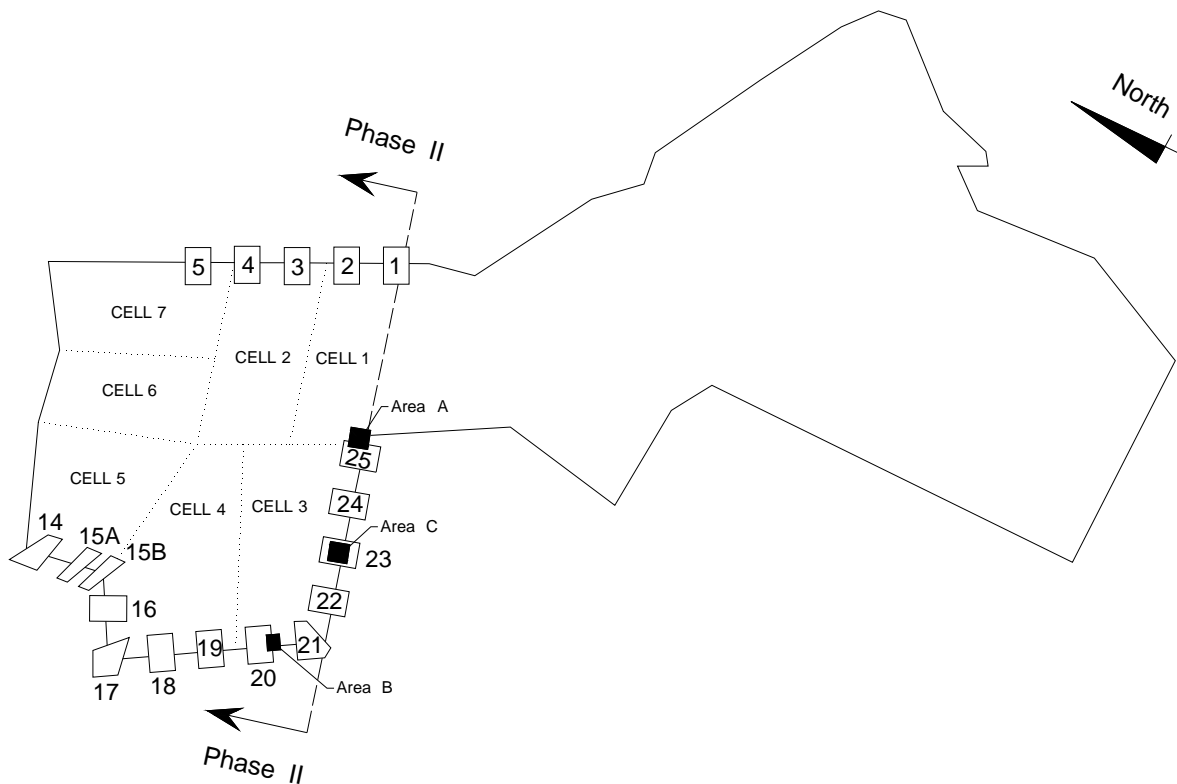
Figure 3-9. Site plan and ground improvement zones.

The blast densification program was conducted in the following sequence: (i) test areas A

and B were blasted during the pilot program in 1998; (ii) test area C was heavily instrumented

and blasted between November 2003 and August 2004; (iii) zones 1, 2, 3, 23, 24, and 25 were

blasted in 2005; (iv) zones 4, 5, 19, 20, 21, 22 were blasted in June 2007; and (v) zones 15A,

15B, 16, 17, 18 were blasted between February 2011 and April 2011.

3.3.1 Blast densification – Pilot program (1998)

GeoSyntec Consultants conducted a pilot program to evaluate the effectiveness of the blast densification design and to gain a better sense of the soil response during blasting (GeoSyntec Consultants, 1998). Two areas with dimensions of 18.3 m x 18.3 m (test area A) and 12.2 m x 12.2 m (test area B) were selected to accomplish these purposes. Test area A consisted of two square grid coverages. The first coverage consisted of nine holes spaced 12.2 m apart and the second coverage of four holes located at the centers of the first coverage grid. The second blast event was detonated one week after the first blast event. Test area B consisted of nine holes distributed in a square pattern and spaced 9.1 m apart. In both test areas, the weight of the charge range from 16 kg to 25.4 kg at each hole and was placed at the middle of the target loose sand layer. The charges were detonated with delays of 18 ms between detonations. The explosive used for this project was Hydromite 860 WWP, which is an emulsion-based waterproof product.

Although ground surface settlements after blasting were on the order of 0.46 m and 0.23 m at the center of test area A and B, respectively, cone penetration resistance and shear wave velocities conducted three years after blasting showed little or no improvement of the ground. Based on these findings, GeoSyntec proposed to conduct a major blast densification and instrumentation program on a nearby zone to gain knowledge about the soil response during and after blasting and to optimize the blast densification design before full-scale field implementation.

3.3.2 Blast densification and instrumentation program (November 2003 – August 2004)

A blast densification and instrumentation program was conducted by GeoSyntec Consultant in an 18.3 m x 18.3 m area. Figure 3-10 shows a plan view of this test area, called test area C.

Four blast coverages were implemented to achieve greater settlements than in the pilot program. The explosive charges were installed at a depth of 10 m and placed in a square grid pattern with a fixed spacing of 9.1 m. The first coverage consisted of nine holes with individual charges of 19 kg and detonation delays of 100 ms between rows. The second coverage consisted of 16 holes with individual charges of 34 kg and detonation delays of 50 ms. The third and fourth coverages consisted of six and seven holes respectively with individual charges of 11 kg each and wait periods between rows of 10 minutes. The explosive used for this project was Hydromite 860 WWP (powder factor 39.7 grams/m^3).
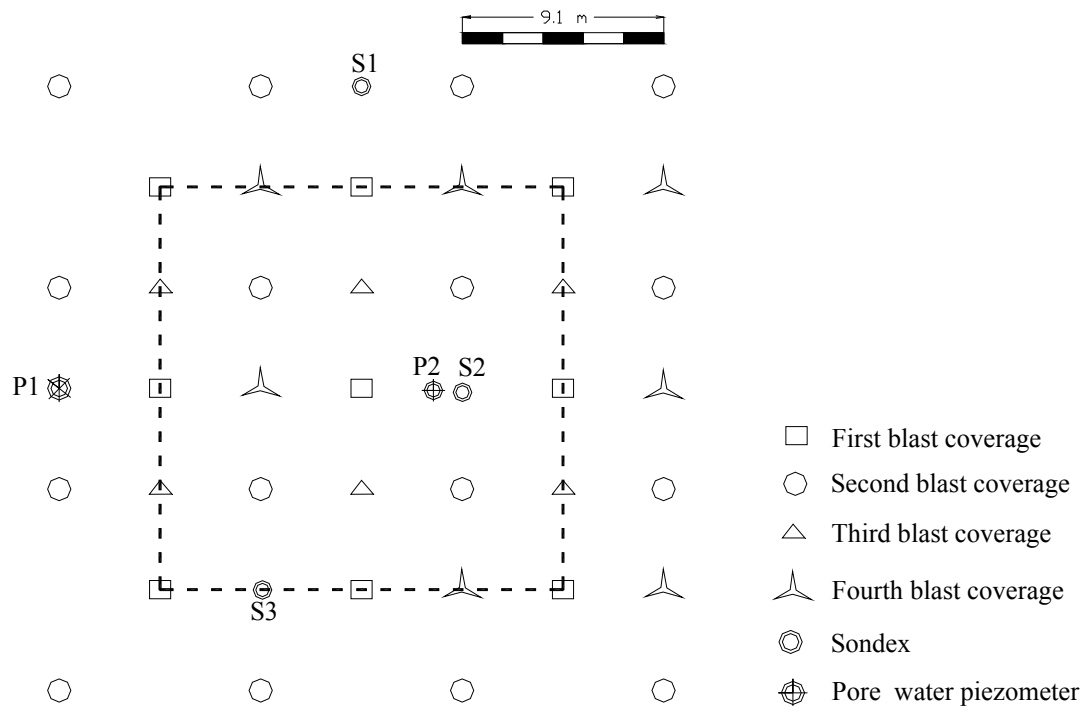
Figure 3-10. Location of the explosives and instrumentation.
After Narsilio et al. (2009)

The monitoring program included a standard optic survey for measuring ground surface settlements, three sondex systems for measuring vertical deformation at depth, geophones for vibration monitoring located at 9, 12, 15, and 18 m away from the perimeter of the blasted zone

along the N-S centerline, sCPTu penetration sounding for measuring soil penetration improvement, ground penetrating radar, and two vibrating wire piezometers for pore water pressure measurements located at the center and along the perimeter of the blasted zone. The following sections present some field results from this testing program. This test section was heavily instrumented and monitored but only the results considered relevant for the purpose of this dissertation are described. For more information, refer to Narsilio et al. (2009).

Ground Surface Settlements: Standard topography surveys were conducted before and after each of the blast events. Figure 3-11 shows the maximum recorded settlements along the centerline of the long direction. The maximum settlement after the fourth blast event was approximately 0.50 m and occurred at the center of the tested zone. The amount of densification achieved incrementally was smaller for each successive blast. The majority of the ground settlements occurred within 24 hours after the blast. Assuming 1-D conditions and all strains occurred in the loose layer, this compression corresponded to an average volumetric strain of 12% in the loose sand layer.
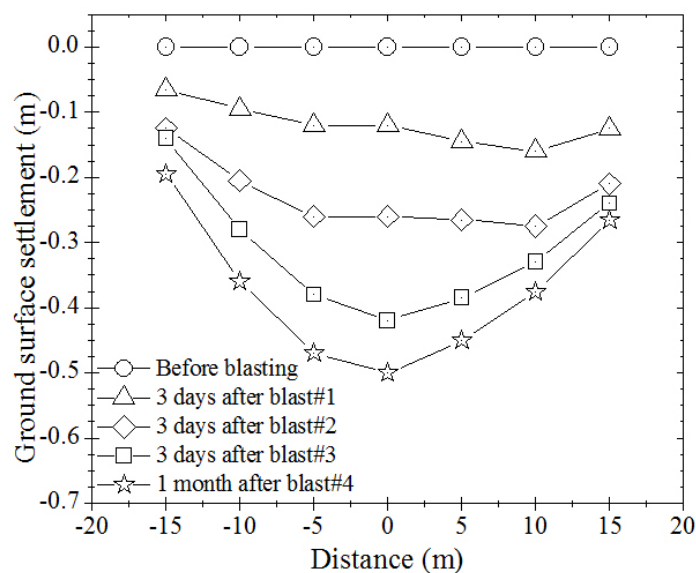
Figure 3-11. Surface settlement during and after blasting – Zone C.

Subsurface settlements: Three sondex tubes were installed in the ground to monitor the subsurface settlements. A sondex tube consists of a corrugated pipe and sensing rings spaced at a regular intervals or at depths of interest. The corrugated pipe and surrounding soil are coupled by filling the gap between the borehole and the sondex pipe with soft grout. This coupling allows the pipe and sensing rings to move as the ground settles. The vertical deformations of the ground after each blast event are measured by lowering the sondex probe down into the pipe to locate each of the sensing rings.

Figure 3-12 shows the typical vertical deformations at the center and on the perimeter of the tested site. These results indicated that the soil above the loose layer (from z=0 to z=-7.5 m) showed little differential vertical movement, indicating that the soil mass between these depths moved as a "rigid" block and the ground surface settlements were mainly due to the densification of the loose sand layer (z=-7.5 m to z=-13 m). The heave recorded between z=-12 m and z=-14m after the first blast event was attributed to the release of tensile stresses in the sondex tube locked in during the installation (Narsilio et al., 2009).
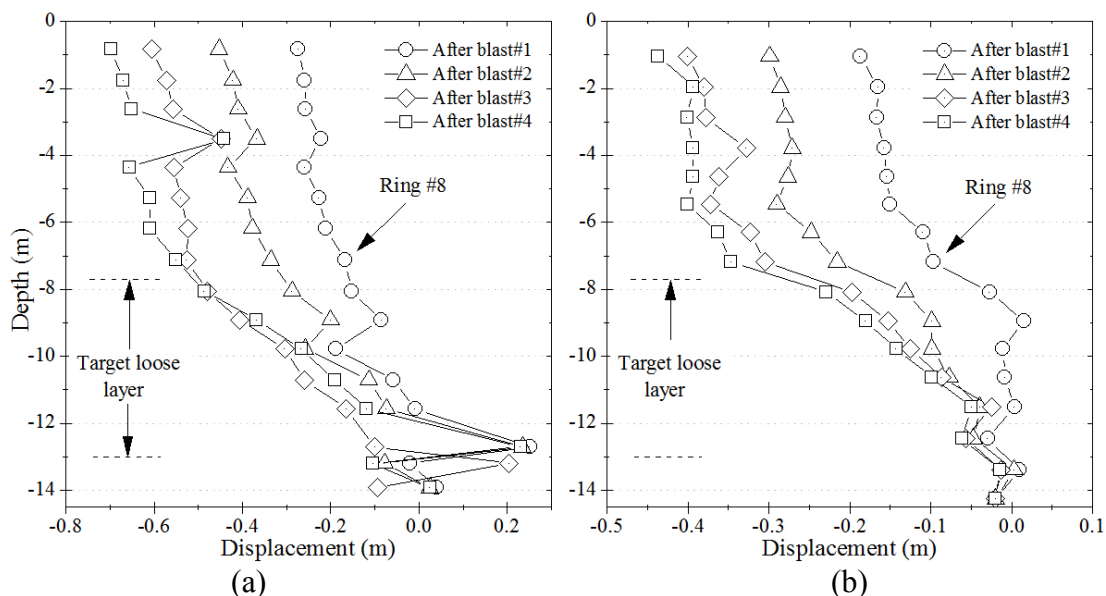
Figure 3-12. Subsurface settlements (a) center and (b) perimeter.
After Narsilio et al. (2009)

Pore water pressure measurements: Two vibrating pore-water pressure piezometers were installed at the center and outside of the test area. Piezometer 1 (P1) and piezometer 2 (P2) were installed at a depth of 10.5 m and 11.5 m, respectively. The pore water pressure was recorded every 2 seconds during the first hour after blasting and every 2 minutes thereafter (Narsilio et al., 2009). The results on Figure 3-13 show that liquefaction was achieved after each blast event, indicating that the mechanism during blast densification hypothesized in section 2.2 is reasonable. The dissipation of the excess pore water pressure occurred in approximately 24 hours.
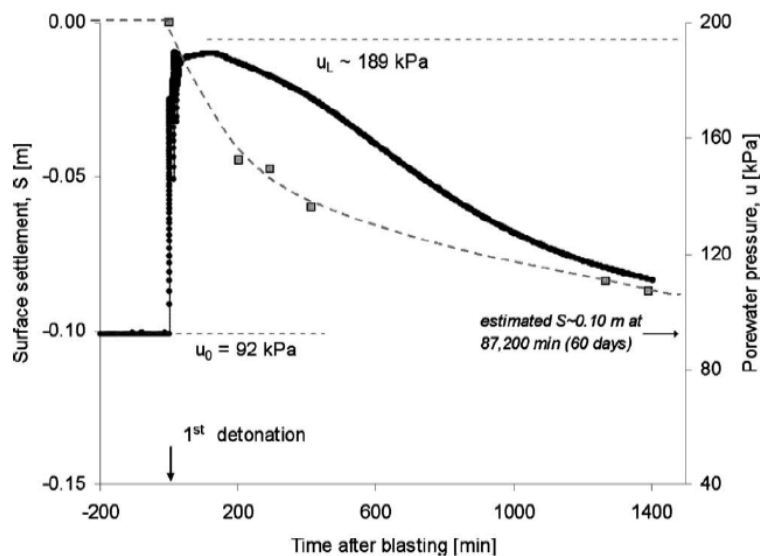
Figure 3-13. Typical pore water pressure dissipation (solid lines) - Settlements (squares).
(Narsilio et al., 2009)

Cone penetration and shear wave velocity tests: Although more than 0.5m of ground surface settlement was recorded after the fourth blast event, seismic CPTu penetration soundings and shear wave velocity tests did not show a clear increase in soil resistance. Figure 3-14 shows the evolution over time of the CPTu and Vs in the loose sand layer (z≈7.5 m – z≈ 12 m). It can be observed that 2.8 years after the fourth blast event there was an increase in soil penetration

resistance in the bottom half of the target layer. However, the top half did not show any increase in tip penetration resistance or shear wave velocity. These results were similar to those obtained in the pilot program (Test area A and B in section 3.3.1) where CPTu and Vs measurements showed little or no soil improvement three years after blast densification.
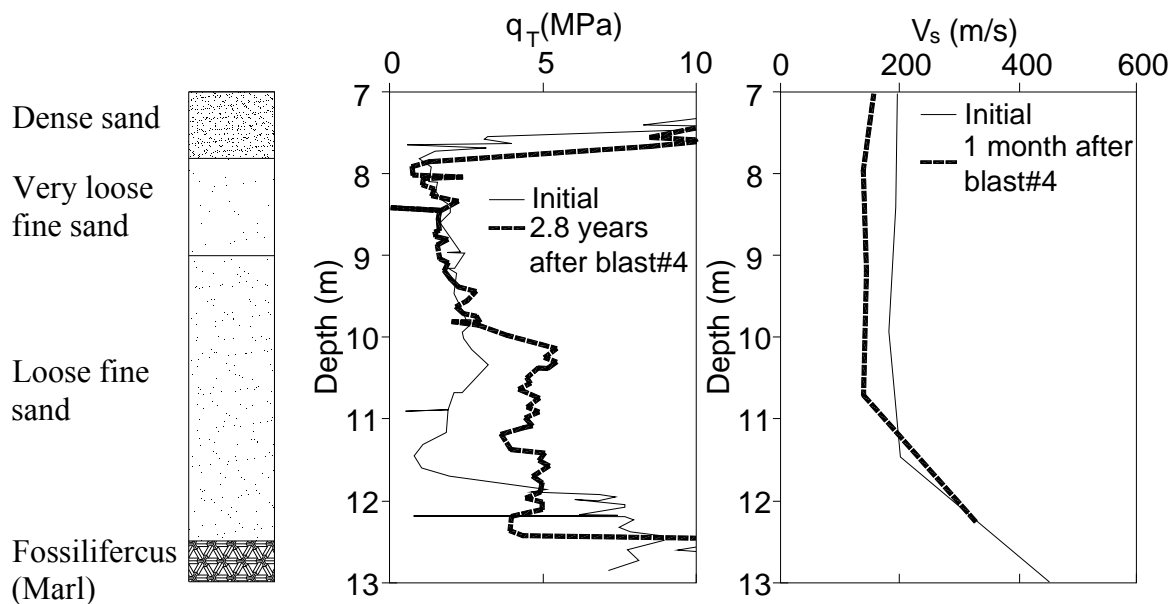
Figure 3-14. Typical CPT tip resistance and Vs before and after blasting – loose layer. After Narsilio et al. (2009) and GeoSyntec Consultants (2005)

3.3.3 Blast densification program (December 2005 - June 2006)

Zones 1, 2, 3, 23, 24, and 25 were blasted by GeoSyntec Consultants between December of 2005 and June of 2006. Table 3-1 lists a summary of seismic CPTu soundings conducted in these zones. The average thickness of the loose sand layer before blasting, inferred from the CPT soundings, varied from 2.4m to 4.1m. In average, the depth to the top of the loose sand layer was 7.6 m. Figure 3-15 shows the blasting configuration in each zone. Zones 1, 2, and 3 were subjected to four blast events each and zones 23, 24, and 25 to three blast events each. A total

weight of approximately 15.4 kg of explosives was placed in each blast hole at a depth of 10 m.

The explosive used for this project was Hydromite 860 WWP.

Table 3-1. Summary of CPT results in zones 1, 2, 3, 23, 24, and 25.

Zone	CPT #	Depth to top of loose sand (m)	Loose ave. layer thick. (m)	# events	CPT values (MPa) before blasting	Ave. Sett. (m)
1	1-1	7.6	3.4	4	2.4	0.38-0.40
	1-2	7.9			3.7	
2	2-1	7.8	2.8	4	2.9	0.38-0.40
	2-2	7.9			3.8	
3	3-1	7.6	2.4	4	1.9	0.33-0.35
	3-2	7.6			2.4	
	3-3	7.9			2.4	
23	23-1	7.6	4.1	3	2.9	0.18-0.20
	C-1	7.8			1.4	
	C-2	7.6			2.9	
24	24-1	7.8	4.0	3	2.7	0.42-0.50
	24-2	7.6			2.9	
25	25-1	7.5	3.7	3	2.4	0.22-0.32
	25-2	7.0			2.5	
	25-3	7.0			2.4	
	A	7.3			1.9	
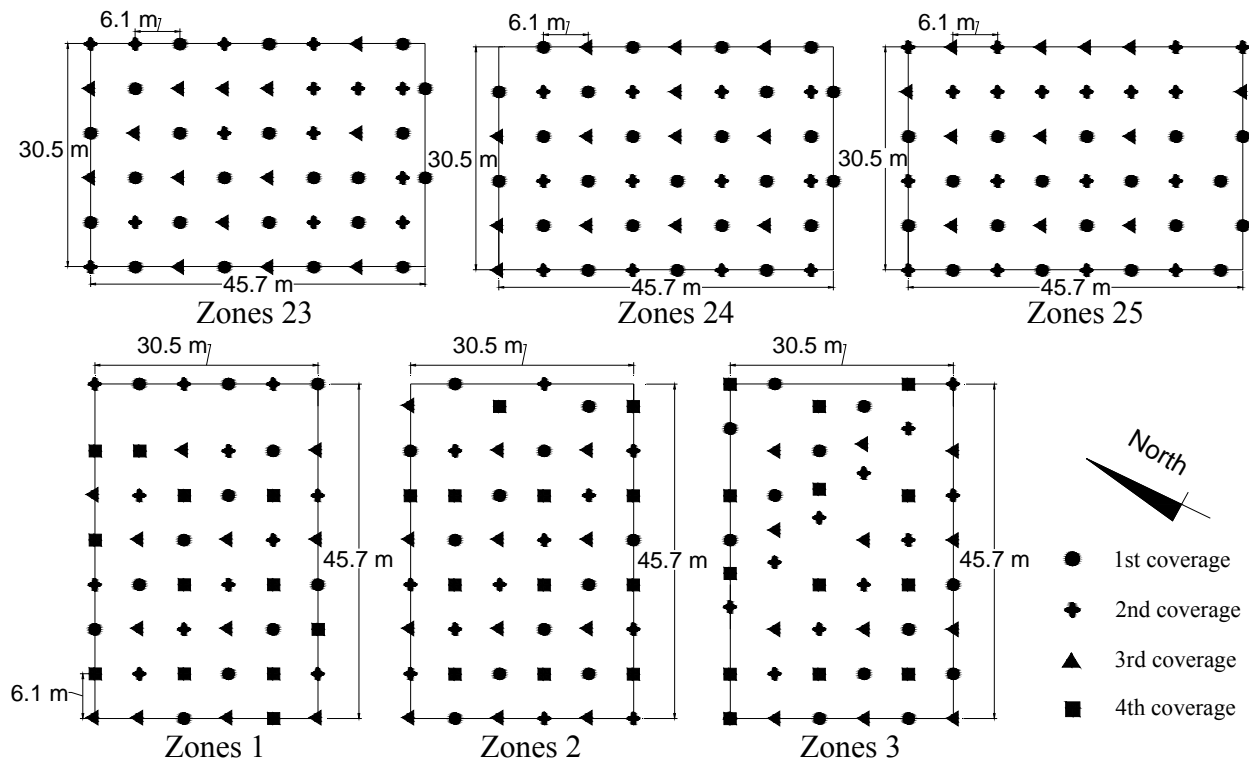
Figure 3-15. Blasting configuration in zones 1, 2, 3, 23, 24, and 25.

Figure 3-16 shows the ground surface settlements along the centerline of the long direction measured after blasting. The survey data showed that the average surface settlements at all zones after blasting varied between 0.18 m and 0.45 m. The concave down shape of the settlement profile shown in zone 23 indicates that either heave was induced at the center of the zone by the energy released during blasting or the soil recently deposited on the ground surface after blasting was not properly removed before the topographic survey.

Figure 3-17 shows the calculated axial strains in zones 23, 24 and 25 after three blast events and in zones 1, 2, and 3 after four blast events. The settlements shown in Figure 3-16 correspond to an average axial strain in the targeted layer of $\varepsilon_a \approx 8\%$ for 3 blast events and $\varepsilon_a \approx 12\%$ for 4 blast events. In general, the cumulative axial strain increases as the number of blast events increases.
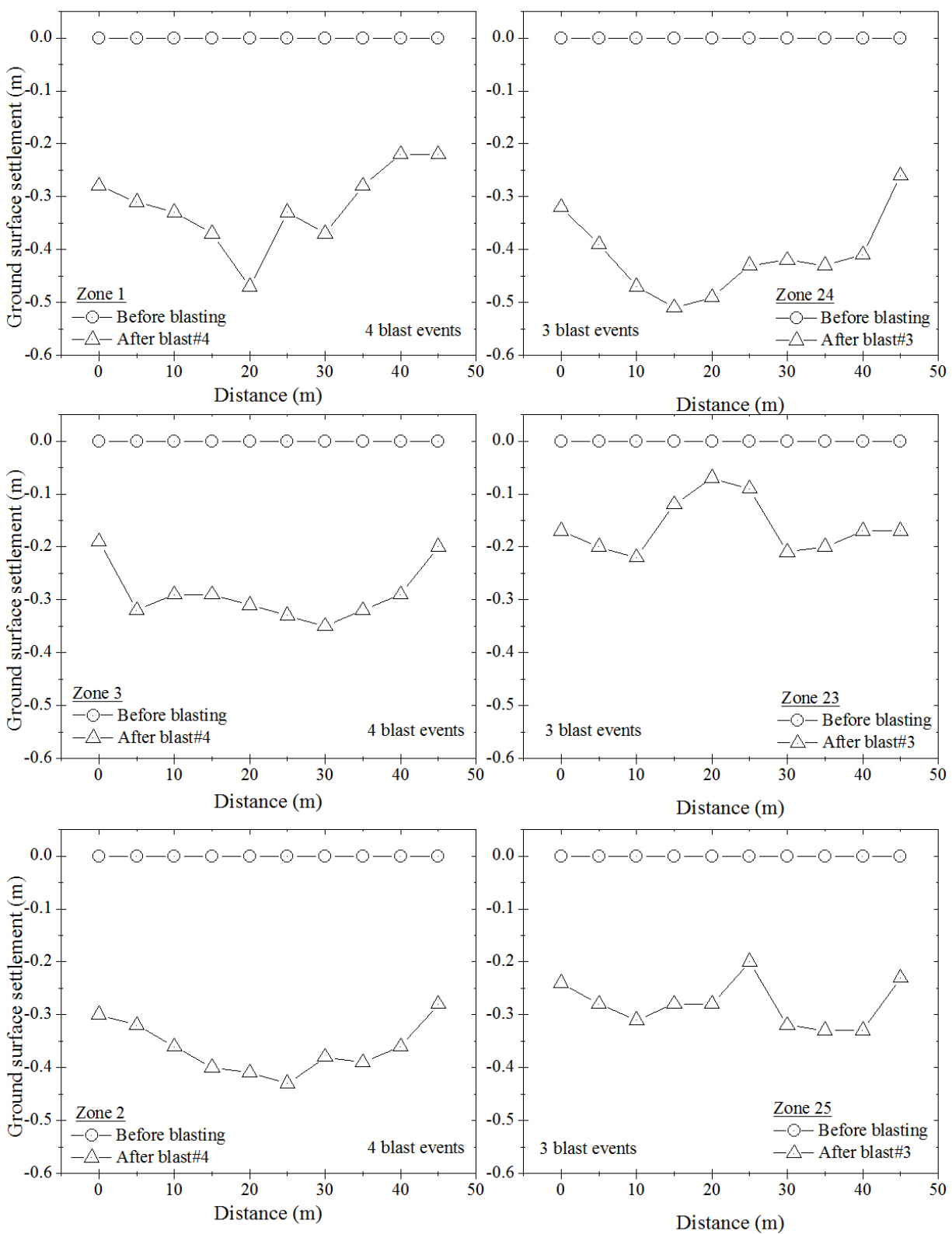
Figure 3-16. Ground surface settlement pre-blasting and post-blasting – Zones 1, 2, 3, 23, 24, and 25.
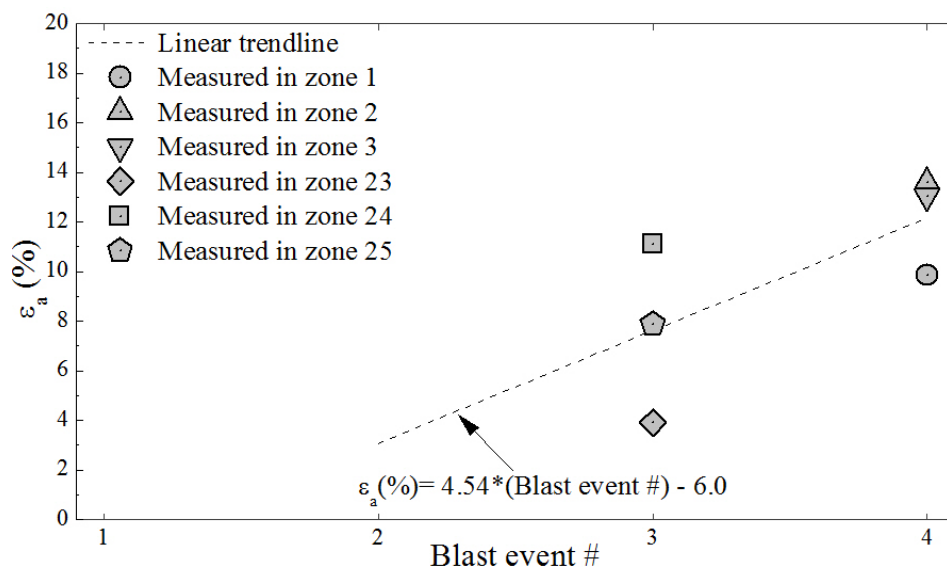
Figure 3-17. Cumulative axial strain after blasting in zones 1, 2, 3, 23, 24, and 25.

3.3.4 Blast densification program (2007)

Zones 4, 5, 19, 20, 21, 22 were blasted in June of 2007 (GeoSyntec Consultants, 2007). CPT

tip resistance soundings were conducted to determine the depths at which the loose sand layer is

encountered. Table 3-2 presents the results from these tests. The thickness of the loose sand layer

varied from 2.1m to 2.8m in zones 4 and 5, and from 2.1m to 3.8m in zones 19, 20, 21, and 22.

In average, the depth to the top of the loose sand layer was 7.3 m.

Table 3-2. Summary CPT results in zones 4, 5, 19, 20, 21, and 22.

Zone	CPT #	Depth to top of loose sand (m)	Loose ave. layer thick. (m)	# events	CPT values (MPa) - before blasting	Ave. Sett. (m)
4	C4-1	7.0	2.8	4	1.9	0.40-0.50
	C4-2	7.0			1.7	
5	C5-1	7.6	2.1	4	1.9	0.20.-0.22
	C5-2	7.0			1.9	
19	C19-1	8.0	3.8	3	1.9	0.31-0.33
	C19-2	8.2			2.1	
20	C20-1	6.8	2.1	3	2.9	0.24-0.26
	C20-2	7.5			1.4	
21	C21-1	7.0	2.1	3	1.8	0.21-0.23
	C21-2	7.3			1.8	
22	C22-1	7.4	3.3	3	1.9	0.18-0.20
	C22-2	7.6			1.4	

Figure 3-18 shows the blasting configuration in each zone. Zones 19, 20, 21, and 22 were subjected to three blast events each and zones 4 and 5 to four blast events each. A total weight of approximately 15.4 kg of explosives was placed in each blast hole at a depth of 10 m. The explosive used for these zones was Hydromite 860 WWP.

Zones 19, 20, and 22

Zones 4 and 5

Zone 21

● 1st coverage
■ 2nd coverage
▲ 3rd coverage
✚ 4th coverage
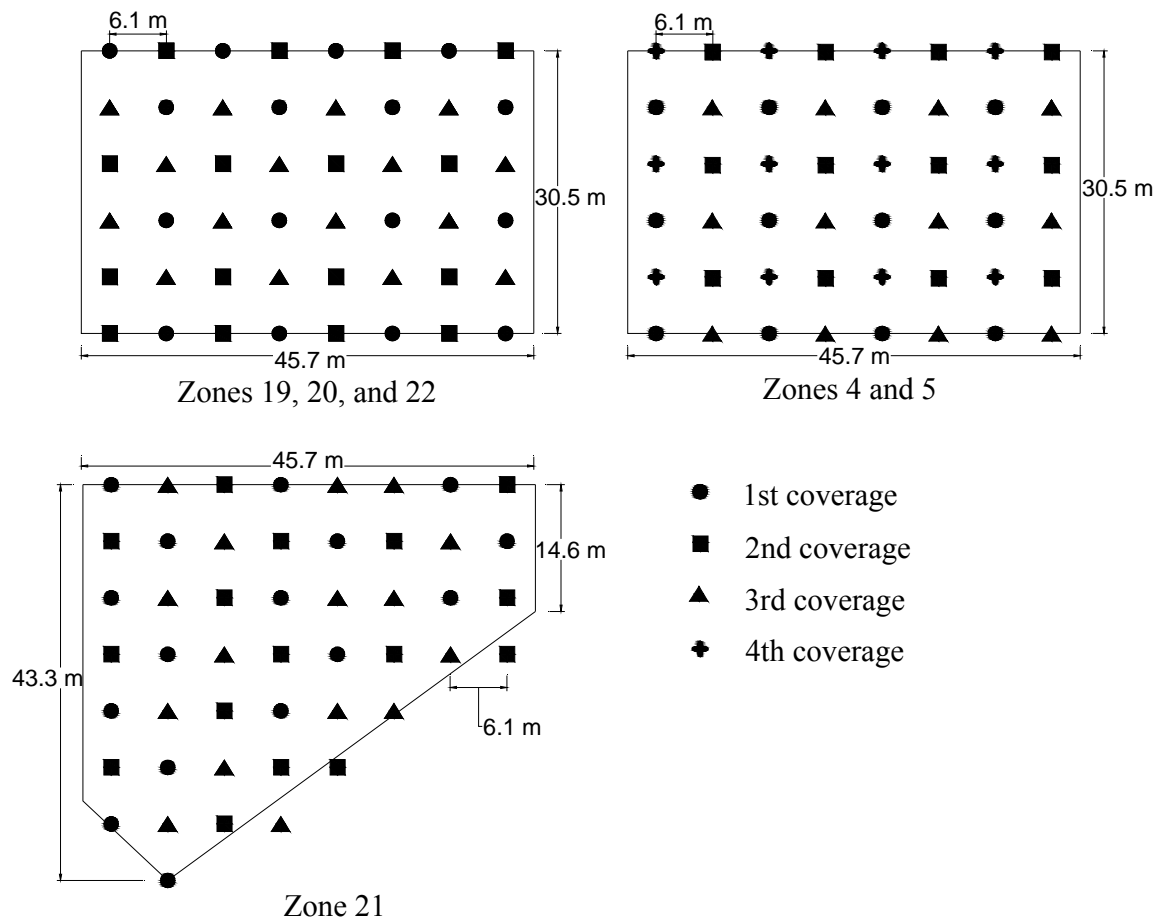
Figure 3-18. Blasting configuration in zones 4, 5, 19, 20, 21, and 22.

Figure 3-19 shows the ground surface settlements after blasting, along the centerline of the blasted zones. The average ground settlements at all zones after blasting varied between 0.18 m to 0.50 m. In general, the maximum settlement occurred at the center of the site and the incremental surface settlement decreased after each consecutive blast. The settlements measured

in zone 4 and 5 were different from the other zones. These differences could be the result of a difficulty to access the monitoring points after blasting - some zones could have been flooded when the topographic survey was conducted (see Figure 7-2) -, or the soil deposited on the ground surface after blasting was not properly removed before the topographic survey. These two observations could explain the heave and the concave down shape of the settlement profile measured at these two zones.

Figure 3-20 shows the cumulative axial strains in zones 4, 5, 19, 20, 21, and 22. The average volumetric strain in the targeted layer was 2%, 6%, 9% and 12% after the first, second, third and fourth blast event, respectively. The volumetric strain computed in zones 4 was not included in this analysis because it was considered inaccurate and unreliable.
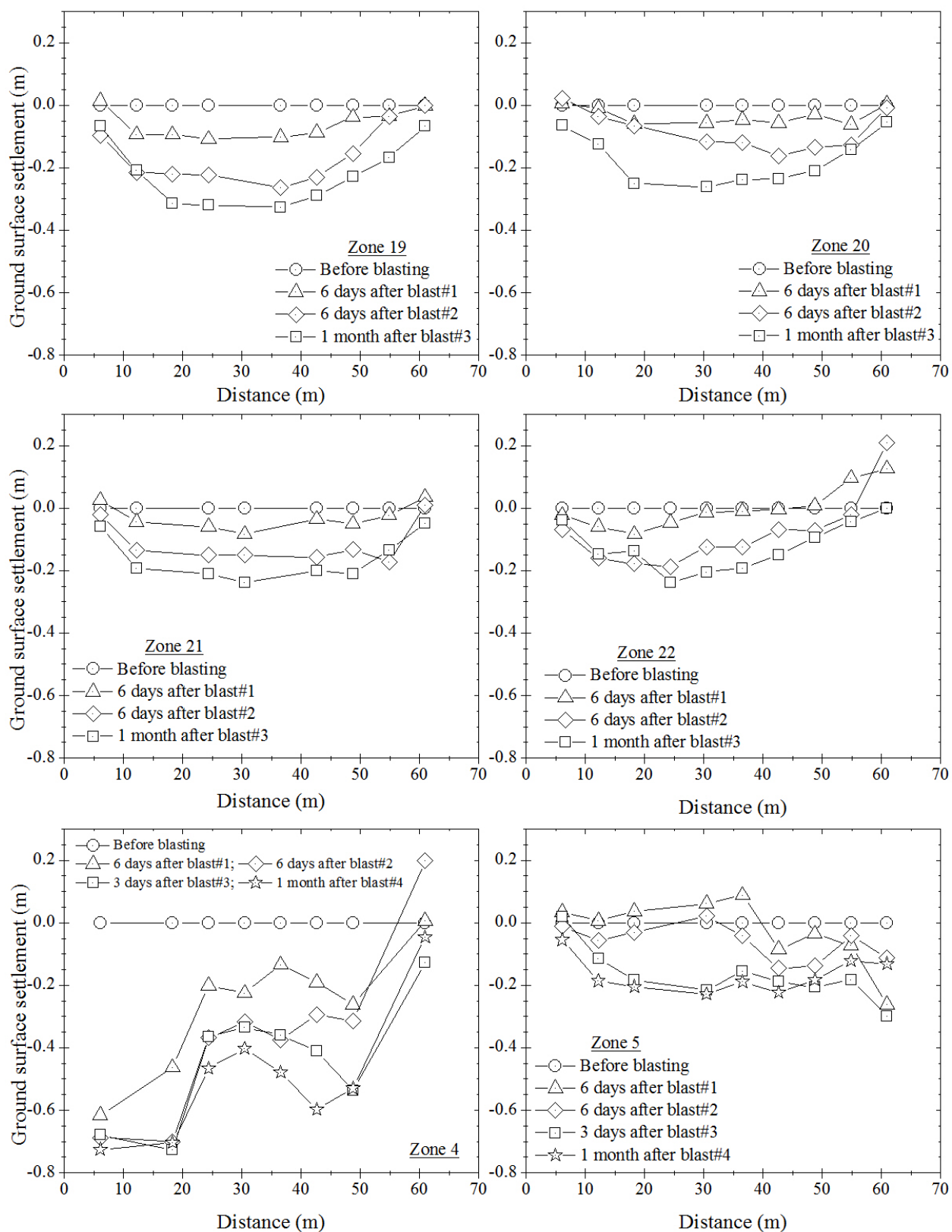
Figure 3-19. Ground surface settlement during and after blasting – Zones 19, 20, 21, 22, 4 and 5.
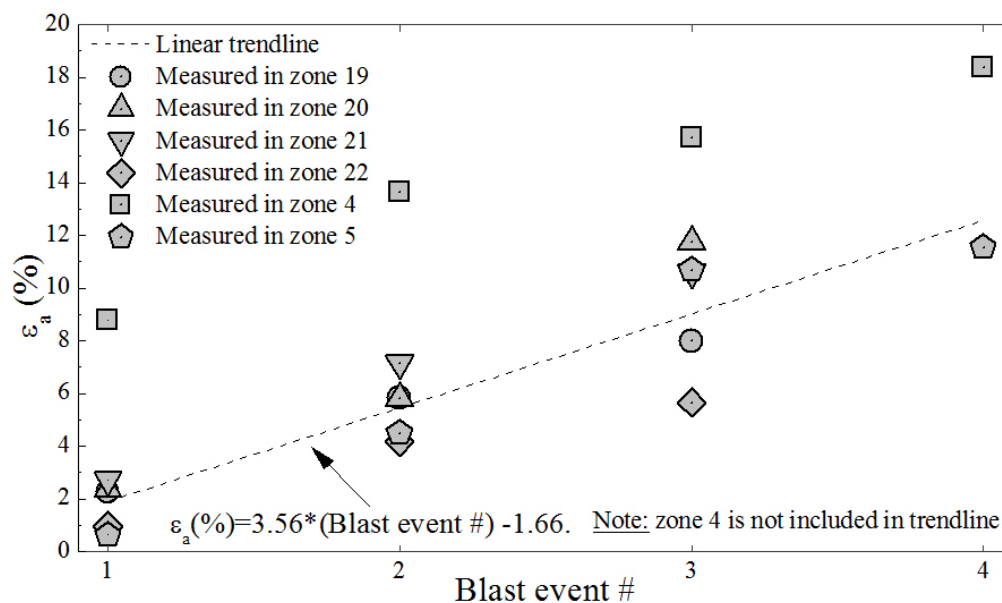
Figure 3-20. Cumulative axial strains in zones 4, 5, 19, 20, 21 and 22.

3.4 Summary

GeoSyntec Consultants has been implementing a large blast densification program at the Oakridge Sanitary Landfill. This work started in 1998 and consists of densifying a potentially liquefiable loose sand layer at a depth from 7.5 m to 13 m. A major blasting and instrumentation test section was conducted between November of 2003 and August of 2004. Since then, blast densification of areas at the site has been conducted in 2005, 2007 and 2011.

The ground surface settlements measured along the centerline of the long direction of each blasted zone showed that densification of the soil mass occurred after blasting and the amount of densification achieved incrementally is smaller for each successive blast. In general, the maximum settlement occurred at the center of the targeted layer and the majority of the settlements were achieved after the second blast event. Sondex tubes installed in the ground to monitor subsurface settlements indicated that the soil mass above the loose layer moved as a "rigid" block and the ground surface settlements were mainly due to the compression of the loose sand layer.

The porewater pressure piezometers installed at the center and outside of zone C showed that liquefaction was induced in the loose layer after each blast event, indicating that the mechanism described in section 2.2 is appropriate to describe the phenomenon of liquefaction. The dissipation of the blast-induced porewater pressure and the ground surface settlements associated with it occurred in approximately 24 hours.

Although the ground surface settled significantly after blasting, seismic CPT penetration soundings and shear wave velocity tests conducted three years after blasting showed little or no improvement of the ground. This apparent indication of a relative lack of "improvement", as indicated by the lack of increase in the tip resistance or shear wave velocities will be studied in the next chapters.

4 BLAST DENSIFICATION AT THE OAKRIDGE SANITARY LANDFILL SITE – NORTHWESTERN EFFORTS IN 2011

The most recent blast densification program was conducted between February and March of 2011. This work was a joint effort between Northwestern University and GeoSyntec Consultants. The data collected by GeoSyntec from the previous work was used to implement a monitoring program similar, but with some additions, to those conducted previously. The main addition to this field program was the use of the BAT probe system to collect groundwater/gas samples to identify the type of gases released during blasting and their in-situ concentrations. Figure 4-1 shows the zones along the perimeter of the landfill that have been improved since 1998. The densification program conducted in 2011 consisted of improving the ground condition of zones 15A, 15B, 16, 17, and 18.

During this phase of the work, GeoSyntec Consultants conducted cone penetration soundings to determine the depth and thickness of the loose layer at these zones, coordinated the installation and detonation of the explosives, and conducted standard topographic surveys along the centerline of the zones before and after each blast event. Northwestern University analyzed the data collected by GeoSyntec, monitored porewater pressures before and after each blast event, and collected and analyzed groundwater/gas samples.
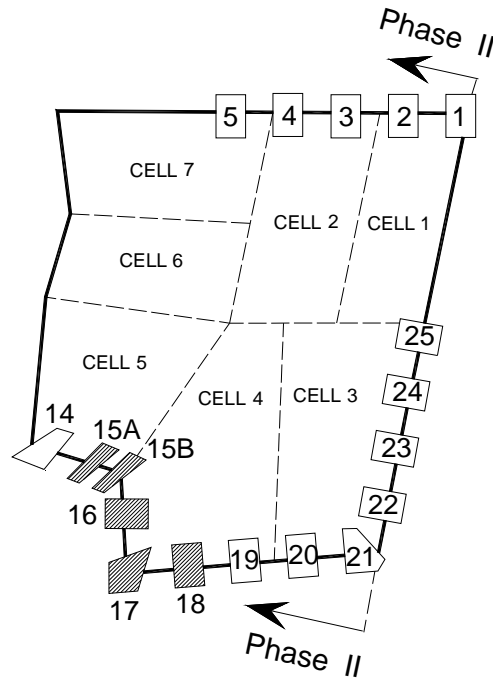
Figure 4-1. Zones blasted in 2011 (black-hatched areas).

4.1 Blasting configuration

Figure 4-2 and Figure 4-3 show the site geometry and blasting configuration of zones 15A, 15B, 16, 17 and 18. A total of four blast coverages were implemented at each zone to achieve the desired ground surface settlement. The explosive charges were placed at a depth of approximately 10 m (middle of loose sand layer) and spaced in a square grid pattern with a fixed spacing of 6.1 m. The explosive used for this project was Hydromite 860, and a total weight of approximately 15.4 kg was placed in each blast hole.
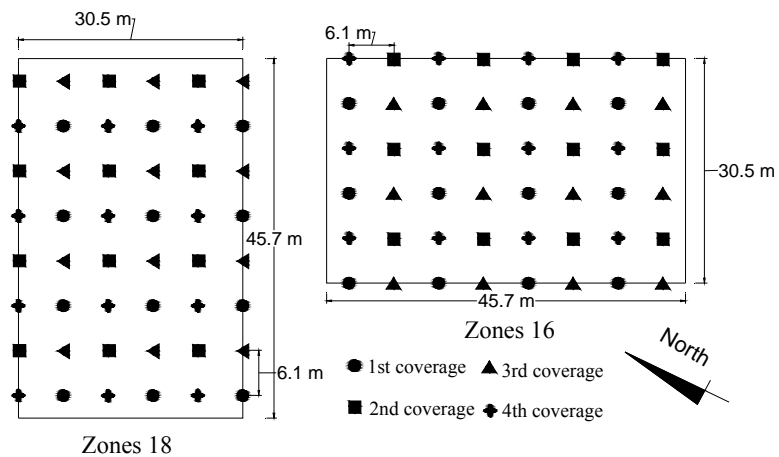
Figure 4-2. Blast configuration of zones 16 and 18.
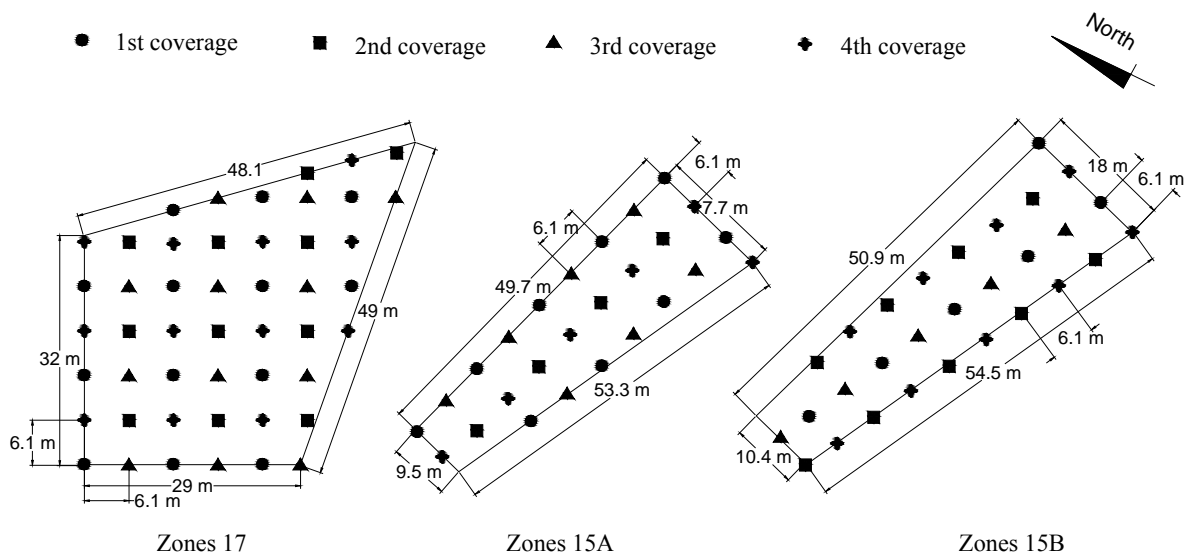
Figure 4-3. Blast configuration of zones 15A, 15B and 17.

4.2 Cone penetration testing

Figure 4-4 shows the CPT soundings were performed before blasting in zones 15A, 15B, 16, 17, and 18 to determine the tip resistance in the loose sand layer and to estimate the depth at which this layer is encountered. The results from these soundings are summarized in Table 4-1. In average, the depth to the top and thickness of the loose sand layer is 7.6 m and 3.85 m, respectively. Only the portions of the sand deposited in a very loose to loose state, N-values < 10

or $^{q_c}/_{P_a} < 4$ MPa (Kulhawy and Mayne, 1990), were considered to contribute to ground surface

settlements after blasting.
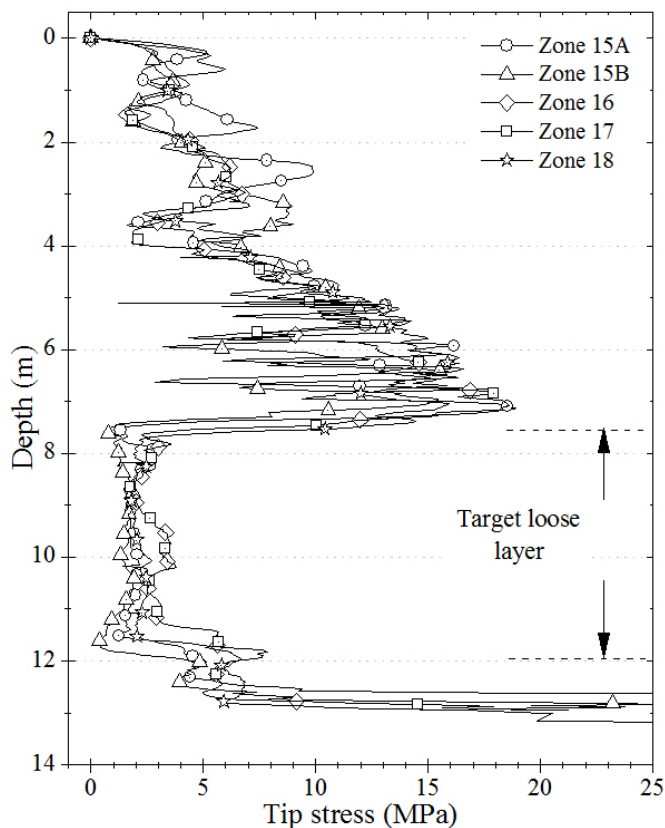
Figure 4-4. Typical CPT results – Zones 15A, 15B, 16, 17 and 18.

Table 4-1. Summary of data from CPT tests in zones 15A, 15B, 16, 17, and 18.

Zone	CPT #	Depth to top of loose sand (m)	Loose ave. layer thick. (m)	# events	CPT values (MPa) - before blasting	Ave. Sett. (m)
18	18-1	7.9	4.1	4	2.1	0.46-0.48
	18-2	7.6			2.0	
	18-3	7.6			1.9	
17	17-1	7.3	3.5	4	2.8	0.50-0.51
	17-2	7.3			1.9	
	17-3	7.0			2.9	
16	16-1	7.5	4	4	2.9	0.36-0.37
	16-2	7.3			2.0	
15A	15A-1	7.3	4	4	2.1	0.38-0.39
	15A-2	7.6			1.9	
15B	15B-1	7.3	3.5	4	1.4	0.43-0.45
	15B-2	7.3			1.8	

4.3 Groundwater and gas sampling

As part of the instrumentation work, Northwestern University installed BAT probes at different locations to monitor pore pressure changes before and after each blast event and to collect groundwater/gas samples. As explained in section 2.6, results from these tests can be used to determine whether or not gases produced and released during blasting are present in the ground at the time of sampling in either dissolved or free form. Figure 4-5 shows the location of the BAT probes in zones 5, 16 and 18.
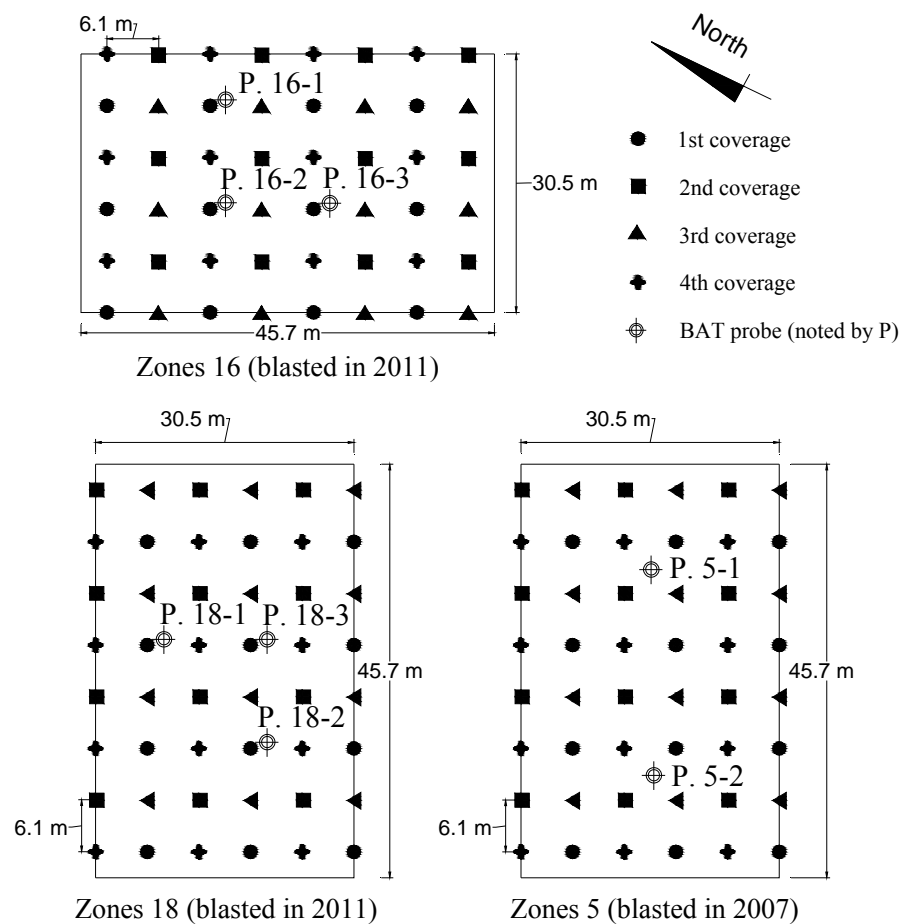
Figure 4-5. Location of BAT probes in zones 5, 16 and 18.

A total of nine BAT probes were installed. As shown in Figure 4-5 and Figure 4-6, three probes were installed in zone 16 and three in zone 18. These two zones were selected because their site geometry and blasting configuration were similar to those ground improvement zones located along the perimeter of the Phase II area. Therefore, the results obtained from these zones can be extrapolated to the other areas. The results from these six probes provided information about the short term concentration of gases after blasting.

Two probes were installed in zone 5 to determine what type of gases and concentrations were still present four years after blast densification. The results from this zone provided valuable information about the persistence of gases after ground improvement.

One more probe was installed approximately 45 m from the corner of zones 16 and 18 (Figure 4-6 – point A). This probe provided information about the horizontal spatial distribution of the gases produced during blasting.
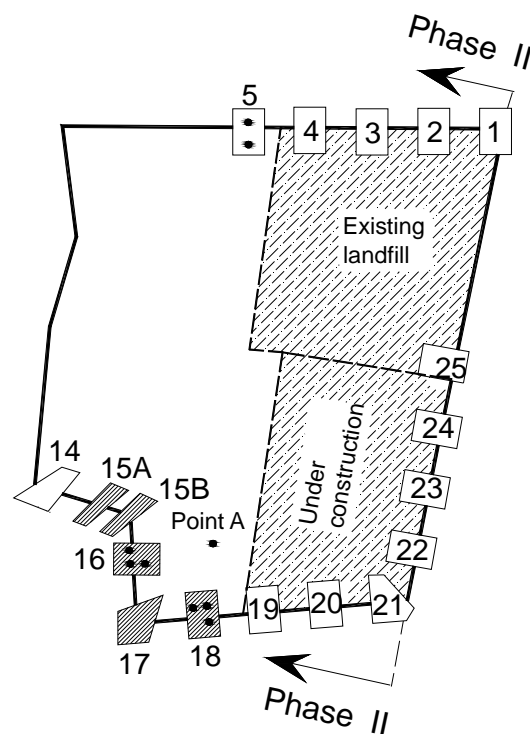
Figure 4-6. Location of the BAT probes and extent of the existing landfill.

Figure 4-6 shows the extent of the actual landfill at the time of sampling. Point A, Zone 5 and

Zone 18 are located approximately 30 m from the edge of the landfill that is being built. Table

4-2 lists the typical gases produced in municipal solid waste landfills and their concentrations

(Qian et al., 2002). Landfill gas is composed of gases that are present in large amounts such as

methane and carbon dioxide and gases that are present in very small amount such as nitrogen,

oxygen, hydrogen and water vapor. The percentage of methane and carbon dioxide make up

more than 90% of the total gas produced in a solid wasted landfill. Since the gases produced

during blast densification are similar to those gases produced in the landfill, a careful

interpretation of the data collected using the BAT probe must be conducted to ensure that the

results are representative of the soil condition after blasting and not from gases that could have

migrated from the landfill. This uncertainty can be overcome by comparing the concentrations of

methane and carbon dioxide detected in the containers with those concentrations expected from

the waste landfill. Very small concentrations of methane and carbon dioxide will indicate that no

gases are migrating from the adjacent landfill.

Table 4-2. Typical gases in municipal solid waste landfills (Taken from Qian et al. (2002)).

TABLE 10.2 Typical Constituents in Municipal Solid Waste Landfill Gas (EMCON,1998)	
Component	Percent
Methane (CH_4)	45 to 58
Carbon Dioxide (CO_2)	35 to 45
Nitrogen (N_2)	< 1 to 20
Oxygen (O_2)	< 1 to 5
Hydrogen (H_2)	< 1 to 5
Water Vapor (H_2O)	1 to 5
Trace Constituents*	< 1 to 3

*NMOCs are among the trace constituents

4.3.1 Preparation and installation of the BAT probes

The preparation and installation sequence of the BAT probes was as follows:

(1) Figure 4-7 shows the filter tip (BAT MkIII standard) as it is being saturated. A total of 40 ml,

four times the volume the filter can hold, of de-aired water was flushed through the filter

from the tip by using a syringe. After saturation, the filter was kept in a bucket under de-aired

water to prevent desaturation.

Figure 4-7. Flushing de-aired water through the filter tip.

(2) Figure 4-8 shows the equipment used to install the filter tip. Using a Geoprobe 8040DT, a

drill pipe was pushed through the ground to approximately 1.5 m above the final depth of the

filter tip. The drill pipe had a circular opening at the tip with a diameter of approximately 4

cm. An inner rod was placed inside the drill pipe to prevent soil from entering the drill pipe

during pipe driving.

(a)   (b)

Figure 4-8. (a) Geoprobe 8040DT and (b) Drill pipe driving.

(3) After pushing the drill pipe to the desired depth, the inner rod was removed and the inside of the drill pipe was filled with water. The filter tip was screwed onto a 2.54 cm adapter pipe (Figure 4-9), while remaining submerged under de-aired water, and the first section of extension pipe was attached to the adapter pipe. Then, the bucket was quickly removed, the filter placed inside the drill pipe, and installation began. Extension pipes were used to reach the desired depth and a thread sealing agent was used at each connection to prevent leakage of water into the pipe.

Figure 4-9. Filter tip and adapter pipe.

(4) After lowering the filter tip through the drill pipe, it was pushed by the Geoprobe 8040DT approximately 1.5 m into the soil to reach the final depth. **Figure 4-10** shows a completed installation.

Figure 4-10. Completed installation of the BAT filter.

The final installation depths of the BAT filters are listed in Table 4-3

Table 4-3. Final installation depths of the filters.

Location	Depth	Observations
Zone 16	10 m	At the middle of loose layer
Zone 18	10 m	At the middle of loose layer
Zone 5	11 m	At the middle of loose layer
Point A	8.8 m	1.5 m below the top of loose layer

The first, second, third, and fourth blast events were conducted on February 23th, March 1st, March 7th, and March 11th of 2011, respectively. The installation of the BAT probes occurred on March 5th, four days after the second blast event and two days before the third blast event. The initial reference values of the in-situ porewater pressures and temperatures were recorded on March 7th, several hours before the third blast event. The excess pore water pressure due to the

second blast event and the installation of the BAT probes had dissipated at the time of the readings as described in section 4.4.

Four sets of groundwater/gas samples were collected during this blast densification program. The first, second, and third set of samples were collected one day after the third blast event, immediately after the fourth blast event, and three days after the fourth blast event, respectively. For this set of samples, the BAT probe was assembled as shown in Figure 2-10 and a vacuum of 85% to 90% was applied to the container from the bottom of the test container housing (refer to session 2.6.1.2) to remove the air trapped in the container and in the sensor cavity. The fourth and last set of samples was collected 27 days after the fourth blast event. For this set of samples, each container was flushed and pre-charged with Helium to minimize the uncertainties in in-situ gas concentration encountered when the vacuum method was used. The containers were pre-charged with a pressure slightly higher than the atmospheric pressure to ensure that contamination with atmospheric gases would not occur at any time during the sampling process. Gas Chromatography (GC) tests were conducted on all the pre-charged containers before sampling to verify that no air was left inside. Helium was chosen to pre-charge the containers because it is an inert gas that is not readily found in the ground, it is not a gas produced by typical explosives, and it is different than the gas used as the carrier gas (argon) in the gas chromatography test.

4.3.2 Results from groundwater/gas samples

After collecting each set of samples, the containers were immediately sent to TRI Air Testing, INC. laboratory for GC tests to analyze the free gas in the headspace of the containers. The concentration of carbon dioxide (CO_2), carbon monoxide (CO), oxygen (O_2), nitrogen (N_2) and methane (CH_4) were determined. The carrier gas used during the GC tests was argon. These

results combined with data regarding the total volume of the BAT container, the amount of pore water sampled, the pressure and temperature in-situ, and the solubility of each gas in pore water are needed to determine if the soil pore fluid was fully saturated with a particular gas or if free gas was present at the test location at the time of sampling. From the detected gases, nitrogen was the only gas contributing to the degree of saturation of the soil, the other gases were found to be dissolved in the pore fluid (Appendix A and B).

Table 4-4 and Table 4-5 summarize the GC results from the vacuumed and pre-charged containers, respectively. For the pre-charged containers, the concentration of helium was not included in this table since it was not part of the sampled gases. The concentrations of CO_2, N_2, and O_2 are expressed in percentage (%) and the concentrations of CO and CH_4 are expressed in ppmv (parts per million by volume). 1 % by volume corresponds to 10,000 ppmv.

Table 4-4. Results from GC tests - vacuumed containers.

Borehole	March 8th										March 11th					March 14th				
	CO$_2$		N$_2$		O$_2$		CO		CH$_4$		CO$_2$	N$_2$	O$_2$	CO	CH$_4$	CO$_2$	N$_2$	O$_2$	CO	CH$_4$
#	(%)		(%)		(%)		(ppmv)		(ppmv)		(%)	(%)	(%)	(ppmv)	(ppmv)	(%)	(%)	(%)	(ppmv)	(ppmv)
P. 16-1	1.8		75.2		19.7		6		41		3.3	73.8	18.7	24	39	-	-	-	-	-
P. 16-2	1.4		77.1		13.8		>2250		3680		2.2	73.2	17.5	4400	3300	2.4	76.0	14.8	4800	3700
P. 16-3	1.4		77.6		18.5		34		208		2.8	72.8	19.7	57	300	2.3	73.2	21.4	10	244
P. 18-1	2.4		78.7		15.9		15		75		3.3	76.5	16	20	124	2.8	72.4	20.6	10	90
P. 18-2	1.5		76.9		17.8		231		140		2.5	75.2	18.5	51	123	2.4	72.2	20.8	14	144
P. 18-3	2.2		77.6		16.4		12		12		3.2	77.0	15.8	24	12	2.0	74.3	19	9	13
P. 5-1	0.4	0.4	79.2	78.3	17.3	19	3	3	230	319	-	-	-	-	-	1.2	74.6	20	4	336
P. 5-2	0.3	0.3	77.7	77.5	17.6	18.7	4	3	301	458	-	-	-	-	-	0.7	74.0	20.9	2	537
Point A	1.6	2.8	78.7	75.8	16	17	12	43	17	22	1.9	77.4	17.4	8	25	-	-	-	-	-

Note: (*) ppmv

ppmv (parts per million by volume)

1 % by volume = 10000 ppmv

Table 4-5. Results from GC tests – Containers flushed and precharged with Helium.

Borehole #	Sample 1				Sample 2				Sample 3				Sample 4				Sample 5				Sample 6			
	CO_2 (%)	N_2 (%)	CO (*)	CH_4 (*)	CO_2 (%)	N_2 (%)	CO (*)	CH_4 (*)	CO_2 (%)	N_2 (%)	CO (*)	CH_4 (*)	CO_2 (%)	N_2 (%)	CO (*)	CH_4 (*)	CO_2 (%)	N_2 (%)	CO (*)	CH_4 (*)	CO_2 (%)	N_2 (%)	CO (*)	CH_4 (*)
P. 16-1		-				-				-				-				-				-		
P. 16-2		-				-				-				-				-				-		
P. 16-3	0.6	8.5	1	89	0.3	6.7	1.2	51	0.4	6.8	<1	83		-				-				-		
P. 18-1	0.4	6.1	1.5	11	0.2	6.2	1.7	10	0.3	6.9	1.6	20		-				-				-		
P. 18-2	0.3	6.3	1.2	13	0.3	6.2	1.0	22	0.3	6.4	1.1	26		-				-				-		
P. 18-3	0.4	7.4	1.7	<1	0.2	5.0	1.3	<1	0.3	5.9	1.4	1.0		-				-				-		
P. 5-1	0.2	6.4	1.5	17	0.1	6.8	<1	39	0.1	5.9	1.7	23	0.1	7.5	1.3	35		-				-		
P. 5-2	0.2	5.1	1.6	13	0.1	6.2	1.7	47	0.1	8.2	1.1	39	0.1	5.4	1.7	33	0.1	7.4	1.0	95	0.2	7.0	1.8	69
Point A	0.4	7.2	2.1	2.0	0.3	6.4	1.5	3	0.3	6.8	2.0	3	0.4	8.0	2.3	8		-				-		

Note: (*) ppmv

ppmv (parts per million by volume)

1 % by volume = 10000 ppmv

Groundwater/gas samples – Vacuumed containers

A total amount of 26 samples were collected using vacuumed containers. Figure 4-11 shows

the concentration of nitrogen detected in the headspace of the containers collected one day after

the third blast event, immediately after the fourth blast event, and three days after the fourth blast

event in zones 16, 18, 5 and point A. The concentration of nitrogen in the blasted layer ranged

from 72.2% to 79.8%. These concentrations are close to those concentrations encountered on the

earth's atmosphere (N_2=78.08%). Therefore, it was decided to flush and pre-charge the

containers with helium for the fourth set of samples to minimize the uncertainties introduced by

the vacuum sampling technique, and to verify that these gases were sampled from the ground and

that the results were not a consequence of the small amount of air left inside the containers after

vacuum had been applied.
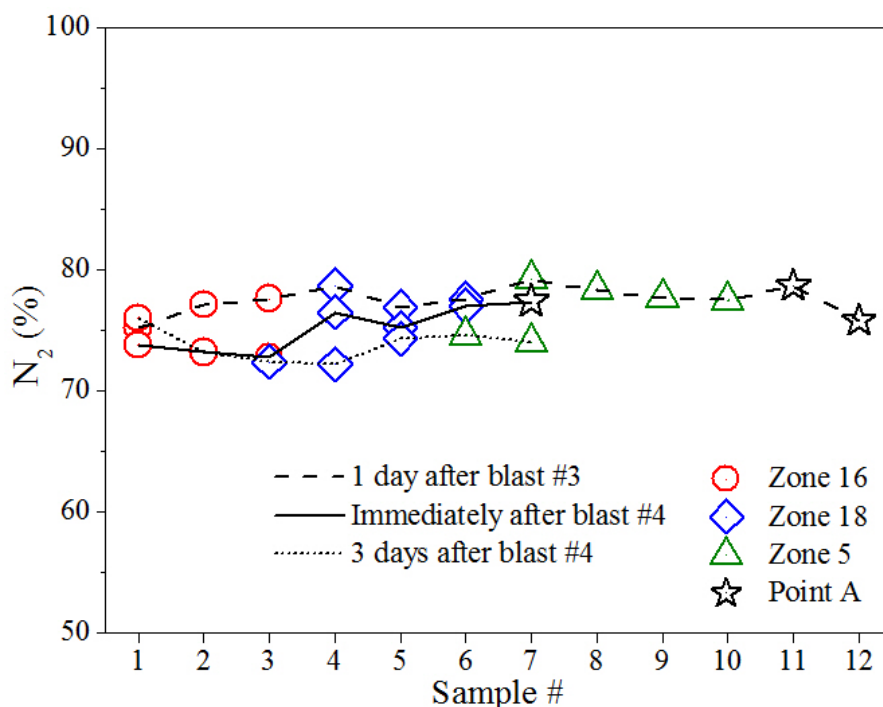
Figure 4-11. Vacuumed containers – concentration of Nitrogen.

Groundwater/gas samples – Containers flushed and precharged with Helium

The total amount of samples collected with the pre-charged containers was 26. Three samples were collected at each location in P. 16-3, P. 18-1, P. 18-2, and P. 18-3; four samples were collected at each location in P. 5-1 and Point A; and six samples were collected in P. 5-2. Figure 4-12 shows the concentration of nitrogen from these samples collected 27 days after the fourth blast event. The concentration of nitrogen ranged from 5.0% to 8.5%.
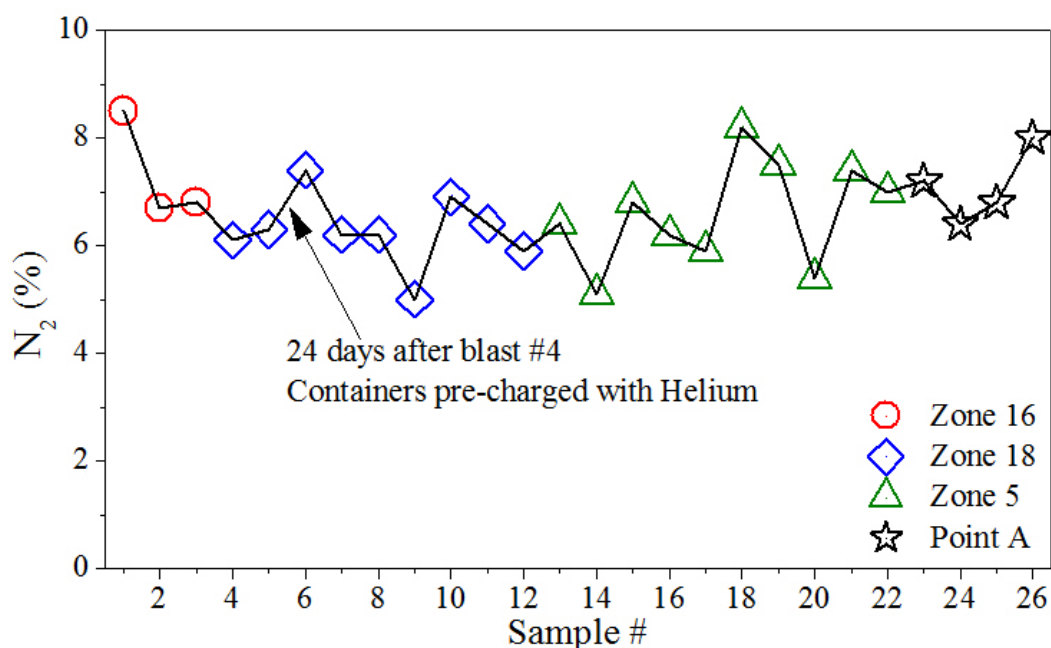
Figure 4-12. Containers pre-charged with Helium – concentration of Nitrogen.

The concentration of nitrogen in the blasted layer ranged from 72.2% to 79.8% when vacuumed containers were used and from 5.0% to 8.5% when pre-charged containers were used. The concentration of gas obtained from these two techniques varied significantly. However, the results alone do not provide any valuable information about whether or not they are present in the ground in either dissolved or free form. The amount of gas that is being sampled is highly dependent on the difference in pressure between the container and the in-situ pressure, and on the

volume of water that enters the container. Therefore, a different approach is needed to determine

the state of the gases (dissolved or free gas) under the in-situ pressures and temperatures.

Degree of saturation of the targeted layer

The concentration of nitrogen in the containers' headspace was used to compute the degrees

of saturation of the targeted layer at the time of sampling. Figure 4-13 shows the degrees of

saturation computed following the procedure proposed by Christian and Cranston (1997). This

procedure is presented in Appendix B. In general, the degrees of saturation varied from 80% to

95% within the tested areas. These degrees of saturation are comparable with those obtained by

Okamura et al. (2006) in sites where the sand compaction piles technique was used to improve

the ground condition.
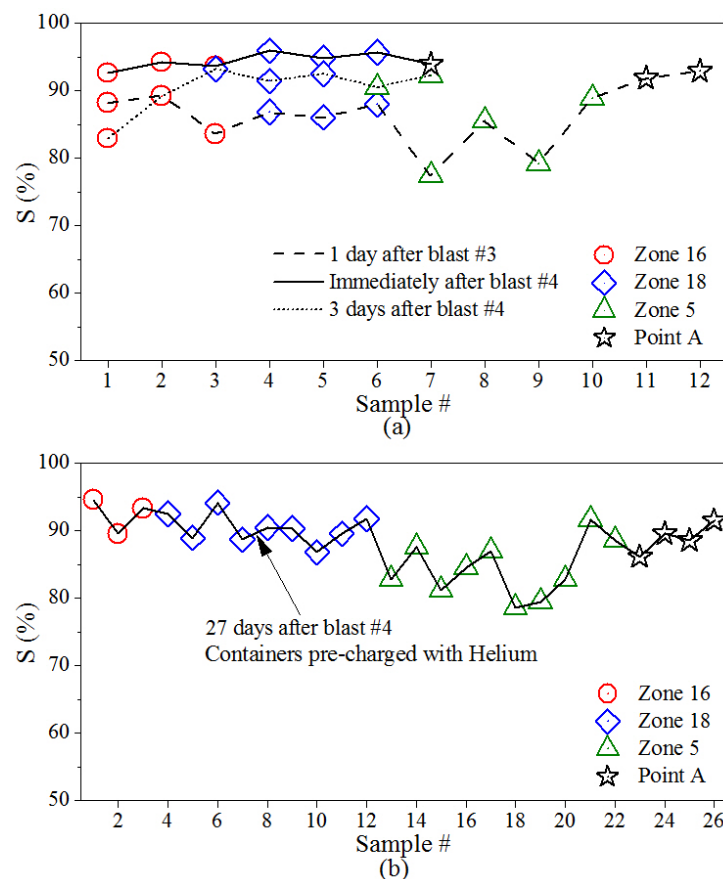
Figure 4-13. Final degrees of saturation in percentage of the soil (a) vacuumed containers and (b) pre-charged containers.

The two sampling techniques, vacuum applied to the container and container flushed and pre-charged with helium, yielded to similar degrees of saturation. Apparently, the small amount of air left in the container after vacuum did not have a significant impact on the final concentration of the sampled gases.

Nitrogen was the only gas contributing to the degree of saturation of the soil, the other gases were found to be dissolved in the pore fluid (Appendices A and B). Samples collected in locations P. 5-1 and P. 5-2 in zone 5 showed that nitrogen was still present in the ground almost four years after ground improvement. This could have been expected since the solubility coefficient of nitrogen is low ($\beta= 0.015$ mL of N_2/ mL of water) and it does not dissolve easily in the pore fluid under the in-situ pressures ($\sigma_v'= 100$kPa). The solubility coefficient of carbon dioxide is 0.83 mL / mL of water, 55 times more soluble in water than nitrogen. Since Nitrogen is persistent in the ground, its influence on the soil behavior must be taken into account when evaluating the behavior of blast-densified sand at a particular ground improvement project.

Point A showed that at approximately 45 m from the corner of zones 16 and 18, the soil has become de-saturated (S=85%-94%). This was not surprising, considering that the first set of samples was collected one day after the third coverage, and the amount of gas that has been previously released by surrounding blasted zones was also significant. Approximately 3000 m^3 of gas is estimated to be produced and released at these zones after ground improvement (Section 2.3.1).

Because point A was located approximately 30 m from the existing landfill (Figure 4-6), it could be speculated that some of the gas produced in the landfill may have migrated to the vicinity and thus contributing to the decrease in the degree of saturation of the soil. However, the principal gases produced in solid waste landfills are methane and carbon dioxide, which were

detected to be present in the soil in very small amounts. The concentrations of methane and carbon dioxide were less than 0.4% and 2.5%, respectively for the vacuumed containers and 0.01% and 0.6%, respectively for the pre-charged containers (appendix A). These gases were computed to be dissolved in the pore fluid at the time of sampling.

Table A-3 (appendix A) lists the parameters required to compute the degree of saturation of the soil at the time of sampling and Appendix B describes the procedure followed to compute the degrees of saturation and provides an illustrative example of the calculations.

4.4 Porewater pressure measurements

The initial reference values for the in-situ pore pressures were recorded six days after the second blast event and one day before the third blast event. The excess pore water pressure due to the second blast event and the installation of the BAT probes had dissipated at the time of the readings. Table 4-6 summarizes the initial porewater pressure readings. The porewater pressures measured in zones 16 and 18 compared well with those pressures measured, at a depth of approximately 10m, by GeoSyntec Consultants in the test section blasted between 2003 and 2004 (Narsilio et al., 2009). The temperature at all the sampling locations was constant and equal to 20.1 $^{\circ}$C

Table 4-6. Initial in-situ pore pressure readings before the third blast event.

Borehole (#)	Pore Pressure (kPa)	Average pore pressure (kPa)
P. 16-1	95.4	
P. 16-2	97.5	95.8
P. 16-3	94.4	
P. 18-1	92.0	
P. 18-2	91.0	92.1
P. 18-3	93.4	
P. 5-1	70.2	70.5
P. 5-2	70.7	
Point A	79.2	79.2

The BAT probe system was used to record the evolution of the excess pore pressure dissipation over time. Figure 4-14 shows the pore pressure dissipation after the third and fourth blast events measured at boreholes P. 16-3 and P.18-3, respectively. Initial liquefaction was induced in these zones after blasting. The pore water pressure was equivalent to the in-situ total vertical stress, indicating that a zero vertical effective stress state was reached in the loose sand layer. The effective in-situ vertical stress in these two zones was approximately 100 kPa. The soil maintained a liquefied state for over a period of 6 to 7 hours and the excess pore pressure decreased to the pre-blasting value in approximately 70 hr. The majority of the blast-induced settlements is expected to occur during this period of time (Narsilio et al., 2009).
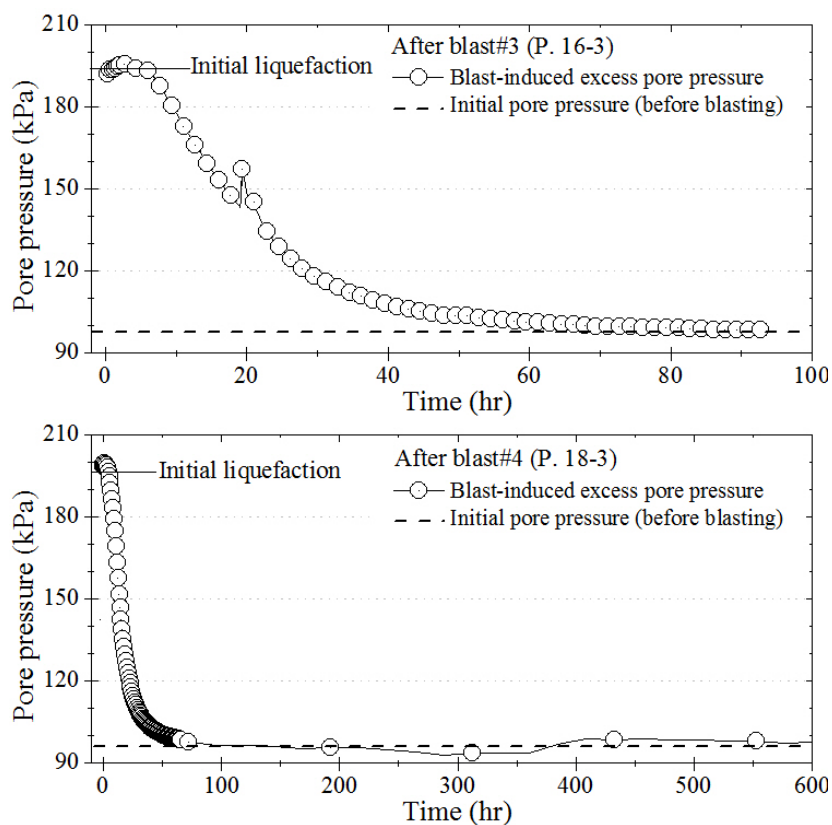
Figure 4-14. Excess pore pressure dissipation over time after blasting.

4.5 Ground surface settlements

Prior to ground improvement, standard topographic surveys along the centerline of each zone were conducted to establish the initial ground surface elevation condition. Ground surface elevations were also conducted after each blast event to measure the cumulative surface settlement at any stage during the blasting program. The monitoring of these surface settlements is essential to assess density changes as a result of blasting, and therefore to evaluate the effectiveness of the blasting program.

The settlement data collected during all the blast densification programs conducted at the Oakridge landfill site showed that the blasted layer, average thickness of 5.5m (t=5.5m), undergoes a one-dimensional consolidation settlement in the vertical direction. In general, these zones experienced a "uniform" settlement over a horizontal distance of about 40 m (B=40m). Because B/t=7 >>1, the one-dimensional consolidation assumption is considered a valid assumption. Figure 4-15 shows the ground settlement survey data collected during and after each of the blast events in zones 15A, 15B, 16, 17 and 18. The average ground settlement after the fourth blast event varied from 0.36m in zone 16 to 0.51m in zone 17.

Figure 4-16 shows the cumulative axial strains after each blast event in zones 15A, 15B, 16, 17 and 18. The axial strain in the targeted layer was 3.5%, 6%, 9% and 11.5% after the first, second, third, and fourth blast event, respectively. Assuming that the initial in-situ void ratio was $e_o = 0.97$ (see section 3.1), the decreased in void ratio after the fourth blast event was $\Delta e = \varepsilon_v(1 + e_o)$=0.74. As will be shown in the next chapter, this void ratio is located below the critical state line where a dilative response is expected and hence, after densification, the soil is not considered susceptible to liquefaction and flow.
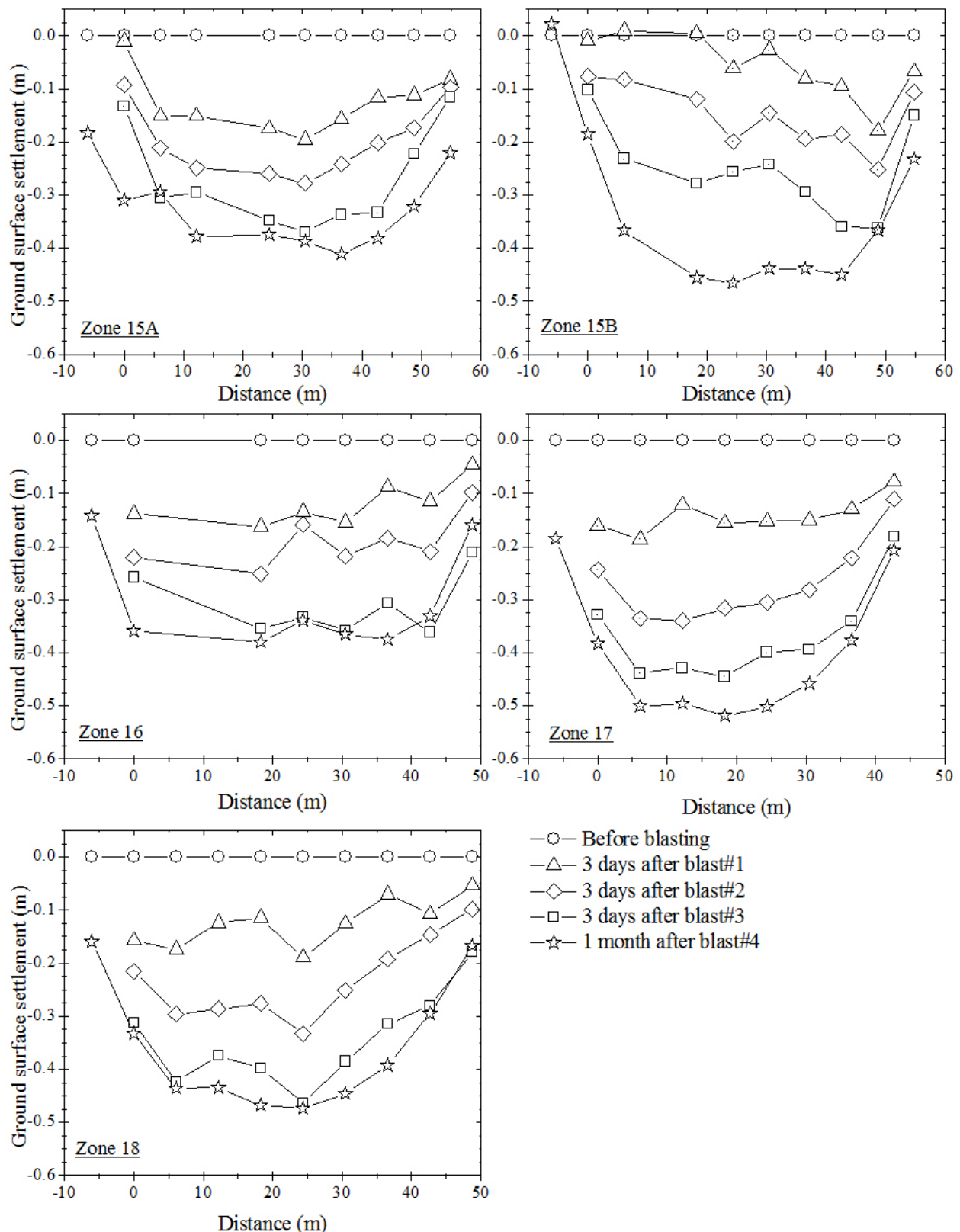
Figure 4-15. Surface settlement during and after blasting – Zones 15A, 15B, 16, 17 and 18.
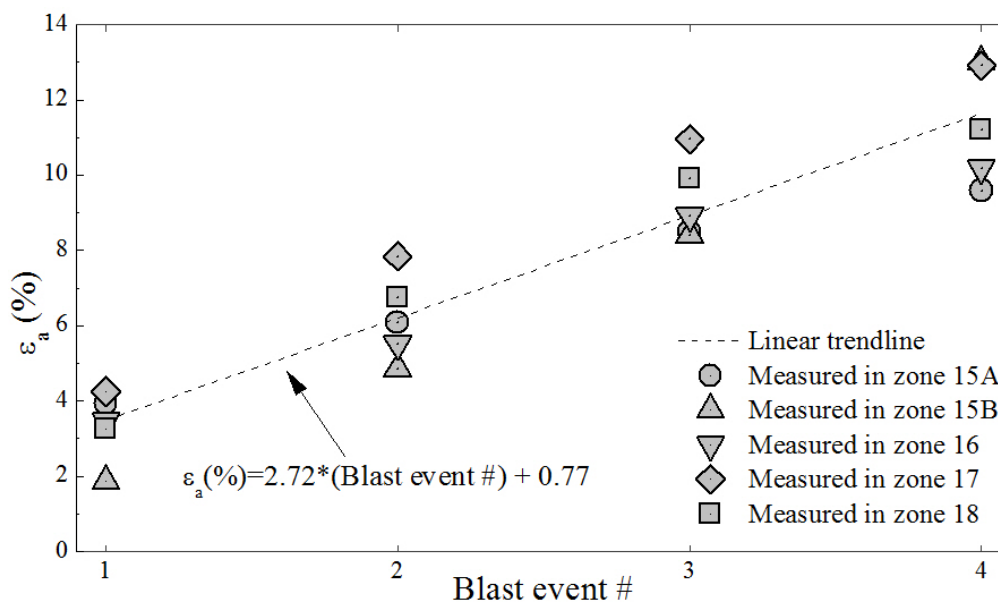
Figure 4-16. Cumulative axial strains in zones 15A, 15B, 16, 17 and 18.

4.6 Summary

The most recent blast densification program at the Oakridge Sanitary Landfill was conducted in 2011. This work was a joint effort between Northwestern University and GeoSyntec Consultants. The blast and monitoring program included cone penetration soundings, standard topographic surveys, porewater pressure measurements, and collection of groundwater/gas samples. The BAT probe system was used for the first time at the Oakridge facility to quantify the type of gases trapped in the soil after ground improvement and their in-situ concentrations.

The maximum settlement occurred at the center of the tested zone and the amount of incremental surface settlement decreased after each consecutive blast. Approximately 65% of the total settlements were achieved after the second blast event. The axial strain in the targeted layer was 3.5%, 6%, 9% and 11.5% after the first, second, third, and fourth blast event, respectively. The corresponding reduction in void ratio makes the improved soil dense enough so that a

dilative response is expected and the soil would not be considered susceptible to liquefaction and flow.

Nitrogen was the only gas contributing to the degree of saturation of the soil, the other gases were found to be dissolved in the pore fluid. The concentration of nitrogen in the container's headspace ranged from 72.2% to 79.8% when vacuumed containers were used and from 5.0% to 8.5% when pre-charged containers were used. These two sampling techniques yielded to similar degrees of saturation. The degrees of saturation computed from these concentrations varied from 80% to 95% within the blasted zones.

The degree of saturation at Point A varied between 85% and 94%. This decrease in saturation is likely the result of the sum of gases released during the current and previous blast densification programs. Because the concentrations of methane and carbon dioxide detected in the container's headspace were very small, gases generated in the landfill were not believed to migrate to the targeted layer and contribute to its decrease in saturation.

Samples collected in zone 5 showed that nitrogen was still present in the ground almost four years after ground improvement. This could have been expected since the solubility coefficient of nitrogen is low and it does not dissolve easily in the pore fluid under the in-situ pressures.

5 LABORATORY MATERIALS AND PROCEDURES

A laboratory testing program was implemented to quantify the influence of gas on the mechanical behavior of medium to dense sands during monotonic and cyclic loading. The laboratory program included the determination of index properties, triaxial compression tests to quantify the soil response as a function of void ratio and degree of saturation, and constrained compression tests to estimate the volume changes that will occur after each blast event. The triaxial compression tests were anisotropically consolidated to in-situ stresses and at void ratios above and below the critical state line. At each void ratio, samples with degrees of saturation varying from 75% to 100% were prepared and then subjected to monotonic and cyclic globally undrained loading. Constrained compression tests were conducted on dry samples at dry densities varying from 13.5kN/m^3 (1.35 g/cm^3) to 15.5kN/m^3 (1.55g/cm^3). The void ratios and degrees of saturation selected for these tests are considered to be representative of those void ratios and degrees of saturation at the Oakridge Landfill site before and after blast densification.

Although nitrogen is the most predominant and longest-lasting gas trapped in the soil after blast densification, it is not easily dissolved in water and high pressures would be required to achieve a desirable degree of saturation, making nitrogen impractical for laboratory work. Instead, carbon dioxide was used since is already available in the laboratory, noncorrosive, nonflammable, and only moderate pressures are required to achieve the target degrees of saturation, as will be discussed later. The undrained shear strength obtained from soils saturated with carbon dioxide are slightly lower (i.e., slightly more conservative) than those obtained from soils saturated with nitrogen (Grozic et al., 2005). The general trend of soils containing gas located above and below the CSL is assumed to be the same for soils saturated with either carbon dioxide or nitrogen.

5.1   Description of loose sands

The sand used for testing was collected in zone 18 during the blast densification program conducted in 2011. Sand samples were collected from the target loose layer at a depth of 10m during drilling of the blast holes for the third blast event. Figure 5-1 shows a typical grain size distribution curve of the sand samples collected at the Oakridge landfill site. The soil is clean, fine grained sand, SP, angular in shape, with little fines. The average uniformity coefficient (C_u) and curvature coefficient (C_c) were 1.63 and 1.03, respectively and the minimum and maximum void ratios were e_{min} = 0.62 and e_{max} = 1.05, respectively. The compression (C_c) and recompression (C_r) indices as determined from the one-dimensional constrained compression tests for a range of working stresses from 50kPa to 400kPa varied from 0.044 to 0.084 for C_c and 0.008 to 0.018 for C_r, respectively. The percentage of fines passing sieve # 200 was less than 1.5% by weight when the dry sieve analysis was conducted. When the washed sieve analysis was conducted, the C_u and C_c coefficients were 1.81 and 1.10, respectively and the percentage of fines passing sieve #200 was 7% by weight. The specific gravity value is 2.66, suggesting that the sand is quartz.

Sand samples collected by GeoSyntec Consultant during the blast densification and instrumentation program conducted between November 2003 and August 2004 were provided to Northwestern University for testing as well. Figure 5-1 shows a comparison between the grain size distributions of the samples collected in 2003-2004 (section 3.2 -Test C) and 2011. Very similar gradations are noted, with the main difference being the percentage of fines passing sieve #60 is greater for the sands collected in 2011.
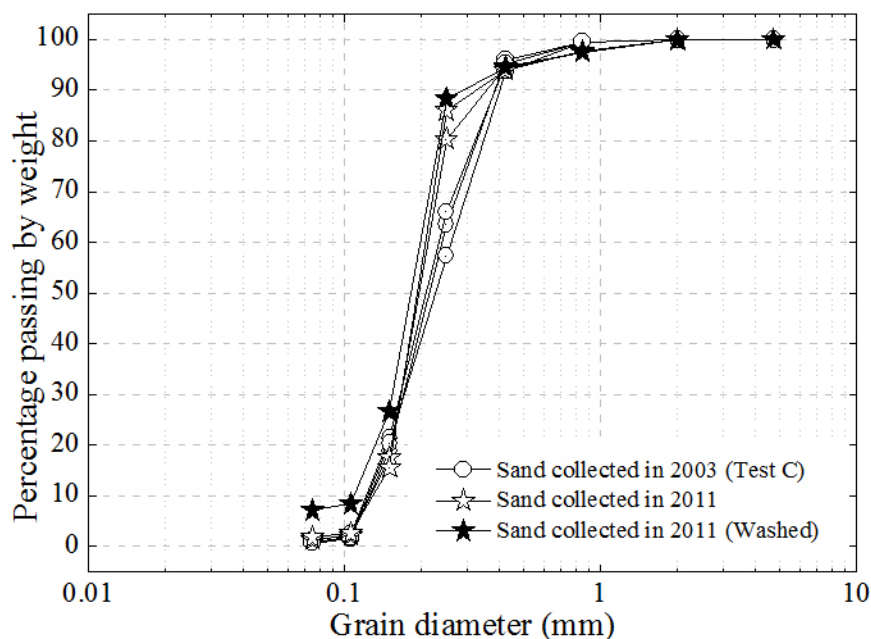
Figure 5-1. Typical grain size distribution at the Oakridge landfill site.

5.2 Equipment description

Figure 5-2 shows a schematic of the testing apparatus and saturation system used to perform the triaxial tests. Experiments were conducted in a Dynamic Triaxial Testing System (DYNTTS) manufactured by *GDS Instruments Ltd*. The DYNTTS system combines a 2-MPa capacity triaxial cell with a dynamic actuator to apply axial forces up to 10 kN and/or axial deformation up to 100 mm. The load or deformation is applied by raising the base of the cell, which is fixed to the actuator unit. Sinusoidal waveforms can be applied cyclically by the actuator at frequencies up to 2 Hz. According to the manufacture specifications, the cell pressure is controlled by a dual channel pneumatic regulator with a resolution of ±0.5 kPa over a pressure range of 0 to 1000 kPa. Water volume changes in the sample are controlled by an Advanced Digital Controller (ADVDPC) with a pressure range of 0 to 2000 kPa and a volumetric capacity of 200 cm^3. The ADVDPC can resolve pressures and volume changes to 0.2 kPa and 1 mm^3,

respectively. Pore pressures are measured via a solid-state pressure transducer connected to the base pedestal which resolves pore pressure to ±0.2 kPa over a range of 2000 kPa. Detailed specifications of this apparatus are provided by Menzies (1988) and Menzies et al. (2002).

A Hong Kong University of Science and Technology (HKUST) pedestal with a bonded High Air Entry Porous Disk (HAEPD) of 100 kPa located atop the bottom pedestal was used to conduct tests with partial saturation. The purpose of the HAEPD was to prevent air or any other gases from passing through the disk. A set of bender elements (BE), one inserted in the top cap and the other in the HKUST pedestal, was used to measure vertical propagation velocities during all phases of the experiments. The BEs and corresponding data acquisition (d/a) system were manufactured by *GDS Instruments Ltd*. The d/a system had a high-speed, 16-bit resolution, and is capable of sampling rates of 200 kHz. BEs were 11-mm-wide, 1-mm-thick and extended about 1 mm into a specimen. The total sample volume change was measured using the HKUST inner cell (Ng et al., 2002) and a high accuracy differential pressure transducer (DPT). The DPT gives measurements ranging from +/- 3.4 kPa (+/- 340 mm of water head), and an accuracy better than 0.1% full-scale pressure output (+/- 3.4 Pa or 0.34 mm of water head). The accuracy of the total volume change system is on the order of 178 mm^3, corresponding to a volumetric strain of 0.09% for a sample 50 mm in diameter and 100 mm in height.

A CO_2 saturation system was developed for replacing the sample pore water with carbonated water and thus to create gassy samples. This procedure is discussed in section 5.3.2.
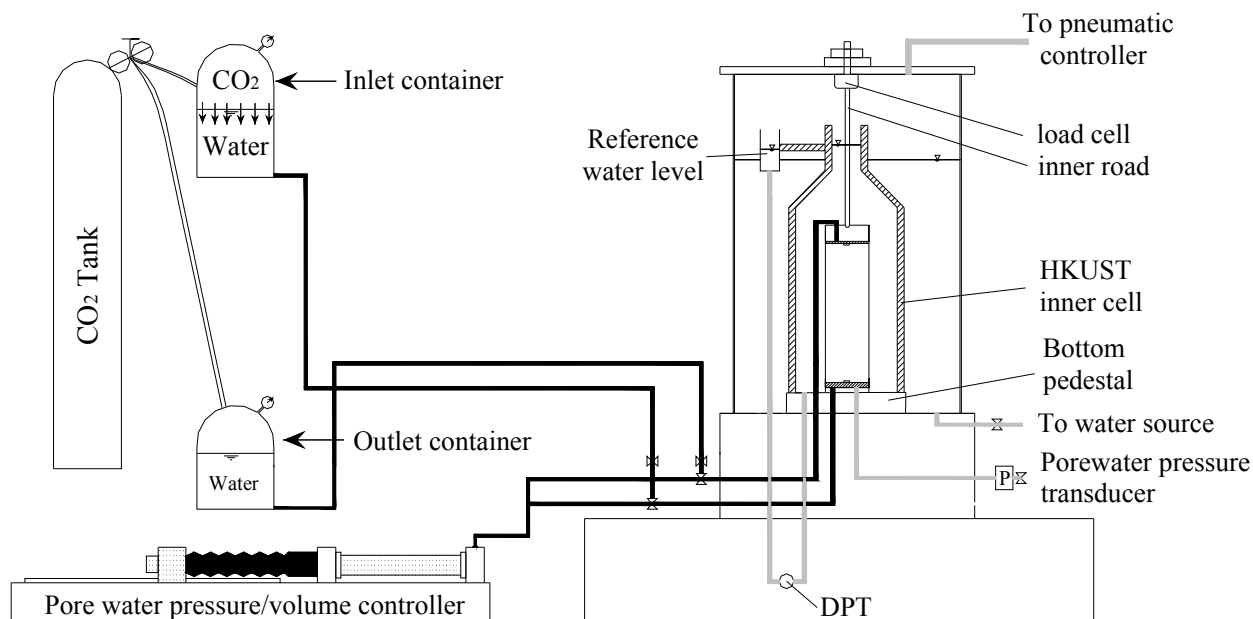
Figure 5-2. Schematic diagram of triaxial apparatus.

The main limitation of the triaxial testing system when configured with the HKUST inner cell was that the inner rod, which was screwed into the bottom of the load cell, was not fixed to the top cap. Therefore, anisotropic cyclic tests with large deviatoric stresses could not be performed. To overcome this limitation, the triaxial testing configuration shown in Figure 5-3 was used to conduct experiments on saturated and gassy samples with a target Cyclic Stress Ratio (CSR) greater than 0.15. The high air entry porous disk was not part of this testing set up, therefore significant amount of gas was lost from the specimens during sample desaturation. The released gas traveled through the lines to the porewater volume controller, making the measurement of water leaving the sample during de-saturation extremely difficult and unreliable. The total volume changes and bender elements measurements were not performed while using this triaxial configuration. This testing configuration was also used to determine the position of the critical state line based on results of saturated undrained compression tests.
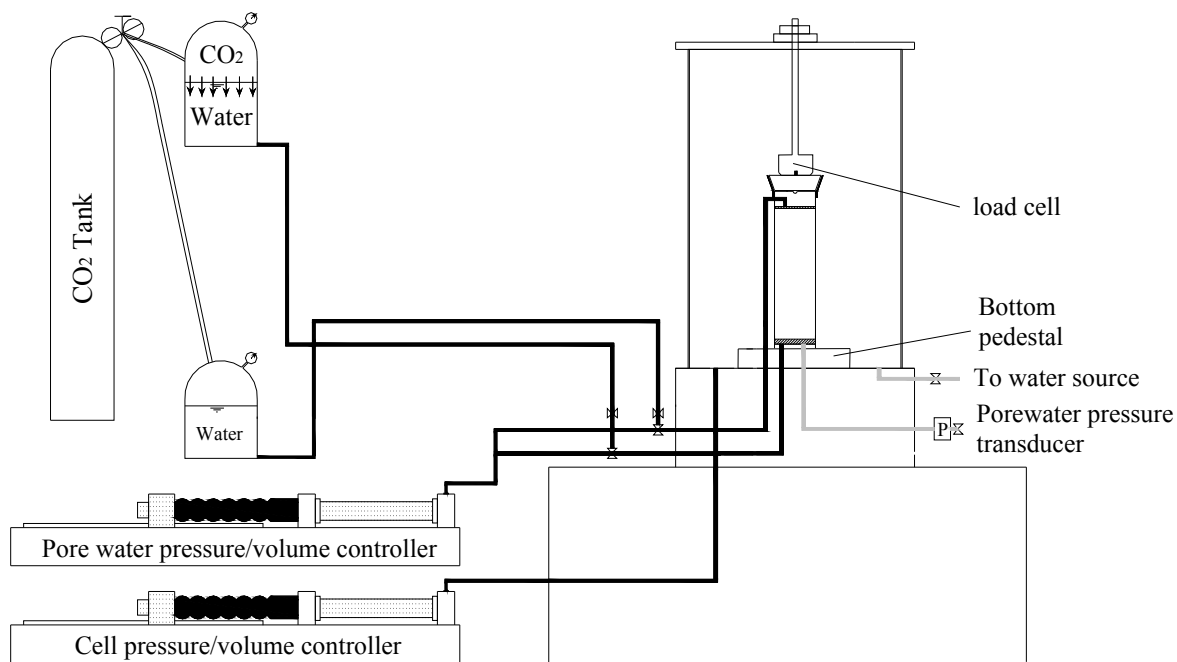
Figure 5-3. Schematic diagram of triaxial apparatus for saturated and gassy samples with CSR>0.15.

5.3 Sample preparation and testing procedures

Most of the knowledge about the mechanical behavior of sands has been derived from the testing of reconstituted specimens. It has been shown that at the same void ratio and effective confining stresses, the undrained response of sands during monotonic or dynamic loads is highly influenced by the sample preparation technique (Oda, 1972; Ladd, 1974; Mulilis et al., 1977; Vaid and Negussey, 1988; Vaid et al., 1999; Vaid and Sivathayalan, 2000; Yamamuro and Wood, 2004; Wijewickreme et al., 2005b; Thomson and Wong, 2008). In this testing program, the majority of the samples were prepared using the water pluviation technique, which is believed to yield more uniform samples and to better reproduce the response of undisturbed samples. An experimental study conducted by Vaid et al. (1999) and Vaid and Sivathayalan (2000) showed that samples prepared using this technique closely mimic the response of

undisturbed samples collected from soils deposited by marine or fluvial action. This is the case for the soils deposited at the Oakridge Landfill site (SCDOT, 2008).

5.3.1   Sample preparation – water pluviation technique

Figure 5-4 shows the water pluviation sample preparation set up. The dimensions of the specimens prepared using the water pluviation technique were approximately 50 mm in diameter and 100 mm in length. The sample preparation procedure was similar to that previously described in detail by Chern (1981 and 1985). To prepare the samples, a known amount of dry sand was poured in a 500 mL glass flask half-filled with de-aired water. The soil and water mixture was boiled under vacuum for about 15 minutes and then the remainder of the flask was filled with de-aired water. The saturated soil was transferred to a 500 mL separatory funnel filled with de-aired water and then allowed to cool overnight. The advantage of the separatory funnel is that it allows good control of the speed of deposition of the grains and amount of soil that is being poured.

Figure 5-4. Sample preparation using the water pluviation technique.

A three split part mold was assembled on the base of the pedestal to hold the membrane in place during sand placement. A vacuum of 20 kPa was applied to the mold to stretch the membrane, after which it was filled with de-aired water. The top and bottom drain lines were filled with de-aired water prior to pouring the sand. The sand was deposited by lowering the tip of the separatory funnel to the bottom of the split mold and then slowly raising the funnel to allow grain settlement. During this process, the tip of the funnel was maintained approximately 10 mm above the top of the sedimented sand surface. After achieving the target height, the sand surface was carefully leveled and the top cap was installed. The top drainage line was kept open during installation of the top cap to allow the trapped air and excess water to flow out of the sample. The least dense samples were formed following this procedure and the denser samples were formed by applying a slight vibration to the mold. The soil left in the separatory funnel was dried and weighed to determine the final sample mass.

After forming the sample, a vacuum of 20 kPa was applied to the sample through the top line and the split mold was carefully removed. The HKUST inner cell was placed on top of the bottom pedestal and then the inner chamber and reference water tube were filled with de-aired water. After assembling the triaxial cell, the main chamber was partially filled with de-aired water and a cell pressure of 20 kPa was applied to the sample and the vacuum released.

To create gassy samples, the backpressure was gradually increased to a pressure range between 300 kPa and 450 kPa, while keeping an effective confining stress of 20 kPa on the specimen. Once the B-value was checked and greater than 0.96, the sample was consolidated to in-situ stresses and then the pore water carefully replaced with carbonated water following the procedure described in section 5.3.2. After the pore water was replaced, the backpressure was gradually lowered to match the in-situ pore water pressure (U_o=100 kPa), while keeping the

applied effective stresses constant, forcing the CO_2 to come out of solution in the form of occluded bubbles. A 60-minute waiting period was enforced to ensure that the pore and air pressures in the sample had time to stabilize before shearing or cyclic loading. Since water was replaced by occluded gas during this process, the degree of saturation of the sample was reduced. Different initial degrees of saturation were achieved by adjusting the pressure at which the CO_2 was dissolved in water.

Although the HKUST pedestal contains an air entry porous disk of 100 kPa to prevent the CO_2 coming out of solution from passing the disk, the bottom drain lines were flushed with de-aired water to remove any CO_2-saturated water and/or gas bubbles still present below the porous disk. This step was conducted prior to de-saturation and before monotonic or cyclic loading, to ensure that the pore water pressure readings during subsequent steps were accurate and reliable.

To create saturated samples, the backpressure was increased, while keeping an effective confining stress of 20 kPa to 100 kPa for the least dense samples and to 250 kPa to 300 kPa for the denser samples in order to prevent cavitation. Once the B-value was checked and greater than 0.96, the sample was consolidated to in-situ effective stresses and then allowed to creep for at least 30 min. The saturated samples were sheared under either undrained or drained conditions; meanwhile the gassy samples were sheared under globally undrained conditions. The rate of shearing for both saturated and gassy samples was 0.20mm/min, corresponding to an axial strain rate of 0.22%/min.

5.3.2 Procedure to replace the sample's pore fluid

As illustrated in Figure 5-2, the circulation system developed for replacing the sample pore water with carbonated water consisted of two high pressure containers partially filled with de-aired water. The circulation system created was similar to that used by Amaratunga and Grozic

(2009). The inlet container was placed 0.8 m above the top of the triaxial cell and the bottom container was placed 0.8 m below the triaxial cell, creating a head difference of approximately 1.5 m. The inlet container was connected to the bottom drain line and the outlet container to the top drain line to create an upward water movement during pore fluid replacement. To produce the CO_2 saturated water, a pressure similar to that of the sample backpressure was applied to both containers using a pressurized CO_2 tank. This pressure was maintained for a period of at least 24 hours, which is considered long enough to fully saturate the water with CO_2 (Knai, 2011). To replace the pore fluid, the top and bottom sample drain lines were opened to allow the CO_2-saturated water to flow by gravity from the inlet container to the sample and from the sample to the outlet container. A total volume of CO_2-saturated water approximately equal to three times the volume of the pore fluid was flushed through the sample to ensure that the pore water was completely replaced with carbonated water. The water replacement process took from 3 to 4 days under an effective mean normal stress of 100 kPa.

5.3.3 Total volume change measurements (HKUST inner cell)

Figure 5-5 shows the system used to measure the total and water volume changes. This system was developed by Ng (2007) at the Hong Kong University of Science and Technology and consists of an inner cell within the main triaxial cell. Here, when a gassy specimen changes volume, a water level change is produced in the inner chamber. The total volume change is measured with a high accuracy differential pressure transducer (DPT) by recording the differential changes in pressure between the water inside the inner cell and the reference water level outside the inner cell. The DPT gives measurements ranging from +/- 3.4 kPa (+/- 340 mm of water head), and an accuracy better than 0.1% full-scale pressure output (+/- 3.4 Pa or 0.34 mm of water head). The accuracy of the total volume change system is on the order of 178 mm³,

corresponding to a volumetric strain of 0.09% for a sample 50 mm in diameter and 100 mm in height.
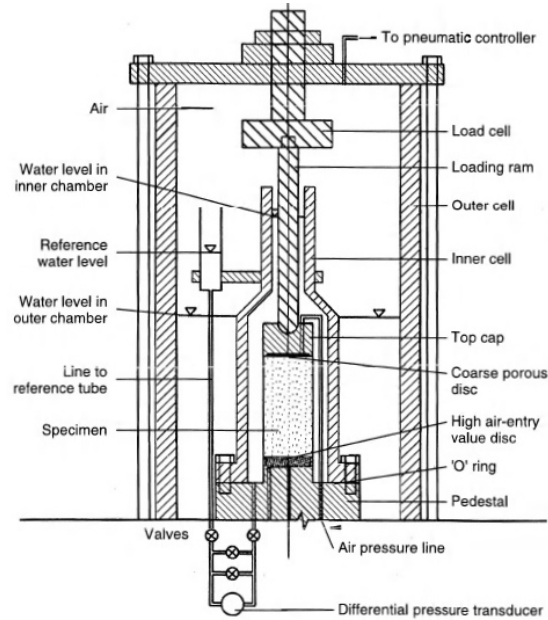
Figure 5-5. Total volume change measurement.
(Ng, 2007)

5.3.4 Shear wave velocity measurements

A set of bender elements, one inserted in the top cap and the other one in the HKUST bottom pedestal, was used to measure the shear wave propagation velocity along the longitudinal axis of the sample. An excitation voltage is applied to the shear wave transmitter (located in the top cap) to cause the bender element to bend and create a flexural wave that travels vertically through the sample. This wave is detected by the receiver located at the bottom of the HKUST pedestal. The shear wave velocity is computed by measuring the travel time of the wave from the source to the receiver. Shear wave measurements are unaffected by the saturation of the sample due to the negligible shear modulus of water. Bender element measurements were taken during consolidation, creep, sample de-saturation, and shear to fully define the effect of changes in

stresses and saturation on the soil elastic response. Details regarding the data reduction techniques have been described by Kim and Finno (2012). The values of the shear wave velocity reported herein were computed using the wave travel time determined by the peak-to-peak method.

5.4 One-dimensional constrained compression

A series of one-dimensional constrained compression (oedometer) tests were conducted on dry samples at various dry densities. The results of these tests were used to estimate the volume change that will occur after each blast event. This approach assumes that the densification of a loose deposit is a direct consequence of the blast induced pore water pressure dissipation and soil re-sedimentation and that no soil volume change will occur during blasting due to the very rapid loading resulting from each blast event.

Figure 5-6 illustrates the proposed method for estimating the expected volume change during reconsolidation from a zero effective vertical stresses to the in-situ vertical stresses. The sketch shows the results of constrained compression tests on specimens initially prepared at two different dry densities, ρ_{d1} and ρ_{d2}. Point A represents the initial state of the sand in the ground. If the blast is large enough to liquefy the soil, and assuming that no volume change occurs during blasting (a good approximation for the very rapid loading resulting from a blast event), the state of the soil element will move to point A'. As the induced pore water pressure dissipates, the soil will reconsolidate along path A'-B, resulting in a void ratio change of $\Delta e1$. A second blast will cause the soil element B to move to point B' (if liquefaction is induced) and will reconsolidate along path B'-C. A similar trend will be assumed for all of the other blast events. In this way, the volume changes measured in the laboratory can be used to predict the volume changes in the

field after each blast event, assuming a family of $e - \sigma_v'$ curves is determined from ρ_d that span

the expected density and effective stress conditions during blasting.
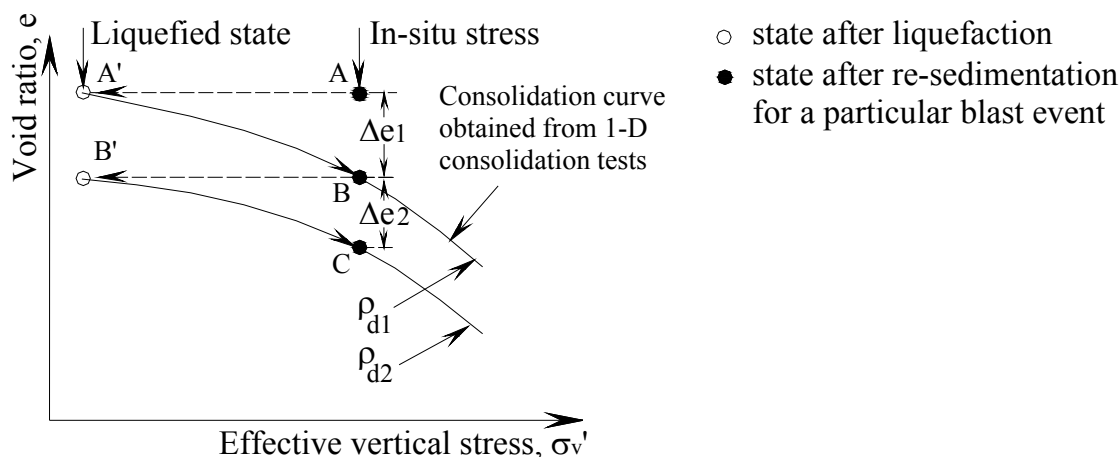
Figure 5-6. Void ratio changes during re-sedimentation after liquefaction.

5.5 Triaxial experimental program

Table 5-1 lists the summary of the triaxial experimental program. A total amount of 45

triaxial compression tests were conducted to determine the response of gassy and saturated sand

samples to monotonic and cyclic loading. The tests were divided into three groups to quantify the

soil's mechanical response as a function of void ratio and degree of saturation. These void ratios

and degrees of saturation are representative of those of the soil condition after blast densification

(see chapter 7). As will be explained in the following sections, moist-tamped (MT) samples were

used to define the critical state line and to complement the cyclic stress ratio vs. number of

cycles data obtained from the water-pluviated (WP) samples. The sample number, test type

(saturated or gassy), void ratio before monotonic or cyclic loading, effective mean normal stress

after consolidation, loading conditions (D:drained or U:undrained), degree of saturation before

monotonic or cyclic loading, loading condition (M: monotonic or C:cyclic), and the purpose of

the tests are presented in the table. For all samples, except samples used to determine the critical

state line, the vertical and horizontal effective stresses after consolidation were 136kPa and

82kPa, respectively.

Table 5-1. Summary of testing program.

Sample	Test type	$e_{cons.} = e_{sh.}$	p' (kPa)	Drainage	S (%)	Loading	Purpose
MT-01	Saturated	0.972	84	CAU	100	M	CSL
MT-02	Saturated	0.845	502	CAU	100	M	CSL
MT-03	Saturated	0.785	1526	CAU	100	M	CSL
MT-04	Saturated	0.993	100	CAU	100	M	CSL
MT-05	Saturated	0.826	697	CAU	100	M	CSL
WP-06	Saturated	0.817	100	CAD	100	M	Shear resistance $e_{aver.}$=0.83
WP-07	Gassy	0.820	100	CAU	94	M	
WP-08	Gassy	0.836	100	CAU	83	M	
WP-09	Saturated	0.841	100	CAU	100	M	
WP-10	Saturated	0.782	100	CAD	100	M	Shear resistance $e_{aver.}$=0.78
WP-11	Gassy	0.797	100	CAU	95	M	
WP-12	Gassy	0.785	100	CAU	91	M	
WP-13	Gassy	0.798	100	CAU	82	M	
WP-14	Saturated	0.775	100	CAU	100	M	
WP-15	Saturated	0.715	100	CAD	100	M	Shear resistance $e_{aver.}$=0.71
WP-16	Saturated	0.703	100	CAD	100	M	
WP-17	Gassy	0.716	100	CAU	98	M	
WP-18	Gassy	0.706	100	CAU	91	M	
WP-19	Gassy	0.692	100	CAU	75	M	
WP-20	Saturated	0.706	100	CAU	100	M	
WP-21	Saturated	0.826	100	CAU	100	C	Cyclic resist. e=0.82
WP-22	Gassy	0.811	100	CAU	89	C	
WP-23	Gassy	0.828	100	CAU	84	C	
WP-24	Saturated	0.791	100	CAU	100	C	Cyclic resist. e=0.78
WP-25	Gassy	0.774	100	CAU	95	C	
WP-26	Gassy	0.783	100	CAU	83.5	C	
WP-27	Saturated	0.706	100	CAU	100	C	Cyclic resist. e=0.70
WP-28	Gassy	0.695	100	CAU	98	C	
WP-29	Gassy	0.687	100	CAU	88	C	
WP-30	Gassy	0.803	100	CAU	N/A	C	Cyclic resist.
WP-31	Gassy	0.757	100	CAU	N/A	C	
WP-32	Gassy	0.728	100	CAU	N/A	C	

Sample	Test type	$e_{cons.} = e_{sh.}$	p' (kPa)	Drainage	S (%)	Loading	Purpose
WP-33	Saturated	0.825	100	CAU	100	C	Defining CSR vs. N
WP-34	Saturated	0.819	100	CAU	100	C	
WP-35	Saturated	0.780	100	CAU	100	C	
WP-36	Saturated	0.782	100	CAU	100	C	
WP-37	Saturated	0.789	100	CAU	100	C	
WP-38	Saturated	0.702	100	CAU	100	C	
WP-39	Saturated	0.707	100	CAU	100	C	Defining CSR vs. N
MT-40	Saturated	0.820	100	CAU	100	C	
MT-41	Saturated	0.843	100	CAU	100	C	
MT-42	Saturated	0.841	100	CAU	100	C	
MT-43	Saturated	0.977	100	CAU	100	C	
MT-44	Saturated	0.983	100	CAU	100	C	
MT-45	Saturated	0.963	100	CAU	100	C	

5.5.1 Determination of the critical state line

Five undrained triaxial compression tests were conducted on reconstituted saturated specimens to determine the position of the critical state line (CSL). As shown schematically in Figure 5-7, the samples were consolidated to stresses higher than the critical state values at a given void ratio, to assure the soil response was fully contractive and the CSL can be determined reliably. Since high void ratios cannot be prepared by using the water pluviation technique and very loose to loose specimens are required to determine reliably the CSL, the samples were prepared by using the moist tamping technique. The procedures presented by Chaney and Mulilis (1978) and Ladd (1978) were followed to prepare the specimens.

Although the effective stress path and stress-strain response are strongly affected by the sample initial fabric (Vaid et al., 1999; Vaid and Sivathayalan, 2000), the steady state condition at high stress levels is not influenced by the method of sample preparation. Samples reconstituted with different preparation techniques converge to the same curve in the *e-q-p'* space, as long as

the soil response is fully contractive (Poulos et al., 1985; Been et al., 1991; Castro et al., 1992; Verdugo and Ishihara, 1996). Been et al. (1991) showed that samples prepared by water pluviation and by moist tamping techniques yield the same critical state line.
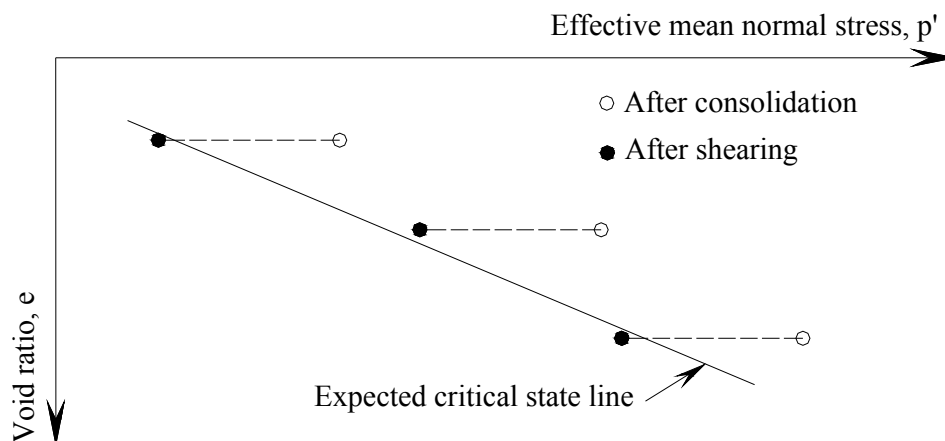
Figure 5-7. Determination of the critical state line.

5.5.2 Fully and partially saturated sand responses at constant effective stress

A series of triaxial compression tests were conducted to determine the response of reconstituted medium dense sand samples to monotonic and cyclic loading. Fully saturated samples (control tests) and partially saturated samples (gassy samples) were conducted to evaluate the effect of gas on the soil shear strength and cyclic resistance to liquefaction.

The control samples were prepared in a saturated state and anisotropically consolidated to in-situ stresses representative of the loose layer at the Oakridge blasting site and to void ratios above and below the critical void ratio (CVR). These samples were performed to define the saturated soil response in both the "loose of critical" and "dense of critical" zones.

Another series of reconstituted samples containing gas were tested to quantify the influence of gas on soil mechanical behavior during monotonic and cyclic undrained loading. Figure 5-8

shows the range of void ratios and degrees of saturation used in this testing program. The gassy samples were consolidated to in-situ stresses and void ratios similar to those of the control tests. At each void ratio, samples with degrees of saturation varying from 75% to 98%, before shearing or cyclic loading, were prepared.

Two set of experiments were performed to determine the soil response as a function of density and degree of saturation. The first set consisted of samples sheared monotonically under undrained condition to quantify the shear strength of saturated and gassy soils. The rate of shearing for both saturated and gassy samples was 0.20 mm/min, or at an axial strain rate of 0.22%/min. The second set consisted of samples sheared cyclically under undrained conditions to quantify the cyclic resistance of gassy samples.
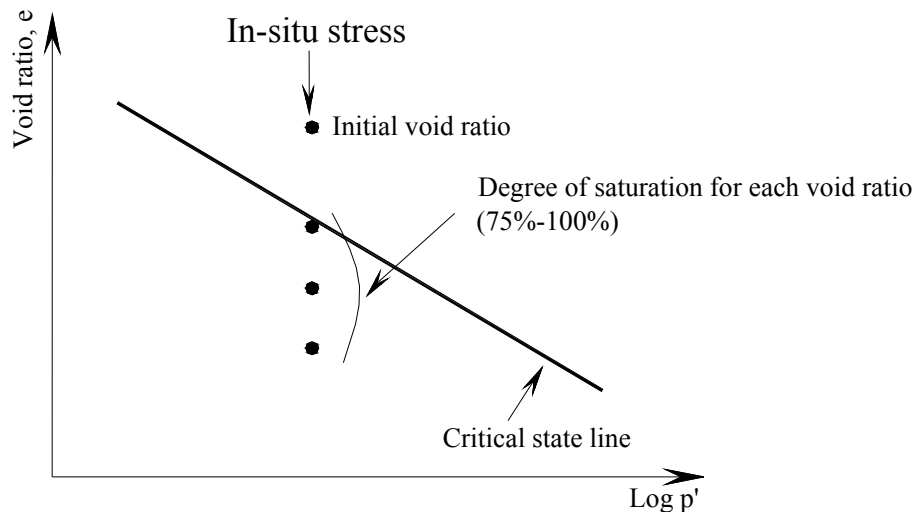
Figure 5-8. Range of void ratios and degrees of saturation.

5.6 Static and cyclic triaxial response of sands

The response of sands to undrained monotonic loading depends on the initial void ratio of the soil, e, and mean normal effective stress, p', acting on it (Robertson and Wride, 1998; Vaid and Sivathayalan, 2000). Figure 5-9 illustrates the undrained response of sands, with void ratios and

state of stresses above and below the critical state line, under monotonic loading. (Robertson and Wride, 1998). In this figure, LSS is the limited strain-softening response, q_{ST} is the static gravitational shear stress, S_u is the ultimate undrained shear strength, SH is the strain-hardening response, SS is the strain-softening response, and US is the ultimate state.
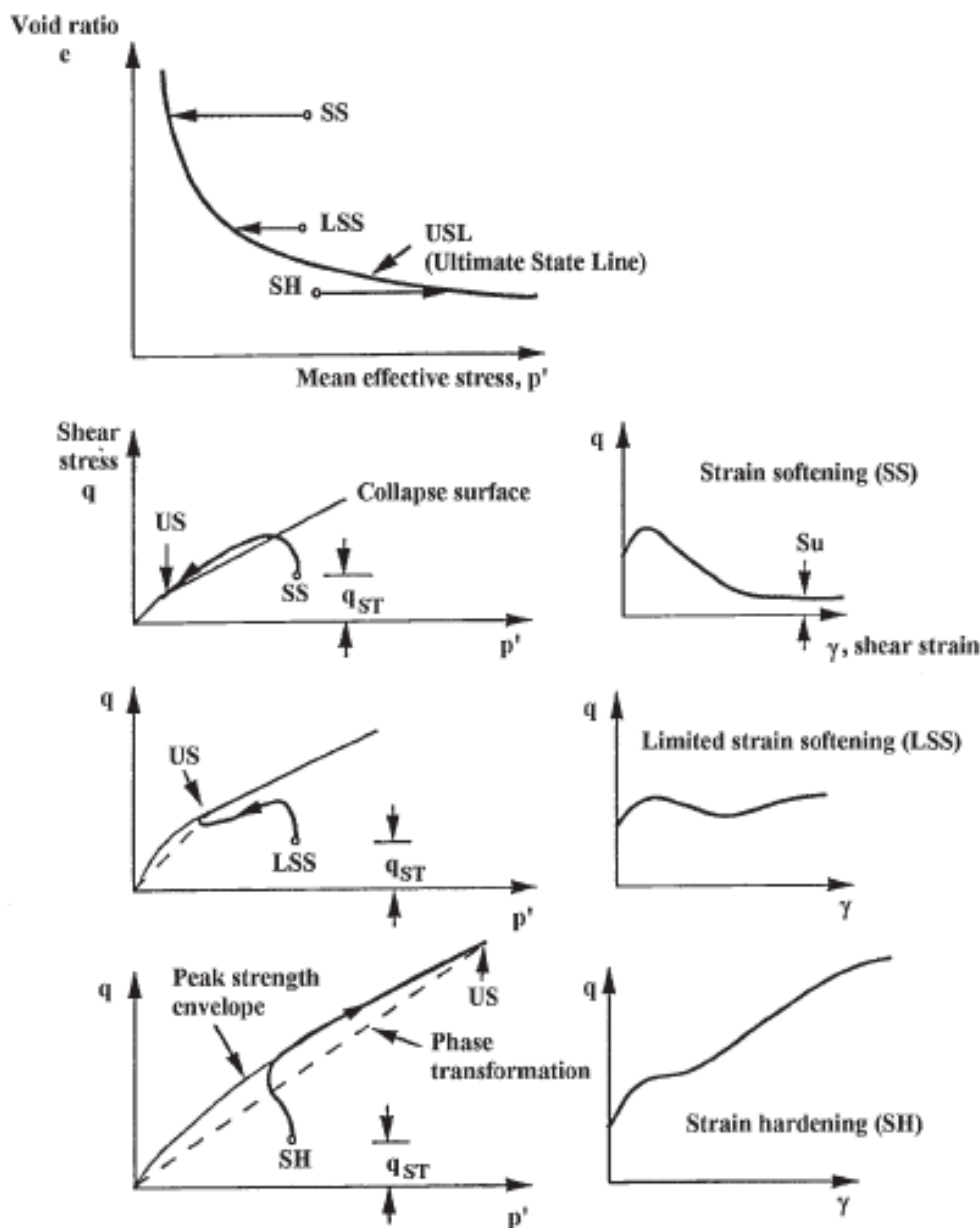
Figure 5-9. Characteristic undrained behavior of sands under static loading. After Robertson and Wride (1998)

Figure 5-9 shows that liquefaction and flow may be triggered in a soil with a state of stresses higher than the ultimate state values at a given void ratio (point SS). At large strains, the soil will strain-soften and eventually it will reach a critical state condition. The response of a soil with an initial void ratio and state of stress above but close to the ultimate state line (critical state line), will show a limited strain softening (LSS) as the soil contracts and then it will change to a strain hardening response as the soil tends to dilate. This behavior continues until the ultimate state is reached. A soil with an initial void ratio and state of stress below the critical state line will strain hardens at large strains until it reaches the ultimate state.

Cyclic triaxial tests have been extensively used to investigate the liquefaction resistance of saturated sands during dynamic loading. Liquefaction refers to the loss of shear strength or development of excessive strains on saturated cohesionless soils due to increase in porewater pressure during dynamic loading. A precise definition of soil liquefaction is given by Sladen et al. (1985)

> *"Liquefaction is a phenomenon wherein a mass of soil loses a large percentage of its shear resistance, when subjected to monotonic, cyclic, or shock loading, and flows in a manner resembling a liquid until the shear stresses acting on the mass are as low as the reduced shear resistance."*

Figure 5-10 shows the response of a cohesionless soil to cyclic undrained loading (Robertson and Wride, 1998). In this figure, q_{ST} and q_{cy} are the applied static and cyclic shear stresses, respectively. In a loose soil, positive porewater pressures will develop during shearing and as a consequence the effective confining stresses are reduced until a steady state condition is reached. If the residual shear strength of the soil is less than the static shear strength, liquefaction and flow will occur. In a dense soil, positive porewater pressures will occur due to the contractive response of the soil at small strains. If the cyclic shear stress is greater than the static shear stress

(q_{cy}>q_{ST}) and shear stress reversal is induced, the soil will reach a transient stress of zero effective stress and it may experience large deformation during cycling loading. If $q_{cy} < q_{ST}$ and there is not shear stress reversal, the soil may not reach a transient stress of zero effective stress and only cyclic mobility with limited deformations will occur.
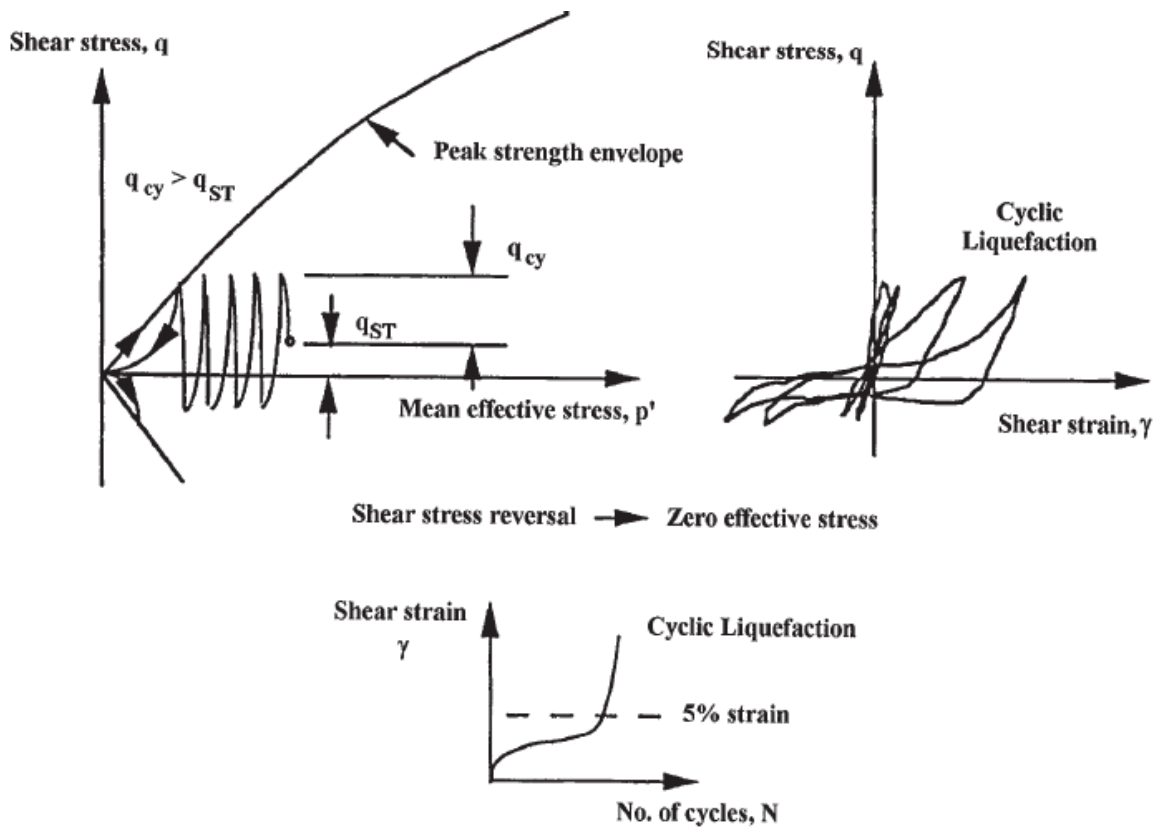
Figure 5-10. Schematic of undrained cyclic behavior of sand illustrating cyclic liquefaction. After Robertson and Wride (1998)

Liquefaction susceptibility of sands has been found to be dependent on the initial void ratio, confining stress and static shear stress. The mechanisms of strain developed during cyclic loading depend on these variables and on the characteristic of the dynamic event (Vaid and Chern, 1983; Vaid et al., 1990; Vaid et al., 2001; Sivathayalan and Ha, 2004; Wijewickreme et al., 2005b). Deformations causing liquefaction occur by four different mechanisms of strain.

These mechanisms are shown and explained in detail by Sivathayalan (2000). Figure 5-11a illustrates the stress-strain and stress path due to strain softening in compression. In this type of strain mechanism, small strains develop until the state of effective stress of the soil reaches the critical state line. At this point, very large strains begin to develop. A similar type of strain softening deformation on contractive sands was observed by Castro (1969). In the strain mechanism shown in Figure 5-11b, large strains develop by limited liquefaction due to strain softening within certain number of cycles, and then the strains become smaller as the soil changes to a strain hardening response. Figure 5-11c and d illustrate the strain mechanisms developed in dense sands. Cyclic mobility is the cause of liquefaction in sands with a state of stress located below the critical state line. Figure 5-11c shows the strain response of a dense sand when the applied cyclic shear stress is greater than the static shear stress ($q_{cy}>q_{ST}$). If a shear stress reversal is induced, the soil will reach a transient state of zero effective stress. Figure 5-11c illustrates the case when the cyclic shear stress is less than the static shear stress and a transient state of zero effective stress is not experienced.
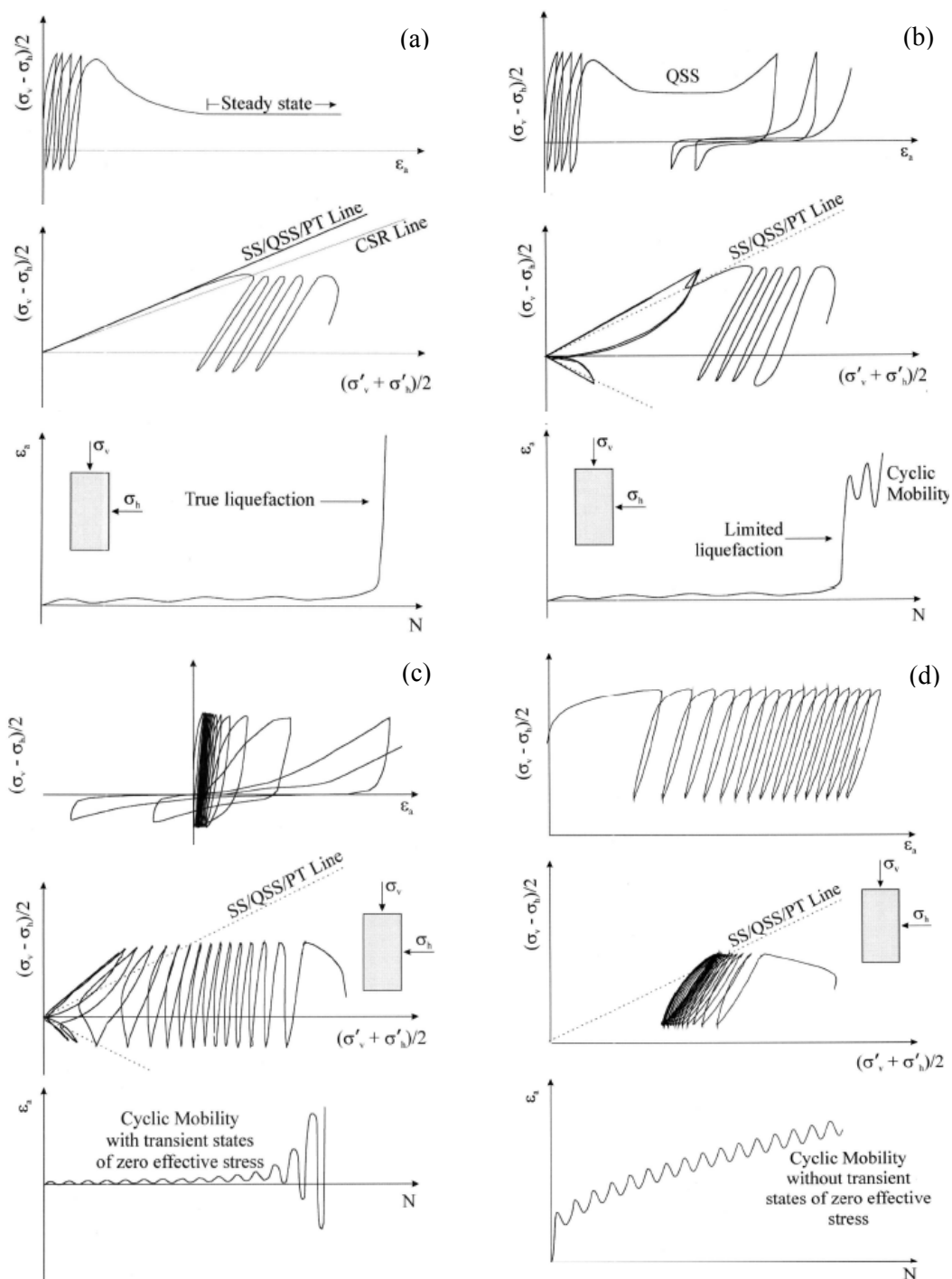
Figure 5-11. Strain mechanisms causing liquefaction (a) steady state deformation following strain softening, (b) strain softening followed by cyclic mobility, (c) cyclic mobility with transient states of zero effective stress and (d) cyclic mobility without transient states of zero effective stress. After Sivathayalan (2000)

5.7 Summary

This chapter describes the index properties of the sand used for testing, summarizes the laboratory testing program implemented to determine the shear resistance and cyclic resistance to liquefaction and flow of saturated and gassy sands and presents the procedure proposed to estimate the volume changes that will occur at the Oakridge landfill site after each blast event.

6   RESULTS OF LABORATORY EXPERIMENTS

Twenty-one one-dimensional constrained compression tests were conducted on dry samples prepared at various densities to estimate the total volume change that will occur after each blast event. Fourty-five triaxial tests were performed to determine the shear resistance and cyclic resistance to liquefaction of medium to dense saturated and gassy sands. The effect of gas on the monotonic and cyclic response of sands is evaluated and discussed in detail.

6.1   One-dimensional constrained compression tests

The procedure used to estimate the void ratio change that will occur after each blast event was explained in section 5.4. Twenty-one oedometer tests on dry samples at dry densities varying from 13.0kN/m^3 (1.30 g/cm^3) to 15.5kN/m^3 (1.55g/cm^3) were performed. Figure 6-1 and Figure 6-2 show the results from the oedometer tests conducted to the sand samples collected by GeoSyntec Consultants during the densification program between 2003 and 2004 (test area C), and to the samples collected by Northwestern University in 2011 (zone 18), respectively.
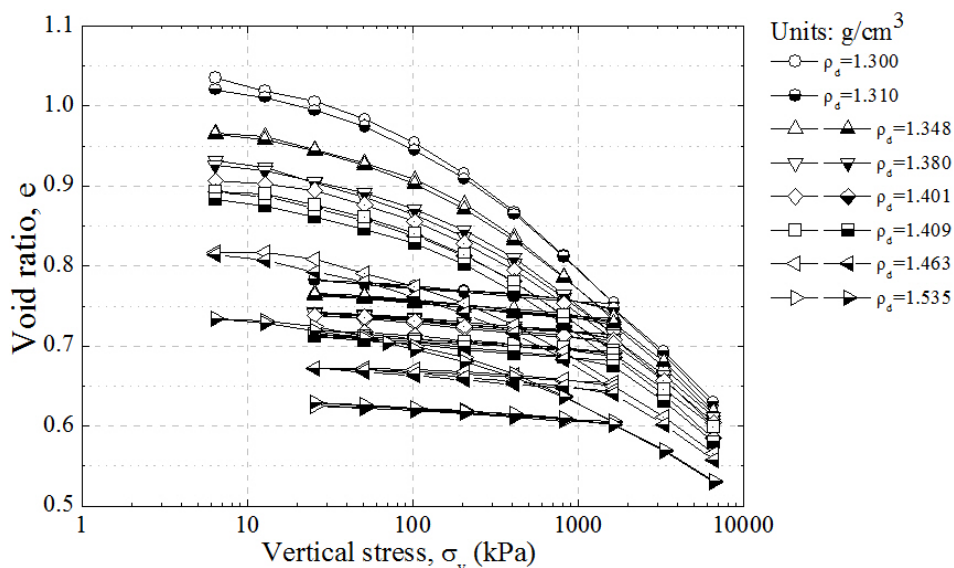
Figure 6-1. One-dimensional constrained compression results from sand samples collected in 2003-2004.
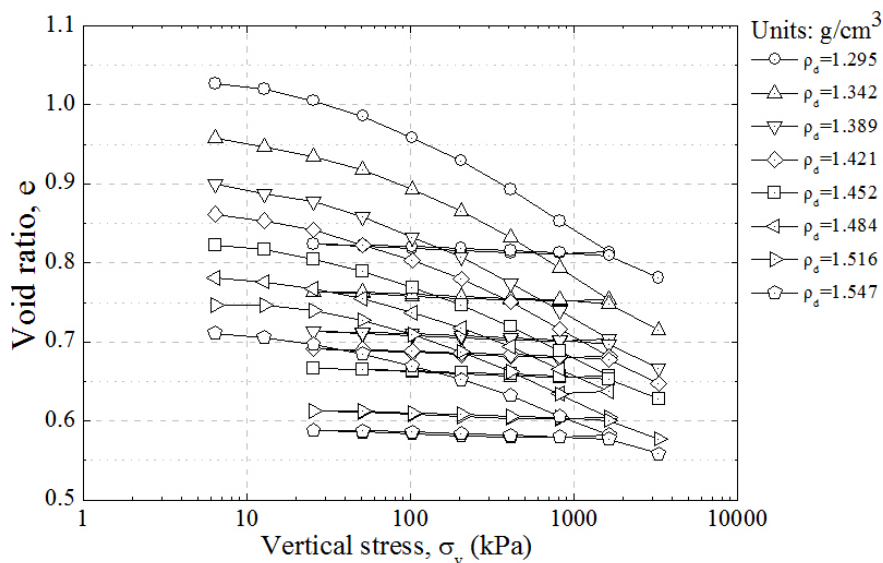
Figure 6-2. One-dimensional constrained compression results from sand samples collected in 2011.

Figure 6-3 shows an illustrative example of how to compute the expected void ratio change after each blast event. In this figure, it is assumed that there is no void ratio change from $\sigma_v' = 0 kPa$ to $\sigma_v' = 6 kPa$ (first load increment). Assuming that the void ratio and in-situ vertical stress acting on the loose sand before blasting are 1.05 and 100 kPa, respectively, the first blast will reduce σ_v' to 0 kPa and the soil will reconsolidate along path a-a', resulting in a void ratio change of 0.073. A second blast will reduce σ_v' to 0 kPa and will cause the soil to reconsolidate along the path b-b', resulting in a void ratio change of 0.067. The same procedure can be followed to compute the expected volume changes for subsequent blasts.
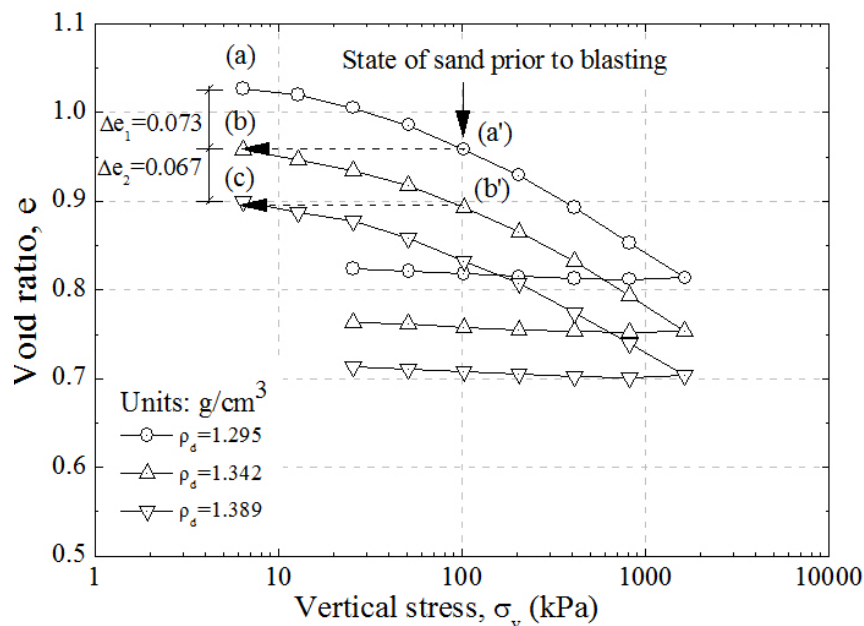
Figure 6-3. Example calculation of expected void ratio change after each blast.

Figure 6-4 shows the expected void ratio and axial strain changes computed from the one-dimensional constrained compression tests.
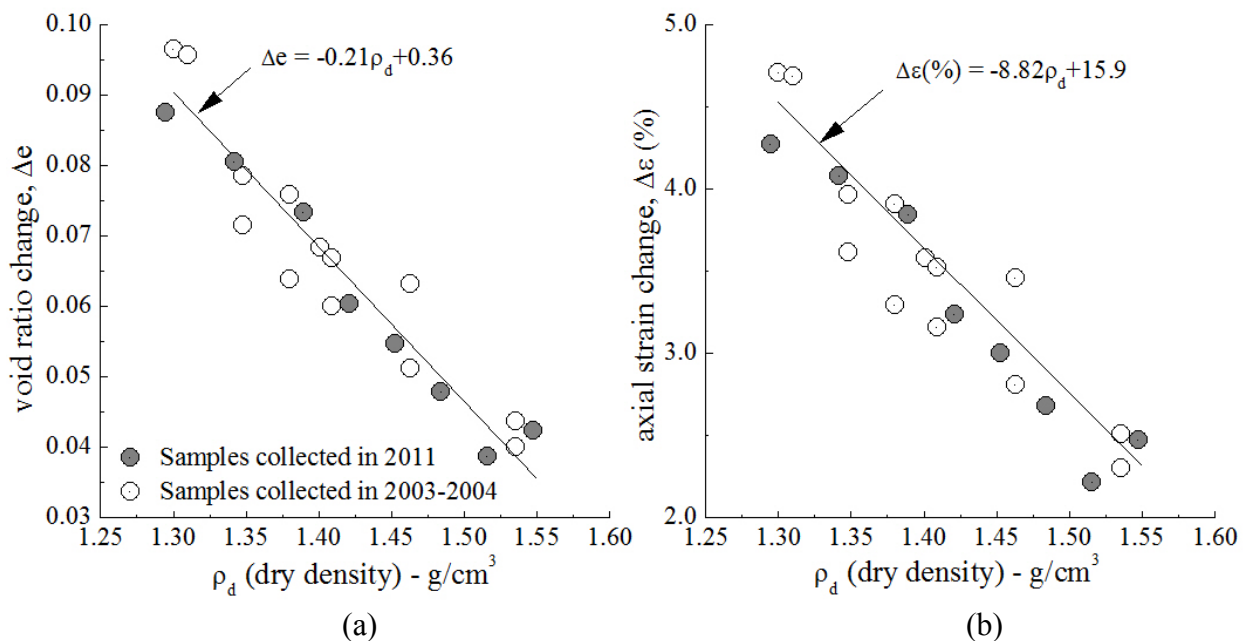
Figure 6-4. (a) Void ratio and (b) axial strain changes versus initial dry density.

Figure 6-4 can be used to estimate the void ratio and axial strain changes that will occur after each blast event at the Oakridge landfill. Figure 6-5 illustrates how to estimate the final void ratio of a soil mass after two blast events. For example, if the in-situ void ratio before blasting is $e_o=0.90$, then the expected void ratio change after the first blast event will be $\Delta e=0.064$ (solid line). With the new void ratio being $e=0.836$, the expected void ratio change after the second blast event will be $\Delta e=0.054$ (dashed line). The final void ratio of the soil mass after two blast events will be approximately $e=0.782$. Note that each successive blast will result in a smaller change in void ratio than the previous blast.
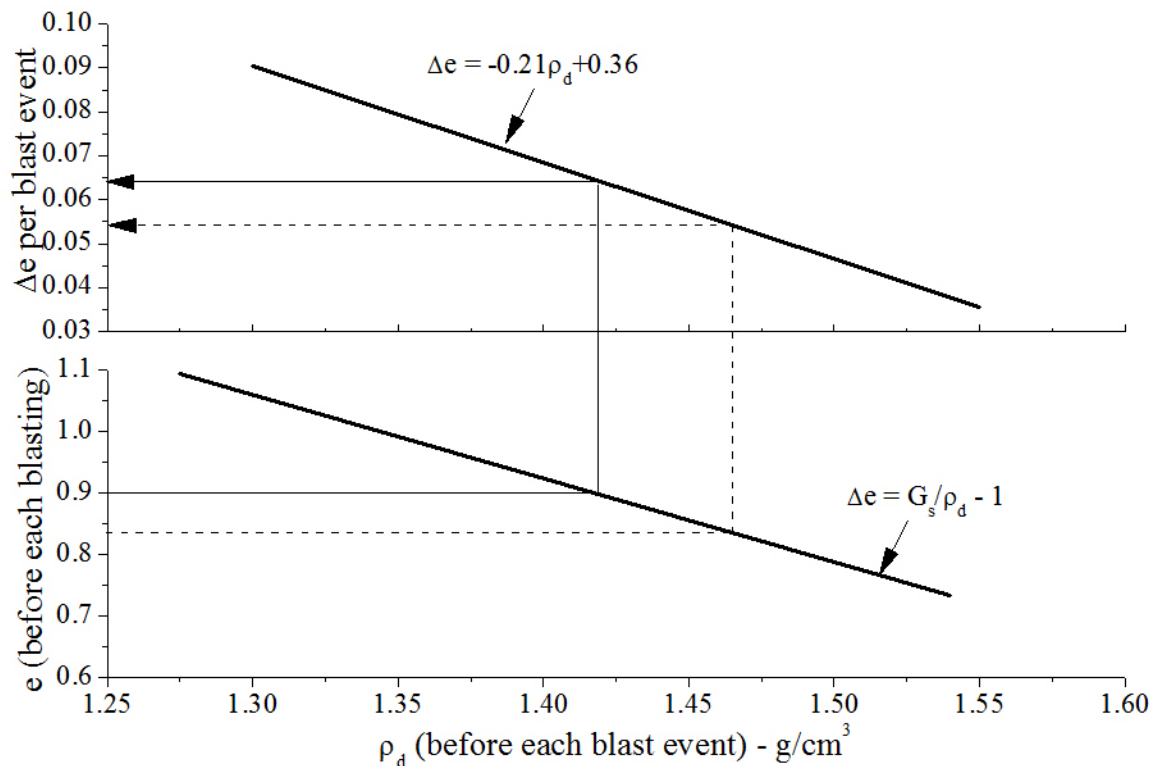
Figure 6-5. Expected void ratio change after each blast event.

6.2 Final sample degree of saturation and volume changes during de-saturation

Figure 6-6 shows the change in backpressure used to force the CO_2 to come out of solution and the final degrees of saturation achieved after this step. The line that best fits the data is $S(\%) = -0.09\Delta_{BP} + 113$, with a square root value of 0.35. Although there is a trend, it is not a highly correlated one. Final degrees of saturation ranging from 82% to 98% were achieved by decreasing the backpressure from 350kPa to 100kPa (Δe=250kPa). It was visually observed that the final degree of saturation was not just a function of the amount of applied backpressure but also of the volume of de-aired water that was replaced in the sample with carbonated water.
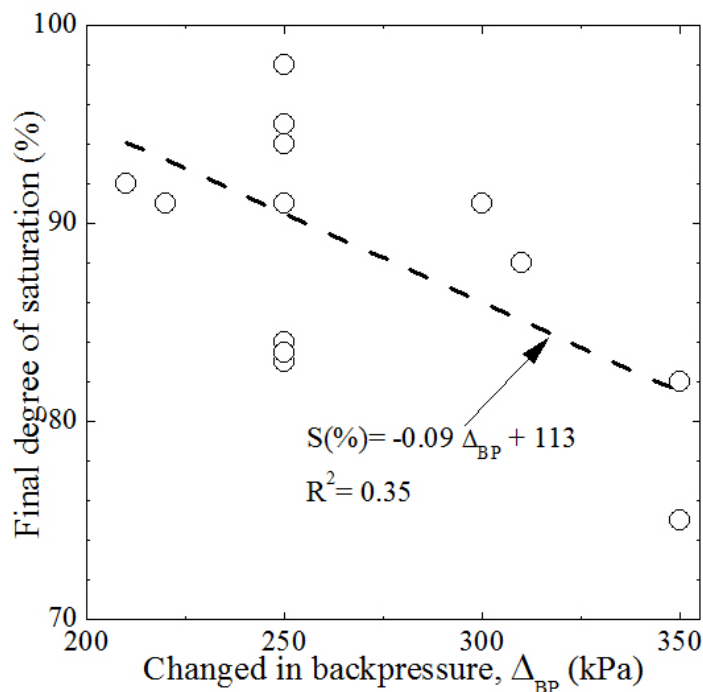
Figure 6-6. Changes in backpressure and achieved final degrees of saturation.

Figure 6-7 shows typical curves of the total volume change occurred during sample de-saturation. It can be observed that no total volume changes occurred during this step, indicating

that the sample void ratio remained constant during the de-saturation process. The final degree of saturation was computed assuming that the amount of water displaced during sample de-saturation was equivalent to the amount of gas released and trapped in the sample.
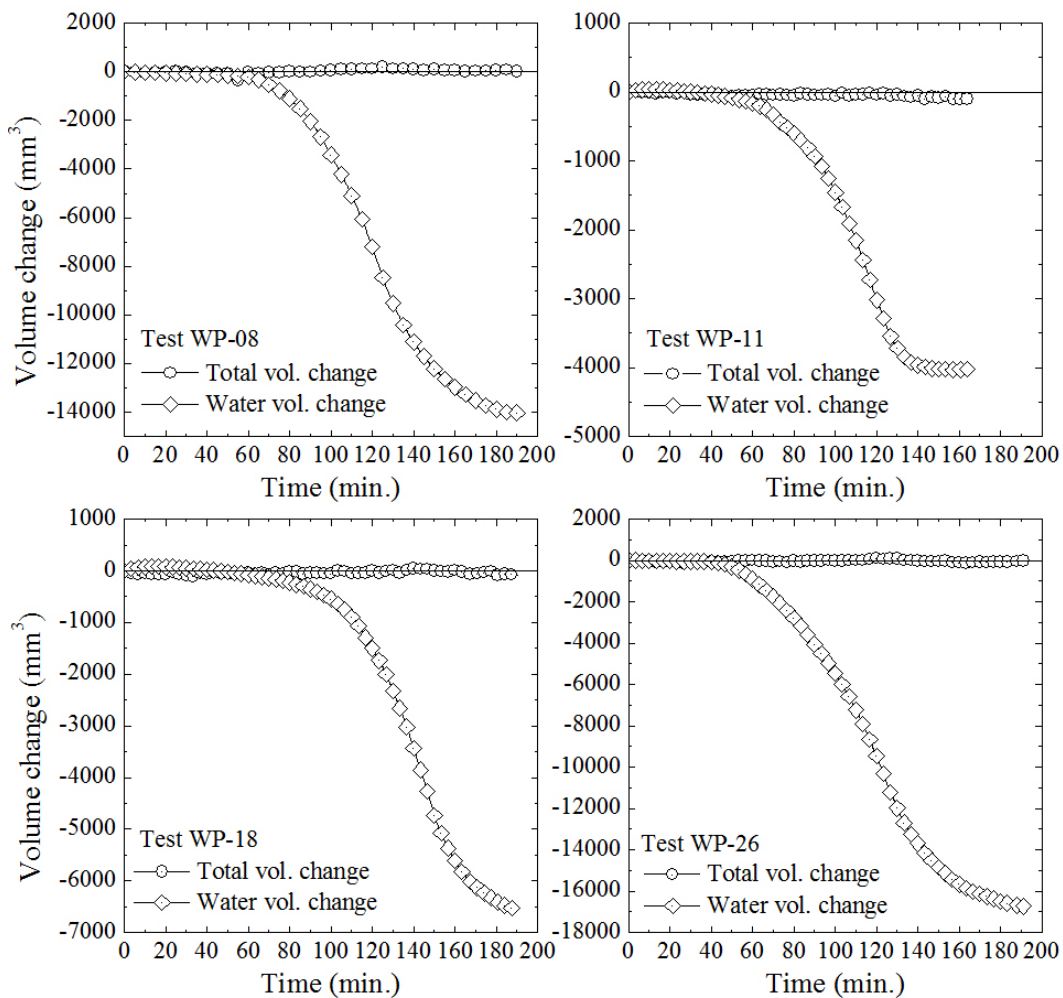
Figure 6-7. Total volume change during sample de-saturation.

6.3 Critical state line

Five displacement-controlled undrained compression triaxial tests were carried out to determine the position of the critical state line. Figure 6-8 shows the position of the critical state line. The specimens were anisotropically consolidated to stresses higher than the critical state

values at a given void ratio, to assure a fully contractive response. Consolidation pressures for these tests varied from 80 kPa to 1600 kPa.
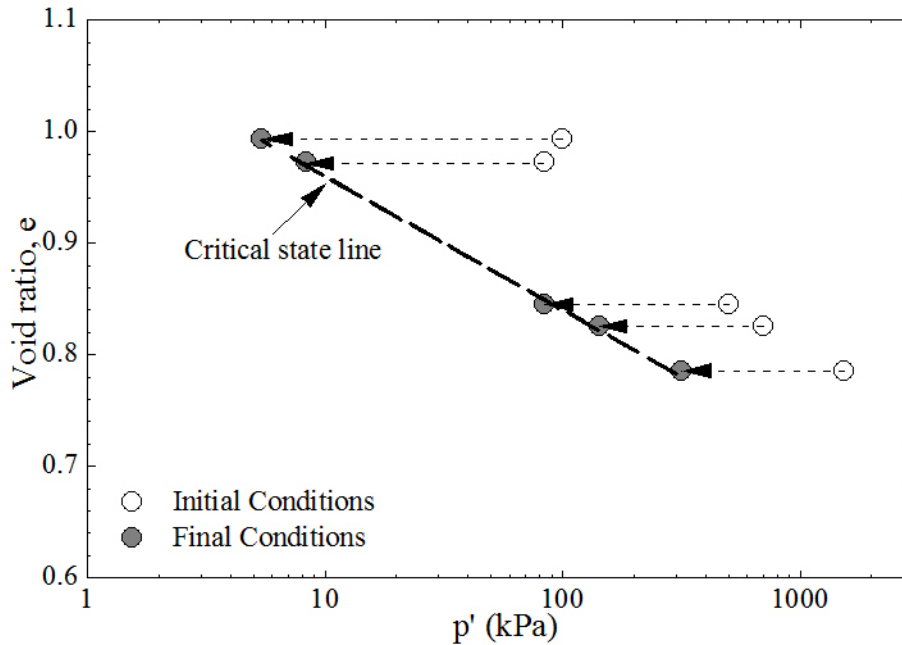
Figure 6-8. Determination of the position of the critical state line.

Figure 6-9 shows the effective stress paths and stress-strain curves for these tests. The effective mean normal stress was evaluated as $p' = (\sigma_1' + 2\sigma_3')/3$ and the deviatoric stress as $q = (\sigma_1' - \sigma_3')$. As can be seen in this figure, the response of the samples was fully contractive and a steady state condition was achieved at large deformations. The line of peaks was also determined from these tests. The critical state friction angle and mobilized friction angle at the line of peaks for these tests are 30.5^o and 17.9^o, respectively.
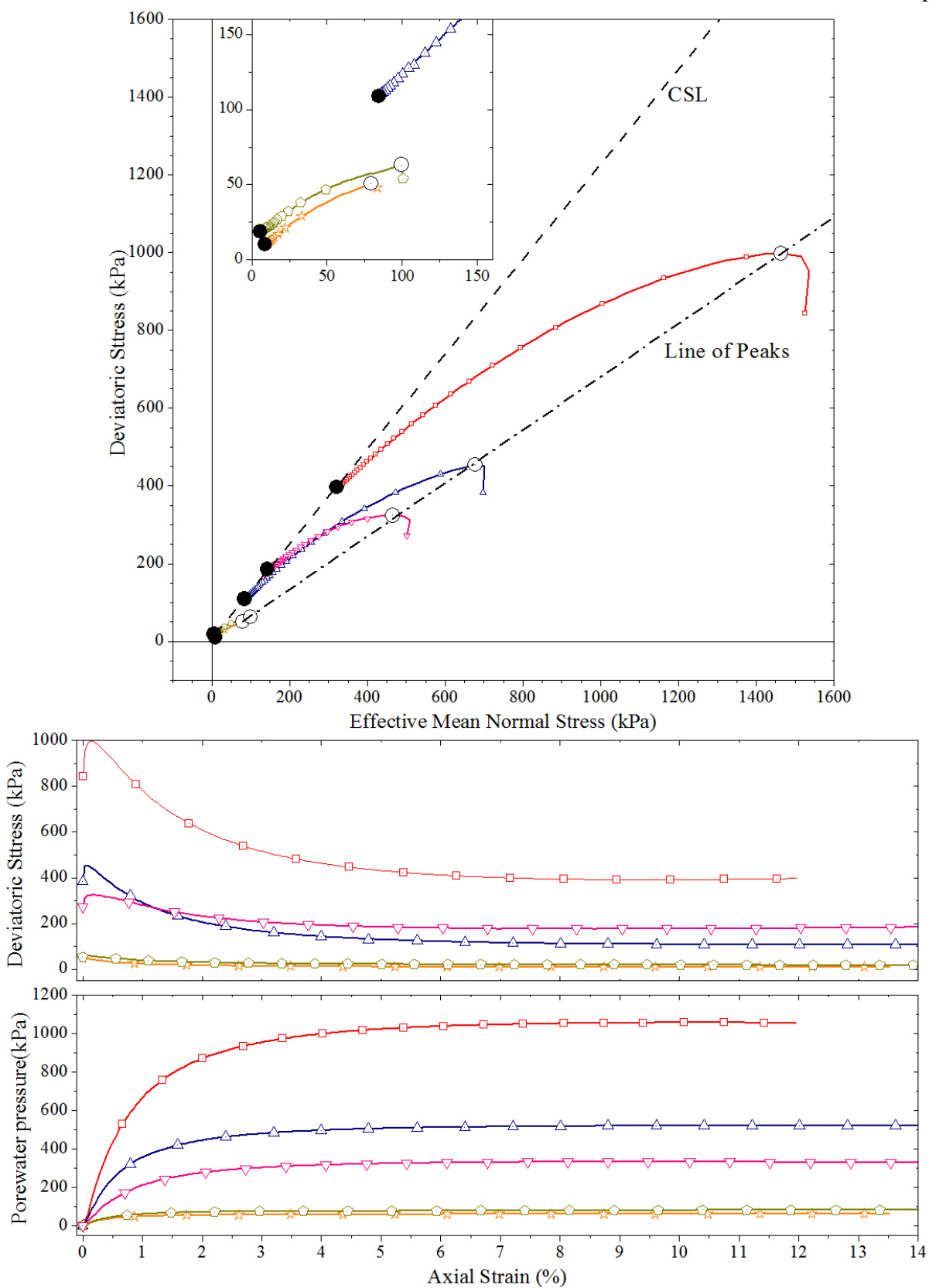
Figure 6-9. Results of undrained TXC tests on loose of critical specimens.

6.4 Computation of the effective stress

Figure 6-10 presents a typical plot of a Soil Water Characteristic Curve (SWCC) for the sand samples collected in 2011. The matric suction is plotted against the degree of saturation of the soil. In a partially saturated soil, the matric suction is defined as the difference between the pore-air pressure, u_a, and the pore-water pressure, u_w. The air-entry value is defined as the matric suction where air starts entering the larges pores in the soil (Fredlund and Rahardjo, 1993).

The triaxial testing configured with the inner cell and high air entry porous disk of 100 kPa (see Figure 5-2) was used to determine the SWCC. To conduct this test, a sample with an initial void ratio of 0.842 was prepared by using the water pluviation technique and following the procedure described in section 5.3.1. For this specimen, the backpressure was slowly increased to a pressure of 220 kPa, while keeping an effective confining stress of 20 kPa. Once the B-value was checked and greater than 0.96, the top drain line was disconnected from the backpressure controller and then connected to the pneumatic controller. This pneumatic controller was used to control the air pressure and the suction applied to the sample. The matric suction was achieved by incrementally reducing the back pressure, while holding the air pressure constant throughout the test ($u_a = 220 kPa$). After each incremental reduction, the water in the sample was allowed to drain until equilibration was obtained. The amount of water that left the sample through the bottom line was measured with the backpressure controller.

The matric suction at a degree of saturation of 78%, which was the lowest degree of saturation computed at the Oakridge landfill, is 2.5kPa. This matric suction is within the range of matric suctions reported in the technical literature for fine sands containing little to no fines (Fredlund and Xing, 1994; Kim and Hwang, 2003; Gitirana and Fredlund, 2004; Lu et al., 2009; Likos et al., 2010). The magnitude of intergranular stress induced by the suction to sands is very

small and the initial matric suction of the sample decreases during monotonic or cyclic loading, as gas is dissolved in the pore fluid (Unno et al., 2008).
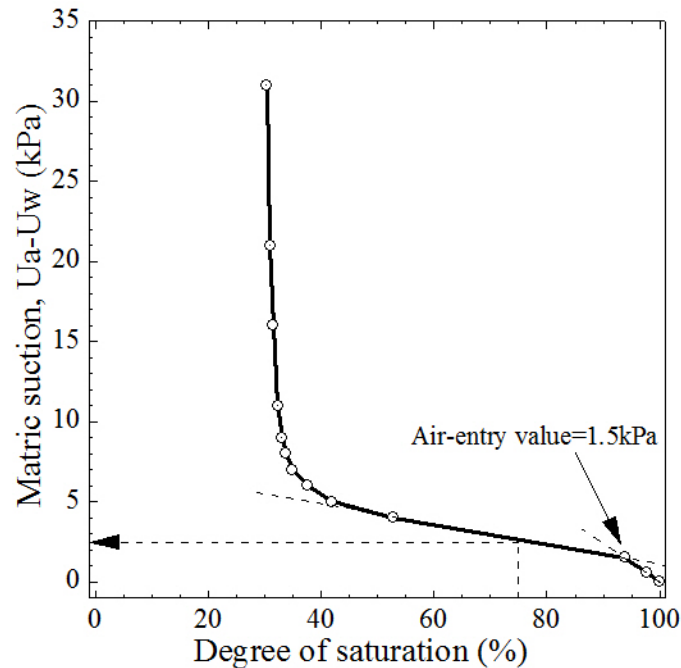
Figure 6-10. Soil water characteristic curve.

Gassy sand is considered a special type of unsaturated soil where the pore gas phase is not connected to the atmosphere and it is surrounded by a fully saturated soil mass (Nageswaran, 1983). Therefore, the only pressure acting on the gassy soil is the hydrostatic pressure. The concept of effective stress developed for saturated soils has been previously used by several authors to analyze the monotonic and cyclic response of loose gassy sand with degrees of saturation varying from 75%-100% (Grozic et al., 1999; Grozic et al., 2000; Amaratunga and Grozic, 2009), and it seems to provide reasonable results.

The effective normal stress can be computed from the classical formulas of unsaturated soil mechanics (Bishop and Blight, 1963):

$$\sigma' = (\sigma - u_a) + \chi(u_a - u_w)$$

where: σ' is the effective normal stress, σ is the total normal stress, u_a is the air pressure, u_w is the pore-water pressure, and χ is a parameter related to the degree of saturation of the soil ($\chi = saturation/100$). For a degree of saturation of 78% and a matric suction of 2.5 kPa, the effective normal stress acting on the soil grains at a depth of 10 m is approximately.

$$\sigma' = (200 - 102.5) + 0.78(102.5 - 100) = 99.5\ kPa$$

The effective stress computed from the classical formulas of saturated soil mechanic is

$$\sigma' = (200 - 100) = 100\ kPa$$

Since the results obtained from these two approaches are similar, for simplicity, the effective stress approach computed from the saturated soil formula was used to analyze the monotonic and cyclic results from the triaxial tests conducted in this study.

6.5 Definition of shear strength

The shear strength of samples sheared under monotonic loading was computed for the saturated undrained and gassy samples as the maximum value of the principal stress ratio in the σ'_1/σ'_3 vs ε_a (%) curve, and as the principal stress difference at the point of maximum dilation angle ($\sigma'_1 - \sigma'_3\ at\ \psi_{max}$) for the drained and gassy samples. The results from these two approaches are compared and discussed in the next section. For the specimens sheared under undrained cyclic loading, failure was defined as the number of cycles needed to induce liquefaction and flow in the loose of critical specimens or to reach an accumulative axial strain of 5% in the dense of critical samples.

6.6   Shear resistance of gassy soils as function of the degree of saturation

Fifteen triaxial compression tests were conducted to measure the shear resistance of saturated and gassy sands as function of density and degree of saturation (Table 5-1). The samples were anisotropically consolidated to an effective mean normal stress of 100 kPa (σ'_{3c} = 82 kPa and σ'_{1c}=136 kPa), except for the densest saturated samples which were consolidated to higher stresses to prevent cavitation during monotonic loading. The triaxial tests were divided into three groups to evaluate the mechanical response of gassy sands at various void ratios. As will be showed in chapter 7, the range of void ratios tested herein was representative of those in-situ final void ratios achieved at the Oakridge landfill after blast densification. Figure 6-11 shows the position of the initial and post-densification average void ratios with respect to the critical state line.
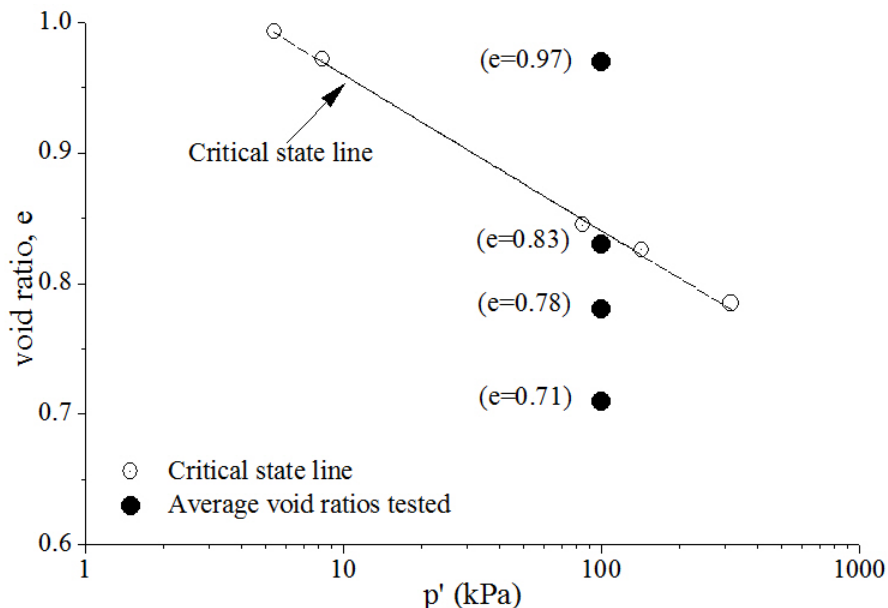
Figure 6-11. Position of void consolidated ratios with respect to CSL.

Figure 6-12 shows the stress-strain response, pore-pressure response and volumetric strain response of the saturated and gassy specimens with an average void ratio of 0.83. The soil

response was highly influenced by the amount of gas in the specimen. Gas had the effect of delaying the development of excess pore water pressure. The greater the amount of gas in the sample or the lower the degree of saturation, the smaller the positive excess pore water pressure.

Table 6-1 lists the shear strength, $q = (\sigma_1' - \sigma_3')$, and mobilized friction angle, ϕ, of the saturated and gassy soils computed using the definition presented in section 6.5. The friction angle of the gassy tests plotted between the saturated undrained and drained friction angles. At the maximum dilation angle, the shear strength of the gassy samples was less than the strength of the drained test. In general, the gassy tests had a friction angle between $1°$ and $2°$ lower than that of the drained test.

Table 6-1. Shear strength and mobilized friction angle ($e_{aver.}$=0.83).

Type	Saturation (%)	At $(\sigma_1'/\sigma_3')_{max}$		At ψ_{max}	
		q (kPa)	ϕ'	q (kPa)	ϕ'
Drained	100	213	34.2	214	34.1
Gassy	94	229	33.3	144	32.1
Gassy	83	196	32.5	181	31.9
Undrained	100	138	31.4		

Figure 6-13 shows the effective stress paths for the specimens with $e_{aver.}$=0.83. The stress path for the gassy sample with S=94% plotted between the saturated undrained and drained tests, meanwhile the gassy sample with S=83% essentially followed the drained stress path. This tendency is an indication that gas has the effect of changing the soil behavior from undrained conditions to drained conditions.
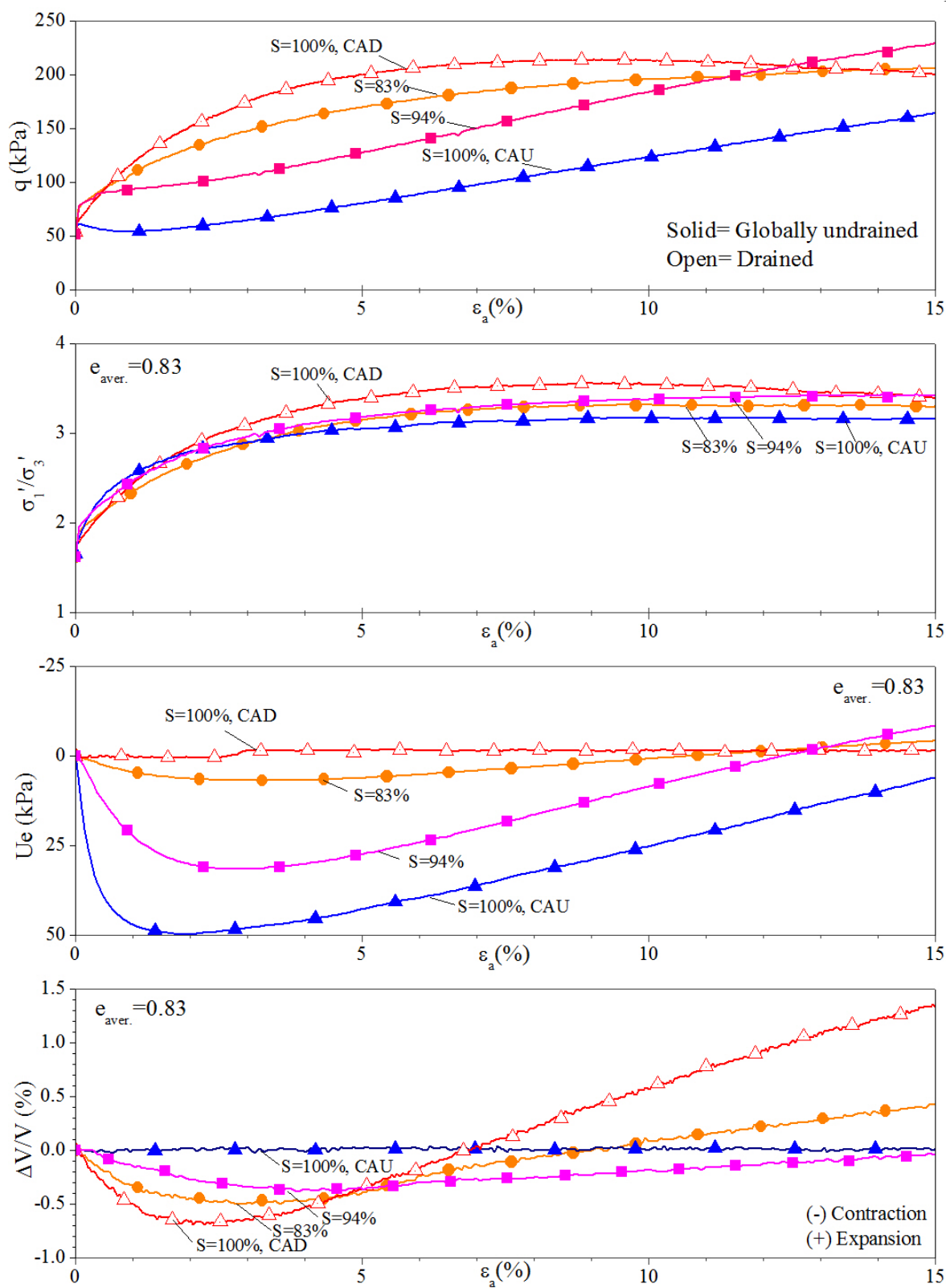
Figure 6-12. Stress-strain response, pore-pressure response and volumetric strain response. Group 1 - e_{ave.}=0.83
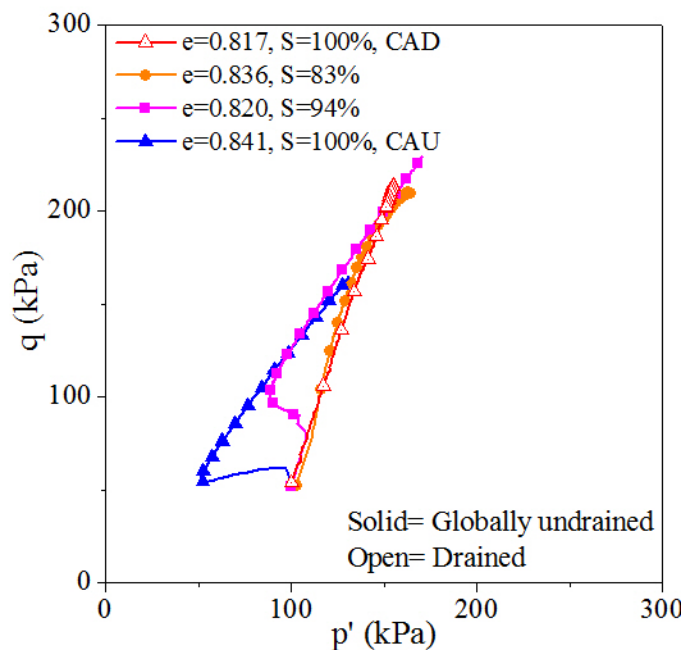
Figure 6-13. Effective stress paths (Group 1 - $e_{ave.}$=0.83).

Figure 6-14 shows the stress-strain response, pore-pressure response and volumetric strain response of the gassy specimens with an average void ratio of 0.78. Table 6-2 lists the shear strengths and mobilized friction angles computed from these tests. The shear strength and mobilized friction angles of the gassy tests were between the saturated drained and undrained values. Gas had the effect of changing the soil response from undrained to drained conditions. Gas made the soil more compressible, therefore reducing the magnitude of excess porewater pressure developed.

The maximum difference between the shear strengths computed at $(\sigma_1'/\sigma_3')_{max}$ and ψ_{max} was less than 12.5%, being slightly greater the values computed from $(\sigma_1'/\sigma_3')_{max}$. The shear strength of samples containing gases was around 60% and 70% of that of the saturated undrained test. In average, the mobilized friction angles of the drained, gassy and undrained tests were 34.3°, 33.7° and 32.4°, respectively.

Table 6-2. Shear strength and mobilized friction angle ($e_{aver.}=0.78$).

Type	Saturation (%)	At $(\sigma_1'/\sigma_3')_{max}$		At ψ_{max}	
		q (kPa)	ϕ'	q (kPa)	ϕ'
Drained	100	219	34.4	217	34.2
Gassy	95	288	33.9	257	33.7
Gassy	91	252	33.6	249	33.6
Gassy	82	240	34.0	210	33.2
Undrained	100	399	32.4		

Figure 6-15 shows the stress path for the saturated and gassy soils. Gas changed the stress-path response from undrained to drained conditions. It can be observed that all the gassy samples followed the saturated drained stress path until the critical state condition was reached, and then moved upwards along the critical state line.
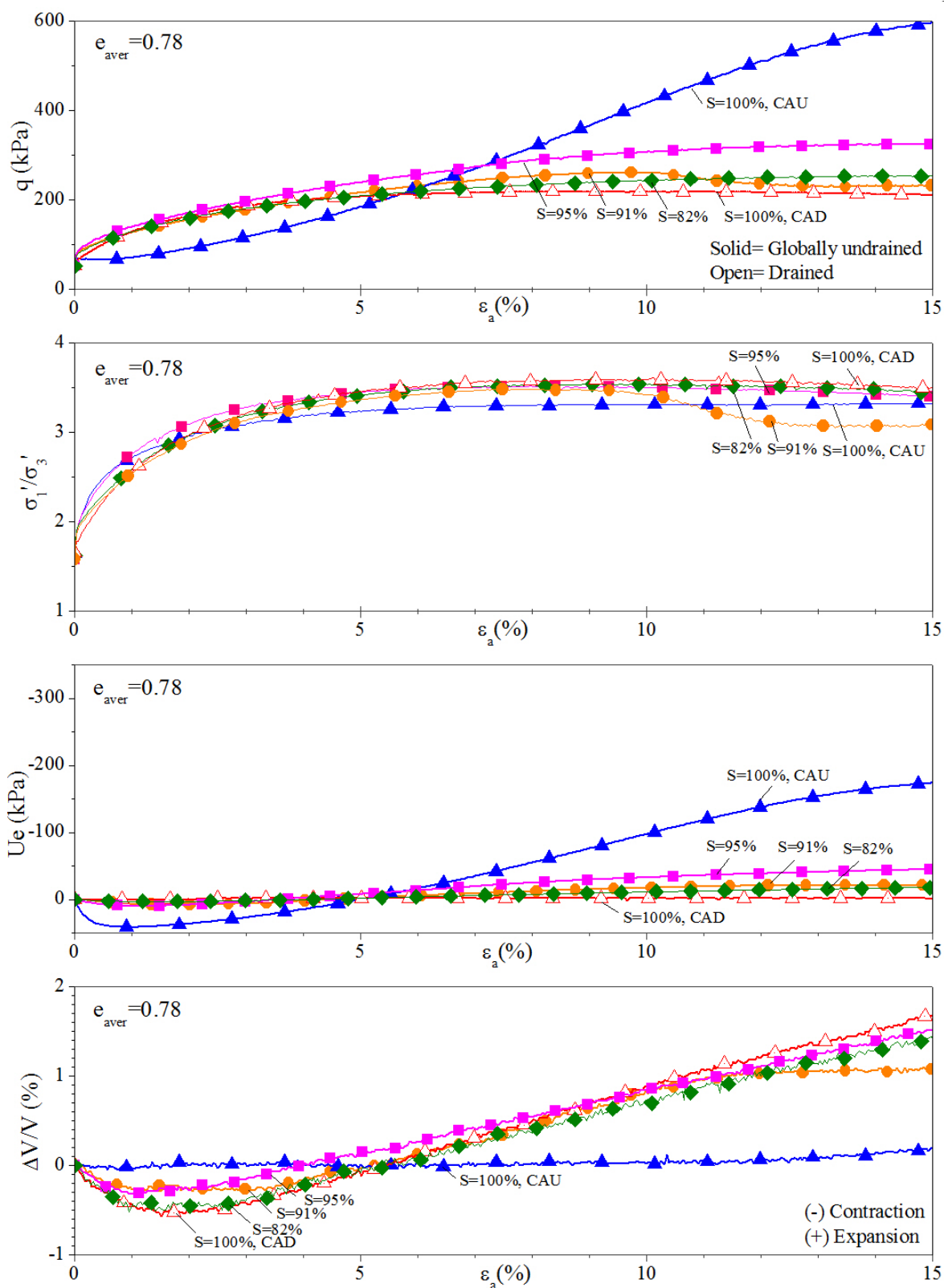
Figure 6-14. Stress-strain response, pore-pressure response and volumetric strain response. Group 2 - $e_{ave.}$=0.78
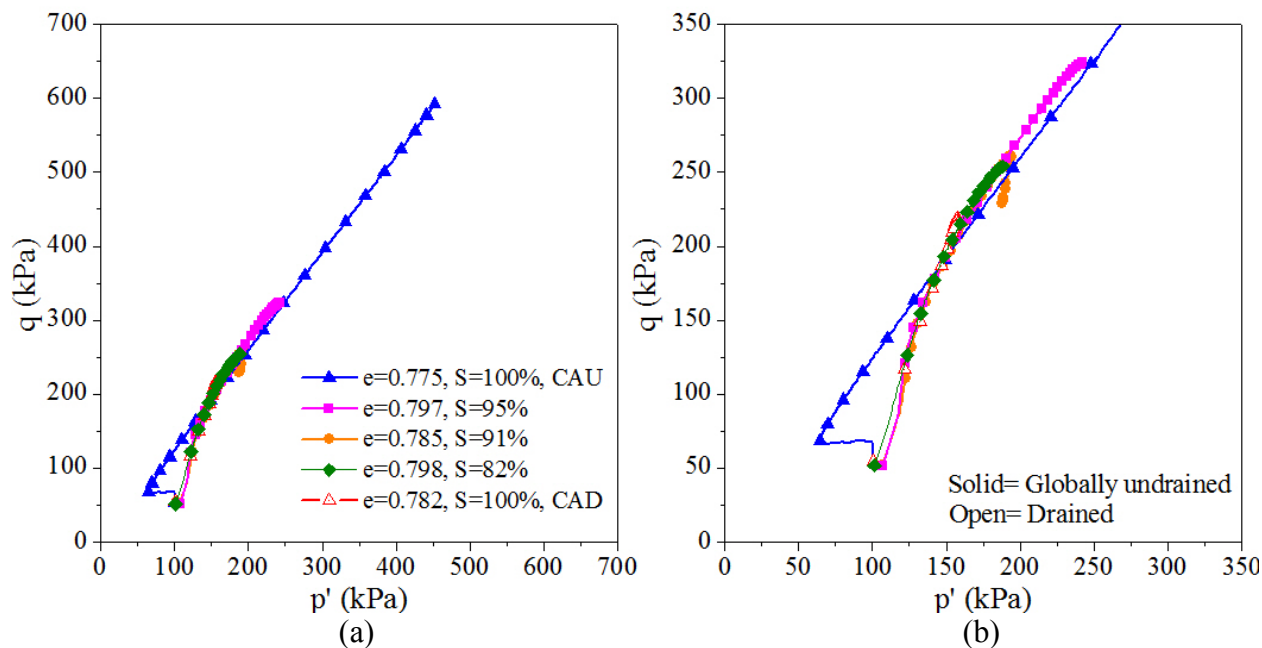
Figure 6-15. (a) Effective stress paths and (b) zoom in of effective stress paths (Group 2 - $e_{ave.}$=0.78).

Figure 6-16 shows the stress-strain response, pore-pressure response and volumetric strain response of gassy specimens with an average void ratio of 0.73. At this void ratio, the shear strength was highly affected by the presence of even small amount of gas (S=98%). The presence of gas made the soil more compressible under undrained conditions, restricting the development of excess pore pressure. At $(\sigma_1'/\sigma_3')_{max}$, the amount of negative U_e developed in the gassy tests was approximately 10 times less than that developed on the saturated undrained specimen.

Table 6-3 lists the shear strengths and mobilized friction angles of the saturated and gassy samples. The maximum difference between the shear strengths and friction angles computed at $(\sigma_1'/\sigma_3')_{max}$ and ψ_{max} was less than 6%, being slightly greater the values obtained from ψ_{max}. The shear strength of gassy samples was between 40% and 50% of that of the undrained saturated sample. Figure 6-17 shows that all the gassy samples followed the saturated drained stress path and once again the soil response was changed from undrained to drained conditions

Table 6-3. Shear strength and mobilized friction angle ($e_{aver.}$=0.71).

Type	Saturation (%)	At $(\sigma_1'/\sigma_3')_{\text{max}}$		At ψ_{max}	
		q (kPa)	ϕ'	q (kPa)	ϕ'
Drained	100	235	35.6	235	35.5
Drained	100	232	35.7	233	35.7
Gassy	98	370	35.5	390	35.3
Gassy	91	315	36.2	321	36.1
Gassy	75	280	37.2	297	37
Undrained	100	701	34.8		
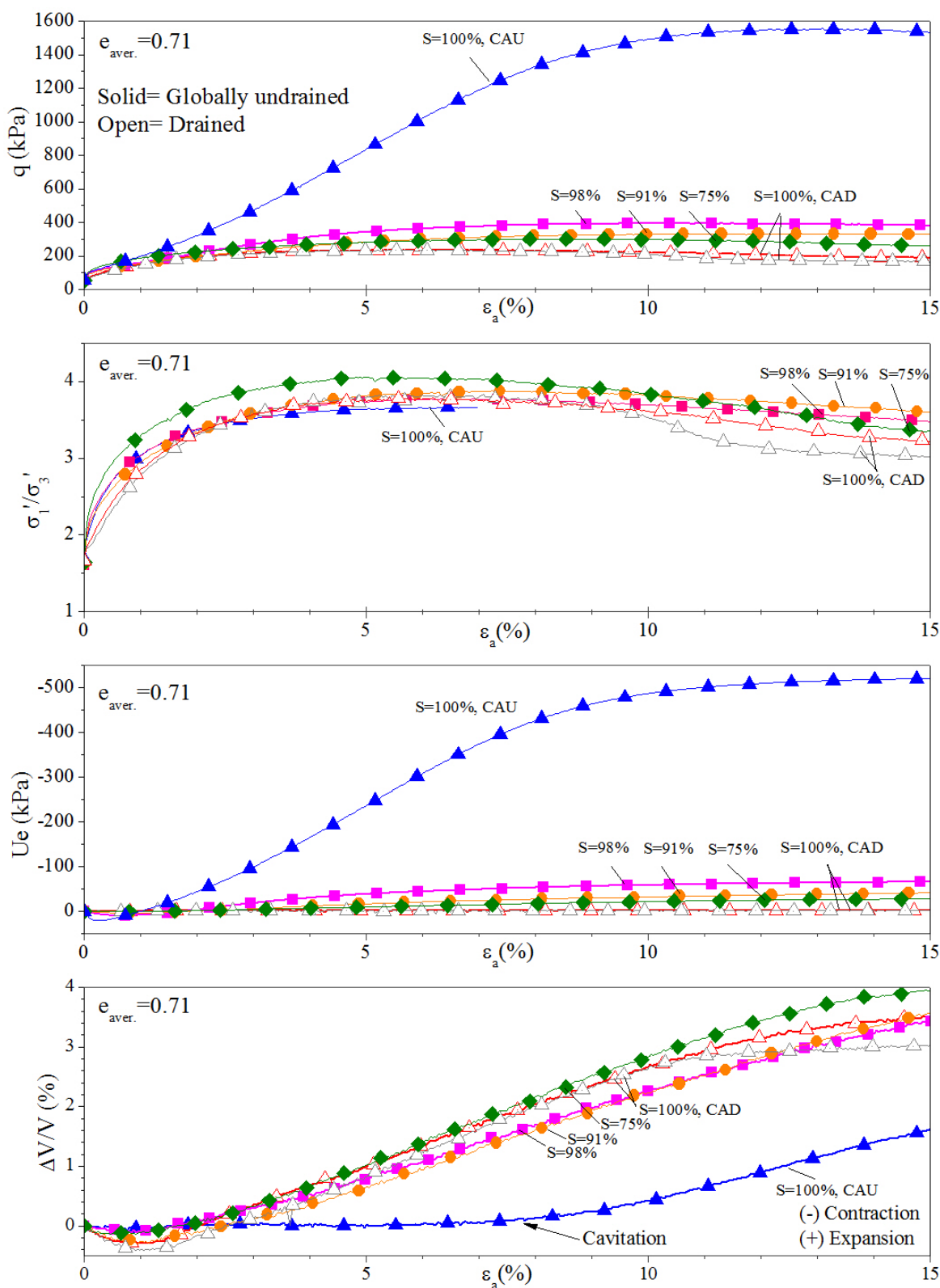
Figure 6-16. Stress-strain response, pore-pressure response and volumetric strain response (Group 3 - $e_{ave.}$=0.71).
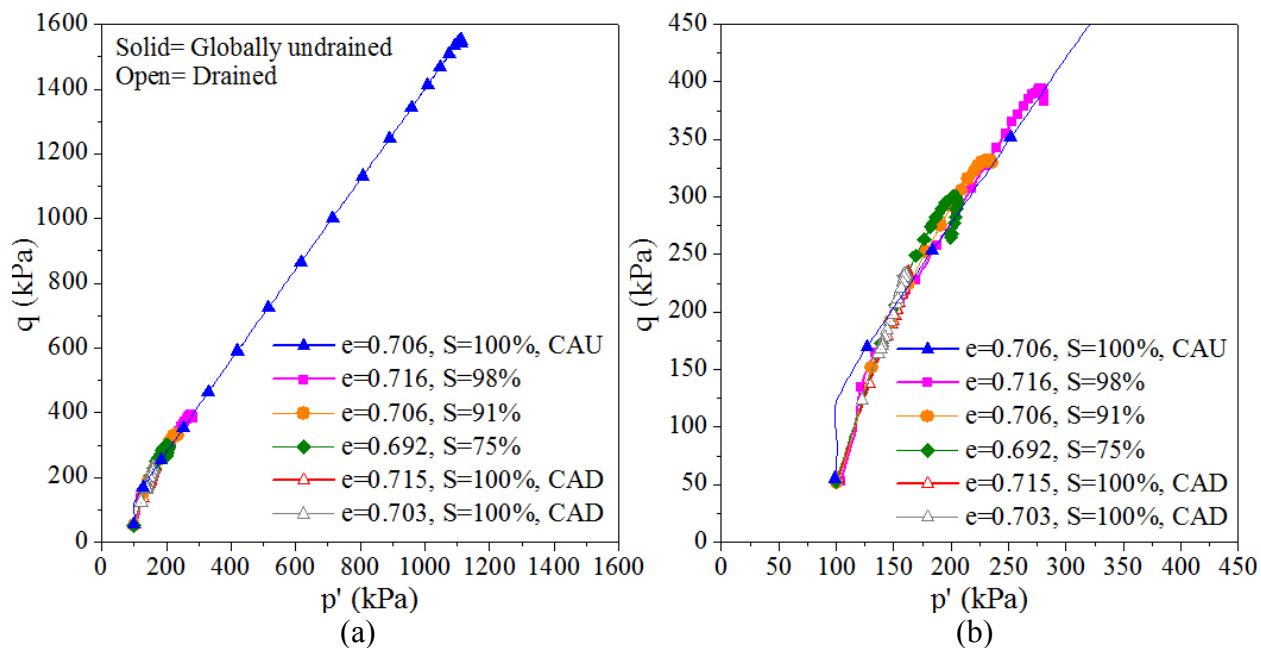
Figure 6-17. (a) Effective stress paths and (b) zoom in of effective stress paths. (Group 3 - $e_{ave.}$=0.71).

Figure 6-18 shows the summary of the shear strength of the tested samples measured at the maximum value of the principal stress ratio and the maximum dilation angle. The presence of even small amounts of gas on medium to dense sands significantly decreases the undrained shear strength of the soil. In general, the undrained shear strength decreases as the amount of gas in the soil increases. Gas makes the soil strength approach the drained values. This effect becomes more pronounced as the soil is denser, suggesting that densification of the soil deposit to values below the critical state line may not be enough to prevent liquefaction and flow. Therefore, the cyclic resistance must be evaluated since the critical state concepts imply that no liquefaction is possible below the critical state line. The shear strength of the soil after blast densification falls between the undrained and drained shear strengths. The drained shear strength slightly increases over the range of void ratios tested.

Two scenarios are proposed to explain the little to no improvement in penetration resistance measured, in some sand deposits, after blast densification. The first scenario is the case where excess porewater pressure is not developed during the field verification tests, in particular the cone penetration test. In this case, the shear strength will increase only slightly over the range of void ratios achieved after blast densification (Figure 6-18). The second scenario is the case where excess porewater pressure is developed during the field tests. In this case, the undrained shear strength after blast densification will be greater than that of the saturated drained condition, but the strength will decrease by the presence of gas. This is the case for the sand deposit at Oakridge landfill, where excess porewater pressures were measured during the cone penetration tests (see Figure 3-7)
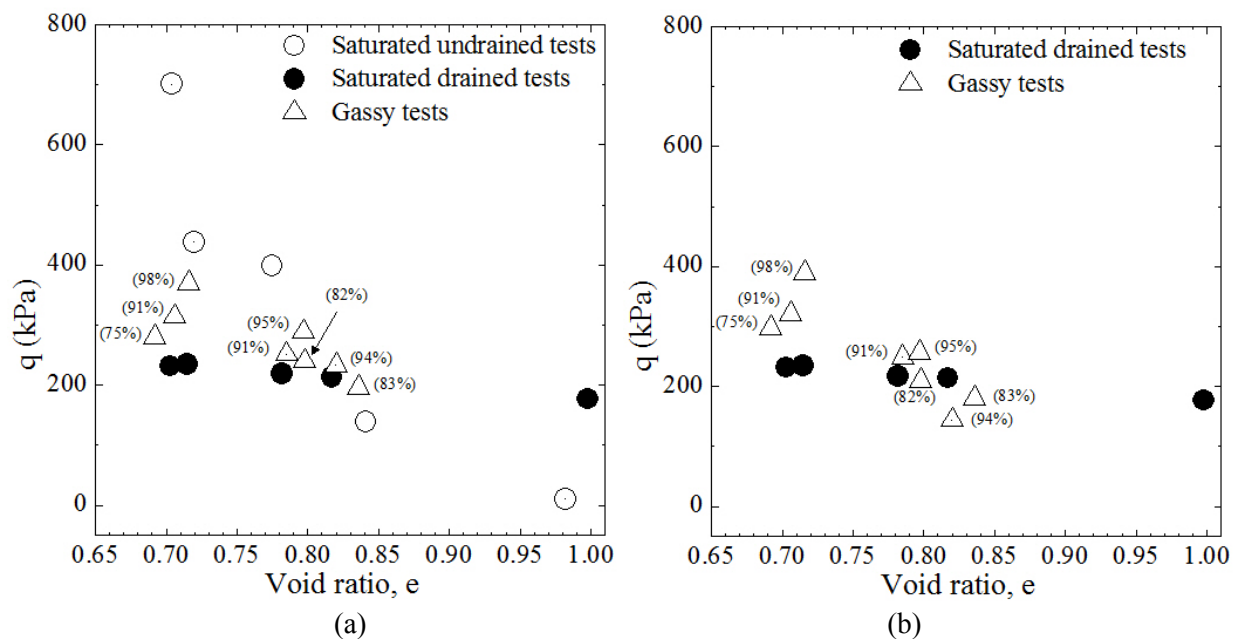
Figure 6-18. Shear strength of tested specimens measured at (a) max. values of σ_1'/σ_3' and (b) ψ_{max}.

Figure 6-19 shows the friction angles of the saturated and gassy samples computed at the peak principal stress ratio, σ_1'/σ_3', and maximum dilation angle, ψ_{max}, and at a constant

effective mean normal stress of 100 kPa. For the sand samples collected at the Oakridge landfill site, the undrained and drained friction angles moderately increased after blast densification with respect to the initial condition. In average, the ϕ'_u and ϕ'_D increased approximately 4.5° over the range of void ratios tested. For the drained tests, this increase in friction angle will be reflected in a slightly increase in shear strength, as observed in Figure 6-18. The friction angle of gassy samples plotted above ϕ'_u and below ϕ'_D at void ratios between 0.77 and 0.84, and above ϕ'_u and ϕ'_D at an average void ratio of 0.71.
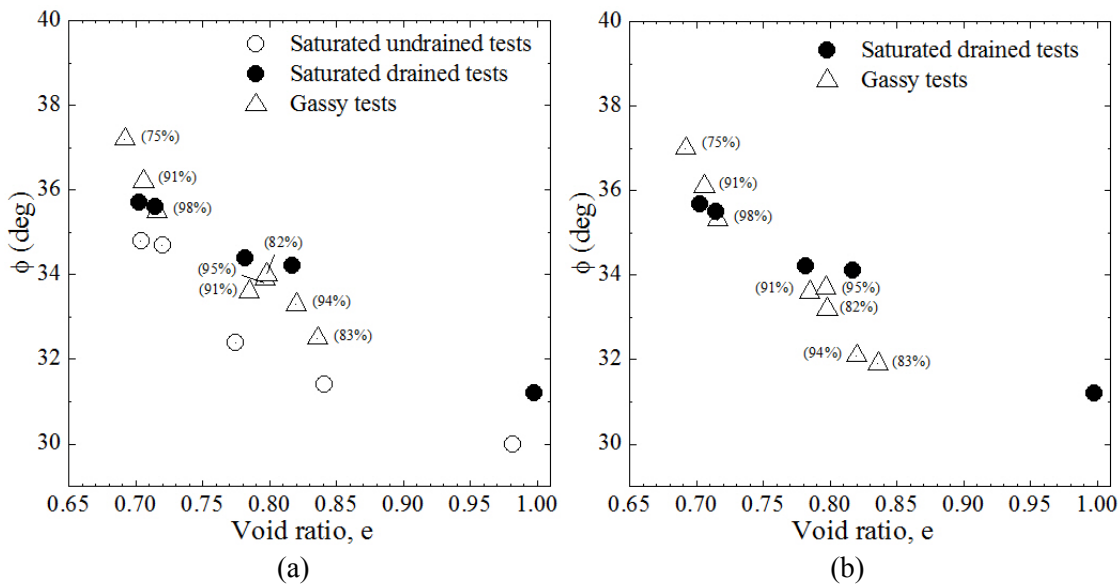
Figure 6-19. Friction angles of tested specimens computed at (a) max. values of σ'_1/σ'_3 and (b) ψ_{max}.

Figure 6-20 shows a comparison between the effective friction angles and shear strengths obtained from the saturated triaxial tests conducted by Knai (2011) on the sand samples provided by GeoSyntec Consultants and those obtained from the saturated triaxial tests conducted on the sand samples collected in 2011. In general, the friction angles, ϕ'_u and ϕ'_D, found in the present study agreed with those friction angles reported by Knai (2011). For the range of void ratios and effective stresses tested in this study, the maximum difference between the undrained and

drained friction angles is 2.8°. Figure 6-20b shows that the drained shear strength slightly increases over the range of the void ratios tested. This range of void ratios is considered to be representative of those in-situ final void ratios after blast densification at the Oakridge landfill site (refer to chapter 7). These two set of experiments show that, for the range of void ratios and effective stresses tested in this study, the drained shear strength slightly increases over the range of densities expected after blast densification.
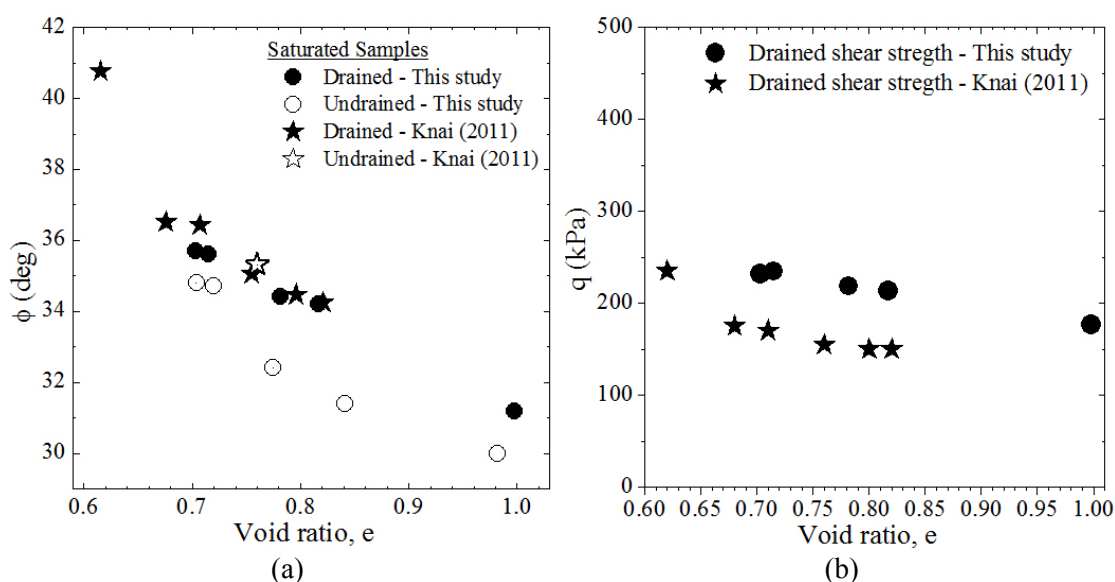
Figure 6-20. Comparison of (a) effective friction angles and (b) shear strengths obtained from triaxial tests conducted on sand samples collected in 2003 and 2011.

6.7 Cyclic resistance to liquefaction of gassy sands as function of density and degree of saturation

Twenty-five cyclic triaxial tests were conducted to measure the cyclic resistance to liquefaction of saturated and gassy sands as function of density and degree of saturation (Table 5-1). The samples were anisotropically consolidated to an effective mean normal stress of 100 kPa (σ'_{3c} = 82 kPa and σ'_{1c}=136 kPa). After consolidation, a cyclic deviatoric load ±ΔF was

applied under globally undrained conditions in the axial direction at a frequency of 0.5Hz. For the denser samples, failure was defined as the development of 5% accumulated axial strain after a certain number of cycles, and for the looser samples it was defined as a sudden loss of strength, causing the sample to flow and develop excessive axial strains. The Cyclic Stress Ratio (CSR) applied to the specimens was defined as $CSR = \Delta\sigma/2\sigma'_v$, where $\Delta\sigma$ was computed as ΔF divided by the sample's cross sectional area.

Figure 6-21 through Figure 6-23 present the cyclic loading response of gassy sands subjected to a CSR=0.15. In these figures, the stress path was plotted in the Lambe's space, where p' and q are defined as $(\sigma'_1 + \sigma'_3)/2$ and $(\sigma'_1 - \sigma'_3)/2$, respectively. For the stress-strain curves, the shear stress was defined as $(\sigma'_1 - \sigma'_3)$. CSR and L. of P. are the critical state line and the line of peaks, respectively. These samples were prepared using the water pluviation technique.

Figure 6-21 shows the stress path, shear stress and induced pore water pressure of the least dense samples ($e_{aver.}$=0.82). For the saturated specimen, the porewater pressure increased to a value between 60 and 65kPa after 7 cycles, and then it remained practically constant. Approximately 50% of the induced porewater pressure (32 kPa) was developed during the first cycle, and an accumulated axial strain of 5% was reached after 16 cycles. On the other hand, the gassy samples with degrees of saturation of 89% and 84% developed an excess porewater pressure of 1.5kPa and 0.5kPa, respectively after 7 cycles. This excess pore pressure is less than 5% of that induced on the saturated samples under the same number of cycles. The gassy samples did not reach the failure line even after 5,000 cycles, indicating that the presence of gas greatly increased the cyclic resistance to liquefaction of these specimens. The maximum accumulative axial strain on the gassy samples was 0.85% after 100 cycles. The amount of axial

strain and excess porewater pressure developed during cyclic loading decreased as the amount of gas increased. For practical reasons, only the first 100 cycles were presented in these figures.

Figure 6-22 shows the stress path, shear stress and induced pore water pressure of the samples with an average void ratio of 0.78. For the saturated specimen, an accumulative axial strain of 5% was reached after 49 cycles. Similar to the response of the least dense samples, approximately 50% of the total induced porewater pressure was reached after the first cycle and then progressively increased until reaching an asymptotic value of $\Delta U = 60kPa$. At 100 cycles, the samples with degrees of saturation of 95% and 83.5% developed an excess porewater pressure of 27.5 kPa and 8 kPa, respectively and an average accumulative axial strain of approximately 0.6%. The sample with a degree of saturation of 95% had an accumulative axial strain of 0.55% at 49 cycles. This axial strain was one-ninth of the axial strain developed on the saturated sample at the same number of cycles. This result is an indication that even small amounts of gas will significantly increase the soil cyclic resistance to liquefaction.

Figure 6-23 shows the stress path, shear stress and induced pore water pressure of the samples with an average void ratio of 0.70. Neither the saturated nor the gassy samples reach the critical state line after 100 cycles. The accumulative axial strain for these samples varied from 0.10% (S=88%) to 0.30% (S=100%). For the sample with a degree of saturation of 98%, the excess positive porewater pressure and accumulative axial strain were about half of those developed for the saturated sample. In general, the amount of axial strain and excess porewater pressure developed during cyclic loading decreased as the amount of gas in the sample increased.

The cyclic response of the saturated tests agreed well with published data of medium to dense sands under similar confining stresses, and subjected to cyclic shear stresses less that the initial static shear applied on the sample (Vaid and Sivathayalan, 2000; Vaid et al., 2001;

Sivathayalan and Ha, 2004). Deformation due to cyclic mobility was the cause of liquefaction for the saturated samples with average void ratios of 0.82 and 0.78. As presented in section 5.6, the mechanism of strain development observed in the saturated samples, large cyclic strains during the firsts cycles and smaller cyclic strains for the subsequent cycles, is a typical response of medium to dense sands where neither contractive response nor transient states of zero effective stress states is responsible for triggering liquefaction (Sivathayalan and Ha, 2004).

Figure 6-24 compares the stress paths, shear stress and excess positive pore water pressure of gassy samples with void ratios before shearing of 0.803, 0.757 and 0.728, when subjected to an average cyclic stress ratio of 0.30. These samples were prepared using the water pluviation technique. As explained in section 5.2, the triaxial testing configuration shown in Figure 5-3 was used to conduct these tests. The final degree of saturation of the gassy samples was not determined since an accurate measurement of the total amount of water leaving the specimen during sample desaturation was not possible with this triaxial testing configuration. These results showed that gassy samples were very stable, even under high values of cyclic loading (CSR=0.30). In general, the denser the sample the smaller the excess porewater pressure and axial strain developed during cyclic loading.

In conclusion, the presence of even small amounts of gas greatly increased the liquefaction resistance of the soil at similar densities. The axial strain developed on the least dense gassy samples was less than 0.8% after 100 cycles, indicating that significant settlements are not expected during an earthquake. Even though the cone penetration tests conducted at the Oakridge landfill showed little to no improvement in penetration resistance after blast densification, the blasted sand layer will not be susceptible to liquefaction and flow, and excessive deformations will not occur if the earthquake loading can be characterized by a CSR equal to 0.30.
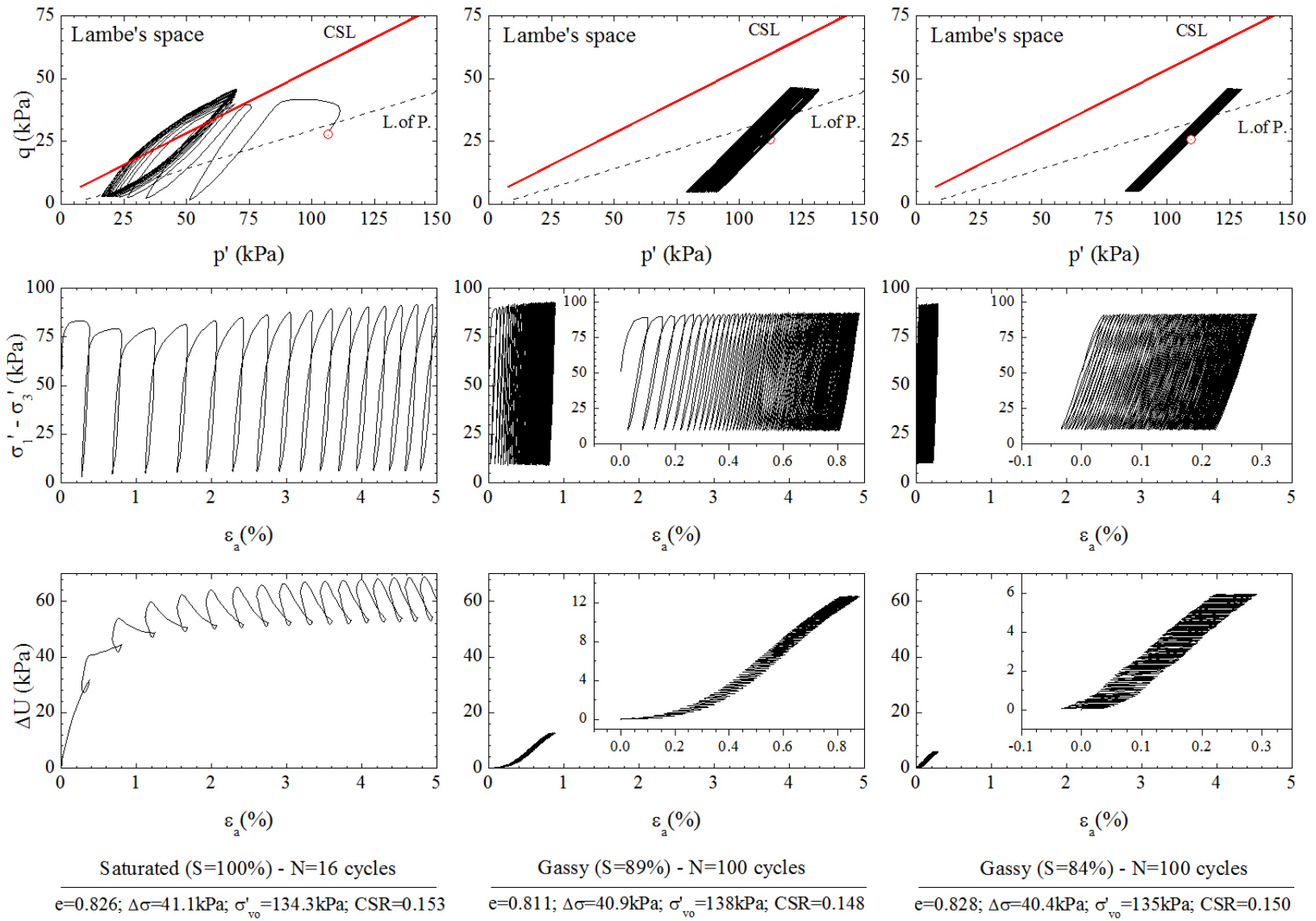
Figure 6-21. Stress path, shear stress and induced pore water pressure (Group 1 - e$_{ave.}$=0.82).
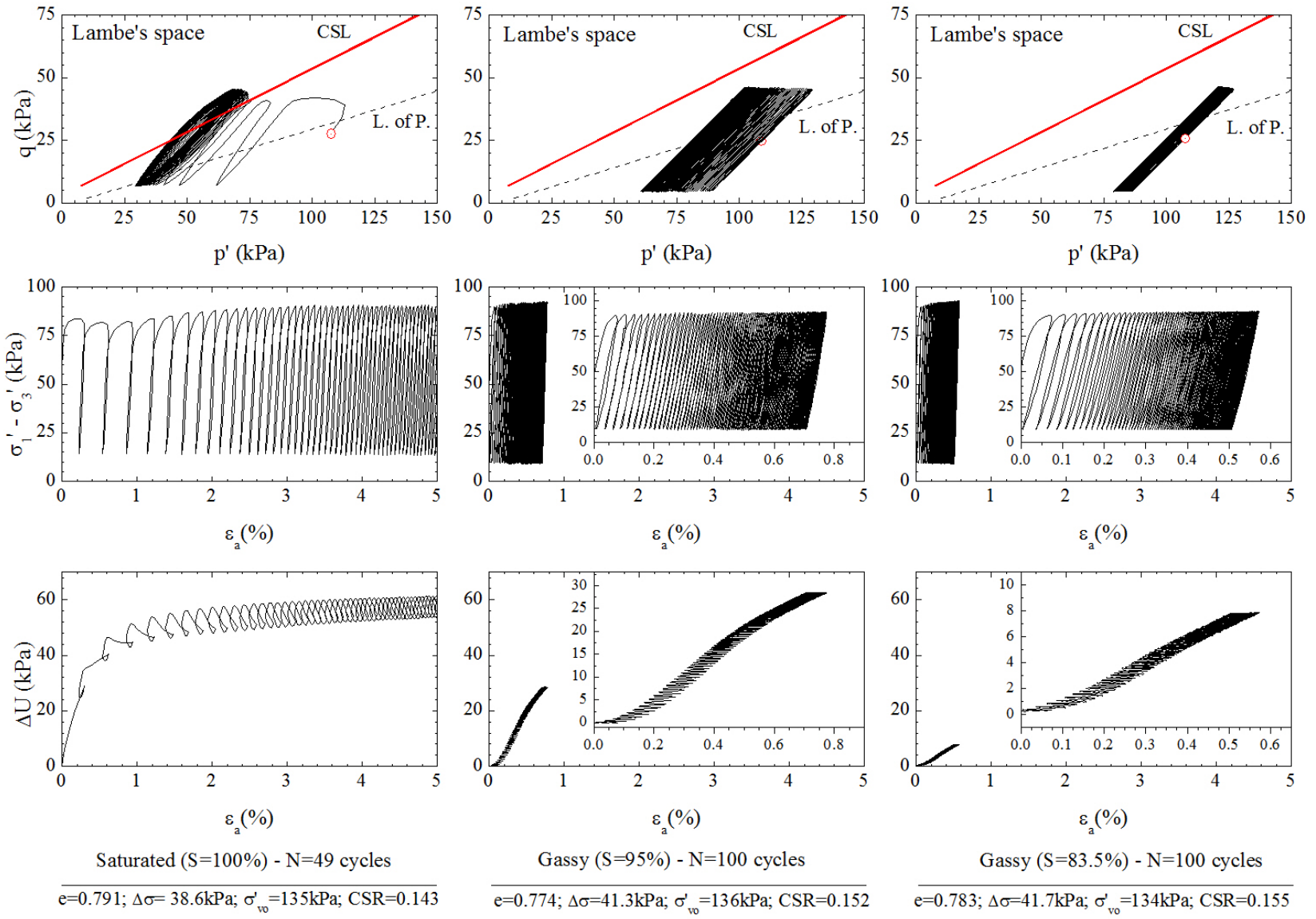
Figure 6-22. Stress path, shear stress and induced pore water pressure (Group 2 - e_{ave.}=0.78).

Saturated (S=100%) - N=49 cycles
e=0.791; Δσ= 38.6kPa; σ'_{vo}=135kPa; CSR=0.143

Gassy (S=95%) - N=100 cycles
e=0.774; Δσ=41.3kPa; σ'_{vo}=136kPa; CSR=0.152

Gassy (S=83.5%) - N=100 cycles
e=0.783; Δσ=41.7kPa; σ'_{vo}=134kPa; CSR=0.155

Saturated (S=100%)

e=0.706; Δσ=40.7kPa; σ'$_{vo}$=136kPa; CSR=0.149

Gassy (S=98%)

e=0.695; Δσ=40.4kPa; σ'$_{vo}$=138kPa; CSR=0.147

Gassy (S=88%)

e=0.687; Δσ=41.1kPa; σ'$_{vo}$=137kPa; CSR=0.149
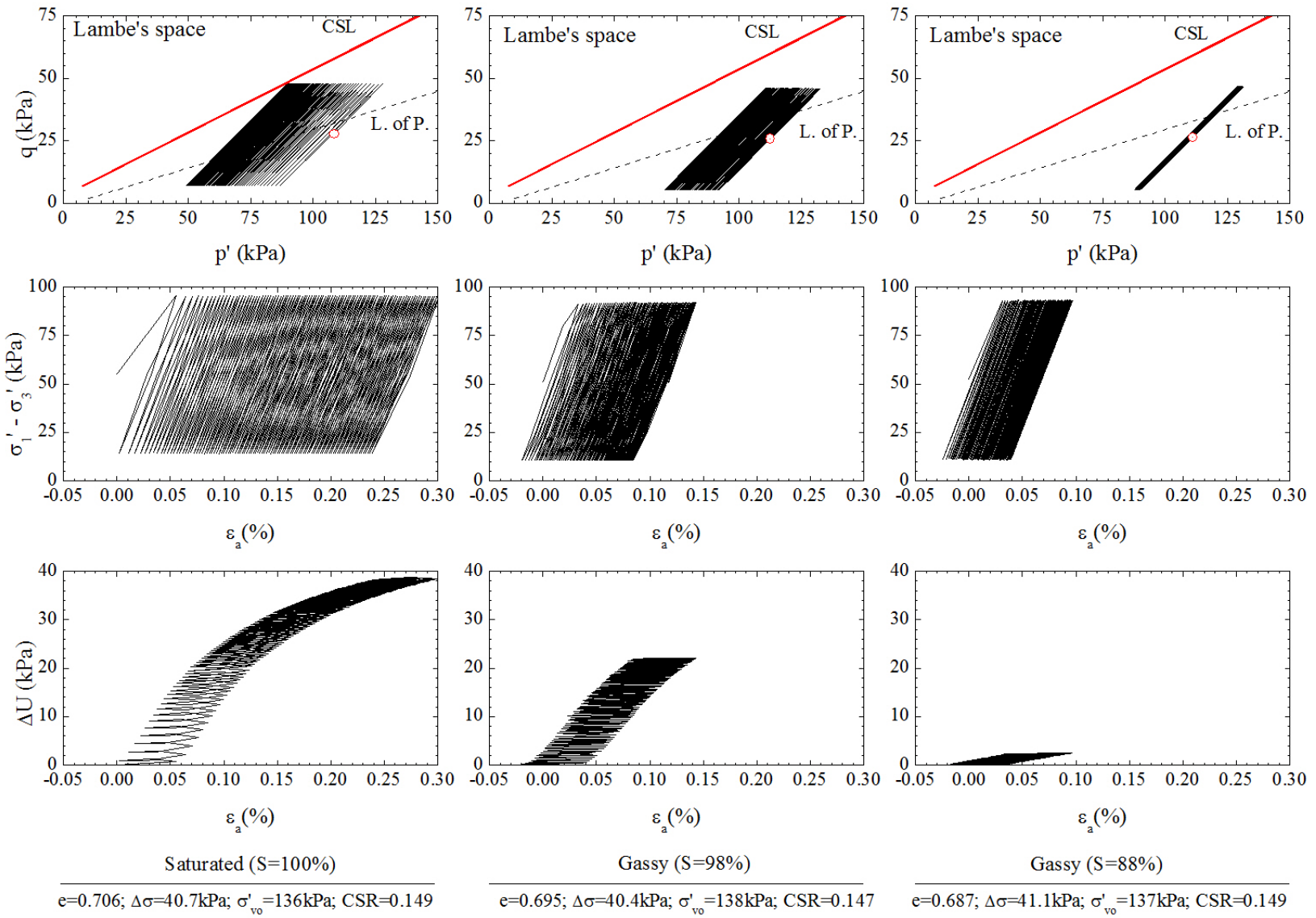
Figure 6-23. Stress path, shear stress and induced pore water pressure (Group 2 - e$_{ave.}$=0.70).
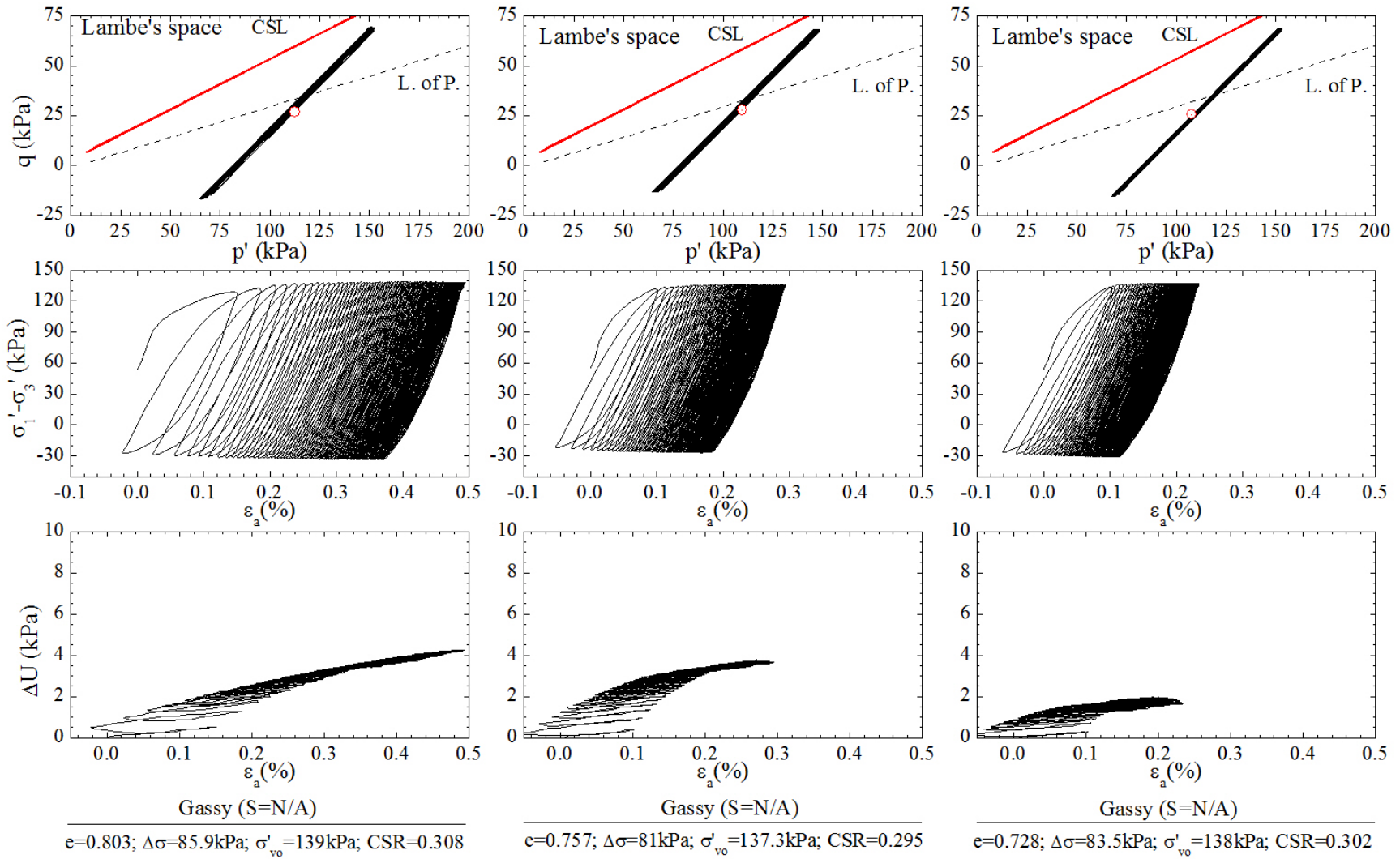
Figure 6-24. Stress path, shear stress and induced pore water pressure (CSR=0.30).

Gassy (S=N/A)

e=0.803; Δσ=85.9kPa; σ'$_{vo}$=139kPa; CSR=0.308

Gassy (S=N/A)

e=0.757; Δσ=81kPa; σ'$_{vo}$=137.3kPa; CSR=0.295

Gassy (S=N/A)

e=0.728; Δσ=83.5kPa; σ'$_{vo}$=138kPa; CSR=0.302

Figure 6-25 compares the cyclic test results of the saturated specimens prepared using the water pluviation and moist tamping techniques. In this figure, the applied cyclic stress ratio was plotted versus the logarithm of the number of cycles needed to induced a flow failure (least dense specimens) or to reach a peak-to-peak accumulative axial strain of 5% (denser specimens). These tests were performed to have a measurement of the cyclic resistance of the saturated soil mass before blasting. Since specimens with void ratios higher than 0.82 were not possible to prepare by water pluviation, samples with an average void ratio of 0.97 were prepared only with moist tamping technique (Table 5-1). In addition, moist-tamped specimens with an average void ratio of 0.83 were also prepared to have a manner of comparison between these two sample preparation techniques. At an average void ratio of 0.82, the cyclic resistance of specimens prepared by water pluviation was approximately 1.5 times greater than those prepared by moist tamping. Since this set of specimens (e=0.82-0.83) was tested at the same void ratio and confining stresses, the differences in liquefaction susceptibility can be attributed to the difference in initial fabric resulting from these two preparation techniques. The results from the liquefaction tests performed on this sand correlated well with data reported in the technical literature in similar sands with little to no fines (Chern, 1981; Steven, 1996; Vaid and Sivathayalan, 2000; Wijewickreme et al., 2005a). Appendix C shows the stress path, shear stress and excess positive pore water pressure response of these tests.
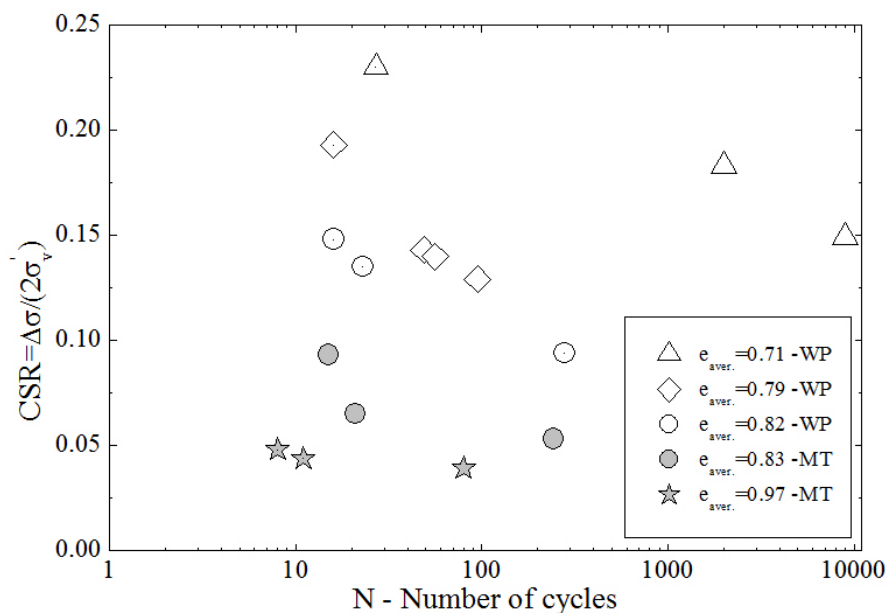
Figure 6-25. CSR vs. N required to induce flow liquefaction or to reach peak-to-peak $\varepsilon_a = 5\%$ on saturated samples.

6.8   Results of bender element measurements

Shear wave velocity measurements were taken during different stages of testing for all the samples. In previous work, Knai (2011) conducted a series of bender element measurements on reconstituted specimens made of the sand samples collected during the 2003-2004 blast densification program. Knai (2011) found that the bender element results obtained by using the peak-to-peak method were less within ±1.2% of those obtained by using the cross correlation and the frequency domain methods. The values of the shear wave velocity reported herein were computed using the wave travel time determined by the peak-to-peak method.

Figure 6-26 shows the summary of the computed values of the normalized elastic shear stiffness plotted versus the normalized mean normal effective stress. These measurements were collected during consolidation of the samples used to determine the shear resistance and cyclic resistance to liquefaction of the soil (from tests WP-06 to WP-32 - Table 5-1). In this testing program all the samples were consolidated in a saturated condition. As expected, G_{BE} increases

with increasing mean normal stress (Jung et al., 2007). The elastic shear modulus was computed

as

$$G_{BE} = \rho V_{BE}^2$$
(Eq. 6-1)

where ρ was the total density of the soil at the time when V_{BE} was measured.
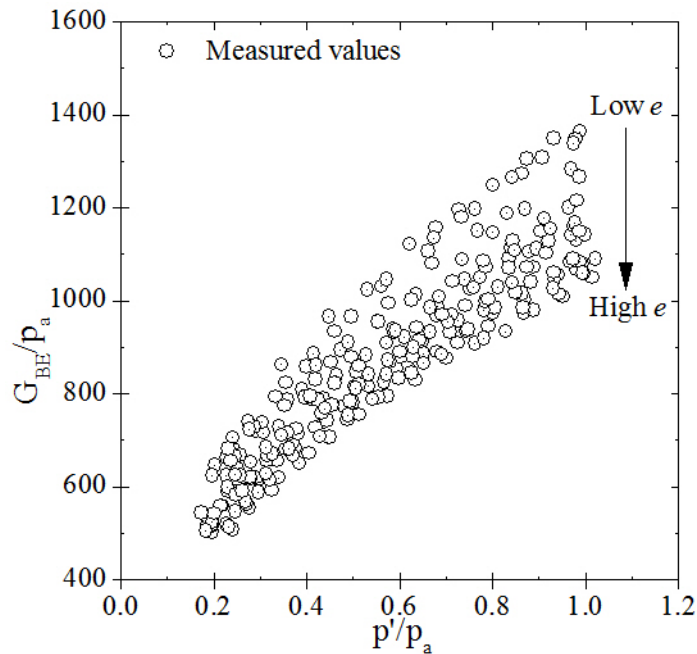
Figure 6-26 Summary of the results from bender element measurements during consolidation.

To account for the variation in density during consolidation, the values of the normalized

elastic shear stiffness shown in Figure 6-26 were related to the sample void ratio following the

procedure presented by Jung et al. (2007). The resulting relationship was expressed as

$$\frac{G_{BE}}{P_a} = Af(e)\left(\frac{p'}{p_a}\right)^n$$
(Eq. 6-2)

where p_a= atmospheric pressure (101.3 kPa); $f(e)$=void ratio function; and A and n = material

constants. Figure 6-27a compares the computed values of $Af(e)$ based on published expressions

with the measured values of $Af(e)$ during consolidation. As can be seen, the measured values of

$Af(e)$ fall within the void ratio functions proposed by several authors. Table 6-4 summarizes the void ratio function, average value of A, and the square of the correlation coefficient (R^2) obtained from seven different expressions. The squared correlation coefficient changes very little between any of these empirical expressions. Therefore, the $f(e)$ proposed by Hardin and Richart (1963) was chosen in this work because it was originally developed for granular soils. Figure 6-27b compares the results of the bender element measured during consolidation with those predicted by Hardin and Richart (1963). The final expression for the normalized shear stiffness was

$$\frac{G_{BE}}{P_a} = 1063 \frac{(2.17-e)^2}{1+e} \left(\frac{p'}{p_a}\right)^{0.48}$$
(Eq. 6-3)
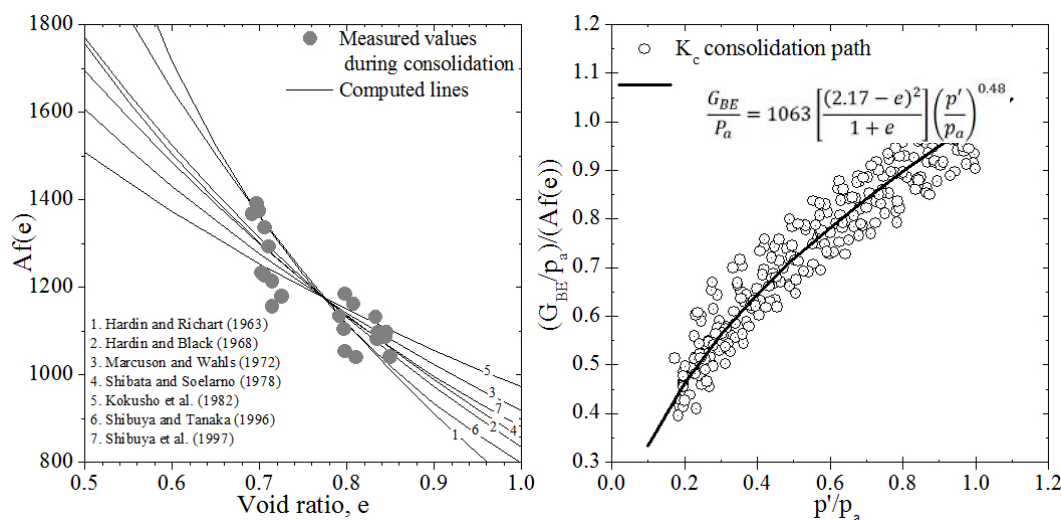
Figure 6-27 (a) Determination of the void ratio function and (b) best fit void ratio function.

Table 6-4 Published expressions of Af(e).

#	Reference	f(e)	Average value of A	Square of the corr. coeff. (R^2)
1	Hardin and Richart (1963)	$(2.17\text{-}e)^2/(1+e)$	1063.1	0.746
2	Hardin and Black (1968)	$(2.91\text{-}e)^2/(1+e)$	454.4	0.745
3	Marcuson and Wahls (1972)	$(4.4\text{-}e)^2/(1+e)$	157.9	0.744
4	Shibata and Soelarno (1978)	$0.67\text{-}e/(1+e)$	5005.5	0.743
5	Kokusho et al. (1982)	$(7.32\text{-}e)^2/(1+e)$	48.5	0.743
6	Shibuya and Tanaka (1996)	$e^{-1.5}$	790.9	0.757
7	Shibuya et al. (1997)	$(1+e)^{-2.4}$	4621.5	0.748

Figure 6-28 through Figure 6-30 show the normalized shear wave velocity during consolidation, creep, desaturation and shear for the samples tested monotonically and with an average consolidated void ratio of 0.82, 0.78 and 0.71, respectively. The values of the shear wave velocity computed from the bender elements were normalized with respect to the shear wave velocity at the end of consolidation.

The shear wave velocity measured during desaturation slightly fluctuates as the CO_2 dissolved in the pore fluid is forced to come out of solution. In general, the shear wave velocity of gassy samples at the end of desaturation, when the pore and air pressures in the sample are stable, varied within ±5% with respect to the values after creep. This small change in shear wave velocity indicates that the sample internal fabric was not significantly altered during gas exsolution. These results are consistent with expectation, since the two main factors influencing the shear wave velocity, void ratio and mean normal effective stress, did not vary much during the gas exsolution stage.

The shear wave velocity of the undrained saturated specimens initially decreased and then increased as the shearing process continued. This effect was more pronounce as the soil became denser. This initial decreased was the result of the development of positive pore water pressures at the beginning of the test. The effect of gas on changing the soil response from undrained to drained conditions was also confirmed with the shear wave velocity measurements. Gas makes the shear wave velocity values to approach the drained values.
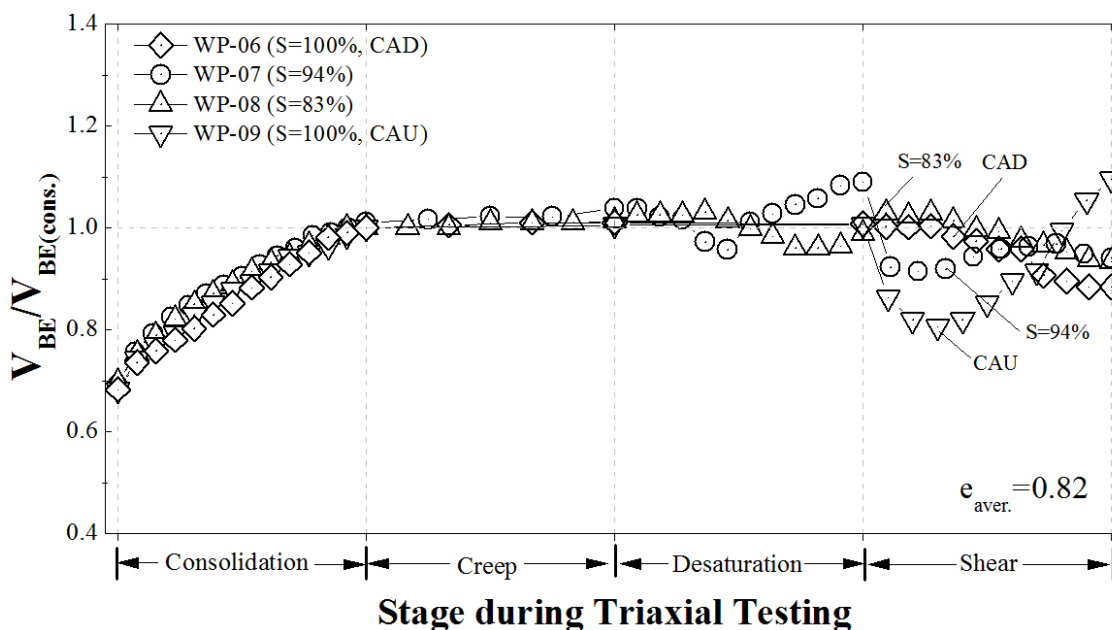
Figure 6-28. Normalized shear wave velocity during the triaxial testing stages (Group 1, $e_{aver.}$=0.82).
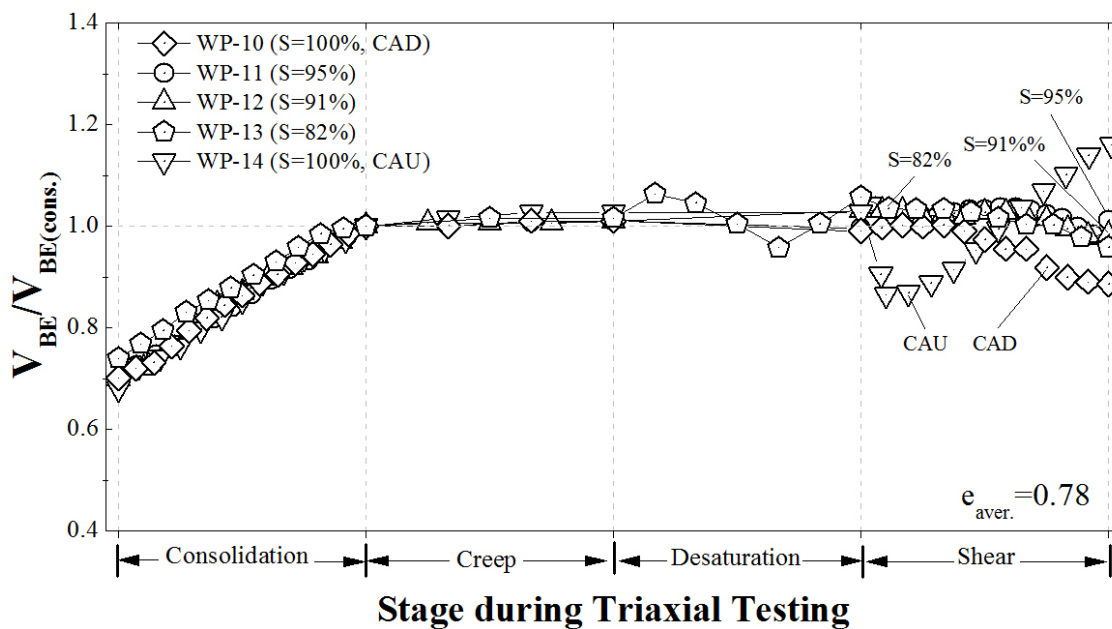
Figure 6-29. Normalized shear wave velocity during the triaxial testing stages (Group 2, $e_{aver.}$=0.78).
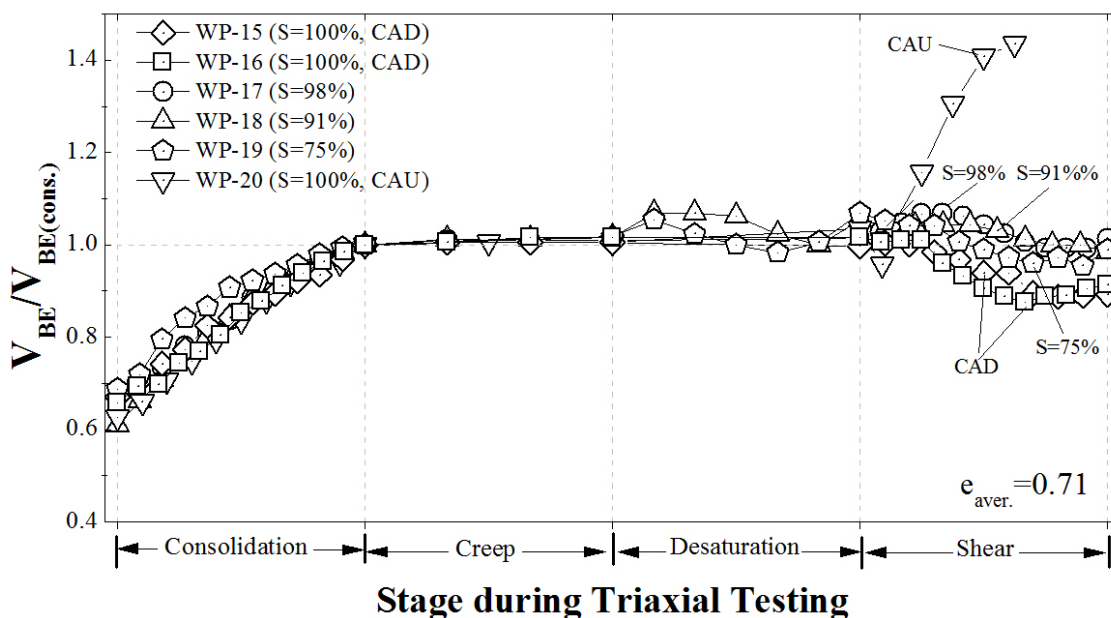
Figure 6-30. Normalized shear wave velocity during the triaxial testing stages (Group 3, $e_{aver.}$=0.71).

6.9 Summary

A one-dimensional constrained compression test was proposed as a simple procedure to estimate the void ratio change that will occur after each blast event. An illustrative example of how to compute the expected void ratio change was described. The position of the critical state line, the definition of the shear strength, the procedure followed to compute the effective stresses, and the shear and cyclic response of medium to dense saturated and gassy sands were presented.

Gas in the sample highly affects the shear strength of medium dense sands. The undrained shear strength is greatly affected by the presence of even small amount of gas and the effect is stronger as the soil becomes denser. The greater the amount of gas in the sample, the smaller the undrained shear strength. Gas has the effect of changing the soil response from undrained conditions to drained conditions. The presence of gas makes the soil more compressible under

undrained conditions, restricting the development of excess pore pressures. The amount of porewater pressure developed on gassy tests is substantially less than that developed on saturated undrained specimens.

Two scenarios are proposed to explain the little to no improvement in penetration resistance, in some sands, measured after blast densification. The first scenario is the case where no excess porewater pressure is developed during the field verification tests. In this case, the shear strength will increase only slightly over the range of void ratios associated with those achieved after blast densification. The second scenario is the case where excess porewater pressure is developed during the field tests. In this case, the shear strength after blast densification will be greater than that of the saturated drained condition, but the strength will decrease by the presence of gas. This is the case for the sand deposit at Oakridge landfill site, where excess porewater pressures were measured during cone penetration tests.

The presence of even small amounts of gas greatly increases the liquefaction resistance of sand regardless of its density. Medium dense sand deposits containing gas will develop very low axial strains during cyclic loading, indicating that significantly settlements are not expected, at least for the CSR tested in this program. Even though the cone penetration tests conducted at the Oakridge landfill showed little to no improvement in penetration resistance after blast densification, the gassy sand layer has significantly increased resistance to liquefaction.

7 COMPARISON OF COMPUTED AND MEASURED SETTLEMENTS

The ground surface settlements measured at the Oakridge landfill during the blast densification programs conducted in 2003-2004, 2005, 2007, and 2011 were used to calculate the void ratio and axial strain changes after each blast event. The volume changes measured at the field were compared with the volume changes computed from the one-dimensional constrained compression tests. The accuracy of the proposed procedure is discussed.

7.1 Measured ground surface settlements

Ground surface settlements were measured by GeoSyntec Consultant in zones 1, 2, 3, 4, 5, 15A, 15B, 16, 17, 18, 19, 20, 21, 22, 23, 24, 25 and Area C, before and after each blast event. Figure 7-1 shows a typical ground surface settlement profile within these zones. The surface settlement profiles of the other zones were previously presented in chapters 3 and 4.
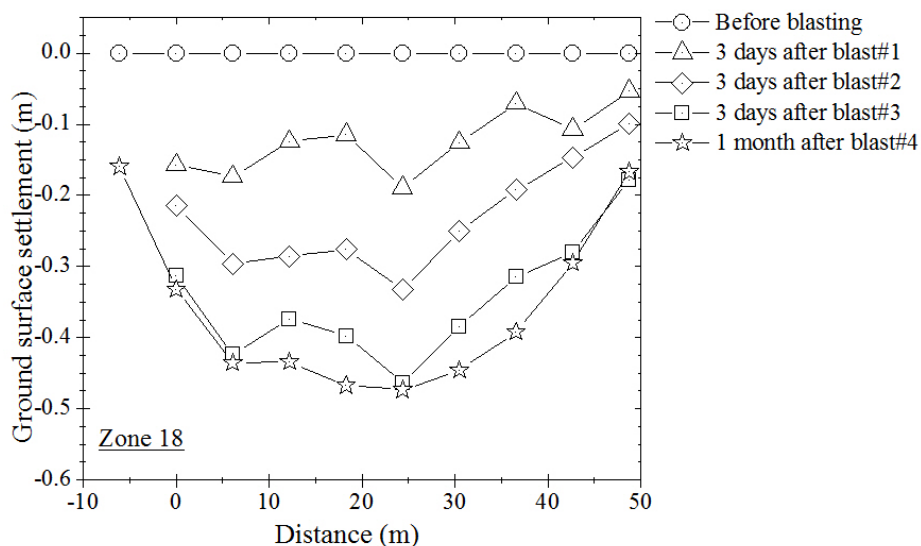
Figure 7-1. Surface settlements measured in zone 18.

In general the maximum settlement occurs at the center of the site and the incremental surface settlements decrease after each consecutive blast. This trend seems to be consistent among the blasted zones except in zones 20, 4, and 5 where no clear trend was observed. Although no physical evidence (photos or videos) of the site condition after blast densification was available for these three zones, this discrepancy could be a result of the difficulty to access the monitoring points to conduct the topographic survey after each blast event, as evidenced in other zones (For example, Figure 7-2) and/or a poorly executed topographic survey (For example, Figure 7-3). For instance, the soil deposited on the ground surface after each blast event was not properly removed at each measuring point before conducting the survey. These two observations could explain the lack of trend in the topographic survey data and the heaving of the soil measured in zones 20, 4, and 5.

Figure 7-2. Ground surface conditions in zones 16 (left) and 18 (right).
Note: accumulated water was from rain. These pictures show the ground surface conditions when the topography survey was conducted.

Figure 7-3. Soil deposited on the ground surface after blasting – Zones 17 and 18.
Note: heave may be measured if deposited soil is not removed.

7.2 Computed and measured void ratio and axial strain changes

The void ratio and axial strain change, Δe and $\Delta\varepsilon(\%)$, measured during and after each of the blast events in all zones were compared with those computed from the procedure presented in section 6.1 based on the one-dimensional constrained compression test. The measured void ratio and axial strain change within each zone after a blast event were computed as:

$$\Delta e = \varepsilon_a(1 + e_b) \qquad \text{(Eq. 7-1)}$$

and

$$\varepsilon_a = {\Delta H}/{H} \qquad \text{(Eq. 7-2)}$$

where ε_a is the induced axial strain by the blast, ΔH was the average surface settlement measured after the blast event; H was the average thickness of the target layer before the blast event; and e_b was the average void ratio of the target layer before the blast event. Figure 7-4 through Figure 7-7 show some typical results of the computed and measured cumulative void ratio and axial strains. Appendix D presents the results for the other zones. Zone C was heavily instrumented prior blasting and carefully monitored during each of the blast events (section 3.3.2). Among the blasted zones, the topographic survey data from this zone is considered to be

the most reliable in terms of measured settlements. The vertical error bars shown in the graphs

represent a plus and minus one standard deviation. The cumulative void ratio and axial strain for

all blasted zones are shown in appendix D.
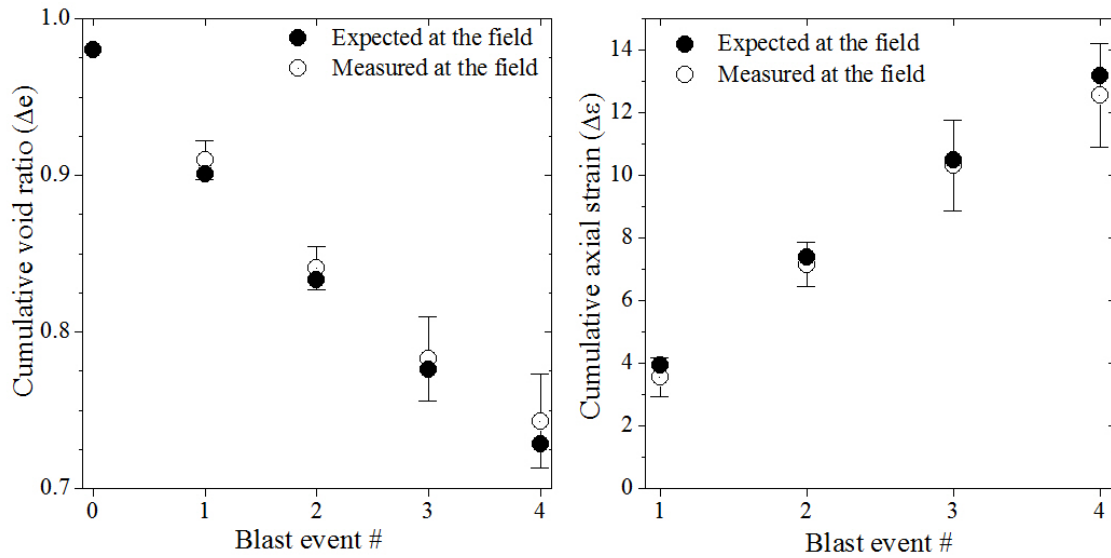
Figure 7-4. Cumulative Δe and Δε (%) after blast densification – Zone C.
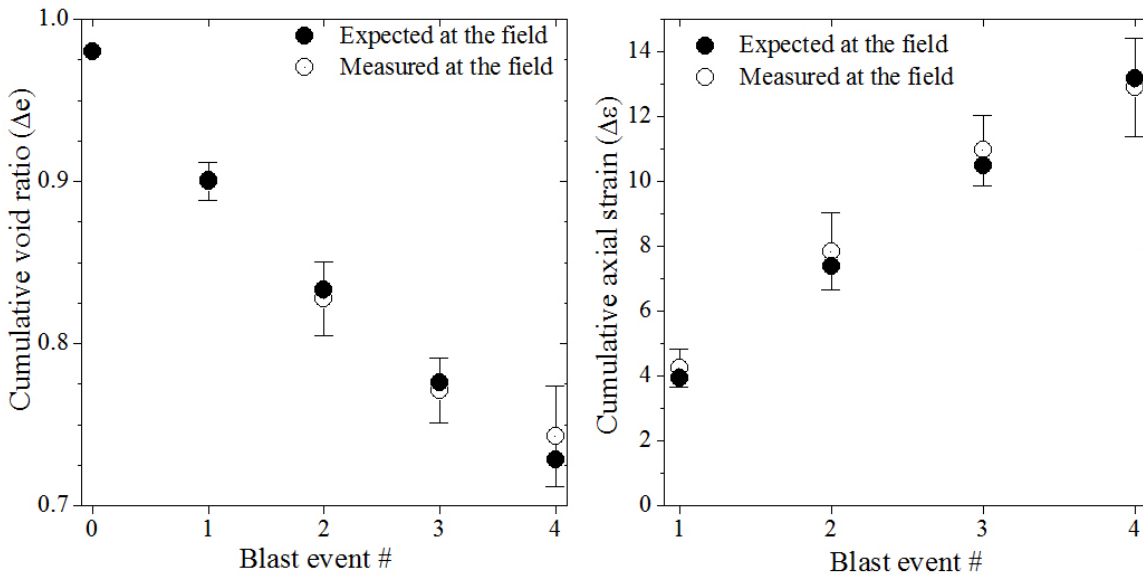
Figure 7-5. Cumulative Δe and Δε (%) after blast densification – Zone 17.
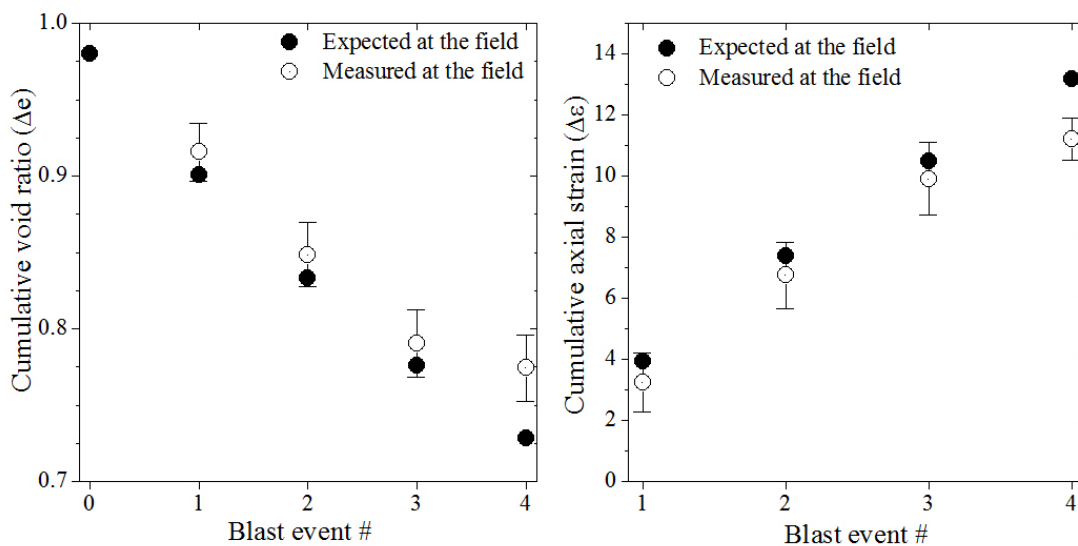
Figure 7-6. Cumulative Δe and Δε (%) after blast densification – Zone 18.
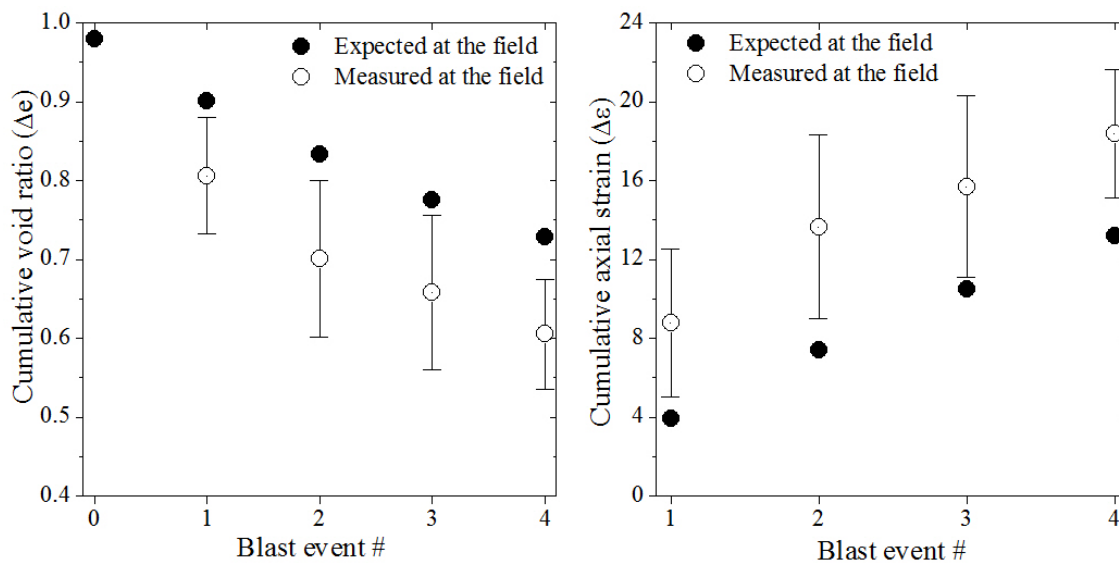
Figure 7-7. Cumulative Δe and Δε (%) after blast densification – Zone 4.

Figure 7-8 shows the cumulative axial strains for all blasted zones, except zone 4. As discussed in section 3.3.4, the surface settlements measured in this section are considered inaccurate and unreliable. The axial strain computed from the 1D constrained compression tests slightly underestimates the average axial strain measured within the blasted zones. However, this

observation should be carefully assessed considering the level of uncertainties and difficulties involved during the topography survey measurements. Some zones were partially or fully flooded during the topographic survey, making difficult the removal of the soil deposited at the measuring points. This could be reflected in a less cumulative axial strain than the one that indeed occurred. The results presented in Figure 7-8 provide a clear indication that the one-dimensional constrained compression test is a simple approach to estimate the amount of axial deformation that will occur within the liquefied layer after blasting. The square root value of the linear trendline of the ground surface settlements measured at the field is 0.815.
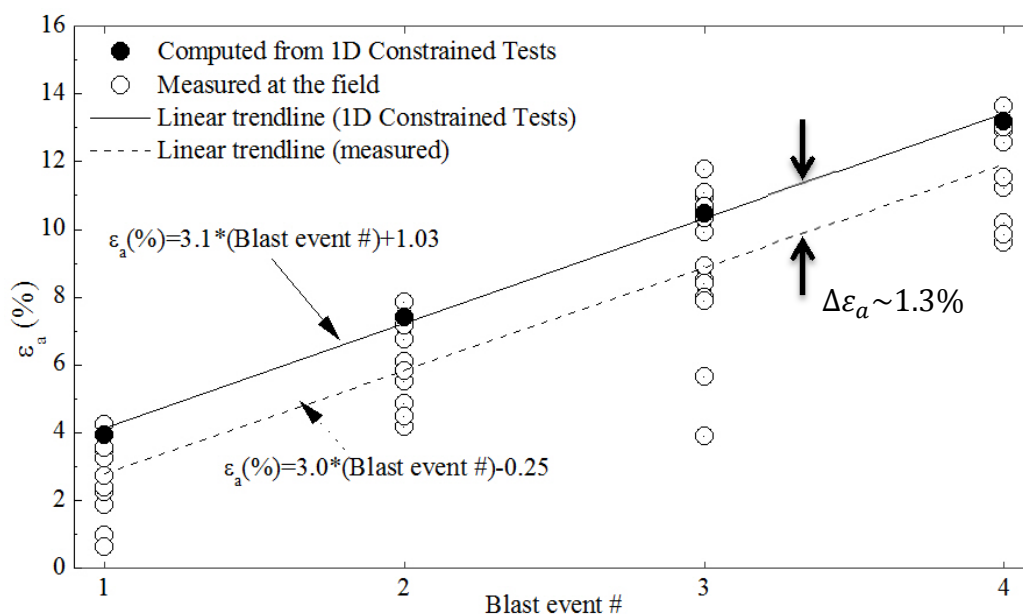
Figure 7-8. Cumulative axial strain for all zones except zone 4.

7.3 Methodology to quantify amount of densification

The procedure presented herein for evaluating the ground improvement and liquefaction resistance after blast densification is based on the concepts of the critical state soil mechanics. The critical state concepts state that a soil with an initial state of stresses below the critical state

line will tend to dilate and thus will not be susceptible to liquefaction and flow. This methodology assumes that liquefaction is induced over the area of interest by the energy released by the explosives.

As shown in chapters 4 and 6, some of the gas released during blast densification can remain trapped in the soil mass for several years. The presence of even small amount of gas on medium dense sands significantly increases the liquefaction resistance and decreases the amount of deformation that the soil will experience during an earthquake. The following steps are proposed to quantify the amount of densification required to prevent liquefaction and flow for a given project. This procedure is conservative since the change in density is the only factor being considered to affect the liquefaction potential. The effect of gas in soil mechanical response is not considered in the proposed procedure, because further research is needed to evaluate the longevity of gas in soils densified with explosives.

Step 1 – Identify the potentially liquefiable layers

Field penetration tests such as the cone penetration test and the standard penetration test can be used to determine the soil stratigraphic and to identify loose sands and silty sands deposits below the groundwater table that are susceptible to liquefaction and flow. The advantage of the cone penetration test over the standard penetration test is that a continuous profile for stratigraphic interpretation is developed and the test results are more consistent and repeatable. The procedure presented by Mayne (2007), in chapter 10, can be used to identify the soils that are prone to liquefaction and flow.

Step 2 – Characterization of the material collected from the loose layer

A complete geotechnical testing program should be conducted on the collected sand sample to evaluate its index and mechanical properties. The laboratory program should be conducted

according to the ASTM specifications and include the visual classification test, sieve analysis test (ASTM D421 & D422), specific gravity test (ASTM D854), and maximum and minimum densities tests (ASTM D4253 & D4254).

Step 3 – Determine the initial in-situ void ratio

It is very important to accurately measure the in-situ void ratio of the liquefiable layers before blasting. This parameter is needed to evaluate the soil liquefaction potential and to estimate the amount of densification needed at a particular project. The in-situ void ratio can be reliably measured by recovering undisturbed samples from the loose sand layer. However, for most practical cases the cost of this alternative is large and almost prohibited. Mayne (2007) present a relationship that can be used to infer the in-situ void ratio from the cone penetration resistance test. This relationship was developed for clean sands with less than 15% fines content. The relative density and in-situ void ratio are computed as follow

$$D_R = 100\left[0.268\, ln\left(\frac{q_t/\sigma_{atm}}{\sqrt{\sigma'_{vo}/\sigma_{atm}}}\right) - 0.675\right] \qquad \text{(Eq. 7-3)}$$

$$e = e_{max} - D_R(e_{max} - e_{min}) \qquad \text{(Eq. 7-4)}$$

where D_R is the relative density in percentage, q_t is the corrected tip cone penetration resistance and σ_{atm} is the atmospheric pressure (1 atm =1 bar = 100 kPa). e_{min} and e_{max} are the minimum and maximum void ratios measured in step 2.

Step 4 – Determine the critical state line (Section 6.3)

Determine the position of the critical state line (CSL) by conducting undrained triaxial compression tests on five or six reconstituted saturated specimens of identical soil. The samples should be consolidated to stresses higher than the critical state values at a given void ratio, to assure a fully contractive response and thus the critical state line can be determine reliable. The

CSL must be defined over a range of void ratios and stresses representative of those in-situ values.

Step 5 – Determine the expected void ratio change as function of the dry density (Section 6.1)

Conduct a series of one-dimensional constrained compression tests on dry samples prepared at various dry densities representative of those densities expected in the field before and after blasting. Follow the procedure presented in section 6.1 to estimate the void ratio change as function of dry density.

Step 6 – Compute the number of blast events needed to achieve the design objective

The amount of densification or the number of blast events required to prevent liquefaction in a given project will depend on the amount of axial deformation that the soil mass will be allowed to experience during an earthquake. Although a soil with a state of stresses below but close to the critical state line is not susceptible to liquefaction and flow, excessive axial deformations can occur during cyclic loading.

Figure 7-9 illustrates the procedure proposed in this step. The first stage consists of estimating the void ratio change that will occur after each one of four or five blast events. These void ratio changes are computed from the results obtained in step 5. The second stage consists of conducting a cyclic triaxial test on a reconstituted saturated sample, at each estimated void ratio. The cyclic stress ratio applied to the samples must be representative of that of the expected earthquake. The third stage consists of quantifying the number of blast events. For practical purposes, the number of passes needed in a given project will correspond to that of the void ratio where the axial strain developed during cyclic loading is acceptable for the project in question.
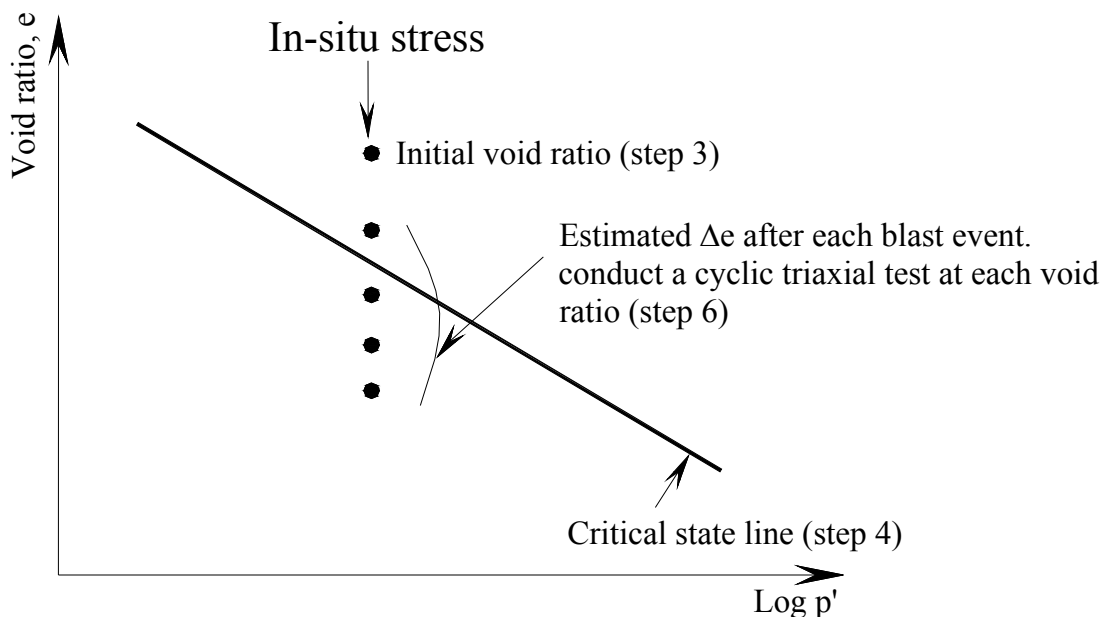
Figure 7-9. Number of blast events needed to achieve desired densification.

Example calculation – number of blast events needed at the Oakridge landfill

The number of blast events needed to prevent liquefaction and excessive axial deformations at the Oakridge landfill site is computed as follow

Step 1: Identify the potential liquefiable layer

CPT soundings performed before blasting in zones 15A, 15B, 16, 17 and 18 showed that a loose sand layer susceptible to liquefaction and flow was found at a depth between 7.6m and 11.5m (Figure 4-4). The average thickness of the liquefiable layer was 3.85m.

Step 2: Characterization of the material collected from the loose layer

A laboratory program was implemented to characterize the sand samples collected in zone 18, from the target loose layer, during the blast densification program conducted in 2011. The soil is clean, fine grained sand, SP, angular in shape, with little fines. The average uniformity coefficient (C_u) and curvature coefficient (C_c) were 1.63 and 1.03, respectively and the minimum

and maximum void ratios were $e_{min} = 0.62$ and $e_{max} = 1.05$, respectively. The percentage of fines passing sieve # 200 was approximately 1.5% and 7% by weight when the dry and wet sieve analysis were conducted, respectively. The specific gravity value is 2.66, suggesting that the sand is quartz.

Step 3: Determine the initial in-situ void ratio

In average, the tip cone penetration resistance for these zones is 2.1 MPa (Table 4-1). The effective vertical stress acting at the middle of the loose sand layer is approximately 100 kPa. From Eq. 7-3 and 7.4, the initial in-situ relative density and void ratio inferred from the CPT soundings are

$$D_R = 100 \left[0.268 \, ln \left(\frac{q_t/\sigma_{atm}}{\sqrt{\sigma'_{vo}/\sigma_{atm}}} \right) - 0.675 \right] = 14\%$$

$$e = e_{max} - D_R(e_{max} - e_{min}) = 0.98$$

Step 4: Determine of the critical state line

Five undrained triaxial compression tests were performed to determine the critical state line. The critical state void ratio, at an effective mean normal stress of 100 kPa, is estimated to be between 0.83 and 0.84 (Figure 6-8).

Step 5: Expected void ratio as function of dry density

Twenty-one one-dimensional constrained compression tests were conducted on dry samples prepared at various densities to estimate the expected void ratio change that will occur after each blast event. At the Oakridge landfill site, the expected void ratio change can be expressed in terms of the dry density before each blast event as follows (Figure 6-5)

$$\Delta e = -0.21\rho_d + 0.36$$

Step 6: Compute the number of blast events needed to achieve the design objective

The in-situ void ratio before blasting was estimated to be 0.98. The final void ratio after the first, second, third and fourth blast event are approximately 0.90, 0.83, 0.78 and 0.73, respectively (Figure 6-5). These void ratios correspond to relative densities of 35%, 50%, 63% and 74%, respectively. Figure 6-21 through Figure 6-23 present the cyclic response of saturated tests consolidated to an average void ratio of 0.82, 0.78 and 0.70, respectively and subjected to a cyclic stress ratio of 0.15. These results showed that even though liquefaction and flow did not occur, the samples with $e_{aver.}$=0.82 and $e_{aver.}$=0.78 experienced considerable axial deformations (i.e., $\varepsilon_a = 5\%$ after 49 cycles for $e_{aver.}$=0.78). For the case of the Oakridge Landfill site, four blast events are considered enough to significantly increase the soil liquefaction potential and to prevent excessive axial strains from developing during an earthquake.

7.4 Summary

The void ratio and axial strain changes measured in all zones, at the Oakridge landfill, during and after each of the blast events were compared with those computed from the one-dimensional constrained compression test. This testing procedure is a practical approach to estimate the amount of axial deformation that will occur within the liquefied layer after each blast event.

8 SUMMARY AND CONCLUSIONS

8.1 SUMMARY

Blasting has been used for several decades to densify loose, saturated sand soil deposits. The effectiveness of blast densification has commonly been evaluated in terms of ground surface settlements and field verification tests, including the cone penetration (CPT), standard penetration (SPT) and shear wave velocity (V_s). Although all case studies available to the author have shown that the loose sand compresses almost immediately after blast densification, in some cases the results from field verification tests provide rather counterintuitive results. Specifically, the CPT tip resistance conducted after blasting often decreases relative to pre-blast values, and in some cases it never increases to levels above the pre-blast levels. This observation raises concerns regarding the future performance of the densified soil mass and begs the question of whether or not the loose sands have been densified to a point where liquefaction and flow is not possible.

During blast densification, large amounts of water vapor (H_2O), carbon dioxide (CO_2) and nitrogen (N_2) are produced and released in the ground. In most applications of blast densification, the absolute pressure acting on the gas is relatively low, leaving open the possibility that some of this gas may remain trapped in the soil for months or even years. Therefore, it is important to study the longevity of these gases and their effect on the mechanical response of soils during monotonic and cyclic loading.

A blast densification program was conducted between February and March of 2011 at a test site located in Dorchester country, SC. This densification program was a continuation of the ground improvement work initiated in 1998 to densify a potentially liquefiable loose layer at a

depth of 10 m. During the 2011 program, standard topographic surveys along the center line of the improved zones were conducted to measure ground surface settlements after each blast event and thus verify that ground improvement had been achieved. A total of nine BAT probes were installed at different locations to collect groundwater/gas samples and to monitor pore pressure and temperature changes before, during and after blasting. Six BAT probes were installed in two zones to obtain information about the short term concentration of gases after blasting. Two more BAT probes were installed in a zone densified in 2005 to determine the type of gases and concentrations that remain four years after blasting. The containers to collect the samples were prepared by either applying vacuum to the containers or pre-charging the containers with helium. The collected samples were sent to a laboratory for a gas chromatograph (GC) test to identify the type of gas present in the soil and to quantify their in-situ concentrations. The results obtained from the BAT probes and GC tests were used to compute the degree of saturation of the soil at the time of sampling.

An experimental program consisting of forty-five triaxial compression tests was conducted to investigate the effect of gas in the mechanical response of sands during monotonic and cyclic loading. These tests were divided into three groups to quantify the shear strength and cyclic resistance to liquefaction of medium dense gassy sands as a function of void ratio and degree of saturation. A vertical pair of bender elements was used to measure the shear wave propagation velocity along the longitudinal axis of the sample during consolidation, creep, sample de-saturation, and shear. Twenty-one one-dimensional constrained compression tests (oedometer tests) on dry samples prepared at various densities were conducted to estimate the amount of volume change that will occur after each blast event. These computed values were compared with volume changes measured at the site.

8.2   CONCLUSIONS

Based on the results of the in-situ testing at the Oakridge facility and the laboratory testing, the following conclusions can be drawn:

The maximum surface settlement occurred at the center of each blasted area and the incremental surface settlements decreased after each consecutive blast.

The porewater pressure measured with the BAT probe immediately after detonation of the explosives equaled the in-situ total vertical stress, indicating that liquefaction was induced in the loose sand layer. The soil maintained a liquefied state for over a period of 6 to 7 hours and the blast-induced pore water pressure decreased to the pre-blasting value in approximately 70 hours.

From the sampled gases, nitrogen was the only gas contributing to the gassy state of the soil. The other gases, carbon dioxide, carbon monoxide, oxygen and methane were found to be dissolved in the soil's pore fluid. Nitrogen was present in the ground in the form of free gas a few days after blasting.

The groundwater/gas samples collected in zone 5 showed that nitrogen was present in the ground in the form of free gas four years after blasting. These measurements indicate that the amount of nitrogen initially trapped in the soil mass after blast densification will remain in the ground for a long period of time, at least for the conditions at the test site.

The percentage of nitrogen detected in the BAT containers' headspace ranged from 72.2% to 79.8% for the vacuumed containers and from 5% to 8.5% for the pre-charged containers. These two sampling techniques yielded similar soil degrees of saturation. The final degree of saturation of the "improved" sand layer varied from 78% to 96% within the tested zones, with an average of 89%. At these degrees of saturation, the gas phase is discontinuous and it is present in the form of occluded gas.

The degree of saturation at approximately 45 m from the corner of zones 16 and 18 varied between 85% and 94%. This gassy state was likely the result of the accumulation of gases released during the current and previous blast densification programs. Because the concentrations of methane and carbon dioxide detected in the container's headspace were very small, gases generated in the landfill were not believed to migrate to the targeted layer and contribute to its gassy state.

Presence of gas greatly affects the shear strength of medium dense sands. The undrained shear strength is affected by the presence of even small amount of gas and the effect is larger as the soil becomes denser. For these dilative soils, the larger the amount of gas and the lower the degree of saturation, the smaller the undrained shear strength and absolute value of excess pore water pressure developed during shear.

In the samples sheared under monotonic conditions, the stress-strain and stress path responses of gassy samples fell between the saturated undrained and drained states. The presence of gas made the soil more compressible under globally undrained conditions, restricting the development of excess pore pressure. The magnitude of porewater pressure developed in gassy samples was substantially less than that developed in the saturated undrained specimens; the denser the specimen, the more pronounced this effect.

The presence of even small amounts of gas greatly increased the liquefaction resistance of the soil regardless of its density. Medium dense sand deposits containing gas developed very low axial strains during cyclic loads, indicating that significantly settlements are not expected during an earthquake represented by the applied loads. For a given cyclic stress ratio, the amount of cumulative axial strain and excess pore water pressure developed during cyclic loading decreased as the amount of gas in the soil increased.

Even though the CPT tests at the Oakridge landfill showed little to no improvement in penetration after blast densification, the gassy sand layer had significantly increased its liquefaction resistance. This observation suggests that the CPT is not a reliable means to verify the increase in liquefaction resistance. Because the gas trapped in the sand resulted in significant increases in cyclic strength, the quantity and distribution of gas should be a better indirect measure of increased liquefaction resistance than either the CPT or SPT.

The BAT probe sampling procedure was found to be a reliable device for collecting groundwater/gas samples. The analytical procedure described herein allowed one to identify the types of gases released during blasting and quantify their in-situ concentrations. These tests are proposed as a means to verify increased liquefaction resistance. Additional testing regarding distribution of gases in a targeted loose soil and the longevity of the gas in occluded form are required for this proposal to be accepted by the profession as a standard verification technique.

The void ratio and axial strain changes measured after each of the blast events compared well with those computed from the procedure proposed herein based on results of the one-dimensional constrained compression test. These results provide a clear indication that this simple procedure is adequate to estimate the amount of volume change that will occur within the liquefied layer after each blast event.

8.3 RECOMMENDATION FOR FUTURE WORK

There are some topics that were not covered in this dissertation and are worth investigating to gain a better understanding of how gas affects the monotonic and cyclic response of soils densified with explosives. The recommended topics for future study are:

1. Distribution of gases: Study the vertical and horizontal distribution of gases in-situ after blast densification.

2. Longevity of gases: Develop a theoretical approach to compare the longevity of gases beneath the water table, and verify the procedure with results of an in-situ test bed.

3. Constitutive modeling of gassy sands: Quantify the response of a three-phase system to monotonic and cyclic loads with a properly-formulated numerical model.

4. Fines content: Investigation of the effect of fines content on the shear strength and cyclic response of gassy sands.

5. Fate of the gases after cyclic loading: Investigate whether or not the gas will dissolve in the pore fluid after multiple seismic events and after substantial waiting periods.

6. Effect of imposed load: Study the effect of loads imposed on the ground after densification.

7. Decrease in shear wave velocity after blast densification: In the present study samples were de-saturated after consolidation. It is proposed to de-saturate the samples before consolidation and to measure changes in shear wave velocities as the samples are consolidated to the in-situ stress.

9 REFERENCES

1. Al-Qasimi, E. M. A., Charlie, W. A., and Woeller, D. J. (2005). "Canadian liquefaction experiment (CANLEX) : Blast-induced ground motion and pore pressure experiments." *Geotech. Testing. J.*, 28(1), 9-21.

2. Amaratunga, A., and Grozic, J. L. H. (2009). "On the undrained unloading behaviour of gassy sands." *Can. Geotech. J.*, 46, 1267-1276.

3. Ashford, S., Weaver, T., and Rollins, K. (2002). "Pore pressure response of liquefied sand in full-scale lateral pile load tests." *Transportation Research Record: Journal of the Transportation Research Board*, 1808(1), 21-29.

4. Ashford, S. A., Rollins, K. M., and Lane, J. D. (2004). "Blast-induced liquefaction for full-scale foundation testing." *J. Geotech. Geoenviron. Eng.*, 130(8), 798-806.

5. Been, K., Jefferies, M. G., and Hachey, J. (1991). "The critical state of sands." *Geotechnique*, 41(3), 365-381.

6. Bishop, A. W., and Blight, G. E. (1963). "Some aspects of effective stress in saturated and partly saturated soils." *Geotechnique*, 13(3), 177-197.

7. Bowman, E. T., and Soga, K. (2003). "Creep, ageing and microstructural change in dense granular materials." *Soils and Foundations*, 43(4), 107-117.

8. Camp, W. M., Mayne, P. W., and Rollins, K. M. (2008). "Cone penetration testing before, during, and after blast-induced liquefaction." *Geotechnical Earthquake Engineering and Soil Dynamics IV*, ASCE, Sacramento, CA, 10.

9. Castro, G. (1969). "Liquefaction of sands." Ph.D thesis, Harvard University, Cambridge, Massachusetts, 231 p. pp.

10. Castro, G., Seed, R. B., Keller, T. O., and Seed, H. B. (1992). "Steady-state strength analysis of lower San Fernando Dam slide." *J. Geotech. Eng.*, 118(3), 406-427.

11. Chaney, R., and Mulilis, J. P. (1978). "Suggested method for soil specimen remolding by wet-raining." *Geotechnical Testing Journal, GTJODJ.*, 1(2), 107-108.

12. Charlie, W. A., and Doehring, D. O. (2007). "Groundwater table mounding, pore pressure, and liquefaction induced by explosions: energy-distance relations." *Reviews of Geophysics*, 45(RG4006), 9 pp.

13. Charlie, W. A., Jacobs, P. J., and Doehring, D. O. (1992a). "Blast-induced liquefaction of an alluvial sand deposit." *Geotech. Testing. J.*, 15(1), 14-23.

14. Charlie, W. A., Lewis, W. A., and Doehring, D. O. (2001). "Explosive induced pore pressure in a sandfill dam." *Geotech. Testing. J*, 24(4), 391-400.

15. Charlie, W. A., Mansouri, T. A., and Ries, E. R. (1981). "Predicting liquefaction induced by buried charges." *Int. Society for Soil Mechanics and Foundation Engineering*, 2(10), 77-80.

16. Charlie, W. A., Rwebyogo, M. F. J., and Doehring, D. O. (1992b). "Time-dependent cone penetration resistance due to blasting." *J. Geotech. Eng.*, 118(8), 1200-1215.

17. Chern, J. C. (1981). "Effect of static shear on resistance to liquefaction." M.A.Sc. Thesis, The University of British Columbia, Vanvouver, Canada, 210 pp.

18. Chern, J. C. (1985). "Undrained response of saturated sands with emphasis on liquefaction and cyclic mobility." Ph.D dissertation, The University of British Columbia, Vanvouver, Canada, 213 pp.

19. Christian, H. A., and Cranston, R. E. (1997). "A methodology for detecting free gas in marine sediments." *Can. Geotech. J.*, 34, 293-304.

20. Christian, H. A., Woeller, D. J., Robertson, P. K., and Courtney, R. C. (1997). "Site investigations to evaluate flow liquefaction slides at Sand Heads, Fraser River delta." *Can. Geotech. J.*, 34(3), 384-397.

21. Dowding, C. H., and Hryciw, R. D. (1986). "A laboratory study of blast densification of saturated sand." *J. Geotech. Eng.*, 112(2), 187-199.

22. Dusseault, M. B. (1979). "Undrained volume and stress change behavior of unsaturated very dense sands." *Can. Geotech. J.*, 16(4), 627-640.

23. Elliott, R. J., Clarke, L., Gohl, B., Fulop, E., Singh, N. K., Berger, K. C., and Huber, F. "Explosive compaction of foundation soils for the seismic upgrade of the Seymour Falls Dam." *Proc., The 35th Annual Conference on Explosives and Blasting Technique*, International Society of Explosives Engineers, Denver, CO, 17 pp.

24. Fourie, A. B., Hofmann, B. A., Mikula, R. J., Lord, E. R. F., and Robertson, P. K. (2001). "Partially saturated tailings sand below the phreatic surface." *Geotechnique*, 51(7), 577-585.

25. Fredlund, D. G., and Rahardjo, H. (1993). *Soil mechanics for unsaturated soil*, John Wiley & Sons, Inc, New York, United States of America.

26. Fredlund, D. G., and Xing, A. (1994). "Equations for the soil-water characteristic curve." *Can. Geotech. J.*, 31(4), 521-532.

27. Gandhi, S. R., Dey, A. K., and Selvam, S. (1999). "Densification of Pond Ash by Blasting." *J. Geotech. Geoenviron. Eng.*, 125(10), 889-899.

28. GeoSyntec Consultants, I. (1998). "Appendix D-3: Final report for ground improvement pilot program."Appendix to 1998 Permit Application, prepared for USA Waste Services, Inc.

29. GeoSyntec Consultants, I. (2005). "Ground improvement results of optimized blast densification program." Oakridge Sanitary Landfill, Dorchester, SC, Final Report - Project Number GD3397. Prepared for USA Waste Services, Inc.

30. GeoSyntec Consultants, I. (2007). "Ground improvement implementation phase II – Zones 4, 5, 19, 20, 21, and 22." Oakridge Sanitary Landfill, Dorchester, SC, Final Report - Project Number GD3989-01. Prepared for USA Waste Services, Inc.

31. Gitirana, J. G. d. F. N., and Fredlund, D. G. (2004). "Soil-Water Characteristic Curve Equation with Independent Properties." *J. Geotech. Geoenviron. Eng.*, 130(2), 209-212.

32. Gohl, W. B., Jefferies, M. G., Howie, J. A., and Diggle, D. (2000a). "Explosive compaction: design, implementation and effectiveness." *Geotechnique*, 50(6), 657-665.

33. Gohl, W. B., Jefferies, M. G., Howie, J. A., and Diggle, D. (2000b). "Explosive compaction: design, implementation and effectiveness." *Geotechnique*, 50(6), 657-665.

34. Gohl, W. B., Tsujino, S., Wu, G., Yoshida, N., Howie, J. A., and J., E. (1998). "Field application of explosive compaction in silty soils and numerical analysis." *Geotechnical Earthquake Engineering and Soil Dynamics III, GSP 75*, ASCE, Seattle, Washington, Vol. 1, 654-665.

35. Grozic, J. L., Robertson, P. K., and Morgenstern, N. R. (1999). "The behavior of loose gassy sand." *Can. Geotech. J.*, 36, 482-492.

36. Grozic, J. L. H., Imam, S. M. R., Robertson, P. K., and Morgenstern, N. R. (2005). "Constitutive modeling of gassy sand behaviour." *Can. Geotech. J.*, 42(3), 812-829.

37. Grozic, J. L. H., Robertson, P. K., and Morgenstern, N. R. (2000). "Cyclic liquefaction of loose gassy sand." *Can. Geotech. J.*, 37, 843-856.

38. Hachey, J. E., Plum, R. L., Byrne, J., Kilian, A. P., and Jenkins, D. V. "Blast densification of a thick, loose debris flow at Mt. St. Helen's, Washington." *Proc., Proc., Vertical and Horizontal Deformations of Foundations and Embankments, GSP 40*, 502–512.

39. Handford, G. T. (1988). "Densification of an existing dam with explosives." *Hydraulic Fill Structures, GSP 21*, ASCE, 750-762.

40. Hardin, B. O., and Black, W. L. (1968). "Vibration modulus of normally consolidated clay." *J. Soil Mech. and Found. Div.*, 94(2), 353-370.

41. Hardin, B. O., and Richart, F. E. J. (1963). "Elastic wave velocities in granular soils." *J. Soil Mech. and Found. Div.*, 89(1), 33-65.

42. Hryciw, R. D. (1986). "A study of the physical and chemical aspects of blast densification of sand." Ph. D. thesis, Northwestern University, Evanston, 229 pp.

43. Jung, Y.-H., Cho, W., and Finno, R. J. (2007). "Defining yield from bender element measurements in triaxial stress probe experiments." *J. Geotech. Geoenviron. Eng.*, 133(7), 841-849.

44. Kim, T.-H., and Hwang, C. (2003). "Modeling of tensile strength on moist granular earth material at low water content." *Engineering Geology*, 69(3–4), 233-244.

45.   Kim, T., and Finno, R. J. (2012). "Anisotropy evolution and irrecoverable deformation in triaxial stress probes." *J. Geotech. Geoenviron. Eng.*, 138(2), 155-165.

46.   Kimmerling, R. E. (1994). "Blast densification for mitigation of dynamic settlement and liquefaction." *Washington State Department of Transportation,* Olympia, WA, Final Report – Project Number WA-RD 348.1.

47.   Knai, H. B. (2011). "Measuring the effect of occluded gas bubbles on stress-strain response of a loose to medium sand." Master's thesis, Northwestern University, Evanston, IL, 64 pp.

48.   Kokusho, T., Yoshida, Y., and Esashi, Y. (1982). "Dynamic properties of soft clay for wide strain range." *Soils Found.*, 22(4), 1-18.

49.   Kulhawy, F. H., and Mayne, P. W. (1990). "Manual on estimating soil properties for foundation design." Cornell University, 291 p.

50.   La Fosse, U., and Rosenvinge IV, T. V. (1992). "Densification of loose sands by deep blasting." *Grouting, Soil Improvement and Geosynthetics*, GPS 30, ASCE, 954-968

51.   Ladd, R. S. (1974). "Specimen preparation and liquefaction of sands." *Journal of the Geotechnical Engineering Division, ASCE*, 100(No. GT10), 1180-1184.

52.   Ladd, R. S. (1978). "Preparing test speciments using undercompaction." *Geotech Test J, GTJODJ.*, 1(1), 16-23.

53.   Liao, T., and Mayne, P. W. "Cone penetrometer measurements during Mississippi embayment seismic excitation experiment." ASCE, Earthquake Engineering and Soil Dynamics, GSP 133 (158), 32.

54.   Likos, W. J., Wayllace, A., Godt, J., and Lu, N. (2010). "Modified direct shear apparatus for unsaturated sands at low suction and stress." *Geotech Test J, GTJODJ.*, 33(4), 1-13.

55.   Lu, N., Kim, T.-H., Sture, S., and Likos, W. J. (2009). "Tensile Strength of Unsaturated Sand." *J. Eng. Mech.*, 135(12), 1410-1419.

56. Marcuson, W. F., and Wahls, H. E. (1972). "Time effects on dynamicshear modulus of clays." *J. Soil Mech. and Found. Div.*, 98(12), 1359-1373.

57. Mayne, P. W. (2007). "NCHRP Synthesis 368, Cone Penetration Testing." National Cooperative Highway Research Program, Transportation Research Board, Washigton, D.C., 118 p.

58. Menzies, B. K. (1988). "A computer controlled hydraulic triaxial testing system." *Adv. Triaxial Testing of Soil and Rock*, ASTM STP 977, 82-94.

59. Menzies, B. K., Hooker, P., Sutton, J. A., and Snelling, K. (2002). "GDS software-based dynamic and seismic laboratory soil testing systems." *A GDS publication.*

60. Mesri, G., Feng, T. W., and Benak, J. M. (1990). "Postdensification penetration resistance of clean sands." *J. Geotech. Eng.*, 116(7), 1095-1115.

61. Michalowski, R. L., and Nadukuru, S. S. (2012). "Static fatigue, time effects, and delayed increase in penetration resistance after dynamic compaction of sands." *J. Geotech. Geoenviron. Eng.*, 138(5), 564-574.

62. Mitchell, J. K., and Solymar, Z. V. (1984). "Time-dependent strength gain in freshly deposited or densified sand." *J. Geotech. Eng.*, 110(11), 1559-1576.

63. Mulilis, J. P., Seed, H. B., Chan, C. K., Mitchell, J. K., and Arulanandan, K. (1977). "Effects on sample preparation on sand liquefaction." *Journal of the Geotechnical Engineering Division, ASCE*, 103(No. GT2), 91-108.

64. Nageswaran, S. (1983). "Effect of gas bubbles on the sea bed behaviour." Ph. D. Thesis, Oxford University, 257 pp.

65. Narin Van Court, W. A., and Mitchell, J. K. (1994). "Soil improvement by blasting." *The Journal of Explosives Eng.*, 12(3), 34-41.

66. Narsilio, G. A., Santamarina, J. C., Hebeler, T., and Bachus, R. (2009). "Blast Densification: Multi-Instrumented Case History." *J. Geotech. Geoenviron. Eng.*, 135(6), 723-734.

67. Ng, C. W. W., and Bruce, M. (2007). "Advanced unsaturated soil mechanics and engineering." Taylor and Francis, Hoboken.

68. Ng, C. W. W., Zhang, L. T., and Cui, Y. J. (2002). "A new simple system for measuring volume changes in unsaturated soils." *Can. Geotech. J.*, 39(3), 757-764.

69. Oda, M. (1972). "Initial fabrics and their relations to mechanical properties of granular material." *Soils and Foundations*, 12(17-36).

70. Okamura, M., Ishihara, M., and Oshita, T. (2003). "Liquefaction resistance of sand deposit improved with sand compaction pile." *Soils and Foundations*, 43(5), 175-187.

71. Okamura, M., Ishihara, M., and Tamura, K. (2006). "Degree of saturation and liquefaction resistances of sand improved with sand compaction pile." *J. Geotech. Geoenviron. Eng.*, 132(2), 258-264.

72. Okamura, M., and Soga, Y. (2006). "Effects of pore fluid compressibility on liquefaction resistance of partially saturated sand." *Soils and Foundations*, 46(5), 695-700.

73. Okamura, M., Takebayashi, M., Nishida, K., Fujii, N., Jinguji, M., Imasato, T., Yasuhara, H., and Nakagawa, E. (2011). "In-Situ Desaturation Test by Air Injection and Its Evaluation through Field Monitoring and Multiphase Flow Simulation." *J. Geotech. Geoenviron. Eng.*, 137(7), 643-652.

74. Okamura, M., and Teraoka, T. (2004). "Shaking table tests to investigate soil desaturation as a liquefaction countermeasure." *Seismic Performance and Simulation of Pile Foundations in Liquefied and Laterally Spreading Ground*, GSP 145, ASCE, 282-293

75. Okamura, M., and Yasuhara, H. (2009). "In-situ test on desaturation by air injection and its monitoring." *International Seminar on Hazard Management for Sustainable Development.* Kathmandu, Nepal, 135-147.

76. Poulos, S. J., Castro, G., and France, J. W. (1985). "Liquefaction evaluation procedure." *J. Geotech. Eng.*, 111(6), 772-792.

77. Qian, X., Koerner, R. M., and Gray, D. H. (2002). *Geotechnical aspects of landfill design and construction*, Prentice-Hall, Inc., Upper Saddle River, New Jersey, 717 p.

78. Rad, N. S., and Lunne, T. (1994). "Gas in soil. I: detection and η−profiling." *J. Geotech. Geoenviron. Eng.*, 120(4), 697-715.

79. Rad, N. S., Vianna, A. J. D., and Berre, T. (1994). "Gas in soil. II: efect of gas on undrained static and cyclic strength of sand." *J. Geotech. Geoenviron. Eng.*, 120(4), 716-736.

80. Raju, V. R., and Gudehus, G. "Compaction of loose sand deposits using blasting." *Proc., Proceedings, 13rd International Conference on soil mechanics and foundation engineering*, New Delhi, India, 1145-1150.

81. Robertson, P. K., and Wride, C. E. (1998). "Evaluating cyclic liquefaction potential using the cone penetration test." *Can. Geotech. J.*, 35(3), 442-459.

82. Rollins, K., Lane, J., Dibb, E., Ashford, S., and Mullins, A. (2005). "Pore pressure measurement in blast-induced liquefaction experiments." *Transportation Research Record: Journal of the Transportation Research Board*, 1936(1), 210-220.

83. Rollins, K. M., and Anderson, J. K. S. (2008). "Cone penetration resistance variation with time after blast liquefaction testing." *Geotechnical Earthquake Engineering and Soil Dynamics IV*, GSP 181, ASCE, 10 pp.

84. Saftner, D. A., Green, R. A., Hryciw, R. D., and Lynch, J. P. (2008). "Instrumentation for the NEESR sand aging field experiment." *GeoCongress 2008: Annual Congress of the Geo-Institute of ASCE,* New Orleans, LA, 8 pp.

85. SCDOT (2008). *SCDOT Geotechnical Design Manual*, South Carolina Geology and Seismicity, Chapter 11, 11-36 p.

86. Schmertmann, J. H. (1987). "Discussion of ``time-dependent strength gain in freshly deposited or densified sand" by James K. Mitchell and Zoltan V. Solymar (November, 1984)." *J. Geotech. Engrg.*, 113(2), 173-175.

87. Schmertmann, J. H. (1991). "The mechanical aging of soils." *J. Geotech. Engrg.*, 117(9), 1288-1330.

88. Schofield, A. N., and Wroth, P. (1968). *Critical state soil mechanics*, McGraw-Hill, 310 p.

89.   Shibata, T., and Soelarno, D. S. "Stress–strain characteristics of clays under cyclic loading." *Proc., Proc., Japanese Society of Civil Engineering*, Tokyo, Japan, No. 279, 101–110 (in Japanese).

90.   Shibuya, S., Hwang, S. C., and Mitachi, T. (1997). "Elastic shear modulus of soft clays from shear wave velocity measurement." *Geotechnique*, 47(3), 593-601.

91.   Shibuya, S., and Tanaka, H. (1996). "Estimate of elastic shear modulus in Holocene soil deposits." *Soils Found.*, 36(4), 45-55.

92.   Sivathayalan, S. (2000). "Fabric, initial state and stress path effects on liquefaction susceptibility of sands." Ph. D dissertation, The University of British Columbia, 307 pp.

93.   Sivathayalan, S., and Ha, D. (2004). "Effect of initial stress state on the cyclic simple shear behaviour of sands." *Cyclic Behaviour of Soils and Liquefaction Phenomena*, Triantafyllidis, ed., 2004 Taylor & Francis Group, London.

94.   Sladen, J. A., D'Hollander, R. D., and Krahn, J. (1985). "The liquefaction of sands, a collapse surface approach." *Can. Geotech. J.*, 22(4), 564-578.

95.   Sobkowicz, J. C., and Morgenstern, N. R. (1984). "The undrained equilibrium behaviour of gassy sediments." *Can. Geotech. J.*, 21, 439-448.

96.   Solymar, Z. V. (1984). "Compaction of alluvial sands by deep blasting." *Can. Geotech. J.*, 21, 305-321.

97.   Solymar, Z. V., Iloabachie, B. C., Gupta, R. C., and Williams, L. R. (1984). "Earth foundation treatment at Jebba dam site." *J. Geotech. Eng.*, 110(10), 1415-1430.

98.   Solymar, Z. V., and Reed, D. J. (1986). "A comparison of foundation compaction techniques." *Can. Geotech. J*, 23(3), 271-280.

99.   Sparks, A. D. W. (1963). "Theoretical considerations of stress equations for partly saturated soils." *Proceedings, 3rd Regional Conference for Africa on Soil Mechanics*, Salisbury, Rhodesia, 215-218.

100.   Steven, L. K. (1996). *Geotechnical Earthquake Engineering*, Prentice Hall, Upper Saddle River, New Jersey, 653 p.

101.   Thomann, T. G. (1990). "Stiffness and strength changes in cohesionless soils due to stress history and dynamic disturbance." Ph.D. Dissertation, University of Michigan, Ann Arbor, MI, 183 pp.

102.   Thomann, T. G., and Hryciw, R. D. (1992). "Stiffness and strength changes in cohesionless soils due to disturbance." *Can. Geotech. J.*, 29(5), 853-861.

103.   Thomas, S. D. (1987). "The consolidation behaviour of gassy soil." Ph. D. Thesis, University of Oxford, 264 pp.

104.   Thomson, P. R., and Wong, R. C. K. (2008). "Specimen nonuniformities in water-pluviated and moist-tamped sands under undrained triaxial compression and extension." *Can. Geotech. J*, 45(7), 939-956.

105.   Tsukamoto, Y., Ishihara, K., Nakazawa, H., Kamada, K., and Huang, Y. (2002). "Resistance of partly saturated sand to liquefaction with reference to longitudinal and shear wave velocities." *Soils and Foundations*, 42(6), 93-104.

106.   U.S.-Army-Corps-of-Engineers (1972). "Systematic drilling and blasting for surface excavations." Engineering Manual, EM 110-2-3800, Office of the Chief, United States Army of Corps of Engineers, Washington, DC, 119.

107.   Unno, T., Kazama, M., Uzuoka, R., and Sento, N. (2008). "Liquefaction of unsaturated sand considering the pore air pressure and volume compressibility of the soil particle skeleton." *Soils and Foundations*, 48(1), 87-99.

108.   Vaid, Y. P., and Chern, J. C. (1983). "Mechanism of deformation during cyclic undrained loading of saturated sands." *International Journal of Soil Dynamics and Earthquake Engineering*, 2(3), 171-177.

109.   Vaid, Y. P., Chung, E. K. F., and Kuerbis, R. H. (1990). "Stress path and steady state." *Can. Geotech. J.*, 27(1), 1-7.

110.   Vaid, Y. P., and Negussey, D. (1988). "Preparation of reconstituted sand specimens." *Advanced Triaxial Testing of Soils and Rock, ASTM STP 977*, 405-417.

111. Vaid, Y. P., and Sivathayalan, S. (2000). "Fundamental factors affecting liquefaction susceptibility of sands." *Can. Geotech. J.*, 37(3), 592–606.

112. Vaid, Y. P., Sivathayalan, S., and Stedman, D. (1999). "Influence of specimen-reconstituting method on the undrained response of sand." *Geotech. Testing. J.*, 22(3), 187-195.

113. Vaid, Y. P., Stedman, J. D., and Sivathayalan, S. (2001). "Confining stress and static shear effects in cyclic liquefaction." *Can. Geotech. J.*, 38(3), 580-591.

114. Verdugo, R., and Ishihara, K. (1996). "The steady state of sandy soils." *Soils and Foundations*, 36(2), 81-91.

115. Weems, R. R., Lemon, E. M., Nelson, M. S., and U.S. nuclear Regulatory Commission (1997). "Geology of the Pringletown, Ridgeville, Summerville, and Summerville Northwest 7.5-minute quadrangles, Berkeley, Charleston, and Dorchester counties, South Carolina." Reston, VA : The Survey; Denver, CO.

116. Wijewickreme, D., Sriskandakumar, S., and Byrne, P. (2005a). "Cyclic loading response of loose air-pluviated Fraser River sand for validation of numerical models simulating centrifuge tests." *Can. Geotech. J.*, 42(2), 550-561.

117. Wijewickreme, D., Sriskandakumar, S., and Byrne, P. M. (2005b). "Cyclic loading response of loose air-pluviated Fraser River sand for validation of numerical models simulating centrifuge tests." *Can. Geotech. J.*, 42(2), 550-561.

118. Xia, H., and Hu, T. (1991). "Effects of saturation and back pressure on sand liquefaction." *J. Geotech. Geoenviron. Eng.*, 117(9), 1347-1362.

119. Yamamuro, J. A., and Wood, F. M. (2004). "Effect of depositional method on the undrained behavior and microstructure of sand with silt." *Soil Dynam. Earthquake Eng.*, 24(9-10), 751-760.

120. Yegian, M. K., Eseller-Bayat, E., Alshawabkeh, A., and Ali, S. (2007). "Induced-Partial Saturation for Liquefaction Mitigation: Experimental Investigation." *J. Geotech. Geoenviron. Eng.*, 133(4), 372-380.

121. Youd, T. L., Idriss, I. M., Andrus, R. D., Arango, I., Castro, G., Christian, J. T., Dobry, R., Finn, W. D. L., Leslie F. Harder, J., Hynes, M. E., Ishihara, K., Koester, J. P., Liao, S. S. C., III, W. F. M., Martin, G. R., Mitchell, J. K., Moriwaki, Y., Power, M. S., Robertson, P. K., Seed, R. B., and II, K. H. S. (2001). "Liquefaction resistance of soils: summary report from the 1996 NCEER and 1998 NCEER/NSF workshops on evaluation of liquefaction resistance of soils." *J. Geotech. Eng.*, 127(10), 817-833.

A. RESULTS FROM GAS CHROMATOGRAPHY TESTS

Table A-1. Results from GC tests - vacuumed containers.

Borehole #	March 8th CO₂ (%)	N₂ (%)	O₂ (%)	CO (ppmv)	CH₄ (ppmv)	March 11th CO₂ (%)	N₂ (%)	O₂ (%)	CO (ppmv)	CH₄ (ppmv)	March 14th CO₂ (%)	N₂ (%)	O₂ (%)	CO (ppmv)	CH₄ (ppmv)
P. 16-1	1.8	75.2	19.7	6	41	3.3	73.8	18.7	24	39	-	-	-	-	-
P. 16-2	1.4	77.1	13.8	>2250	3680	2.2	73.2	17.5	4400	3300	2.4	76.0	14.8	4800	3700
P. 16-3	1.4	77.6	18.5	34	208	2.8	72.8	19.7	57	300	2.3	73.2	21.4	10	244
P. 18-1	2.4	78.7	15.9	15	75	3.3	76.5	16	20	124	2.8	72.4	20.6	10	90
P. 18-2	1.5	76.9	17.8	231	140	2.5	75.2	18.5	51	123	2.4	72.2	20.8	14	144
P. 18-3	2.2	77.6	16.4	12	12	3.2	77.0	15.8	24	12	2.0	74.3	19	9	13
P. 5-1	0.4 / 0.4	79.2 / 78.3	17.3 / 19	3 / 3	230 / 319	-	-	-	-	-	1.2	74.6	20	4	336
P. 5-2	0.3 / 0.3	77.7 / 77.5	17.6 / 18.7	4 / 3	301 / 458	-	-	-	-	-	0.7	74.0	20.9	2	537
Point A	1.6 / 2.8	78.7 / 75.8	16 / 17	12 / 43	17 / 22	1.9	77.4	17.4	8	25	-	-	-	-	-

Note: (*) ppmv

ppmv (parts per million by volume)

1 % by volume = 10000 ppmv

Table A-2. Results from GC tests – Containers flushed and precharged with Helium.

Borehole #	Sample 1 CO$_2$ (%)	N$_2$ (%)	CO (*)	CH$_4$ (*)	Sample 2 CO$_2$ (%)	N$_2$ (%)	CO (*)	CH$_4$ (*)	Sample 3 CO$_2$ (%)	N$_2$ (%)	CO (*)	CH$_4$ (*)	Sample 4 CO$_2$ (%)	N$_2$ (%)	CO (*)	CH$_4$ (*)	Sample 5 CO$_2$ (%)	N$_2$ (%)	CO (*)	CH$_4$ (*)	Sample 6 CO$_2$ (%)	N$_2$ (%)	CO (*)	CH$_4$ (*)
April 7th																								
P. 16-1	-				-				-				-				-				-			
P. 16-2	-				-				-				-				-				-			
P. 16-3	0.6	8.5	1	89	0.3	6.7	1.2	51	0.4	6.8	<1	83	-				-				-			
P. 18-1	0.4	6.1	1.5	11	0.2	6.2	1.7	10	0.3	6.9	1.6	20	-				-				-			
P. 18-2	0.3	6.3	1.2	13	0.3	6.2	1.0	22	0.3	6.4	1.1	26	-				-				-			
P. 18-3	0.4	7.4	1.7	<1	0.2	5.0	1.3	<1	0.3	5.9	1.4	1.0	-				-				-			
P. 5-1	0.2	6.4	1.5	17	0.1	6.8	<1	39	0.1	5.9	1.7	23	0.1	7.5	1.3	35	-				-			
P. 5-2	0.2	5.1	1.6	13	0.1	6.2	1.7	47	0.1	8.2	1.1	39	0.1	5.4	1.7	33	0.1	7.4	1.0	95	0.2	7.0	1.8	69
Point A	0.4	7.2	2.1	2.0	0.3	6.4	1.5	3	0.3	6.8	2.0	3	0.4	8.0	2.3	8	-				-			

Note: (*) ppmv

ppmv (parts per million by volume)

1 % by volume = 10000 ppmv

Table A-3. Parameters required to compute the degree of saturation of the soil.

85%-90% vacuum applied to containers					Containers flushed and pre-charged with Helium							
Borehole #	P_o (kPa)	P_c (kPa)	V_w (mL)	V_{gc} (mL)	C_{N2} (%)	Borehole #	P_v (kPa)	P_o (kPa)	P_c (kPa)	V_w (mL)	V_{gc} (mL)	C_{N2} (%)	C_{He} (%)
March 8th						April 7th							
P. 16-1	244	52	18.5	16.5	75.2	P. 16-3 (S1)	73	197	133	15.3	19.7	8.5	88.4
P. 16-2	251	122	25.9	9.1	77.1	P. 16-3 (S2)	122	197	174	10.8	24.2	6.7	88.7
P. 16-3	248	85	20.3	14.7	77.6	P. 16-3 (S3)	101	197	174	14.2	20.8	6.8	88.6
P. 18-1	219	80	22.4	12.6	78.7	P. 18-1 (S1)	114	195	192	13.4	21.6	6.1	89.3
P. 18-2	218	78	21.9	13.1	76.9	P. 18-1 (S2)	131	195	193	10.7	24.4	6.2	89.3
P. 18-3	218	65	21.4	13.6	77.6	P. 18-1 (S3)	99	195	192	16.3	18.7	6.9	89.1
P. 5-1 (1)	171	78	20	15.1	79.2	P. 18-2 (S1)	131	194	192	10.7	24.4	6.3	89.4
P. 5-1 (2)	171	49	20.1	14.9	78.3	P. 18-2 (S2)	115	194	192	11.8	23.2	6.2	89.1
P. 5-2 (1)	172	78	20.7	14.3	77.7	P. 18-2 (S3)	123	194	191	11.9	23.1	6.4	89.3
P. 5-2 (2)	172	62	23.8	11.2	77.5	P. 18-3 (S1)	128	197	181	10.1	24.9	7.4	88.6
Point A (1)	186	121	29.3	5.7	78.7	P. 18-3 (S2)	136	197	188	9.3	25.7	5.0	91.0
Point A (2)	186	85	28.1	6.9	77.4	P. 18-3 (S3)	123	197	192	12.4	22.6	5.9	90.1
March 11th						P. 5-1 (S1)	132	172	171	7.8	27.3	6.4	89.6
P. 16-1	297	27	14.7	20.3	73.8	P. 5-1 (S2)	119	172	171	10.5	24.5	6.8	88.8
P. 16-2	306	52	22	13.1	73.2	P. 5-1 (S3)	138	172	171	6.7	28.3	5.9	89.3
P. 16-3	297	38	18.6	16.4	72.8	P. 5-1 (S4)	124	172	171	9.5	25.5	7.5	87.4
P. 18-1	295	34	21.4	13.6	76.5	P. 5-2 (S1)	147	173	171	5.2	29.8	5.1	90.4
P. 18-2	297	39	21	14	75.2	P. 5-2 (S2)	126	173	172	9.5	25.6	6.2	89.3
P. 18-3	295	38	22.3	12.8	77	P. 5-2 (S3)	136	173	172	8.0	27.0	8.2	86.3
Point A	188	37	23.3	11.7	75.8	P. 5-2 (S4)	140	173	172	6.8	28.2	5.4	90.1
March 14th						P. 5-2 (S5)	103	173	171	14.2	20.8	7.4	87.8
P. 16-2	208	51	16.6	18.4	76	P. 5-2 (S6)	119	173	172	11.4	23.6	7.0	88.8
P. 16-3	206	46	19.9	15.1	73.2	Point A (S1)	127	182	180	10.1	24.9	7.2	87.7
P. 18-1	202	44	22.9	12.2	72.4	Point A (S2)	120	182	180	11.4	23.6	6.4	89.5
P. 18-2	200	37	20.1	14.9	76	Point A (S3)	121	182	180	11.2	23.9	6.8	88.8
P. 18-3	201	45	22.5	12.5	74.3	Point A (S4)	104	182	176	14.6	20.4	8.0	87.7
P. 5-1	175	35	19.9	15.1	74.6	$T_o = T_c = 293.15^oK$; $P_1 = 101.3\ atm$; $T_1 = T_v = 298.15^oK$;							
P. 5-2	174	50	24.2	10.9	74	$V_t = 35mL$; $\beta_{(N2)1} = 0.015$; $\beta_{(N2)o} = 0.016$; $\beta_{(He)1} = 0.0015$							

Table A-4. Final degrees of saturation in percentage of the soil.

Borehole #	85%-90% vacuum applied to containers				Containers flushed and pre-charged with Helium (April 7th)											
	March 8th		March 11th	March 14th	Sample 1		Sample 2		Sample 3		Sample 4		Sample 5		Sample 6	
					(*)	(**)	(*)	(**)	(*)	(**)	(*)	(**)	(*)	(**)	(*)	(**)
P. 16-1	88		93	-	-		-		-		-		-		-	
P. 16-2	89		94	83	-		-		-		-		-		-	
P. 16-3	84		94	89	95	94	90	88	93	93	-		-		-	
P. 18-1	87		96	93	93	92	89	88	94	94	-		-		-	
P. 18-2	86		95	91	89	88	90	90	90	90	-		-		-	
P. 18-3	88		96	93	87	85	90	89	92	91	-		-		-	
P. 5-1	77	86	-	91	83	81	88	86	81	80	84	83	-		-	
P. 5-2	79	89	-	92	79	77	87	86	79	77	83	81	92	90	89	87
Point A	92	93	94	-	86	85	90	89	89	88	91	90	-		-	

Note: Samples on March 11th were collected during the first six hour after blasting, when the soil was still in a liquefied state.
(*) Computed using Eq. B-3
(**) Computed using Eq. B-4

B. CALCULATION OF DEGREE OF SATURATION

Calculation procedure for in-situ degree of saturation

Rad and Lunne (1994) proposed the following equation to determine if the gases sampled with the BAT probe are present at the test location in dissolved and/or free form. The term η_j indicates how saturated the in-situ pore fluid is with gas j. An η_j value larger than 100% indicates that the pore fluid is fully saturated with gas j, and that free gas is present at the test location.

$$\eta_j = \frac{[(V_t - V_w) + V_w H_{cj}](MF_j x 10^{-6})}{V_w H_{oj}} \frac{S_o}{S_c} \frac{P_c}{P_o} \frac{T_o}{T_c} x 100 \qquad \text{(B-1)}$$

where η_j = water-gas saturation for gas j

V_t = total volume of BAT container (cm^3)

V_w = volume of water in BAT container (cm^3)

MF_j = concentration (mole fraction) of the in-situ gas of interest in BAT container

S_o, S_c = salinity of in-situ pore water (g/L) and water in BAT container (g/L)

P_o, P_c = in-situ absolute pore pressure and final absolute pressure in BAT container (atm)

T_o, T_c = in-situ absolute and final absolute temperature in BAT container (^{o}K)

H_{oj}, H_{cj} = solubility coefficient of gas j in-situ and in BAT container (cm^3/cm^3)

The main limitation of this approach is that a η_j value larger than 100% does not provide valuable information about the level of the degree of saturation of the soil. To overcome this limitation, Christian and Cranston (1997) developed an alternative procedure to quantify the degree of saturation in term of conventional soil mechanics terminology, as described below:

1. Determine if the pore fluid is fully saturated with gas j as follows (this solution is equivalent to that proposed by Rad and Lunne (1994)).

$$S_{jo} = 10^{-6} \frac{C_j P_1 T_o (V_{g1} + \beta_{j1} V_w)}{P_o T_1 \beta_{jo} V_w} x100 \tag{B-2}$$

where C_j = concentration (mole fraction) of gas j in BAT container (ppmv)

P_1 = absolute final sample pressure in the laboratory at NTP (atm)

P_o = in-situ absolute pore pressure (atm)

T_1, T_o = sampler temperature in the laboratory at NTP and in-situ (^{o}K)

V_w = volume of water in BAT container (cm^3)

β_{j1}, β_{jo} = Bunsen coefficient describing the solubility of gas j in pore fluid in the

laboratory and in-situ (liters of gas j / liters of pore fluid)

V_{g1} = total volume of gas in the headspace of BAT container at NTP (cm^3)

When the containers are pre-charged with a compound gas, V_{g1} is computed as

$$V_{g1} = \frac{P_v V_{cont}}{T_v} x \frac{10^6 T_1}{C_{He} P_1} - \beta_{(He)1} V_w \tag{B-3}$$

where P_v = absolute final pressure of BAT container after pre-charging (atm)

$T_v = T_1$ = temperature of BAT container after pre-charging (atm)

V_{cont} = total volume of BAT container (cm^3)

R = universal gas constant (0.082 L$^.$atm/(mol$^.$K))

C_{He} = concentration (mole fraction) of gas Helium in BAT container (ppmv)

An alternative procedure to determine V_{g1} is as follows:

By conservation of mass, and assuming that no gas molecules were lost at any of the stages

during sampling and GC testing, V_{g1} can be computed as

$$V_{g1} = \frac{P_c V_{gc} T_1}{T_c P_1} \tag{B-4}$$

where P_c, T_c = final absolute pressure and temperature in BAT container (atm, ^{o}K)

V_{gc} = total volume of gas in the headspace of BAT container after sampling (cm³)

2. If the pore fluid is fully saturated with gas j $(S_{jo} > 100\%)$, the total of free gas in-situ is computed as

$$V_{go} = \frac{RT_o}{P_o}\sum_{j=1}^{n}\eta_{gjo} \tag{B-5}$$

where η_{gjo}= total number of moles of gas j in the gaseous phase at in-situ conditions

η_{gjo} is computed as $\eta_{total(j)} - \eta_{wjo}$; where

$\eta_{total(j)} = \eta_{g(j)1} + \eta_{w(j)1}$ and $\eta_{wjo} = \frac{P_o\beta_{jo}V_w}{RT_o}$ respectively.

$\eta_{g(j)1}$ and $\eta_{w(j)1}$ are equal to $\eta_{g(j)1} = 10^{-6}\frac{C_jP_1V_{g1}}{RT_1}$ and $\eta_{w(j)1} = 10^{-6}\frac{C_jP_1\beta_{j1}V_w}{RT_1}$ respectively.

3. The degree of saturation is computed as

$$S(\%) = \frac{V_w}{(V_w+V_{go})}x100 = \frac{V_w}{\left(V_w+\frac{RT_o}{P_o}\sum_{j=1}^{n}\eta_{gjo}\right)}x100 \tag{B-6}$$

The degree of saturation computed using Eq. B-3 is slightly greater than those computed using Eq. B-4. A plausible explanation is that a small amount of gas molecules could have been lost during any of the stages during sampling or GC testing.

Example of computation of the soil degree of saturation

Compute the degree of saturation of sample 1 collected at P. 16-3 location. The absolute pressure in the BAT container before sampling (after vacuum) and after sampling were $P_v = 72.5kPa$ and $P_c = 132.5kPa$ respectively. The in-situ absolute pressure and temperature at the time of sampling were $P_o = 197.5\ kPa$ and $T_o = T_c = 293.15°K$ respectively. The total volume of BAT container was $V_t = 35\ cm^3$ and the volume of pore water sampled was $V_w = 15.3\ cm^3$. From the gas chromatography test, the concentrations of Nitrogen and Helium

detected were $C_{N2} = 85000 \, ppmv$ (8.5 %) and $C_{He} = 915000 \, ppmv$ (91.5 %) respectively.

These parameters were also used for the calculations: $\beta_{(N2)1} = 0.015$, $\beta_{(N2)o} = 0.016$, $\beta_{(He)1} = 0.0015$, $P_1 = 101.3 \, atm$, $and \, T_1 = T_v = 298.15^o K$.

Pore fluid/gas saturation

The water/gas saturation for Nitrogen as proposed by Rad and Lunne (1994) is as

$\eta_{(N2)}$

$$= \frac{[(0.035L - 0.0153L) + 0.0153L * 0.016] * 85000 * 10^{-6}}{0.0153L * 0.016} x \frac{1.31atm}{1.95atm} x \frac{293.15K}{293.15K} x100$$

$\eta_{(N2)} = 465$ % (pore fluid is supersaturated with Nitrogen)

The water/gas saturation for Nitrogen as proposed by Christian and Cranston (1997)

$$S_{(N2)o} = 10^{-6} \frac{85000 * 1atm * 293.15K * (V_{g1} + 0.015 * 0.0153L)}{1.95atm * 298.15K * 0.016 * 0.0153L} x100$$

$$V_{g1-Eq(B-3)} = \frac{1.31atm * (0.035L - 0.0153L) * 298.15K}{293.15K * 1atm} = 0.026L$$

$$V_{g1-Eq(B-4)} = \frac{0.72atm * 0.035L}{293.15K} x \frac{10^6 * 298.15K}{915000 * 1atm} - 0.0015 * 0.0153L = 0.028L$$

$S_{(N2)o-Eq(B-3)} = 459$ % (pore fluid is supersaturated with Nitrogen)

$S_{(N2)o-Eq(B-4)} = 494$ % (pore fluid is supersaturated with Nitrogen)

Degree of saturation, S(%)

Computing V_{g1} by using Eq. (B-3)

$$\eta_{g(N2)1-Eq(B-3)} = 10^{-6} \frac{85000 * 1atm * 0.026L}{0.082L * \frac{atm}{mol * K} * 298.15K} = 9.04x10^{-5} mol$$

$$\eta_{w(N2)1-Eq(B-3)} = 10^{-6} \frac{85000 * 1atm * 0.015 * 0.0153L}{0.082 \frac{L * atm}{mol * K} * 298.15K} = 7.98x10^{-7} mol$$

$$\eta_{total-Eq(B-3)} = 9.12x10^{-5}mol$$

$$\eta_{w(N2)0-Eq(B-3)} = \frac{1.95atm * 0.016 * 0.0153L}{0.082\frac{L*atm}{mol*K} * 293.15K} = 2.00x10^{-5}mol$$

$$\eta_{g(N2)0-Eq(B-3)} = 7.12x10^{-5}mol$$

$$V_{go-Eq(B-3)} = \frac{0.082L\frac{L*atm}{mol*K} * 293.15K * 7.12 * 10^{-5}mol}{1.95atm} = 8.76x10^{-4}L$$

$$S(\%)_{Eq(B-3)} = \frac{0.0153L}{(0.0153L + 8.76 * 10^{-4}L)}x100 = 94.6\%$$

Computing V_{g1} by using Eq. B-4

$$\eta_{g(N2)1-Eq(B-4)} = 10^{-6}\frac{85000 * 1atm * 0.028L}{0.082L * \frac{atm}{mol*K} * 298.15K} = 9.73x10^{-5}mol$$

$$\eta_{w(N2)1-Eq(B-4)} = \eta_{w(N2)1-Eq(2-3)} \text{ and } \eta_{w(N2)o-Eq(2-4)} = \eta_{w(N2)0-Eq(2-3)}$$

$$\eta_{total-Eq(B-4)} = 9.81x10^{-5}mol$$

$$\eta_{g(N2)0-Eq(B-4)} = 7.81x10^{-5}mol$$

$$V_{go-Eq(B-4)} = \frac{0.082L\frac{L*atm}{mol*K} * 293.15K * 7.81 * 10^{-5}mol}{1.95atm} = 9.63x10^{-4}L$$

$$S(\%)_{Eq(B-4)} = \frac{0.0153L}{(0.0153L + 9.63 * 10^{-4}L)}x100 = 94.0\%$$

C. RESULTS OF CYCLIC TRIAXIAL TESTS

**Figure C-1. CSR vs. N (Group 1 - e$_{ave.}$=0.82) – WP.**

WP; S=100%; N=16

e=0.826; Δσ=39.7kPa; σ'$_{vo}$=134.3kPa; CSR=0.148

WP; S=100%; N=23

e=0.819; Δσ=36.4kPa; σ'$_{vo}$=134.6kPa; CSR=0.135

WP; S=100%; N=280

e=0.825; Δσ=25.4kPa; σ'$_{vo}$=135kPa; CSR=0.094
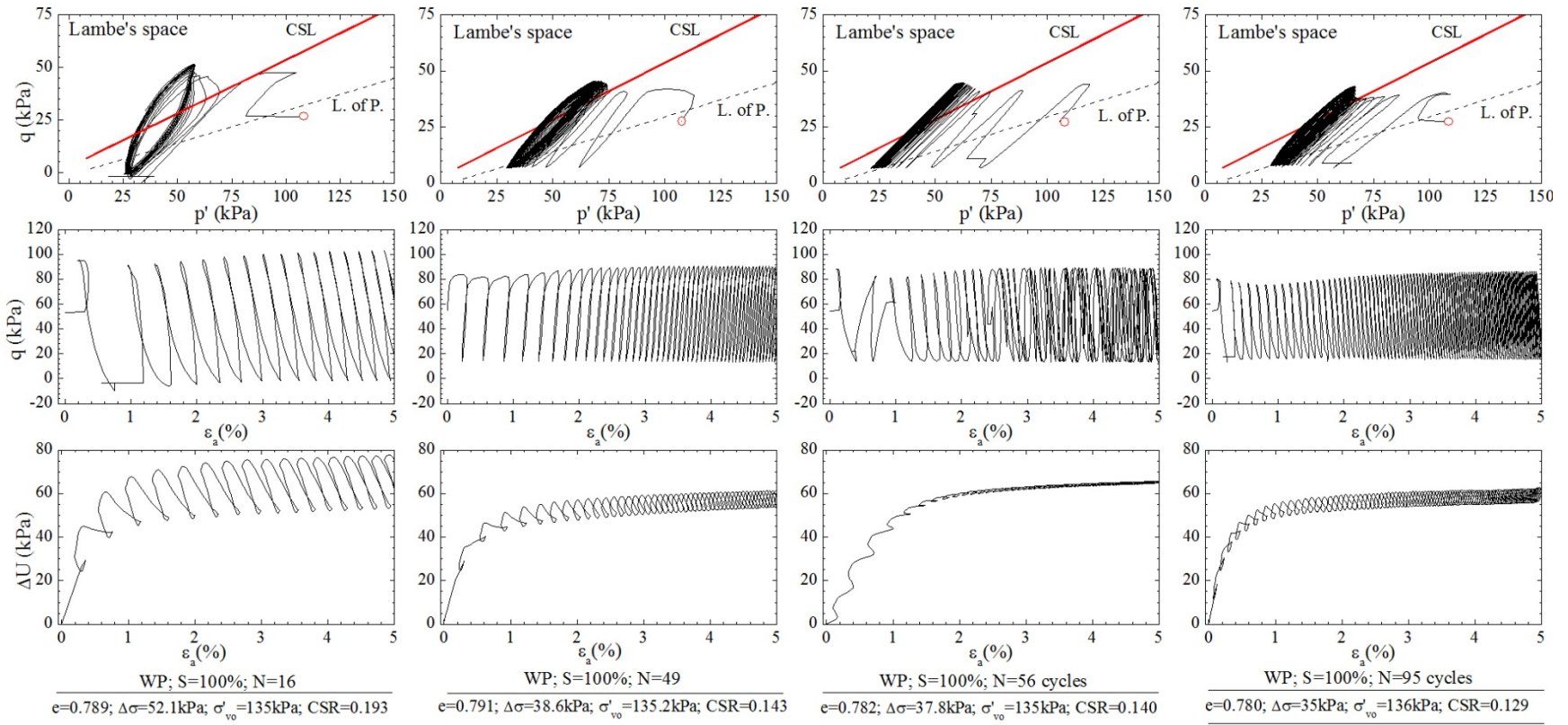
Figure C-2. CSR vs. N (Group 2 - e_ave.=0.79) – WP.

WP; S=100%; N=16

e=0.789; Δσ=52.1kPa; σ'vo=135kPa; CSR=0.193

WP; S=100%; N=49

e=0.791; Δσ=38.6kPa; σ'vo=135.2kPa; CSR=0.143

WP; S=100%; N=56 cycles

e=0.782; Δσ=37.8kPa; σ'vo=135kPa; CSR=0.140

WP; S=100%; N=95 cycles

e=0.780; Δσ=35kPa; σ'vo=136kPa; CSR=0.129

WP; S=100%; N=27

e=0.702; Δσ=62.1kPa; σ'$_{vo}$=135.1kPa; CSR=0.23

WP; S=100%; N=2000 cycles (*)

e=0.707; Δσ=50.9kPa; σ'$_{vo}$=139.4kPa; CSR=0.182

WP; S=100%; N=9000 cycles (*)

e=0.706; Δσ=40.5kPa; σ'$_{vo}$=136.1kPa; CSR=0.149
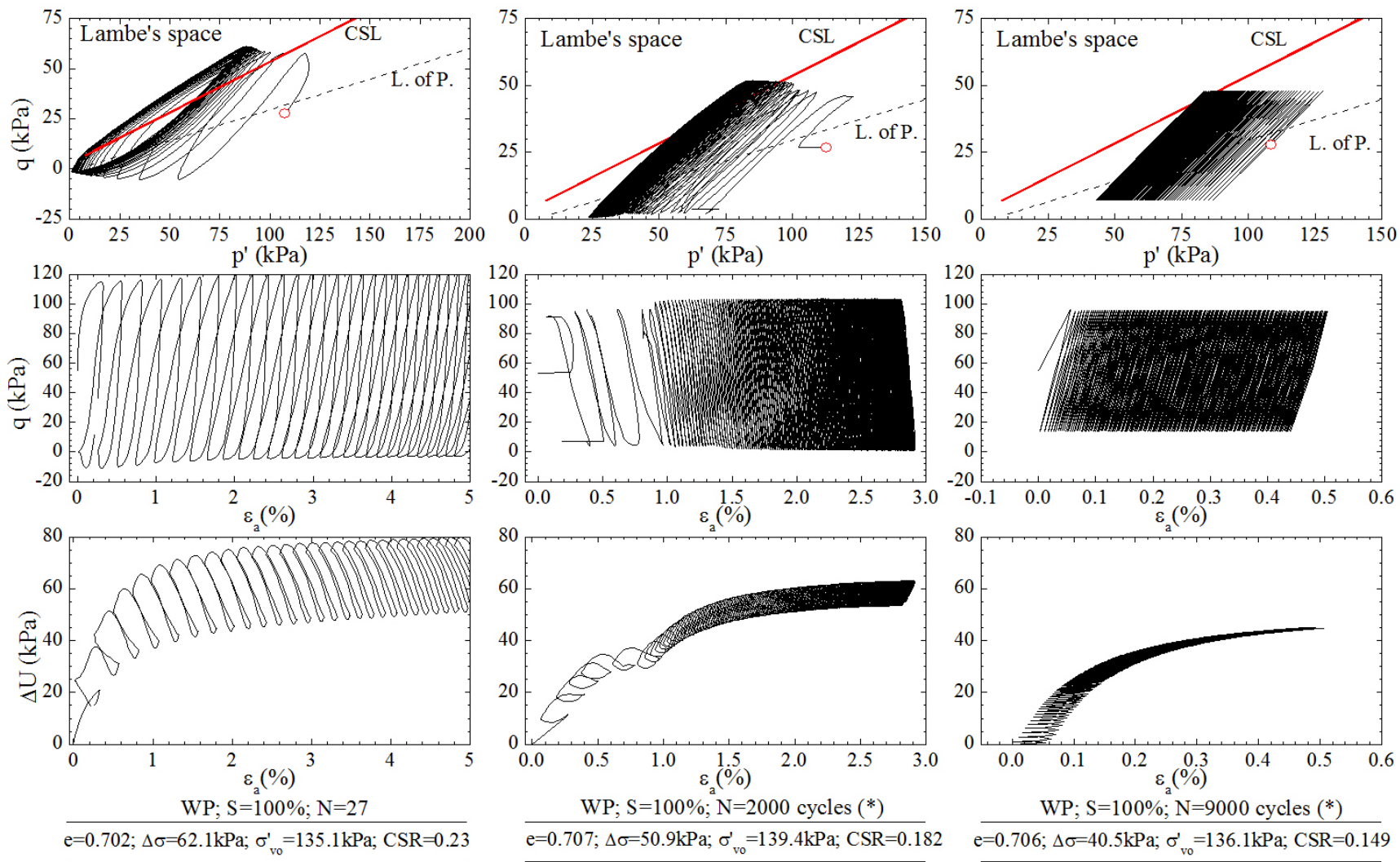
(*) For easy reference, only 200 cycles are plotted

Figure C-3. CSR vs. N (Group 3 - e$_{ave.}$=0.71) – WP.
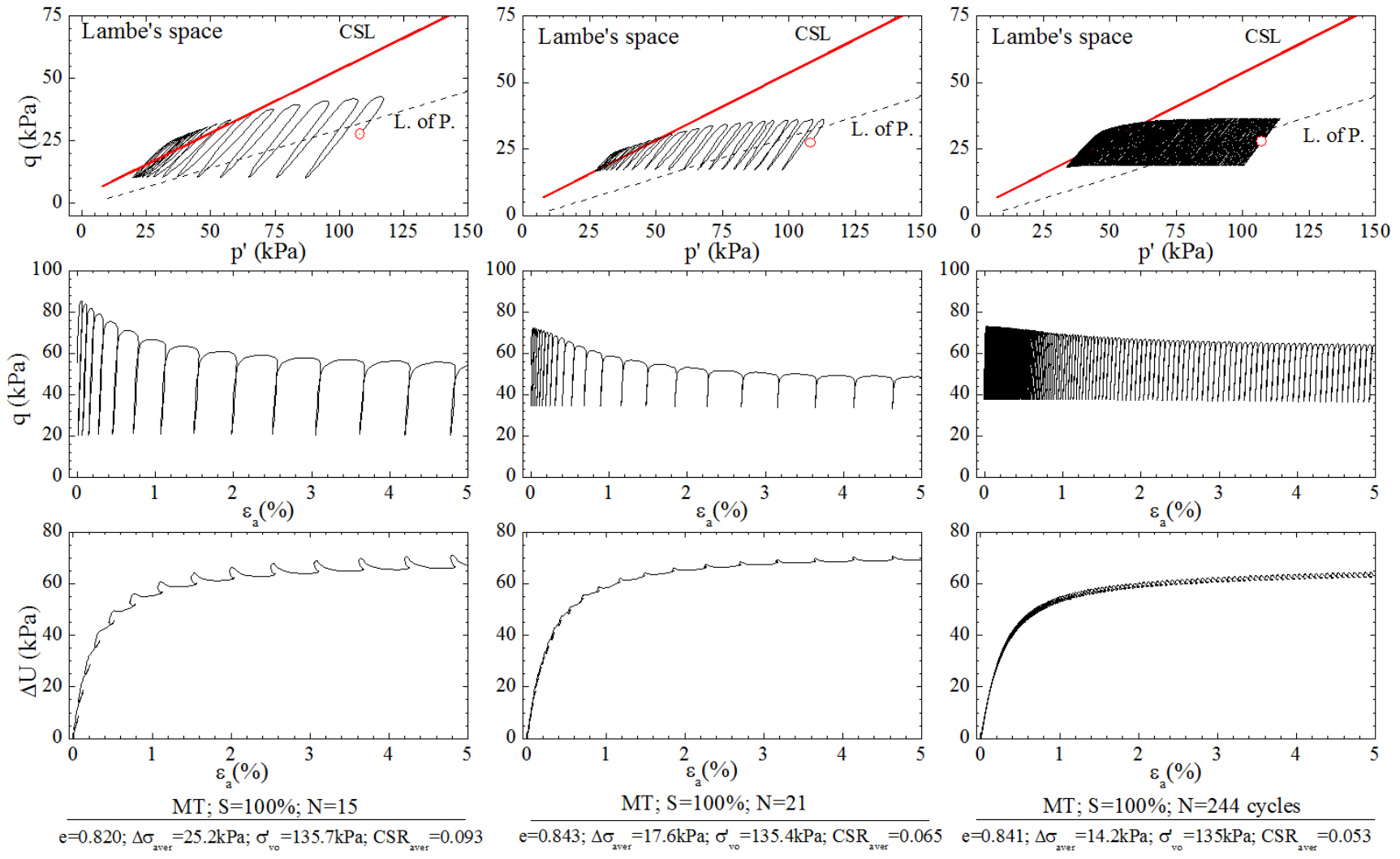
Figure C-4. CSR vs. N (Group 1 - e_ave.=0.83) – MT.

MT; S=100%; N=15

$e=0.820$; $\Delta\sigma_{aver}=25.2$kPa; $\sigma'_{vo}=135.7$kPa; $CSR_{aver}=0.093$

MT; S=100%; N=21

$e=0.843$; $\Delta\sigma_{aver}=17.6$kPa; $\sigma'_{vo}=135.4$kPa; $CSR_{aver}=0.065$

MT; S=100%; N=244 cycles

$e=0.841$; $\Delta\sigma_{aver}=14.2$kPa; $\sigma'_{vo}=135$kPa; $CSR_{aver}=0.053$
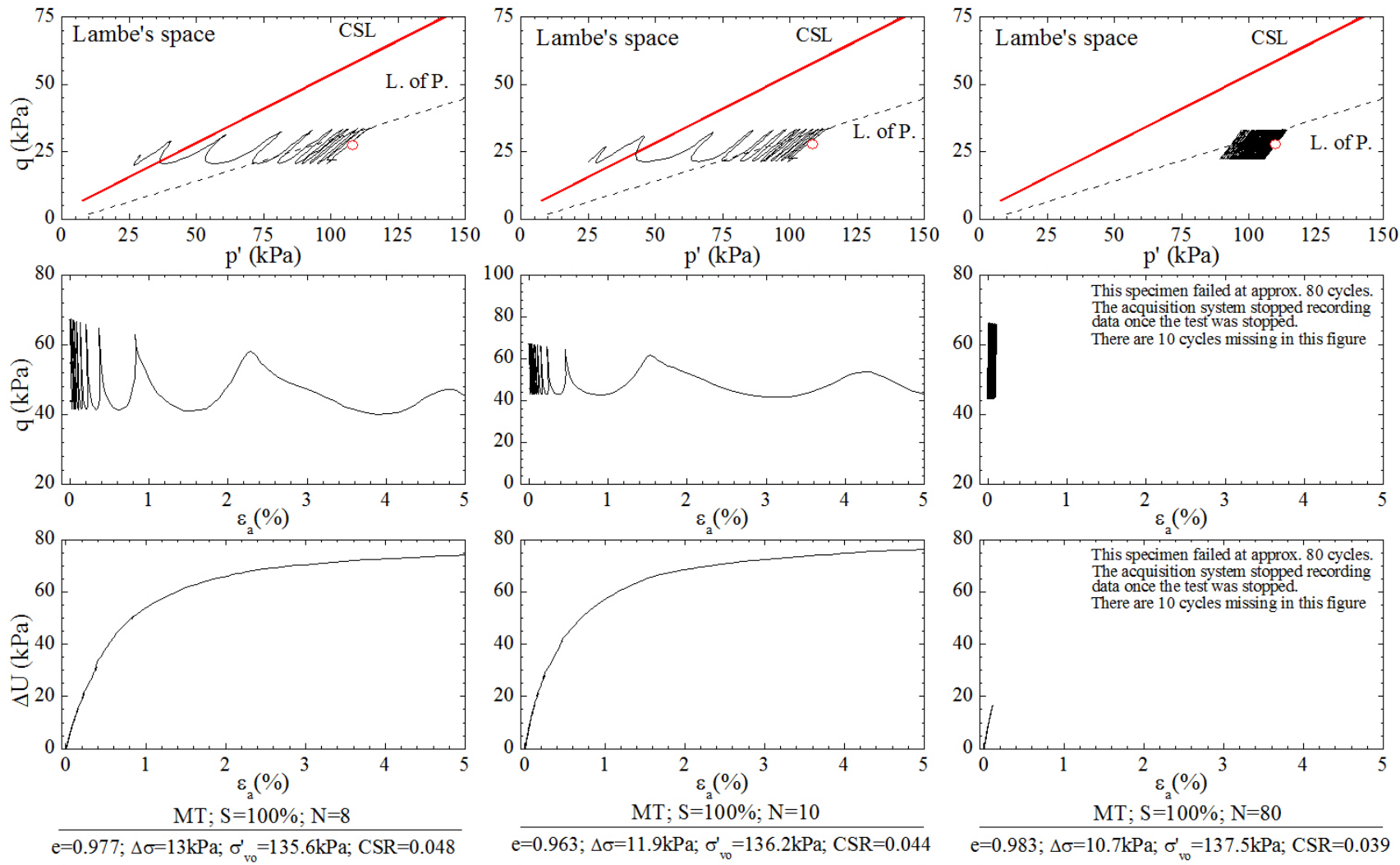
Figure C-5. CSR vs. N (e_ave.=0.97) – MT.

D. COMPUTED AND OBSERVED SETTLEMENTS
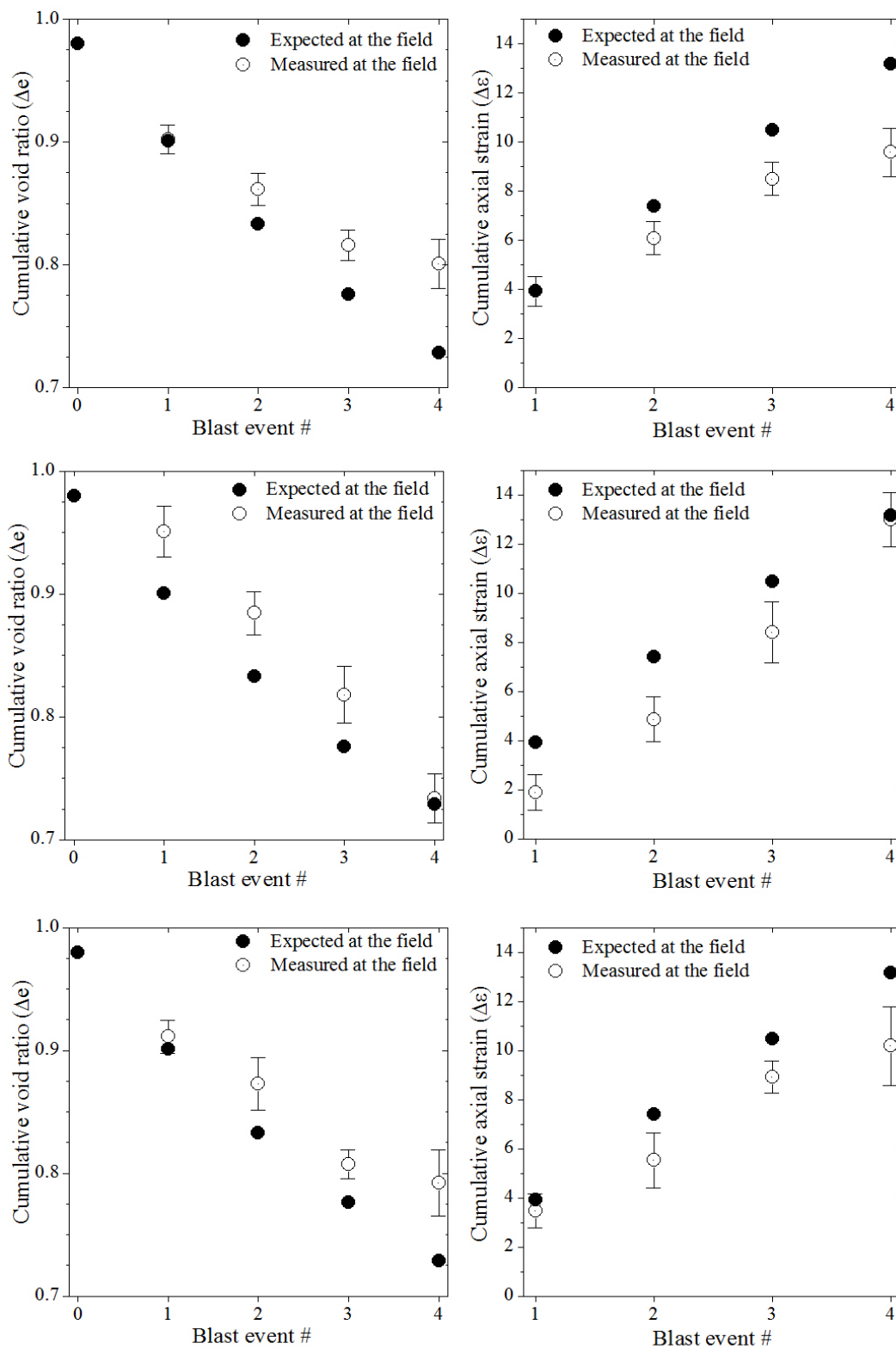
Figure D-1. Cumulative void ratio and axial strain (%) – Zones 15A, 15B, and 16 (from top to bottom).
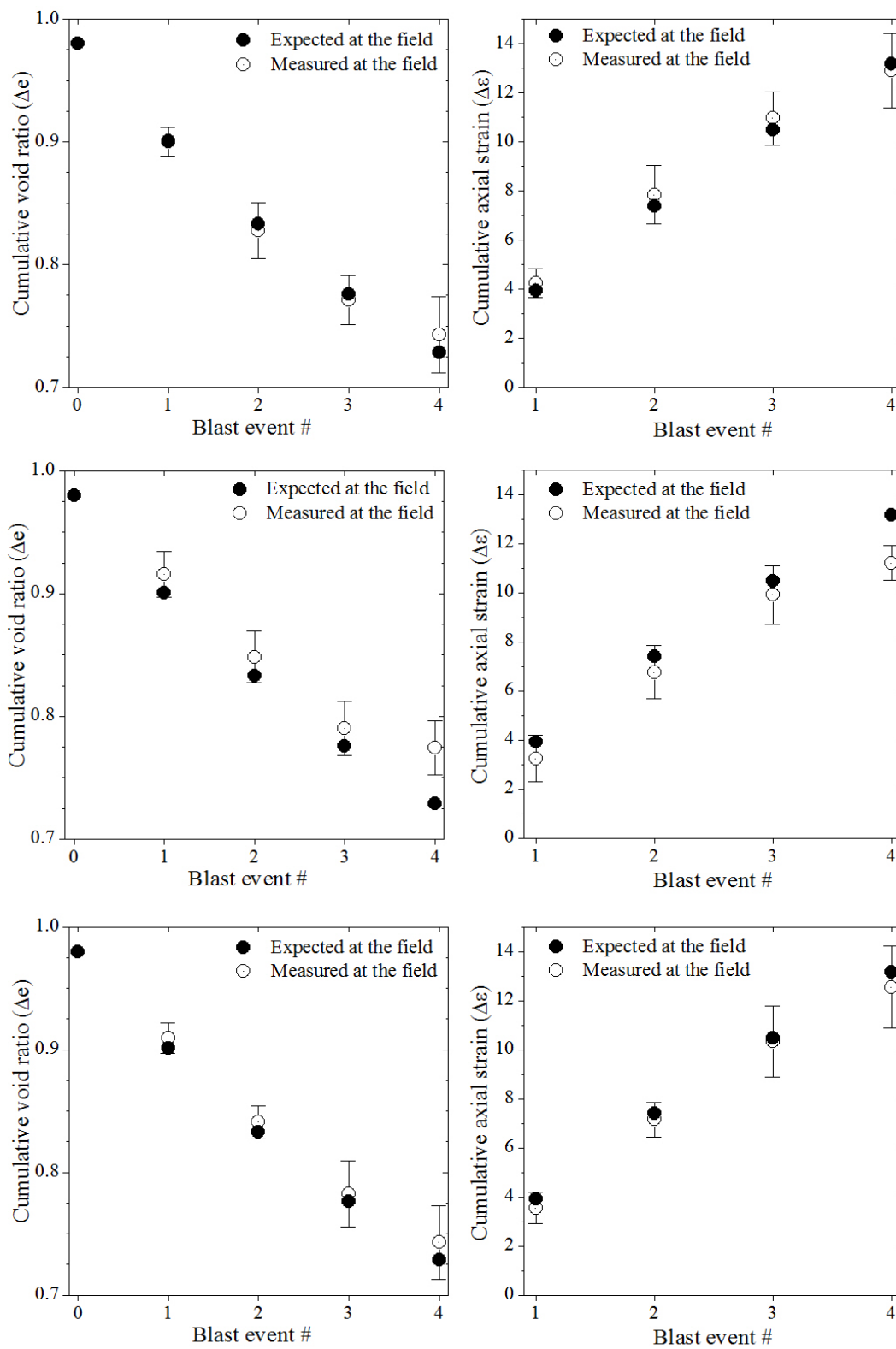
Figure D-2. Cumulative void ratio and axial strain (%) – Zones 17, 18, and C (from top to bottom).
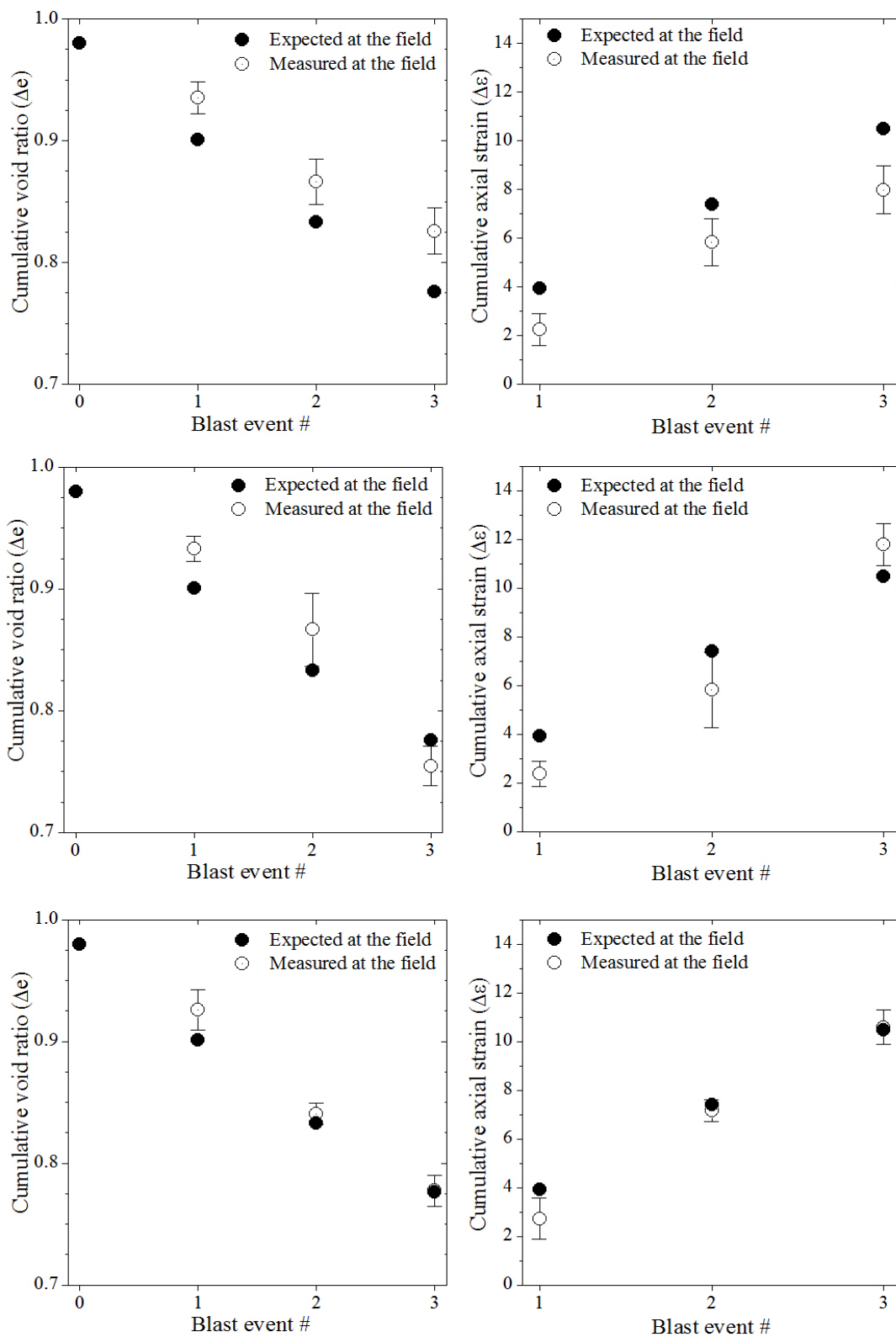
Figure D-3. Cumulative void ratio and axial strain (%) – Zones 19, 20, and 21(from top to bottom).
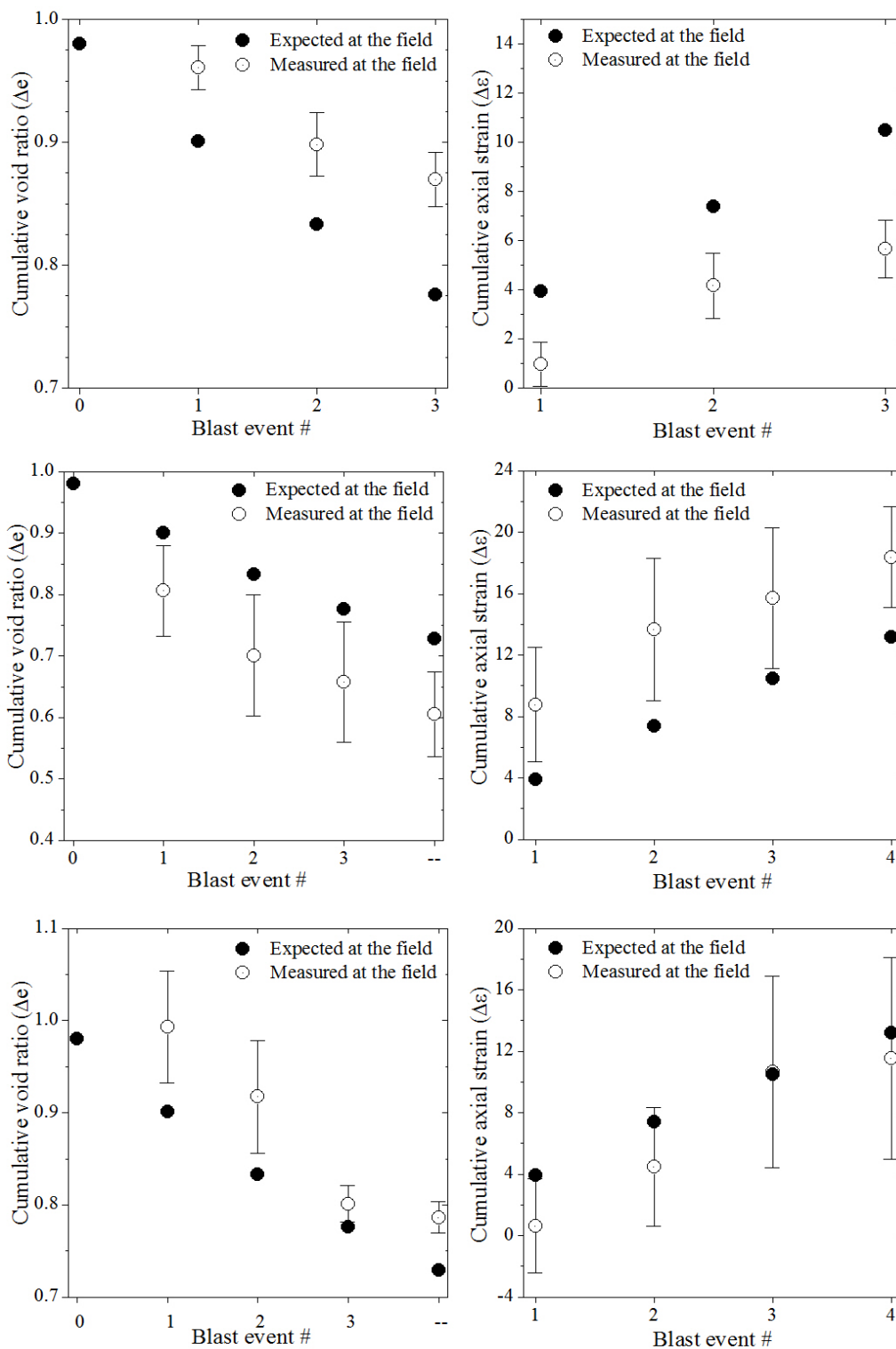
Figure D-4. Cumulative void ratio and axial strain (%) – Zones 22, 4, and 5 (from top to bottom).